Metamorphism and geodynamics of the Proterozoic Kabul Block: Preservation and modification of crustal fragments within an orogenic zone

by

Stephen Paul Collett

MGeol., University of Leicester, 2011

Supervised by

Prof. Ing. Shah Wali Faryad, CSc.

A thesis submitted in partial fulfilment of the requirements for the degree

of

Doctor of Philosophy in Geology

at

The Institute of Petrology and Structural Geology, Faculty of Science, Charles University in Prague

June, 2015

To my grandfather, Thomas Hamilton

(1925-2013)

Whose example of good humour and perseverance in the face adversity continues to inspire

Declaration

I certify that the work presented in this thesis 'Metamorphism and geodynamics of the Proterozoic Kabul Block: Preservation and modification of crustal fragments within an orogenic zone' is my own work or the product of collaboration with other members of the research team. Credit is given in each of the parts to those involved in their composition. None of the material presented here has been accepted for the award of any other degree or diploma in my name, in any university or other tertiary institution; and, to the best of my knowledge contains no material previously published or written by another person, except where due reference has been made in the text.

In:

Date: Stephen Collett MGeol.

Research student

1   Abstract

The Kabul Block is a lenticular crustal fragment that, along with the Farah, Helmand, and Nuristan terranes, is situated within a tectonic zone known as the Afghan Central Blocks. The Afghan Central Blocks form within the collision zone between the Indian, Eurasian, and Arabian plates. The Kabul Block consists of a highly-deformed crystalline basement overlain by weakly-deformed Late Paleozoic-Mesozoic sediments. U/Pb SHRIMP analysis of zircon cores from the lowermost basement formations (the Sherdarwaza and/or Khair Khana) indicates the presence of a Neoarchean component (~ 2700 Ma), while the majority of zircon cores yield a range of Early Paleoproterozoic ages (2200 - 2500 Ma). The Sherdarwaza and Khair Khana Formations are comprised of migmatite and orthogneiss with minor marble, quartzite, and amphibolite that reached granulite-facies conditions. Conventional geothermobarometry and phase equilibria modelling on well preserved granulite-facies assemblages indicates that the rocks reached conditions of approximately 850 °C at up to 7 kbar of pressure. Textural relations indicate that this was a strongly temperature dominated event. U/Pb SHRIMP dating of zircon rims and U-Th-Pb dating of monazite inclusions in granulite-facies garnet suggest that this event occurred in the late Paleoproterozoic (~ 1750 - 1900 Ma).

The granulite-facies assemblages are overprinted by a younger, amphibolite-facies metamorphism, and are unconformably overlain by amphibolite-facies rocks belonging to younger formations (the Kharog and Welayati) that lack paragenetic evidence for a preceding high-grade metamorphism. The Welayati Formation crops-out extensively in the south of Kabul City and consists of a variety of mica-schists and garnet-amphibolites, which contain textural relations suitable for the construction of a pressure-temperature (P-T) path. Inclusion assemblages in porphyroblastic garnet yield P-T conditions of around 525 °C and 6 kbar. Chemical zonation in garnet and phase equilibria modelling indicates that from this point garnet grew during a pressure increase of ~ 3.5 kbar over a temperature increase of ~ 125 °C. A subsequent period of near isothermal decompression of up to 2 kbar is recorded by plagioclase and biotite porphyroblasts which overgrow and cross-cut the main foliation. Ar/Ar dating of mica and U-Th-Pb dating of monazite has been used to constrain both the amphibolite-facies overprint in the Sherdarwaza and Khair Khana Formations, and the metamorphism in the Welayati Formation to the Early-Mid Neoproterozoic (~800 - 850 Ma).

Subsequent deformation and metamorphism is evidenced by the transformation of the amphibolite- and granulite-facies assemblages to lower-grade phases and by the partial resetting of geochronological systems. The lack of equilibrium assemblages precludes the constraining of P-T conditions for these transformations and the age relations are not clearly resolved. However, north from the Kabul Block, in the Western Hindu Kush, Paleozoic and Cenozoic metamorphic events are observed. Eocene pressure dominated amphibolite-facies metamorphism is recorded in Cretaceous meta-granitoids. This metamorphism occurred as a result of indentation tectonics resulting in the wedging of the Kabul Block between the Helmand and Nuristan Terranes.

2   Abstrakt

Kábulský blok je čočkovitý fragment zemské kůry, který se spolu s Farah, Helmand, a Nuristan terány nachází v tektonické zóně známé jako ,Afghan Central Blocks', které jsou situované v kolizní zóně mezi indickou, euroasijskou, a arabskou deskou. Kábulský blok je složen z vysoce deformovaného krystalinikého basementu překrytého slabě deformovanými svrchnopaleozoického-mezozoickými sedimenty. U / Pb SHRIMP analýza zirkonových jader z nejspodnější formace krystalinického basementu (Sherdarwaza a / nebo Khair Khana) indikuje Neoarcheanského stáří (~ 2700 Ma), zatímco většina zirkonvých jader spadá do spodněPaleoproterozoických věků (2200 - 2500 Ma). Sherdarwaza a Khair Khana formace jsou složeny především z migmatitů a ortorul, minoritně s mramory, křemenci, a amfibolity, které dosáhly podmínek granulitové-facie. Konvenční geotermobarometry a modelování fázových rovnovah v dobře zachovalých minerálních asociacích granulitové facie naznačuje, že horniny dosáhly podmínek přibližně 850 ° C při tlaku až 7 kbar. Texturní vztahy ukazují na dominantně teplotní event . U / Pb SHRIMP datování okrajů zirkonu a U-Th-Pb datování monazitových inkluzí v granátech granulitové facie naznačují, že tato událost nastala v pozdním Paleoproterozoiku (~ 1750-1900 Ma) .

Asembláž granulitové facie je přetištěna mladší metamorfózou v amfibolitovéfacii a je diskordantně překryta horninami amfibolitové facie náležící mladší formaci (Kharog a Welayati), která postrádá paragenezi předchozího vysokého stupně metamorfózy. Welayati Formace je výrazně rozšířena na jihu Kábulu a je tvořena různými varietami svorů a granátických amfibolitů, které obsahují texturní vztahy vhodné pro určování teplotně tlakových podmínek. Inkluze v porphyroblastech granátu naznačují teplotně tlakové podmínky okolo 525 ° C a 6 kbar. Chemická zonálnost v granátu a modelování fázové rovnováhy indikuje, že od tohoto bodu granát rostl s nárůstem tlaku o ~ 3,5 kbar a teploty o 125 ° C. Následná téměř izotermální dekomprese až do 2 kbar je zaznamenána plagioklasem a biotitickými porfyroblasty které přerůstají a přetínají hlavní foliaci. Ar / Ar datování slíd a U-Th-Pb datování monazitů byla použita k určení stáří jak přetisku v amfibolitové facii ve Sherdarwaza a Khair Khana formaci, tak k určení stáří metamorfózy ve formaci Welayati, což odpovídá spodně až středně Neoproterozoickému stáří (~ 800 - 850 Ma).

Následnou deformaci a metamorfózu dokládá transformace asembláže amfibolitové a granulitové facie do nižších fází a částečný restart geochronologických systémů. Nedostatek rovnovážného složení vylučuje určení P-T podmínek této transformace a ani stáří není jasně vyřešeno. Nicméně severně od Kábulského bloku, v západním Hindúkuš jsou jasně pozorovány paleozoické a kenozoické metamorfní eventy. Eocení tlakově dominantní metamorfóza v podmínkách amfibolitové facie je zaznamenána v křídových meta-granitoidech. Tato metamorfóza je způsobena indentační tektonikou která dává vzniknout vklínění Kábulského bloku mezi Helmand a Nuristan terány.

3   Acknowledgements

This project would not have been possible without the support of my supervisor Shah Wali Faryad. Wali has patiently and tirelessly guided me through the research process and the standard of the work presented here has been improved immeasurably thanks to his involvement. Furthermore, without Wali it is almost certain I would never have been able to experience and carry out fieldwork in Kabul and for that I'm eternally grateful.

Also I would like to acknowledge Prof. Mike Petterson who is presently with the Secretariat of the Pacific Community and was formerly my masters project supervisor at the University of Leicester, Mike first introduced me to the topic of metamorphism in Afghanistan and without his encouragement I would not have pursued the PhD.

Thanks also to the many colleagues and students I have worked with at the Institute of Petrology and Structural Geology who have made me feel so welcome here in the Czech Republic and for the numerous discussions both geologically related and not, over countless piva.

I would also like to thank the Grant Agency of Charles University, the Czech Sciences Foundation, the British Council, and the Faculty of Science at Charles University all of whom have provided the financial means to complete this project.

And finally thank you to all the friends and family both in the Czech Republic and beyond who have supported and encouraged me throughout the duration of my studies.

4   Format of the thesis

This thesis is presented in six parts comprising an introduction to the topic, four articles published in international impact factor journals, and conclusions derived from this work. The introduction describes the physical geography of Afghanistan and the study region around Kabul, followed by an outline of the historical geological activities in the region and an overview of the present understanding of the tectonic framework of Afghanistan and the stratigraphical relations present within the Kabul Block. Finally, an outline of the various objectives of this research project is presented.

Each of the articles deals with a different aspect of the crustal evolution of the Kabul Block and surrounding regions. The first two articles establish constraints on the early history of the Kabul Block through investigation of the metamorphic basement. Textural relations amongst minerals are used to establish metamorphic events and the pressure-temperature (P-T) history of these events are examined through thermodynamic modelling and geothermobarometric calculations. In the first article we assess granulite-facies assemblages preserved in the lowermost basement formations, the granulites occur as lenses and boudins within migmatite and gneiss and record textures which indicate a polyphase metamorphic history. The second article investigates micaschists which belong to a younger sequence that unconformably overlies the granulite-facies formation in the south of Kabul. The construction of well constrained P-T paths are possible in the mica-schist owing to the preservation of prograde zoning garnet and textural relations between minerals.

The third article investigates the age relations of the processes identified in the first two articles. Using a combination of geochronological dating techniques, including: U/Pb zircon, U-Th-Pb monazite, and Ar/Ar mica it is possible to identify probable protolith ages and constrain the timing of metamorphism and deformation events. Additionally, assessment of the geochemical signature of the basement rocks and the age relations and geochemistry of similar Precambrian terranes prefaces a discussion of the historical evolution of the Kabul Block.

The fourth article differs from the previous three as it does not directly investigate the evolution Kabul Block. The article explores magmatic and metamorphic events within the Western Hindu Kush; examining samples collected from the three major mountain passes (Ghor Band, Salang, and Panjshir) that traverse the Hindu Kush Mountains north from Kabul. The results are informative regarding the tectonic evolution of this region and also relating to the latter history of the Kabul Block and its eventual docking with the Eurasian continent.

The final part of the thesis outlines the various conclusions drawn from this work, assessing how much of the original objectives have been fulfilled and what issues remain to be resolved.

5   List of published articles

- Collett, S., Faryad, S. W., & Mosazai, A. M. (2015). Polymetamorphic evolution of the granulite-facies Paleoproterozoic basement of the Kabul Block, Afghanistan. Mineralogy and Petrology. doi:10.1007/s00710-015-0371-9

  - Authors contribution: Partial involvement in the fieldwork and sampling, responsible for the petrographic descriptions, majority of the collection of minero-chemical data, as well as the thermobarometry and pseudosection modelling. Discussion produced by the student following detailed consultations with the supervisor.

- Collett, S., & Faryad, S. W. (2015). Pressure-temperature evolution of Neoproterozoic metamorphism in the Welayati Formation (Kabul Block), Afghanistan. Journal of Asian Earth Sciences. doi:10.1016/j.jseaes.2015.06.002

  - Authors contribution: Partial involvement in fieldwork and sampling, responsible for the petrographic descriptions the majority of the minero-chemical data and the thermobarometry. Direction of the paper largely the students work with suggestions from the project supervisor.

- Faryad, S. W., Collett, S., Finger, F., Sergeev, S. A., Čopjaková, R., & Siman, P. (2015). The Kabul Block (Afghanistan), a segment of the Columbia Supercontinent, with a Neoproterozoic metamorphic overprint. Gondwana Research. doi:10.1016/j.gr.2015.02.019

  - Authors contribution: Partial involvement in fieldwork and sampling, conducted some of the petrographic descriptions and acquisition of minero-chemical data, responsible for the study of geochemistry. Discussion primarily the project supervisor with collaboration from the student.

- Faryad, S. W., Collett, S., Petterson, M., & Sergeev, S. A. (2013). Magmatism and metamorphism linked to the accretion of continental blocks south of the Hindu Kush, Afghanistan. Lithos, 175, 302-314.

  - Authors contribution: Limited involvement in the fieldwork and sampling. responsible for the pseudosection modelling and the chapter on geochemistry. Discussion primarily the work of project supervisor with input and consultation with the student.

I certify that the above records an accurate representation of the involvement of the research student in the aforementioned research papers.

Signed:_____

Prof. Ing. Shah Wali Faryad, CSc.

Project supervisor

Contents

Part I

Introduction

1   Geographic position of the Kabul Block

Afghanistan is located at the juncture of Central, Western and Southern Asia, sharing borders with Pakistan to the east, Iran to the west, and Turkmenistan, Uzbekistan, and Tajikistan to the north. Additionally, Afghanistan shares a short (approximately 35 km long) border with China in the far north east of the country. The geographical landscape is dominated by the Hindu Kush Mountains, which rise as an approximately 800 km long ridge that stretches from Central Afghanistan to Northern Pakistan (Fig. 1). The mountains act as a geographical divide between the Amu Darya River valley in the North and the Indus River valley in the south and east. Elevations are highest in the north east at the border with Pakistan diminishing towards the western margin of the range. To the south and west the mountains give way to plateaus and desert that straddles the border with Iran. The north of the country is defined by fertile plains that border the Amu Darya River.
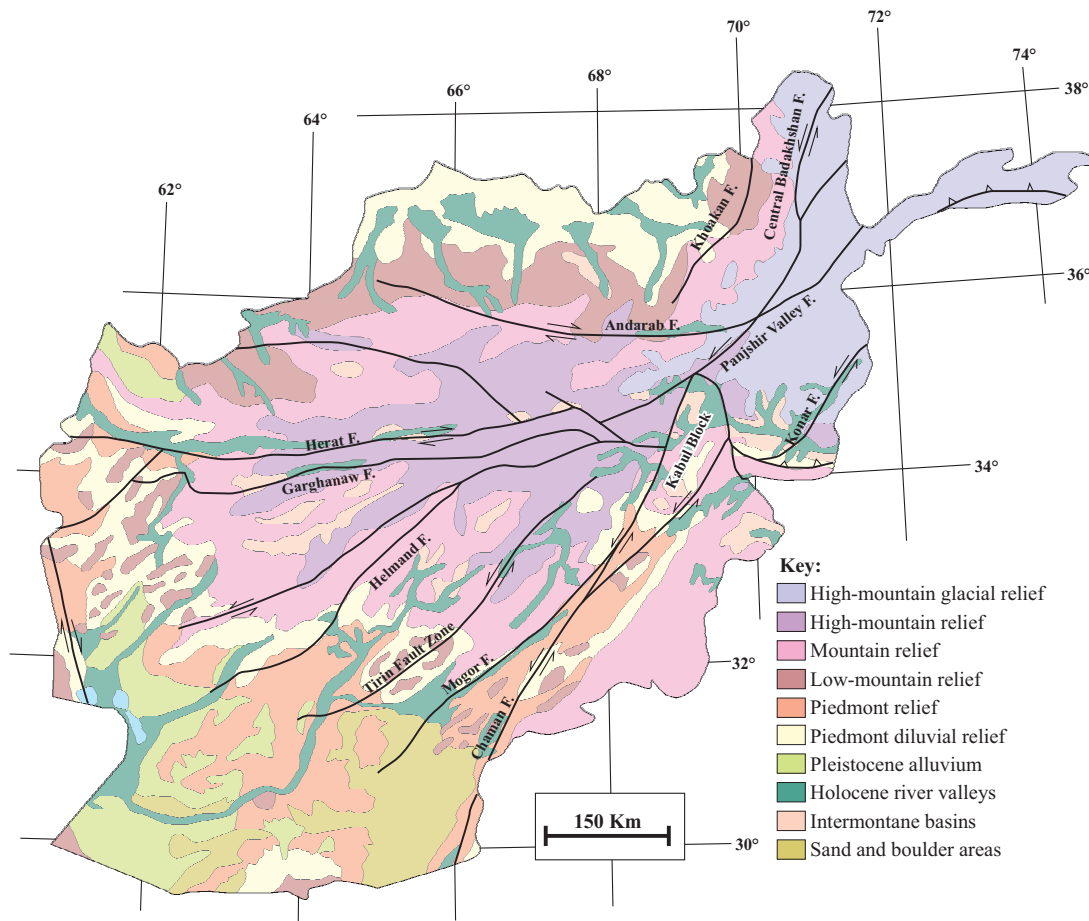
Figure 1: Geomorphological map of Afghanistan (adapted from: http://www.aims.org.af/maps/national/national_atlas/10_geomorphology.jpg (last accessed 3ʳᵈ June 2015)) overlain by the tectonic subdivision by Treloar and Izatt (1993). High mountain relief of the Hindu Kush mountains concentrated in the north east of the country. The Kabul Block sits in the foothills of the Hindu Kush Mountains and is characterised by Holocene river valley, intermontane basins, and medium mountain relief.

The Kabul Block is situated in the east of the country in the southern foothills of the Hindu Kush Range.

The area primarily consists of a sedimentary basin drained by the Panjshir River in the north and the Kabul River in the south. The Hindu Kush Mountains define the northern and eastern margins of the basin while the western margin buttresses the Paghman mountain chain. Rugged hills rise above the basin most prominently in the area immediately around the city of Kabul and in the Kohi-Safi district north east from the city. Vegetation is scarce in the area around Kabul, but more prominent in the drainage basin of the Panjshir River and its tributaries north from the city. The climate is semi-arid with precipitation concentrated primarily as snow during the winter months. Temperatures are generally cool in comparison to similar latitudes, reaching summer highs of around 35 °C, owing to the elevation of the area.

2   History of geological research

Afghanistan has long represented an area of geological interest, its situation at the juncture of major tectonic blocks providing a complex and spectacular geological framework. It is rich in natural resources including rare and precious stones, which have been exploited since the Neolithic times. Some of the world's oldest mines are thought to have been established in Afghanistan, in particular lapis lazuli extraction in the Badakhshan province in North East Afghanistan is considered to have originated as much as 10,000 years ago. The deep blue colour of the lapis lazuli stone, owing to the presence of the S^{3-} radical in the mineral lazurite (Boros et al. 2010), was prized in ancient art and jewellery and can be found in archaeological sites across Mesopotamia and extending to Ancient Egypt and the Mediterranean.

The foundations for the present day understanding of Afghan geology were laid by pioneering work in the late 19th and early 20th century. Investigation was conducted along the primary caravan trails and up to the foothills of the Hindu Kush Mountains. These early works (e.g. Griesbach, 1885 and Hayden, 1911) outlined the general stratigraphic make-up of the area and were collated by Mennessier (1963) in his 'stratigraphic guide' to Afghanistan.

Real advancement into the geological understanding of the region however, didn't initiate until the establishment of the National Geological Survey in 1955. Co-operative studies between the Afghan Geological Survey and teams of geoscientists from Germany, Italy, France, and the Soviet Union led to the first extensive mapping and prospecting operations (Fig. 2).

German geological mission

The collaboration with German geoscientists primarily focussed on the mapping of geologically significant areas in the south of the country through a combination of aerial photography and field data. Summation of this data was compiled by Wittekind and Weppert (1973) and Wolfart and Wittekindt (1980). Further to the geological mapping Andritzky (1967, 1971) studied the crystalline basement rocks in the Kabul area and first interpreted the Kabul Block as representing a dome like structure. Additionally, Andritzky (1971) provides age data for the basement rocks recording K-Ar ages of 928+/-8 Ma and 644+/-6 Ma from samples of gneiss and biotite schist respectively.

Italian geological mission

The Italian works in the region focussed primarily on the study of igneous complexes in the Western Hindu Kush, Badakhshan and Wakhan areas in the north and north east of the country (e.g. Desio

Histogram of the publication language of articles and reports on Afghanistan geology

Kernel density plot of year of publication of articles and reports on Afghanistan geology
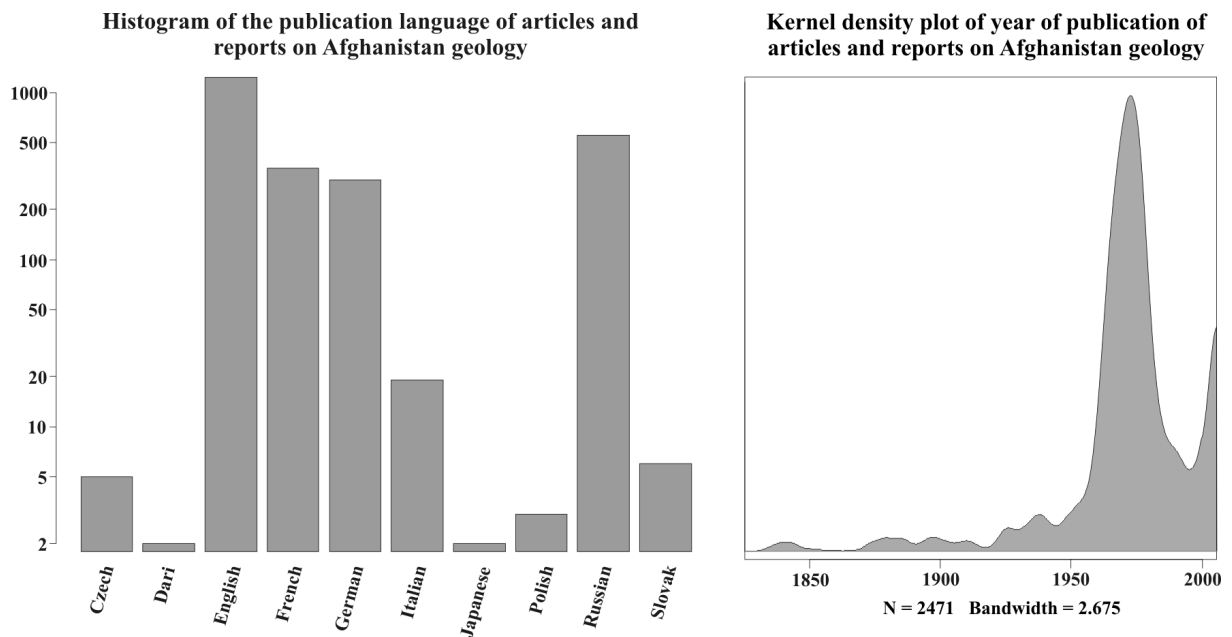
Figure 2: Histogram of the language of publications on the geology of Afghanistan and Kernel density plot of the publication year. The data used comes from a database of all publications on Afghanistan to 2007 produced by Eppinger et al. (2008)

et al. 1964; 1965; 1968). These works provided links between the structures of Afghanistan and the neighbouring Eastern Hindu Kush and Pamir ranges.

French geological mission

French geological studies in the area encompassed a broad range of topics, including broad stratigraphical studies (e.g. Lappparent and Mennessier, 1962; Mennessier, 1963); study of the Cenozoic volcanism (e.g. Lapparent and Bordet, 1963; Bordet, 1969); paleontological investigation (e.g. Mennessier, 1968; Leven, 1971); metamorphic studies of blue-schists in the Bamyan area (Fabries and Lang, 1970) and gneiss in the Maydan and Wardak regions (Blaise et al. 1971); and large-scale interpretation of the structural evolution (e.g. Boulin, 1972; Mennessier, 1977). Furthermore, within the Kabul area Tapponnier et al. (1981) conducted investigation of ultra-mafic (ophiolite) bodies and large scale tectonic movements. The margins of the Kabul Block are flanked by two ophiolite belts and these were interpreted to mark the Indus-Tsangpo suture between India and Eurasia, in Afghanistan.

Afghan-Soviet co-operation

By far the most comprehensive work in this region was conducted under the auspices of U.S.S.R. and Afghanistan economic co-operation. This co-operation was initiated in the late 1950's in the form of oil and gas prospecting within the northern part of Afghanistan. This combined extensive geological, geophysical, and structural studies that are described by Bratash et al. (1970). In addition to prospecting for oil and gas, extensive exploration for solid mineral deposits was conducted and the first countrywide geological mapping produced (Kafarsky et al. 1975). A comprehensive summary of these works and of the overall geology and mineral resources of Afghanistan are given in Abdullah and Chmyriov (1977). This work incorporates all of the known stratigraphical and structural knowledge at the time and was translated into English as part of the British Geological Survey mission in Afghanistan (Abdullah and

Chmyriov, 2008). In addition to these aforementioned works between 1977 and 1981 a team of Soviet and Afghan geologists conducted the most extensive study of the basement rocks of the Kabul town area. This is preserved as an unpublished geological report with 1:25000 maps at the Afghanistan Geological Survey (Karapetov et al. 1981).

Post U.S.S.R. invasion geological studies

Following the Soviet invasion (24th December, 1979) and the ensuing conflicts, geological activity within the country ground towards a halt. However, small advances were made during this period through the re-analysis of old data and samples, satellite and airborne imagery as well as improved knowledge of the surrounding regions. Debon et al. (1987) provided a comprehensive analysis of the different intrusive belts within Afghanistan, identifying multiple generations of plutonism linked to periods of subduction. Large scale structural analysis by Boulin (1988, 1991) led to the distinction of the country into distinct areas of Hercynian and Eocimmerian orogenisis. These ideas were furthered by Treloar and Izatt (1993) who sought to link these different orogenic events to the adjacent regions of Himalayan tectonics. Leven (1997) re-examined the stratigraphical relations to investigate paleogeographic and paleotectonic implications. New petrological studies calculating mineral reactions, metamorphic conditions and fluid controls by Faryad (1999, 2002) were undertaken on samples previously collected from the Hindu Kush Mountains. Badshah et al. (2000) compiled new geological mapping for a region of Eastern Afghanistan based on cross border relations in Pakistan and previously published materials.

Post U.S.A.-led invasion geological activity

Some geological activity has returned to the country subsequent to the American-led invasion (7th October 2001). Once again this activity has mainly focussed towards resource prospecting and geological mapping. The United States Geological Survey (USGS) undertook digitising of the older Soviet-Era maps with a countrywide 1:850000 map compiled by Doebrich and Wahl (2006) and smaller scale (1:250000) quadrangle maps compiled by Bohannon and Turner (2007). Bohannon (2010a, b) also produced new geological maps of the Kabul area based on remote sensing techniques and some limited field geology. These maps were accompanied by a breakdown of the stratigraphical and structural relations based on the previous literature and these new findings.

3   Geology of the Afghan region

Owing to its position at the juncture between three major continental masses (the Eurasian, Indian, and Arabian Plates) and its composition of diverse micro-continental fragments Afghanistan has some of the most complex and varied geology in world. These tectonic fragments were incorporated onto the southern margin of Eurasia during the Mesozoic and early Cenozoic prior to the closure of the Tethys Ocean and collision of the Indian Plate (Fig. 3).

Several different attempts have been made to classify each of the contiguous terranes, the most comprehensive of which by Leven (1997) identified as many as 28 distinct tectonic provinces (Fig. 4). Broadly speaking however, the country can be sub-divided into three principal zones. The northern portion, identified as the Turan plate in the classification of Leven (1997) or the North Afghan Tajik Block (Treloar and Izatt, 1993), represents the stable southern margin of Eurasia. In the south east the Katawaz Basin is interpreted as a flexural basin located on the western margin of the Indian Plate (Treloar and
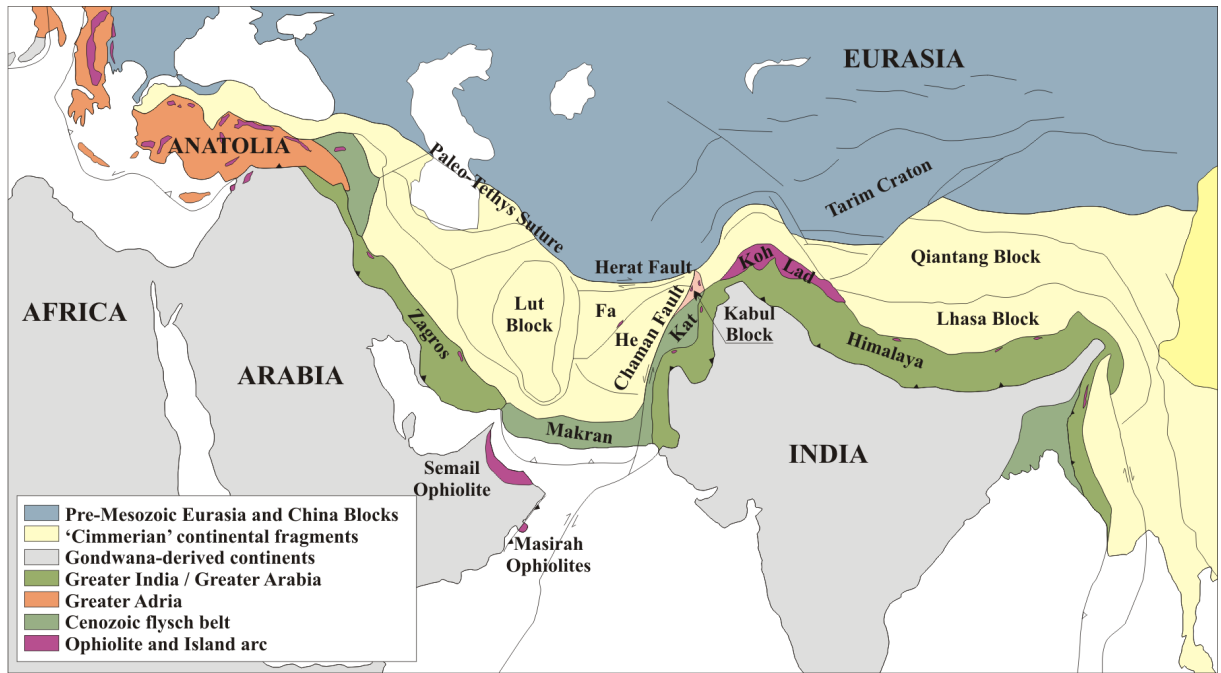
Figure 3: Regional tectonic map of the India-Arabia-Eurasia collision zone after Gaina et al (2015). Fa = Farah Block; He = Helmand Block; Kat = Katawaz Basin; Koh = Kohistan island arc; Lad = Ladakh Island Arc.

Izatt, 1993) and as such the north-western extreme of the Indian continent. Between these two extremes lies a series of north east – south west aligned fragments that includes the Farah, Helmand, Kabul, and Nuristan Blocks. Collectively these tectonic fragments are known as the Afghan Central Blocks (Fig. 5).

1- Turan Plate
2- Turkmenistan Folded Area
3- Rudi-Tchal Structural Zone
4- Sourkhob Structural Area
5- Darvaz-Transalay
6- Jaway-Kurgovad
7- Faizabad-Khazret
8- South Pamir
9- Western Hindu Kush
10- Bamyan Structural Zone
11- Herat Zone
12- Kohi Gardana
13- Alijan Block
14- Farah Block
15- Chagcharin Zone
16- Harrirod Zone
17- Hagigak/Paghman
18- Helmand Block
19- Tarnak Zone
20- Kabul Block
21- Nuristan Block
22- South Badakhshan Massif
23- Koh-e Belandtarin
24- Kunar Zone
25- Katawaz Basin
26- Helmand Basin

Figure 4: Tectonic subdivision of Afghanistan after Leven (1997), the numbered list of tectonic provinces corresponds to the numbered areas on the figure.
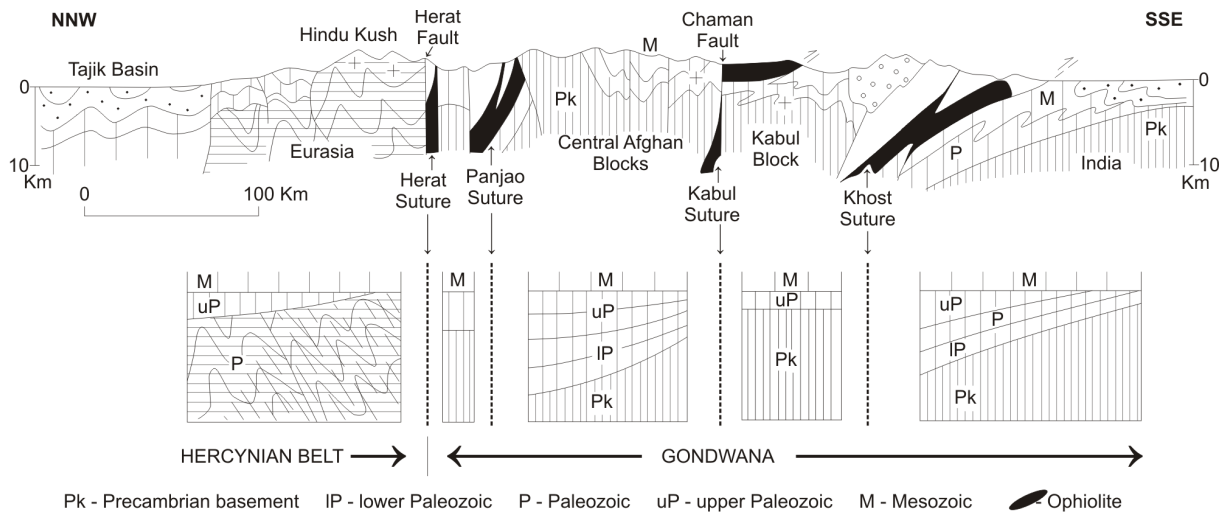
Figure 5: Simplified cross section through Eastern Afghanistan after Tapponnier et al. (1981).

These central blocks are separated from the Eurasian margin by a major suture zone (the Herat Panjshir Suture Zone) that bisects Afghanistan from the north-eastern corner to the border with Iran in the west. Although only very limited ophiolitic material is preserved within the Herat-Panjshir Suture Zone, biogeographical and structural considerations indicate significant paleogeographic separation (Tapponnier et al. 1981). Stöcklin (1977) pointed out that the continental basement rocks of the terranes south of the Herat Panjshir Suture Zone (HPSZ) lack Paleozoic deformation, which is pervasive north of the HPSZ. Moreover a transition in Permian stratigraphy and fusulinid assemblages either side of the HPSZ clearly indicates a Gondwanan origin for those terranes south of the suture (Leven, 1997). The rocks belonging to the Eurasian margin are carbonate-facies and fusulinid bearing indicating a tropical shelf environment, in contrast those south of the suture zone are siliciclastic and fusulinid absent, containing cold-water bryozoans, brachiopods, and bivalves typical of Perigondwanan seas. Furthermore, within the HPSZ Leven (1997) also identified several small tectonic fragments and proposed significant lateral displacement based on the Permian fusulinida assemblages.

Prior to the onset of rifting in the early Mesozoic the terranes south of the HPSZ were situated on the margins of the Gondwanan supercontinent, separated from Eurasia by the Paleotethys Ocean (Şengör, 1988; Treloar and Izatt, 1993). Northwards subduction of the Paleotethys Ocean beneath the Eurasian continent is evidenced by the presence of Triassic calc-alkaline intrusions in the Hindu Kush, north of the HPSZ (Desio, 1965; Debon, 1978). Ophiolitic material in the Panjao Suture zone (between the Farah and Helmand Blocks), along the Chaman Fault (between the Helmand and Kabul Blocks), and the Khost Suture Zone (Between the Kabul Block / Katawaz Basin and the Indian Plate) is thought to indicate a multiple subduction setting (Tapponnier et al. 1981). Collision between Eurasia and the Afghan Central Blocks is therefore considered to have been a poly-phase process involving multiple collisions during the Cimmerian Orogeny (Fig. 6).

Tapponnier et al. (1981) place the first collision, between the Farah Block and the Southern Eurasian margin, in the early Jurassic. This collision resulted in tectonic compression in the Hindu Kush. Subsequent suturing of the Helmand Block along the Panjao Suture Zone occurred in the late Jurassic. Intense Upper Jurassic / Lower Cretaceous folding in central Afghanistan as recorded by Wittekindt and Weippert (1973) is probably related to this collision. The timing relations are further supported by the stratigraphy, with Upper Jurassic-Cretaceous sediments deposited on the Farah Block while the Helmand Block is covered by Cretaceous sediments only (Abdullah and Chmyriov, 1977). The timing of the collision of the Nuristan Block is less clear; however, Cretaceous calc-alkaline intrusives are pervasive
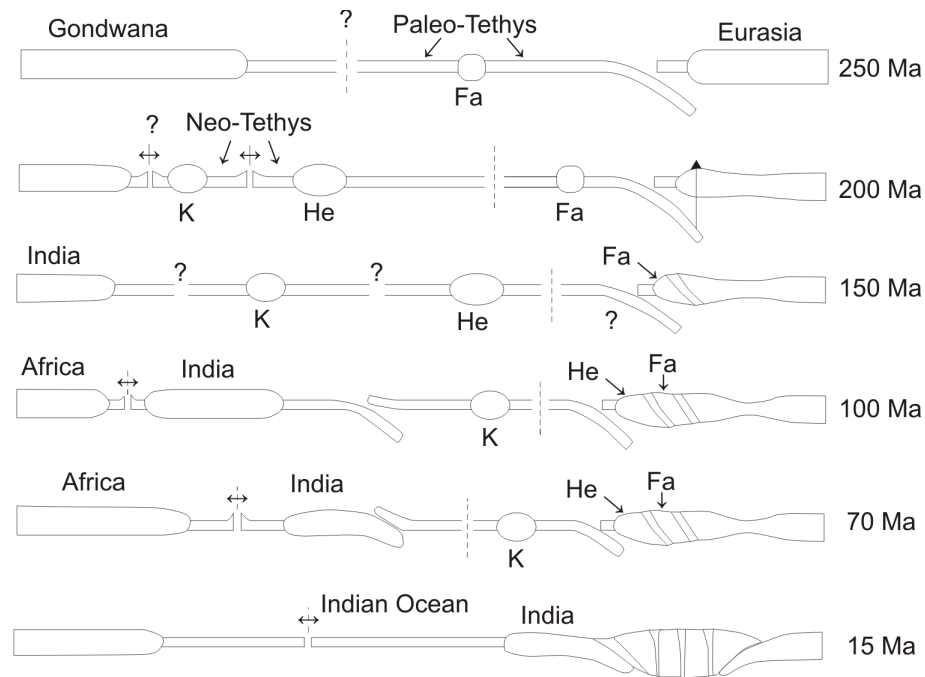
Figure 6: Schematic cross sections showing the closure of Tethys and opening of the Indian Ocean providing a tectonic framework for Afghanistan (Tapponnier et al. 1981). Widths of ocean basins and relative size of continental blocks are not represented to scale. Fa = Farah Block; He = Helmand Block; K = Kabul Block.

through the Farah, Helmand, and Nuristan Blocks (Debon, 1987, Faryad et al. 2013) indicating these terranes were probably contiguous along the Southern Eurasian margin by the early Cretaceous.

In contrast, the Kabul Block lacks either Cretaceous sediments or intrusives (Abdullah and Chmyriov, 1977) and its relations to the other Afghan Central Blocks are the subject of debate. In the proposed models of Tapponnier et al. (1981) the Kabul Block is treated as an exotic terrane, separate from either the Indian Plate or the other Central Afghan Blocks. Suturing of the Kabul Block to the Eurasian continent is proposed in the late Cretaceous / early Paleocene and between the Kabul Block and India in the Eocene (Molnar and Tapponnier, 1975; Tapponnier et al. 1981). Treloar and Izatt (1993) took this idea even further suggesting that the Kabul Block could represent a fragment of the Indian Plate displaced by strike-slip motions during the Himalayan Orogeny. In contrast to this, Şengör (1984) considers the Kabul Block to have affinity to the Helmand Block. The presence of ophiolitic material along the Chaman Fault (between the Kabul and Helmand Blocks) is suggested to have been dragged along as the Kabul Block itself was forced into present location by the northward movement of India, during and following its collision with Asia. Either way, the Kabul Block must have been contiguous with the Helmand and Nuristan Blocks by the Eocene owing to the presence of a granitoid intrusion belt across all three blocks (Debon, 1987).

Timing of the collision between India and Eurasia in the Afghanistan portion of the collision zone is usually considered to have occurred around 55 Ma (Klootwijk et al. 1991; Beck et al. 1996). Tapponnier and Molnar (1975) estimated that subsequent to collision India continued to penetrate up to 2000 km into the Eurasian continent at a rate of around 4-5 cm a year. This continental shortening was partly compensated for by crustal thickening but within Afghanistan it was primarily absorbed by horizontal movements along strike-slip faults and the westward squeezing of the Afghan Central Blocks (Tapponnier et al. 1981). The lateral extrusion was interpreted as being controlled by the reactivation of the pre-existing faults and sutures; the Herat-Panjshir Suture Zone, Panjao Suture, and Chaman Fault (Searle, 1991). Treloar and Izatt (1993) challenge this interpretation, based on deformation and structural char-

acteristics they suggest collision between India and the Afghan segment of the Eurasian margin didn't occur until as late as the Pliocene. Although lateral movement along the Herat-Panjshir Suture Zone is recorded in the Oligo-Miocene there is little evidence for movement subsequent to that. Instead crustal shortening associated with the indentation of India was accommodated by inversion of the Katawaz basin.

4   Stratigraphy of the Kabul Block

As previously discussed the Kabul Block is often classified as part of the Afghan Central Blocks, but its relations with the surrounding terranes are somewhat unclear. The Block has an elongate ovoid shape, up to 200 km in length and approximately 70 km wide. It is completely fault bounded, the Chaman Fault in the west separates the Kabul Block from the Helmand and extends south past the Afghanistan-Pakistan border. Along its north eastern margin the Kabul Block is separated from the Nuristan Block by the Altimoor Fault (Treloar and Izatt, 1993). A complex array of faults known as the Ghazni Fault connects the Chaman and Altimoor faults in the south east and delineates the boundary with the Katawaz Basin. The far northern tip of the Block also comes into contact with the Herat-Panjshir Suture Zone, the major Eurasian – Afghanistan suture. Each of the fault systems, with the possible exception of the Herat-Panjshir Suture Zone, record evidence for Quaternary activity (Ruleman et al. 2007).

The Kabul Block itself is composed of a highly deformed crystalline basement overlain by various Paleozoic to Jurassic sediments (Fischer, 1971; Abdullah and Chmyriov, 1977). Peridotite nappes, underlain by a schistose melange are thrust onto the eastern and western margins of the Block (Mennessier, 1976; Tapponnier et al. 1981). Eocene-Oligocene granitoid intrudes the south of the Block (Abdullah and Chmyriov, 1977; Debon, 1987) and much of the surface geology is covered by unconsolidated Cenozoic sediments (Bohannon, 2010) (Fig. 7).

Precambrian basement

Within the basement rocks either two (Bohannon, 2010), three (Abdullah and Chmyriov, 1977), or four (Karapetov et al. 1981) distinct formations are described. In decreasing age these are the Khair Khana, Sherdarwaza, Kharog, and Welayati Formations.

Khair Khana Formation

The Khair Khana Formation, as described by Karatepetov et al. (1981) consists of granulite facies xenoliths of possible Archean age that occur within the Sherdarwaza Formation in the Khair Khana hills north-west of Kabul. The rocks are defined by the occurrence of ortho- and/or clinopyroxene in orthogneiss. The Khair Khana Formation is also notable for the lack of marble and calc-silicates (Karapetov et al. 1981). Abdullah and Chmyriov (1977) do not mention such lithologies or formations, while Bohanon (2010) considers the Khair Khana Formation indistinct from the Sherdarwaza.

Sherdarwaza Formation

The Sherdarwaza Formation consists of various migmatites, gneiss, schist, marble, amphibolite, and quartzite (Abdullah and Chmyriov, 1977). The Sherdarwaza is mostly exposed in the hills that surround

Key:

- Holocene conglomerate and sandstone
- Holocene fan alluvium and colluvium
- Pleistocene conglomerate and sandstone
- Pliocene conglomerate and sandstone
- Miocene conglomerate and sandstone
- Eocene clay and shale
- Paleocene conglomerate and sandstone
- Late Cretaceous sandstone and siltstone
- Late Triassic siltstone and sandstone
- Late Triassic volcano-sedimentary melange (Kotagai series)
- Late-Middle Triassic sandstone and siltstone
- Early-Middle Triassic limestone and dolomite
- Late Permian limestone and dolomite
- Early Permian-Carboniferous sandstone and siltstone
- Early Carboniferous volcano-sedimentary series
- Late Devonian sandstone and siltstone
- Early-Middle Devonian limestone and dolomite
- Late Silurian-Devonian limestone and dolomite
- Silurian sandstone and siltstone
- Ordovician sandstone and siltstone
- Vendian-Cambrian marble and quartzite
- Mesoproterozoic metamorphic rocks
- Proterozoic gneiss and granite
- Paleoproterozoic gneiss, marble, quartzite

- Oligocene granite
- Eocene ultra-mafics
- Early Cretaceous gabbro and monzonite
- Triassic granite
- Early Carboniferous ultra-mafics

- Faults

N

50 Km

Figure 7: Geological map of the Kabul Block and surrounding regions after Kafarsky et al. (1975); adapted from the digitised versions of Bohannon and Turner (2005), Lindsay et al. (2005), and Maldonado and Turner (2005).

Kabul city, in the Koh-i-Sofe Mountains to the east of the city, and in a small area in the south of the Block. The gneiss and migmatite are more common from the northern localities while schist is more abundant in the south (Bohannon, 2010). The gneiss is the most abundant lithology it is typically biotite, garnet-biotite or quartz-muscovite variety depending on its constituent minerals (Abdullah and Chmyriov, 1977). Textures also vary between lepidoblastic, granoblastic and porphyroblastic varieties that range in scale from being micro-laminated to coarsely banded (Bohannon, 2010). Quartz, K-feldspar and plagioclase typically constitute up to 85 % of the gneiss (Abdullah and Chmyriov, 1977; Bohannon, 2010). Areas described as migmatite contain rapidly alternating dark, biotite-rich, and light, quartz-feldspathic rich layers (Abdullah and Chmyriov, 1977). The migmatite is usually K-Feldspar-rich and garnet absent (Collett, 2011). Schist is usually biotite rich, although epidote-biotite-muscovite, muscovite, staurolite-garnet-muscovite, and other varieties are also reported (Abdullah and Chmyriov, 1977; Bohannon, 2010). The marble occurs as single beds or lenses within the schist, gneiss, and migmatite; it has a light-grey to white colour and includes bands of silicate minerals (Abdullah and Chmyriov, 1977). Amphibolite is present throughout the Sherdarwaza Formation, developing as thin beds or lenses consisting predominantly of hornblende and plagioclase; variable amounts of biotite, quartz and epidote are also present (Abdullah and Chmyriov, 1977). Texturally the amphibolite is typically nematoblastic with a schistose structure.

Kharog Formation

The Kharog Formation overlies the Sherdarwaza Formation with an apparent disconformity but with no pronounced angular unconformity (Abdullah and Chmyriov, 1977). It is defined based on stragraphical relations in the Kharog Mountains, south of Kabul. It consists of a basal conglomerate interbedded with quartzite, with crystalline schist, gneiss, amphibolite and marble at the top. The extent and distribution of the Kharog Formation is unclear. Karapetov et al. (1981) mapped areas to the south and west of Kabul as belonging to the Kharog Formation that on other geological maps (Kafarsky, 1975; Bohannon, 2010) is considered part of either the Sherdarwaza or Welayati Formations. Karapetov et al. (1981) considered the Kharog Formation to be older than the Sherdarwaza; however, given the petrography and structural relations of the Kharog Formation it is not clear how they came to that conclusion. Bohannon (2010) only maps a small area of Kharog rocks in the Aynak district south east of Kabul, and speculates that it may be undifferentiated from the Welayati Formation.

Welayati Formation

The Welayati Formation is described as resting conformably on the Kharog Formation and is comprised of crystalline schist at the base, amphibolite in the middle and alternating crystalline schist and amphibolite at the top (Abdullah and Chmyriov, 1977). The Welayati Formation crops-out extensively in the area to the south of Kabul City, as well as in the Koh-i-Sofe Mountains, north west of Kabul, and along the Altimoor Fault Zone. The crystalline schists are represented by biotite, staurolite-garnet-biotite, biotite-quartz, muscovite-quartz, and muscovite varieties (Abdullah and Chmyriov, 1977) texturally these rocks are lepidoblastic to porphyroblastic and show a high degree of folding and deformation. The amphibolite is nematoblastic and is composed predominantly of hornblende and plagioclase with minor epidote, biotite and rare garnet. One body of amphibolite occurring in the Chehel Sotoon area, south of Kabul, is identified as separate from the Welayati Formation in the map of Karapetov et al. (1981). Based on its textural relations Abdullah and Chmyriov (1977) identified this amphibolite as of volcanic origin.

Vendian - Cambrian meta-sediments

In the area surrounding the Aynak copper deposit the Welayati Formation is unconformably overlain by the Vendian to Cambrian age Loy Khwar and Gulkhamid Formations (Abdullah and Chmyriov, 1977; Bohannon, 2010). The Loy Khwar Formation is a meta-sedimentary sequence that plays host to the copper mineralisation. It is lithologically varied, composed of dolomitic marble, carbonaceous quartz-schist, quartz-biotite-dolomite-schist, and quartzite (Bohannon, 2010). The rocks have been metamorphosed to the upper greenschist - lower amphibolite facies and are therefore of lower grade than the underlying basement rocks. The rocks are assigned a Vendian to Cambrian age based on stromatolite remnants and the occurrence of the algae Tannuofia (Mennesier, 1968; Abdullah and Chmyriov, 1977). The Gulkhamid Formation is a sequence of metamorphosed intermediate volcanic rocks, it consists of conglomerate, meta-sandstone and schistose tuff at the base and tuffs, breccias and tuffaceous sandstones of andesitic to dacitic composition at the top (BGS, 2005; Bohannon, 2010). Abdullah and Chmyriov, (1977) do not describe these rocks, in part because they were considered part of the Welayati Formation. However, the BGS (2005) pointed out they overlie the Loy Khwar Formation and therefore cannot be Welayati (Bohannon, 2010).

Carboniferous - Permian volcano-sedimentary sequence

Carboniferous to Lower Permian age rocks crop-out in the south of the Kabul Block. These consist of low grade phyllite and slate enclosing interbeds and lenses of limestone, dolomite, sandstone, conglomerate, and minor volcanics (Abdullah and Chmyriov, 1977). The volcanics which are primarily basaltic occur within the lower part of the series only. The assigned age of the rocks is based on rare organic material including fusulinids, brachiopods, and crinoids, which are primarily preserved in the upper part of the series.

Khengil Series (Permian - Jurassic)

The Khengil Series is a sequence of Permian to Jurassic age carbonate rocks that occur predominantly along the eastern margin of the Kabul Block and rests unconformably above the Precambrian basement (Fischer, 1971; Bohannon, 2010). Fischer (1971) identified seven distinct units within the Khengil Series these consist of a basal conglomerate of Guadalupian age (1), late Permian reef limestone (2), Lower Triassic ceratiten-bearing limestone (3), Middle to Upper Triassic limestone, dolomite, and tuff (4), Jurassic ammonite-bearing limestone (5), Jurassic belemnite-bearing limestone (6), and undifferentiated limestones of mostly Jurassic age (7).

Kotagai Melange (Undetermined - Eocene (?))

The Kotagai Melange is a volcano-sedimentary sequence which unconformably overlies the Khengil Series (Abdullah and Chmyriov, 1977). The rocks are strongly deformed with a modest overprint of thermal metamorphism (Bohannon, 2010). At least nine different units are identified within the Kotagai Melange including various limestones, meta-sandstone, shale, basaltic schist, andesite, and serpentinized basalt (Bohannon, 2010). The age range of the melange is unclear owing to a lack of fossils and no radiometric dating has been carried out. Abdullah and Chmyriov (1977) suggest a Cretaceous to Eocene age, while Mennessier (1976) inferred that some parts of the melange may be as old as the late Paleozoic. As the rocks are pervasively deformed and metamorphosed they have clearly been transported to

their present position overlying the largely undeformed Khengil Series. Furthermore, Bohannon (2010) observed Sherdarwaza gneiss overlying the Kotagai Melange in the southern Koh-i-Sofe.

Cover sequences (Neogene - Holocene)

Neogene fine grained sediments and conglomerate, known as the Lataband Series occur extensively throughout the Kabul Block infilling the intermontane basins (Bohannon, 2010). In addition unconsolidated Pleistocene and Holocene alluvial deposits are widespread in the flood plains of the Kabul and Panjshir rivers.

Igenous complexes

Ultramafic nappes

Ultramafic complexes are mapped as klippen along both the eastern and western margins of the Kabul Block (Kafarsky et al. 1975; Tapponier et al. 1981). These rocks are thrust atop the Kotagai Melange in the east and the Carboniferous-Permian meta-sediments in the west (Bohannon, 2010). The ultramafic complexes are predominantly peridotite with minor dunite, harzburgite, and serpentinite (Benham et al. 2009). The upper part of the complexes is composed of layers of ultramfic and mafic material with the uppermost sections consisting of layered gabbro. Chromitites in the Logar Complex, south west of Kabul, are rich in platinum group elements and interpreted to be produced from a boninitc magma in a supra-subduction setting (Benham et al. 2009).

Granitoid intrusives (Eocene - Oligocene)

A granitoid body of Eocene-Oligocene age is mapped in the south of the Kabul Block. The granitoid intrudes the Precambrian basement and Carboniferous-Permian meta-sediments (Abdullah and Chmyriov, 1977). Texturally the rock is porphyritic with an idiomorphic granular groundmass. Phenocrysts are commonly plagioclase and microcline and the groundmass is composed of approximately equal amounts of plagioclase, K-feldspar and quartz with minor biotite and muscovite (Abdullah and Chmyriov, 1977).

5   Structure of the Kabul Block

The Precambrian basement rocks are strongly deformed with intense folding. In the centre of the Block most of the folding strikes in an easterly direction, while at the margins the structures trend in parallel with the fault boundaries. As such the Kabul Block is considered to form an east-west trending dome-like structure (Andritzky, 1967; Abdullah and Chmyriov, 1977; Karapetov et al. 1981). The degree and timing of metamorphism within the Precambrian basement is poorly constrained. U/Pb zircon age dating has previously indicated a Paleoproterozoic age for the basement rocks (Faryad, 2009; Bohannon, 2010; Collett, 2011) while K/Ar and Ar/Ar dating of micas gave Neoproterozoic ages (Andritzky, 1971; Faryad, 2009). Although the rocks are known to have reached granulite-facies conditions (Karapetov et al. 1981) and extensive migmatization indicates significant degrees of partial melting, the only constraints on the P-T conditions were recorded by (Russians) as 650-800 °C and 4-9 kbar.

The overlying Carboniferous-Lower Permian sediments and, Permian-Jurassic Khengil Series only records gentle simple brachyform folding. The fold axes trend parallel to the boundaries of the Block further emphasizing the dome-like structure (Abdullah and Chmyriov, 1977).

The Kotagai melange has strong penetrative deformation and folding and was emplaced by large thrust faults (Fischer, 1971). Unlike the largely unmetamorphosed sediments of the Khengil Series the melange was metamorphosed in intermediate pressure conditions recorded by garne-bioitite-chloritoid schists (Tapponnier et al. 1981). Mennessier (1976) suggested that significant transport to the north west was needed in order to explain the melange's present position. Bohannon (2010) goes further, having observed melange above the Sherdarwaza gneiss in the northern Koh-i-Sofe Mountains and below the Sherdarwaza in the southern Koh-i-Sofe, he interprets the Kabul Block as consisting of two contrasting environments. The Paleozoic-Jurassic sediments underlain by highly deformed crystalline basement representing one environment and the schistose melange and overlying ultramafic rocks the other. These two contrasting environments were tectonically juxtaposed by a complex low-angle fault system that Bohannon (2010) termed the Kotagai Roof Fault and Kotagai Overthrust. Bohannon (2010) envisioned the Kabul Block to therefore represent a backstop within a subduction system. The melange is interpreted to continue at depth below the Precambrian basement, while some fragments were thrust onto the Kabul Block along the Kotagai Overthrust (Fig. 8).
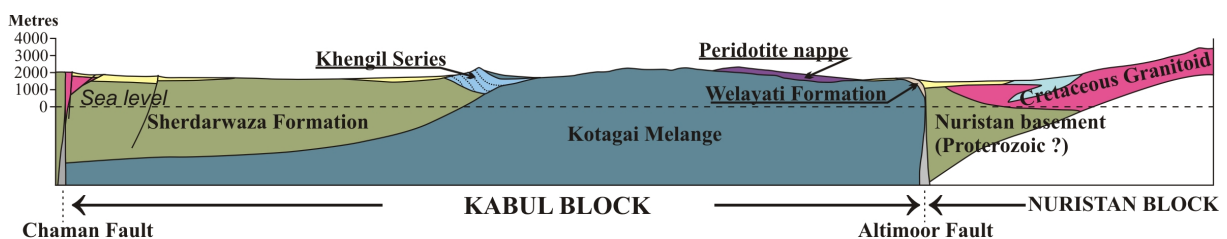
Figure 8: ESE-WNW interpretative cross section through the Kabul Block after Bohannon (2010). The Kotagai Melange is considered to continue at depth beneath the Precambrian basement based on observed relations in the Koh-i-Sofe Mountains.

Tapponnier et al (1981) interpreted the ultramafic rocks thrust onto the Kabul Block as part of the Kabul-Altimur ophiolite complex. They suggested the ophiolite complex was emplaced from northwest to south east before the Paleocene and represents the suture between the Kabul Block and the Central Afghan Blocks. The model of Bohannon (2010) challenges this, suggesting the ultramafic rocks are fragments of sub-crustal lithosphere peeled off the roof of the subduction system and emplaced from the opposite direction. The interpretation of Tapponnier et al. (1981) conforms to the Kabul Block having an isolated or Indian affinity while the model of Bohannon (2010) would support a closer relationship with the Afghan Central Blocks as suggested by Şengör (1984).

6   Objective

There are significant gaps in our understanding of the Kabul Block and its various units. Much of the available literature for the area is either incomplete or outdated. The fact that Bohannon (2010) with only very limited field studies was able to identify stratigraphic relationships that were previously unreported and challenge the prior interpretations highlights this knowledge gap. The primary objective of this project is therefore to resolve some of these outstanding issues regarding the geology and structure of the Kabul Block. Unfortunately, the situation within the country remains precarious and this limits the potential scope of the project, especially in regards to the structure relations beyond the city of Kabul.

However, the Precambrian basement crops-out extensively in the vicinity of Kabul and large areas of this can be accessed in relative safety. These exposures include the granulite-facies assemblages of the Khair Khana Formation described by Karapetov et al. (1981), various well preserved gneiss, schist and migmatite belonging to the Sherdarwaza Formation, and an area of Welayati and/or Kharog Formation in the south of the City. In addition some fieldwork was possible from roadside cuttings in the passes of the Hindu Kush Mountains north from Kabul. These rocks are sampled from areas beyond the northern margins of the Kabul Block and can provide insights into the history of orogenesis for the southern Eurasian margin.

The samples that comprise this study have been collected from multiple localities over the course of several field seasons and cover a wide variety of different lithologies (Figs. 9 & 10; Appendix A). A classical petrological study of these samples incorporating petrographical, geochemical, thermobarometric, and geochronological analyses has been undertaken in order to resolve the evolution of the Kabul Block. The objectives for this project can therefore be broken down into several different tasks as follows:

- Distinguishing the metamorphic character of the basement rocks of the Kabul Block, through the identification of reaction textures and microstructural trends.

- Quantification of the pressure-temperature (P-T) conditions recorded within the rocks and constraining of a possible P-T path.

- Deciphering relative absolute time scales and residence times for both the protolith emplacement and metamorphism.

- Through comparative study with similar Precambrian terranes resolving the historical origins of the Kabul Block and its place within global-scale orogens.

- Identification of the role of the Kabul Block during the convergence and eventual collision between the Eurasian and Indian continents.
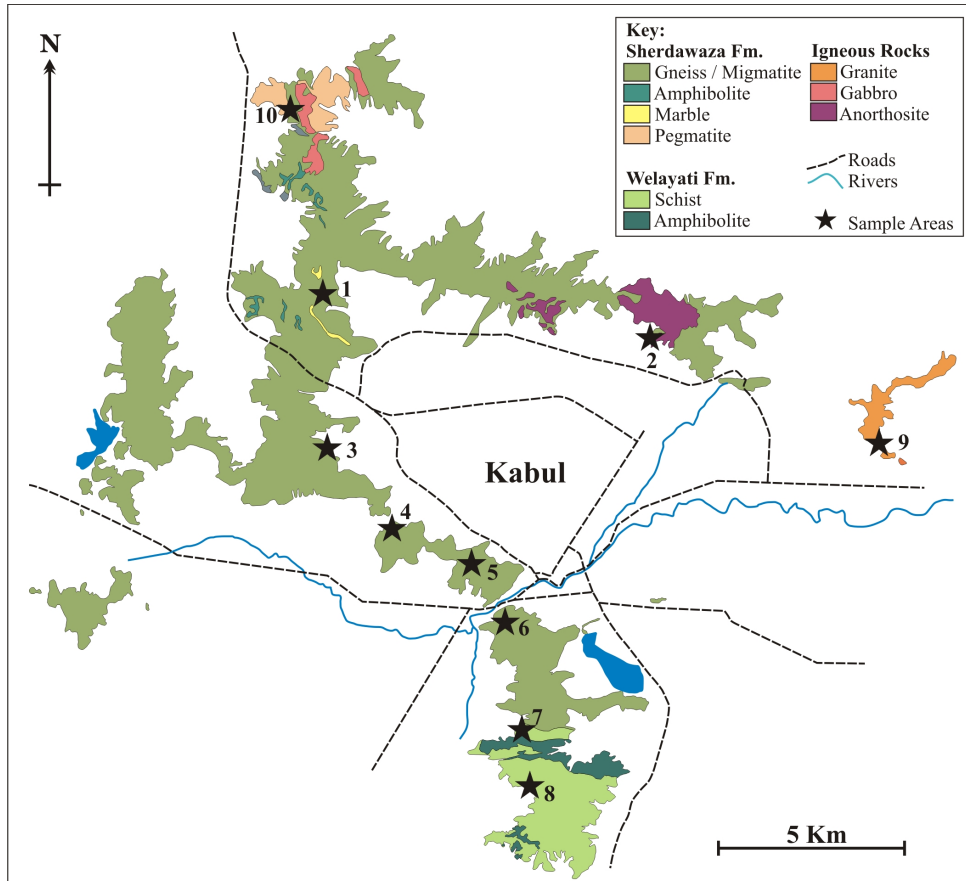
Figure 9: Geological map of the area around Kabul City after Bohannon (2010). Sample areas are identified by black stars and numbers which correspond to the locality number in the Appendix (A).
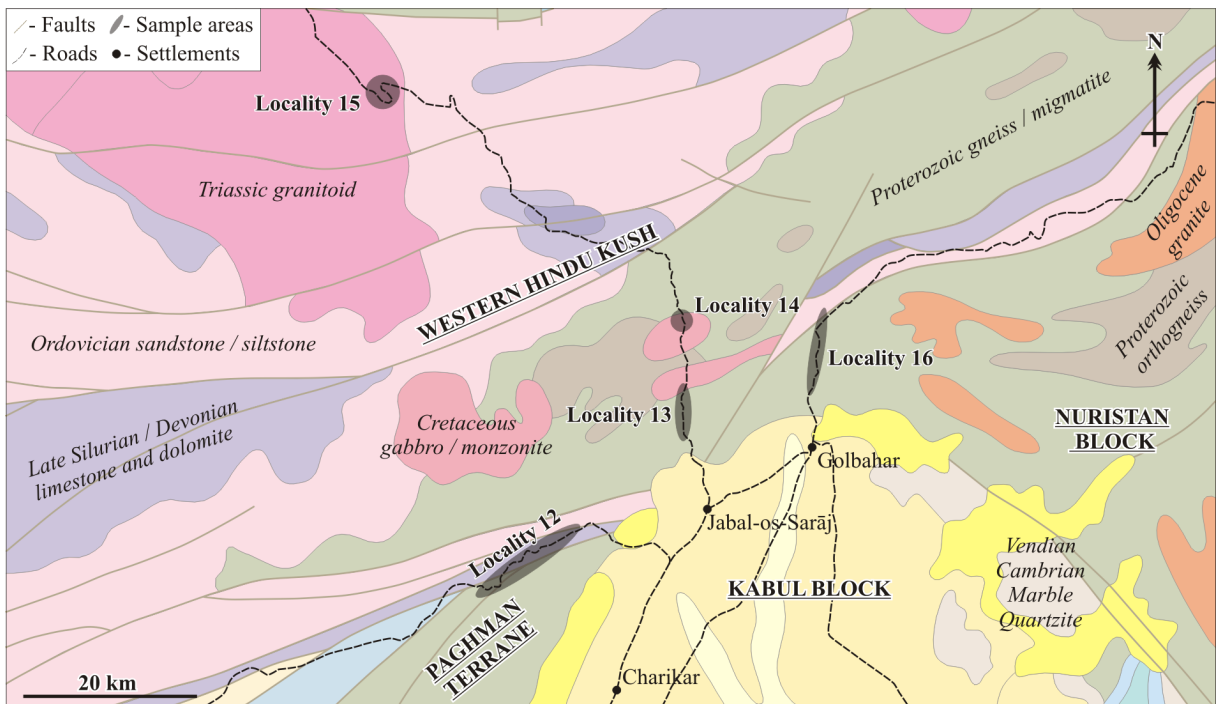
Figure 10: Geological map of the sampling locations in the Hindu Kush after Kafarsky et al. (1975). Unit colours correspond to key in Fig. 7.

Part II

Polymetamorphic evolution of the granulite-facies Paleoproterozoic basement of the Kabul Block, Afghanistan

Stephen Collett[1*], Shah Wali Faryad[1] & Amir Mohammad Mosazai[2]

[1]Institute of Petrology and Structural Geology, Charles University, Prague, Albertov 6, 12843 Prague 2, Czech Republic

[2]Department of Geology and Mines, Kabul Polytechnic University, Kabul, Afghanistan

[*]Corresponding author e-mail: colletts@natur.cuni.cz

Abstract

The Kabul Block is an elongate crustal fragment which cuts across the Afghan Central Blocks, adjoining the Indian and Eurasian continents. Bounded by major strike slip faults and ophiolitic material thrust onto either side, the block contains a strongly metamorphosed basement consisting of some of the only quantifiably Proterozoic rocks south of the Herat-Panjshir Suture Zone. The basement rocks crop-out extensively in the vicinity of Kabul City and consist predominantly of migmatites, gneisses, schists and small amounts of higher-grade granulite-facies rocks. Granulite-facies assemblages were identified in felsic and mafic siliceous rocks as well as impure carbonates. Granulite-facies conditions are recorded by the presence of orthopyroxene overgrowing biotite in felsic rocks; by orthopyroxene overgrowing amphibole in mafic rocks and by the presence of olivine and clinohumite in the marbles. The granulite-facies assemblages are overprinted by a younger amphibolite-facies event that is characterized by the growth of garnet at the expense of the granulite-facies phases. Pressure-temperature (P-T) conditions for the granulite-facies event of around 850 °C and up to 7 kbar were calculated through conventional thermobarometry and phase equilibria modeling. The younger, amphibolite-facies event shows moderately higher pressures of up to 8.5 kbar at around 600 °C. This metamorphism likely corresponds to the dominant metamorphic event within the basement of the Kabul Block. The results of this work are combined with the lithostratigraphic relations and recent geochronological dating to analyze envisaged Paleoproterozoic and Neoproterozoic metamorphic events in the Kabul Block.

1   Introduction

Afghanistan is composed of a complex collage of mostly Gondwanan derived terranes which were accreted onto the southern margin of Eurasia prior to, and during, the India Eurasia collision (Şengör 1984; Boulin1991). The terranes are incorporated into three distinct tectonic zones (Fig. 1), the north consists of the Afghan - Tajik Platform, stable blocks that have been part of the Eurasian continent since the Paleozoic (Brookfield and Hashmat 2001). In the south-east the Katawaz basin, a large flexural basin (Treloar and Izatt 1993), represents the northern extension of the Makran accretionary complex and the north-western continental margin of the Indian plate. In between these are the Afghan Central Blocks, a series of NE-SW aligned tectonic blocks that collided with Eurasia throughout the Mesozoic and into the early Cenozoic. Geotectonic and/or paleogeographic interpretation of the area is mostly based on Cenozoic-Mesozoic sedimentary cover sequences and Alpine tectonics (e.g. Boulin 1991; Treloar and

Izatt 1993; Faryad et al. 2013) and there is scarce information regarding the basement rocks and their metamorphic history. The Afghan Central Blocks include three blocks, the Kabul, Helmand, and Farah (Fig. 1); however, the relations of the Kabul Block to the other Afghan Central Blocks are the subject of controversy. According to Tapponnier et al. (1981) and Treloar and Izatt (1993) the Kabul Block represents a detached crustal fragment of the Indian continent which became accreted to the Afghan Central Blocks in the Paleocene. Contrary to this view, Andritzky (1967) and Abdullah and Chmyriov (1977) consider the Kabul Block as part of the Afghan Central Blocks. While Proterozoic, and even Archean, rocks are known north of the Herat-Panjshir suture, in the Western Hindu Kush (e.g. Wallbrecher 1974; Schreyer and Abraham 1975; Faryad 1999, 2002), there are only limited Precambrian basement exposures within the Afghan Central Blocks (Kafarsky et al. 1975).
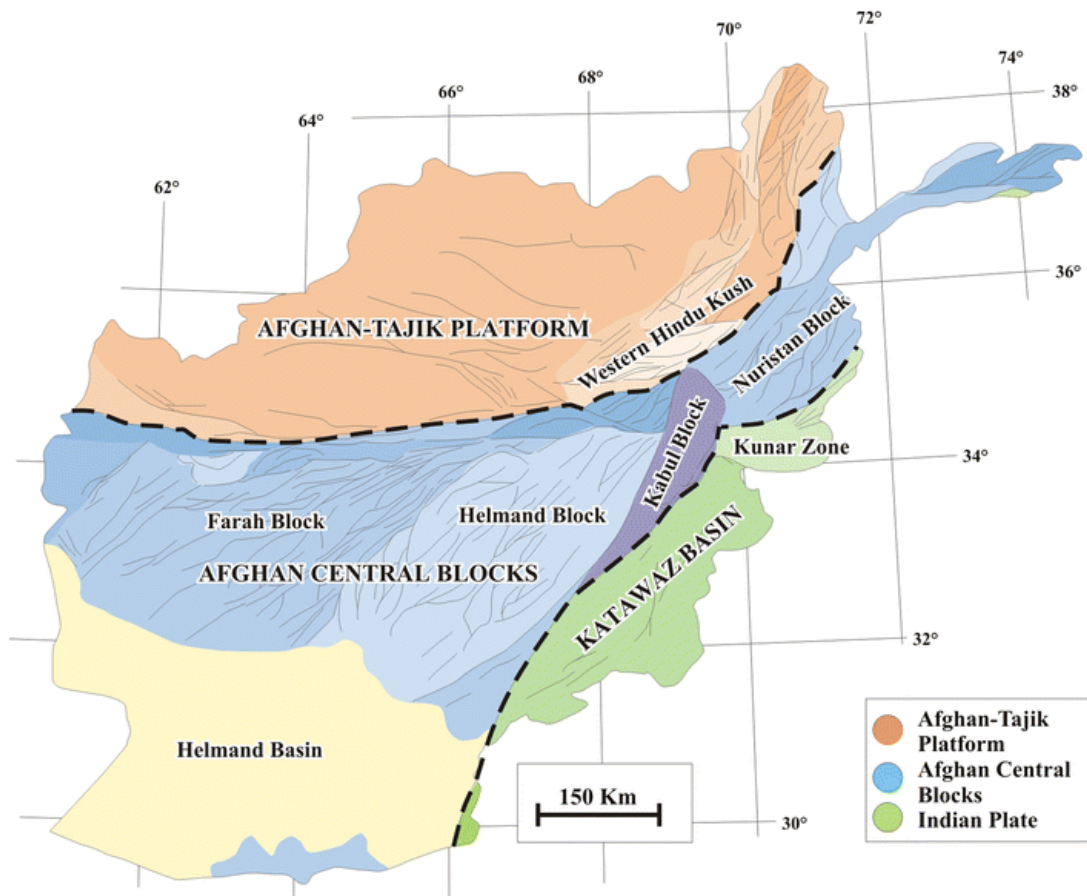
Figure 1: Tectonic outline of Afghanistan according to Boulin (1991), Leven (1997) and Bohannon (2010). The country can be divided into three tectonic zones: the Eurasian zone contains the Afghan-Tajik Platform and the Western Hindu Kush. In the South East the Katawaz basin represents the furthest extent of the Indian Plate. The Afghan Central Blocks, Kabul Block, and Nuristan Block indicate the Eurasian-India boundary

The Kabul basement rocks are typically subdivided into three formations (the Sherdarwaza, Kharog, and Welayati), that are assumed to differ in age and metamorphic character (Abdullah and Chmyriov 1977). Karapetov et al. (1981) distinguished one more formation with granulite facies metamorphism, the Khair Khana Formation, and suggested it to be of Archean age. The high-grade basement rocks exposed around Kabul are migmatite and show strong deformation and recrystallization to low-grade assemblages. A polymetamorphic history of the Kabul basement rocks was recently considered by a combination of geochronological data, including: U-Pb SHRIMP on zircon, Ar-Ar on micas, and U-Th on monazite (Faryad et al. 2015). An Archean age (~2700 Ma) for the basement rocks from the Sherdarwaza Formation was confirmed by UPb data on zircon from orthogneiss. Most of the data recorded early

Paleoproterozoic ages between 2200–2500 Ma (Faryad et al. 2009; Bohannon2010; Faryad et al. 2015). The younger ages are partly affected by Paleoproterozoic metamorphism (1800–1900 Ma) that was confirmed by U-Pb data on zircon rims with inherited core ages, and U-Th on monazite inclusions in garnet. A Neoproterozoic age of metamorphism (900 – 820 Ma) was obtained by Ar-Ar and U-Th data both from the Sherdarwaza and overlying Welayati formations (Faryad et al. 2015).Similarageswererecordedby K-Ar dating (Andritzky 1971) of micas, which yielded Neoproterozoic metamorphic cooling ages of between 920 and 670 Ma.

This paper focuses on mineral textures and extent of highgrade rocks from the Sherdarwaza Formation that are exposed beneath the other basement rocks of Kabul Block. By investigation of mineral assemblages and their textural relations, it is aimed to analyze their polymetamorphic history as assumed by the geological relations of the different lithologies and age dating. As most of the basement rocks show strong deformation and reequilibration, the granulites, as the most competent rocks with well-preserved granulite-facies mineral assemblages and with various growth textures were investigated. P-T (pressure-temperature) conditions for different metamorphic events are constrained by conventional geothermobarometry and pseudosection modeling.

2   Regional geology

The Kabul Block is an approximately 200 km long and up to 50 km wide tectonic block bounded by major strike slip faults (Fig. 2). The Chaman Fault (locally the Paghman Fault) defines the western margin and separates the Kabul Block from the other Afghan Central Blocks. The Altimoor Fault separates the Kabul Block along its eastern margin from the Nuristan Block in the north-east; whereas, the Ghazni fault zone defines its boundary with the Katawaz Basin in the south-east. The northernmost tip of the Kabul Block reaches the Western Hindu Kush and the Herat-Panjshir Suture Zone, the major Eurasia – Afghan Central Blocks suture.

The basement rocks are mostly exposed within the core of the Kabul Block (Fig. 2), thought to represent an east–west trending dome-structure (Andritzky 1967; Karapetov et al. 1981). They are overlain by un-metamorphosed to low-grade Late Paleozoic to Cenozoic volcano-sedimentary sequences (Fesefeld 1964; Andritzky 1967; Fischer1971; Abdullah and Chmyriov 1977). Late Paleozoic (Carboniferous-Permian) sequences overlie the basement units in the southern part of the block. They are represented by low-grade phyllites, shales, marbles and meta-conglomerates. The Khengil Series, an upper Permian-Triassic cover sequence, consists of a basal conglomerate overlain by limestones and minor tuffs (Fischer 1971). Large peridotite sheets underlain by a Jurassic volcano-sedimentary sequence exhibiting a moderate thermal overprint (Kotagai Mélange, Fig. 2b) are thrust onto both the western and eastern margin of the block (Mennessier 1976; Abdullah and Chmyriov 1977). In the east, the ultra-mafic thrust sheet is described as belonging to the Khost ophiolite complex (Tapponnier et al. 1981). The ultra-mafic rocks in the south and west of the block occur as klippen, thrust atop the un-metamorphosed sedimentary cover. Tapponnier et al. (1981) interpreted these ultramafic rocks as distinct from those in the north-east, referring to them as the Kabul ophiolite complex. The south of the Kabul Block is intruded by a series of granitic rocks of Eocene-Oligocene age that continues through the Afghan Central Blocks and eastwards to the Nuristan Block. They are related to continental collision subsequent to oceanic subduction between the Indian and Eurasian plates (Debon et al. 1987). Much of the block is covered by a thick layer of unconsolidated Cenozoic sediments (Abdullah and Chmyriov 1977).

The basement rocks are represented by thick Proterozoic metamorphosed volcano-sedimentary sequences that have been sub-divided into three distinct formations (e.g. Abdullah and Chmyriov 1977). In terms
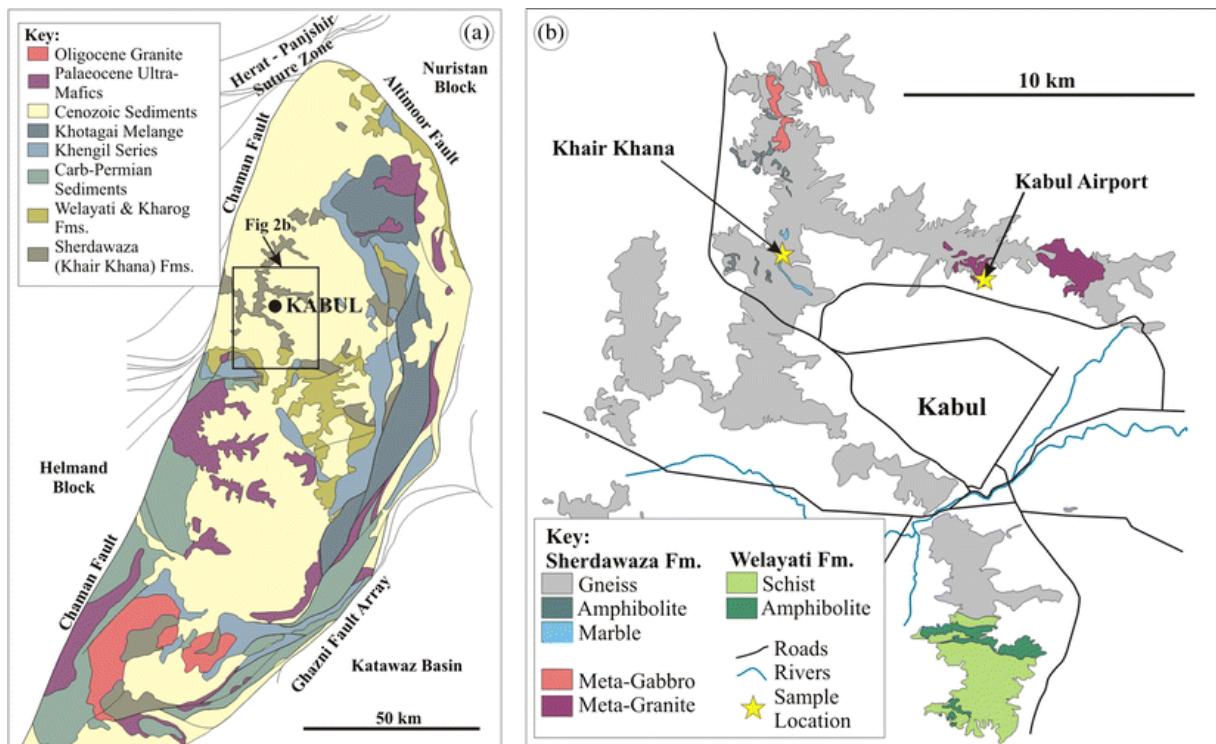
Figure 2: Geology of the Kabul Block and the study area. (a) Schematic geological map of the Kabul Block after Kafarsky et al. (1975). (b) Geology of the Kabul City area after Karapetov et al. (1981) and Bohannon (2010). The samples for this study came from Khair Khana to the north-west of the City and nearby to the Kabul Airport in the north of the city

of decreasing age and metamorphic degree these are the Sherdarwaza, Kharog, and Welayati Formations (Fig. 2, 2b). The Sherdarwaza Formation is represented mostly by migmatites and gneisses with intercalated layers of quartzite, amphibolite and marble. Several meta-igneous bodies of syenitic and dioritic composition are also exposed within the Sherdarwaza Formation (Fig. 2b). Granulite-facies rocks, recognized by the presence of orthopyroxene in quartz-feldspathic lithologies, are exposed within the Sherdarwaza Formation at Khair Khana to the north west of Kabul where they form small outcrops enveloped by quartz-feldspathic gneisses, schists and migmatites. The relations of the granulites and the surrounding rocks are not clear. In most cases the contact is formed by strongly foliated rocks. The granulites from Khair Khana were first described by Slavin et al. (1972) as Proterozoic orthogneisses. However, Karapetov et al. (1981) suggested they may represent xenoliths of an older, possibly Archean, formation.

The extent and distribution of the Kharog Formation is poorly understood. It consists of metaquartzite, crystalline schists, gneisses, amphibolites, and marbles (Abdullah and Chmyriov 1977) and was defined based on stratigraphical relations in the Kharog Mountains, south of Kabul. It overlies the Sherdarwaza Formation with an apparent disconformity (but with no pronounced angular unconformity). The Welayati Formation is assumed to lie conformably above the Kharog Formation and crops-out to the south and north east of Kabul. It consists of garnetiferous amphibolites and a variety of crystalline schists, including: biotite, staurolite-garnet-biotite, muscovite-kyanite-garnet schists, and muscovite quartzites (Abdullah and Chmyriov 1977). Neither the Kharog, nor the Welayati preserve paragenetic evidence for a high-grade granulite-facies metamorphism.

3   Sampling and analytical techniques

Sampling for this study was conducted within the area to the north of Kabul identified by Karapetov et al. (1981) as preserving high-grade granulite-facies assemblages. More than 100 samples were collected for this study include granulites and various types of migmatites and gneisses or their retrogressed – mylonitized products that comprise the Sherdarwaza Formation. The samples of granulite with well-preserved high-grade assemblages, selected for detailed study, come from two localities north of Kabul City. At the Khair Khana locality (Fig. 2b), felsic granulites with orthopyroxene occur as elongate bodies within strongly foliated garnet-absent migmatites, typical of the Sherdarwaza Formation. The felsic granulite includes small (<25 cm diameter) lenses of mafic granulite; while, granulite-facies assemblages are also observed in adjacent calc-silicates and impure marble. The second, Kabul Airport locality (Fig. 2b), is characterized by an outcrop of orthogneiss overlain by the Sherdarwaza migmatite. The orthogneiss is significantly coarser grained than the surrounding rocks and shows weaker foliation. The contact between the gneiss and surrounding migmatite is disturbed by the presence of a younger unmetamorphosed dyke. Representative samples of felsic granulite, mafic granulite, calc-silicate, and orthogneiss were selected to undergo detailed petrographic evaluation. Table 1 shows the minerals present in each of the studied samples.

Table 1: Minerals present in selected samples of granulite facies rocks. All mineral abbreviations after Whitney & Evans (2010).

Sample	Opx	Cpx	Ol	Amp	Bt	Grt	Pl	Kfs	Qtz	Ilm	Ap	Other
Felsic Granulite												
F74/6	x				x	x	x	x	x	x	x	Zrn
af159c	x				x	x	x	x	x	x	x	Zrn
af101	x			o	x	x	x	x	x	x	x	Zrn, Mnz
C30/13	x			o	x	x	x	x	x	x	x	Zrn, Mnz
Mafic Granulite												
F16/9	x			x	x	x	x		x	x		Ep, Mag
Impure Marble												
F72/6		o	x	x	x						x	Cc, Dol,
C8/12		o	x	o	x					o	o	Cc, Dol, Chu, Ttn,
Orthogneiss												
C44/12					x	x	x	x	x	x	o	Sil, Mnz, Zrn
C47/12					x	x	x	x	x	x		Sil, Mag, Mnz, Zrn
C3/13					x	x	x	x	x	x	o	Sil, Sp, Mnz, Zrn

o - indicates presence in trace amounts

Analyses of chemical compositions of the constituent minerals were performed using a CAMECA SX 50 electron microprobe at the Institute of Mineralogy and Crystal Chemistry, University of Stuttgart, which is equipped with four wavelength-dispersive spectrometers. The following standards were used: pyrope (Si, Al, Mg), andradite (Ca, Fe), jadeite (Na), spessartine (Mn), K-silicate glass (K), Ba-silicate glass (Ba), NaCl (Cl), as well as natural rutile (Ti) and topaz (F). The operating voltage was 15 kV using a beam current between 10 and 15 nA, and the beam was focused to a 1- to 2-μm diameter except for mica, for which an 8- to 10-μm beam was used. Supplementary analyses were also conducted using an EDX-SEM at Charles University in Prague. Ferric iron in garnet and orthopyroxene was calculated based on the scheme of Droop (1987). Molecular formulae for amphibole were calculated following the IMA2012 guidelines (Hawthorne et al. 2012) using the method of Locock (2014). Representative chemical analyses are presented in Tables 2, 3, 4, 5, 6, and 7.

Table 2: Representative orthopyroxene analyses

Rock	Felsic Granulite							Mafic Granulite		
Sample	F74/6			Af159c		Af102		F16/9		
Texture	Coarse Grained		Inc. Grt	Coarse Grained		Coarse Grained		Coarse Grained		
Position	Core	Rim	Rim	Core	Rim	Core	Rim	Core	Rim	Rim
SiO_2	48.35	49.39	49.55	48.77	48.80	49.78	49.29	49.98	49.84	50.11
TiO_2	0.07	0.15	0.12	0.14	0.16			0.11	0.24	0.11
Al_2O_3	2.47	1.29	1.37	1.81	1.46	2.21	1.77	0.87	1.01	1.09
FeO	34.40	34.39	36.04	34.73	35.47	31.70	33.68	32.86	33.11	31.70
MnO	0.65	0.46	0.49	0.36	0.46	1.62	1.00	1.01	0.75	0.50
MgO	13.88	13.67	12.94	13.67	12.96	14.68	14.03	14.67	15.12	15.73
CaO	0.27	0.30	0.35	0.25	0.27	0.22	0.24	0.37	0.13	0.30
Na_2O	0.04			0.05			0.06			
Total	100.13	99.65	100.87	99.78	99.57	100.21	100.07	99.87	100.20	99.54
Oxygen	6	6	6	6	6	6	6	6	6	6
Si	1.902	1.959	1.953	1.929	1.946	1.945	1.939	1.966	1.950	1.962
Ti	0.002	0.005	0.003	0.004	0.005			0.003	0.007	0.003
Al	0.115	0.060	0.064	0.084	0.069	0.102	0.082	0.040	0.047	0.050
Fe^{3+}	0.081	0.013	0.024	0.053	0.029	0.009	0.044	0.021	0.039	0.019
Fe^{2+}	1.051	1.127	1.164	1.096	1.154	1.027	1.064	1.060	1.045	1.018
Mn	0.022	0.015	0.017	0.012	0.015	0.054	0.033	0.034	0.025	0.017
Mg	0.814	0.808	0.760	0.806	0.770	0.855	0.823	0.860	0.882	0.918
Ca	0.011	0.013	0.015	0.011	0.011	0.009	0.010	0.016	0.005	0.012
Na	0.004			0.004			0.005			
Total	4.000	4.000	4.000	4.000	4.000	4.000	4.000	4.000	4.000	4.000
X_{Mg}	0.434	0.418	0.392	0.424	0.398	0.454	0.434	0.448	0.458	0.474

4 Petrography

Felsic granulite

Four samples (F74/6, af159c, af101, and C30-13, Table 1) of orthopyroxene-bearing quartz-feldspathic gneisses have undergone detailed petrographic study and mineral chemistry analysis. These are medium to coarse grained and composed of a granoblastic matrix of plagioclase (30–45 %), quartz (20–30 %), and K-Feldspar (10–15 %). Variable amounts of biotite (10–20 %), orthopyroxene (up to 6 %), garnet (up to 8 %), and ilmenite (2–5 %) are also present. Accessory phases include apatite, zircon and in some cases also graphite.

Orthopyroxene occurs as sub-idioblastic to xenomorphic grains of approximately 0.5 – 2 mm diameter. The orthopyroxene is partially replaced by fine grained domains of biotite, quartz, and rare amphibole (Fig. 3a) while a small number of grains are enclosed by porphyroblastic garnet (Grt_{II}) (Fig. 3b). Compositionally the orthopyroxene has an X_{Mg} ratio of 0.40–0.45, exhibiting slight decreases towards the rim. The best preserved grains have an Al concentration of up to 0.12 a.f.u., which decreases significantly for more strongly replaced grains with most grains showing a typical range of 0.08–0.04 a.f.u.

Based on the textural relations three different varieties of garnet are present in the felsic granulites. Accessory amounts of small (less than 0.2 mm in diameter) grains (Grt_I) occur in plagioclase in samples af101 and C30/13. This garnet is characterized by the highest X_{Mg} (up to 0.24) and spessartine content (~7 mol%) with comparatively low grossular (5–7 mol%). Poikiolitic and xenomorphic porphyroblasts (Grt_{II}), up to 6 mm in diameter is present in all the samples; these contain inclusions of orthopyroxene, Ti-rich biotite (Bt_I) and quartz (Fig. 3b). The garnet porphyroblasts have X_{Mg} ratios of 0.16–0.21; compared to the inclusions in plagioclase they have higher grossular content (6.5–10.5 mol%), but spessar-

Table 3: Representative garnet analyses

Rock	Felsic Granulite								Mafic Granulite		Orthogneiss					
Sample	F74/6	F74/6	F74/6	F74/6	af159c	af159c	af101	af101	F16/9	F16/9	C44/12	C44/12	C44/12	C47/12	C47/12	C47/12
Mineral	Grt_{II}	Grt_{II}	Grt_{III}	Grt_{III}	Grt_{II}	Grt_{II}	Grt_{I}	Grt_{III}	Grt	Grt	Grt_{I}	Grt_{I}	Grt_{II}	Grt_{I}	Grt_{I}	Grt_{II}
Position	Core	Rim			Core	Rim	Core				Core	Rim		Core	Rim	
SiO_2	37.20	37.17	37.48	37.35	37.09	37.13	37.17	37.11	36.65	37.13	38.27	37.68	37.23	37.96	37.53	37.30
Al_2O_3	20.53	20.30	21.42	21.01	20.68	20.96	21.11	20.75	20.79	20.93	21.80	21.56	20.85	21.53	21.40	21.18
FeO	33.17	33.90	30.62	31.86	34.25	33.41	31.34	31.63	31.64	31.19	29.59	31.72	33.04	29.84	32.34	32.98
MnO	1.27	1.12	0.71	1.00	0.95	0.96	3.16	1.66	1.70	0.74	0.67	0.60	0.79	0.49	0.55	0.65
MgO	4.61	3.79	2.35	3.21	4.74	3.70	5.20	2.76	3.34	3.60	8.77	6.98	4.09	8.84	6.42	3.99
CaO	2.71	3.58	7.51	5.41	2.48	3.59	1.89	6.23	5.01	6.46	0.77	1.38	3.32	0.87	1.77	3.26
Total	99.48	99.86	100.08	99.85	100.18	99.74	99.87	100.13	99.13	100.05	99.87	99.92	99.32	99.53	100.01	99.36
Oxygens	12	12	12	12	12	12	12	12	12	12	12	12	12	12	12	12
Si	2.982	2.983	2.986	2.986	2.959	2.977	2.962	2.970	2.959	2.957	2.973	2.963	2.989	2.962	2.960	2.991
Al	1.945	1.927	2.012	1.982	1.952	1.984	1.986	1.963	1.983	1.970	1.998	2.001	1.976	1.984	1.993	2.002
Fe^{3+}	0.065	0.080	0.001	0.028	0.079	0.034	0.046	0.060	0.052	0.064	0.025	0.032	0.032	0.047	0.042	0.006
Fe^{2+}	2.159	2.196	2.039	2.102	2.206	2.206	2.042	2.058	2.085	2.013	1.897	2.054	2.187	1.900	2.091	2.205
Mn	0.086	0.076	0.048	0.068	0.064	0.065	0.213	0.113	0.116	0.050	0.044	0.040	0.054	0.032	0.037	0.044
Mg	0.551	0.453	0.280	0.383	0.563	0.442	0.617	0.329	0.402	0.428	1.016	0.818	0.489	1.028	0.755	0.477
Ca	0.233	0.308	0.641	0.464	0.212	0.309	0.161	0.534	0.433	0.551	0.064	0.116	0.286	0.073	0.150	0.280
Total	8.021	8.023	8.007	8.013	8.035	8.018	8.028	8.026	8.030	8.034	8.018	8.024	8.011	8.028	8.028	8.006
$X_{Fe^{2+}}$	0.971	0.965	0.999	0.987	0.965	0.985	0.978	0.972	0.976	0.969	0.987	0.985	0.986	0.976	0.980	0.997
X_{Mg}	0.203	0.171	0.121	0.154	0.209	0.167	0.232	0.138	0.162	0.175	0.352	0.285	0.183	0.351	0.265	0.178
Alm	71.28	72.40	67.79	69.67	72.45	73.00	67.33	67.83	68.68	66.17	62.79	67.83	72.51	62.64	68.94	73.35
Spss	2.84	2.51	1.60	2.25	2.10	2.15	7.02	3.72	3.82	1.64	1.46	1.32	1.79	1.06	1.22	1.46
Prp	18.19	14.94	9.31	12.69	18.49	14.63	20.34	10.84	13.24	14.07	33.63	27.01	16.21	33.89	24.89	15.87
Grs	7.69	10.15	21.31	15.38	6.96	10.23	5.31	17.60	14.26	18.11	2.12	3.83	9.48	2.41	4.95	9.31

$X_{Fe^{2+}} = Fe^{2+}/(Fe^{2+}+Fe^{3+})$; $X_{Mg} = Mg/(Mg+Fe^{2+})$

Table 4: Representative biotite analyses

	Felsic granulite				Mafic Granulite					Orthogneiss				
Sample	F74/6	F74/6	F74/6	F74/6	Af159c	Af159c	Af101	F16/9	F16/9	C44/12	C44/12	C44/12	C47/12	C47/12
Texture	Inc. Grt Bt_I	Inc. Opx Bt_I	Symp Bt_{II}	Matrix Bt_{III}	Symp Bt_{II}	Matrix Bt_{III}	Matrix Bt_{III}	Inc. Opx Bt_I	Matrix Bt_{II}	Inc. Grt Bt_I	Matrix Bt_{II}	Symp Bt_{III}	Inc. Grt Bt_I	Matrix Bt_{II}
SiO_2	35.48	34.98	35.37	36.99	37.13	37.46	36.49	35.36	35.87	36.84	37.43	36.95	37.86	37.16
TiO_2	5.47	5.11	4.84	2.96	4.60	2.68	2.82	3.94	1.47	2.35	2.49	1.22	2.38	2.83
Al_2O_3	14.73	13.97	14.44	14.98	13.67	14.45	15.64	13.92	15.34	15.93	15.77	18.67	16.24	17.85
FeO	21.12	20.96	19.89	19.13	18.40	19.20	17.44	21.46	19.61	16.38	14.60	15.22	16.54	14.08
MnO	0.14	0.14	0.07	0.06		0.06	0.03		0.13	0.19	0.06		0.12	0.12
MgO	8.93	9.52	9.94	11.79	10.98	10.75	12.09	10.24	11.84	12.29	14.13	13.77	12.48	13.21
CaO			0.03			0.08							0.09	0.08
Na_2O	0.11	0.12		0.05	0.13	0.19		0.14	0.14	0.19	0.06	0.08	0.06	
K_2O	9.43	9.65	9.50	9.86	9.78	9.60	9.76	9.47	9.78	9.87	9.90	9.65	9.89	9.88
F	0.40	0.65	0.95	0.22	0.93	0.35	0.37	0.41	0.23	0.32	0.30	0.57	0.33	0.41
Cl^-	0.29	0.18	0.80	0.16	0.45	0.27	0.27	0.19	0.34	0.64	0.43	0.32	0.27	0.23
Total	95.58	95.28	95.83	96.09	96.06	95.09	94.90	95.13	94.75	94.81	95.11	96.44	96.14	95.85
Oxygen	22	22	22	22	22	22	22	22	22	22	22	22	22	22
Si	5.478	5.478	5.513	5.617	5.694	5.762	5.585	5.531	5.573	5.633	5.634	5.483	5.670	5.520
Ti	0.635	0.602	0.567	0.338	0.530	0.310	0.325	0.464	0.172	0.270	0.282	0.136	0.268	0.316
Al	2.681	2.579	2.653	2.681	2.471	2.620	2.822	2.566	2.809	2.871	2.798	3.266	2.867	3.126
Fe	2.727	2.746	2.592	2.430	2.360	2.470	2.233	2.807	2.548	2.095	1.838	1.889	2.071	1.749
Mn	0.019	0.019	0.010	0.008		0.008	0.003		0.017					0.015
Mg	2.055	2.223	2.309	2.669	2.510	2.465	2.758	2.388	2.742	2.801	3.172	3.048	2.786	2.926
Ca			0.005			0.013							0.014	0.013
Na	0.034	0.035		0.013	0.038	0.057		0.042	0.042	0.056	0.019	0.023	0.017	
K	1.857	1.928	1.888	1.910	1.913	1.884	1.906	1.889	1.938	1.925	1.902	1.827	1.889	1.872
Total	19.492	19.611	19.537	19.666	19.516	19.588	19.632	19.688	19.841	19.652	19.644	19.673	19.582	19.537
X_{Mg}	0.430	0.447	0.471	0.524	0.515	0.499	0.553	0.460	0.518	0.572	0.633	0.617	0.574	0.626

$X_{Mg} = Mg/(Mg+Fe)$

Table 5: Representative feldspar analyses

	Felsic granulite						Mafic granulite		Orthogneiss						
Sample	F74/6			Af159c			F16/9		C44/12						C47/12
	Coarse Grained		Pl_{II}	Coarse Grained		Pl_{II}	Coarse Grained		Perthite		Antiperthite		Matrix Pl		Matrix Pl
Texture	Core	Rim	Rim	Core	Rim	Rim	Core	Rim	Host	Exsol	Host	Exsol	Core	Rim	Core
SiO_2	59.16	60.37	61.24	58.45	58.15	61.84	50.47	58.86	64.51	60.36	60.31	65.23	61.06	60.73	60.38
Al_2O_3	25.95	25.18	24.13	25.98	26.92	23.79	30.92	25.91	18.83	24.99	25.05	18.75	24.76	24.29	24.79
Fe_2O_3			0.16	0.34			0.56					0.14			0.12
CaO	7.38	6.54	5.27	7.52	6.27	5.01	13.38	7.08	0.09	6.34	6.13	0.43	5.72	5.66	6.07
Na_2O	7.32	7.83	8.39	7.30	8.29	8.76	3.94	7.22	1.04	7.97	8.11	1.79	8.40	8.37	8.20
K_2O	0.27	0.26	0.06	0.08	0.08	0.17		0.08	15.07	0.20	0.19	13.15	0.08	0.16	0.07
BaO									0.78			0.62			
Total	100.08	100.18	99.25	99.67	99.71	99.57	99.27	99.15	100.33	99.86	99.77	100.12	100.02	99.21	99.63
Oxygen	8	8	8	8	8	8	8	8	8	8	8	8	8	8	8
Si	2.638	2.683	2.736	2.622	2.604	2.753	2.317	2.643	2.979	2.689	2.689	2.989	2.711	2.719	2.696
Al	1.364	1.319	1.270	1.374	1.421	1.248	1.673	1.371	1.025	1.312	1.316	1.013	1.296	1.282	1.305
Fe			0.006	0.013			0.022					0.005			0.005
Ca	0.353	0.311	0.252	0.362	0.301	0.239	0.658	0.341	0.005	0.303	0.293	0.021	0.272	0.271	0.290
Na	0.633	0.675	0.727	0.635	0.720	0.756	0.351	0.629	0.093	0.689	0.701	0.159	0.723	0.727	0.710
K	0.015	0.015	0.003	0.005	0.005	0.010		0.005	0.888	0.012	0.011	0.769	0.004	0.009	0.004
Ba									0.014			0.011			
Total	5.004	5.003	4.994	5.010	5.049	5.006	5.021	4.988	5.004	5.005	5.009	4.968	5.007	5.008	5.009
An	35.23	31.12	25.68	36.11	29.33	23.78	65.24	34.97	0.47	30.18	29.16	2.23	27.32	26.96	28.93
Ab	63.24	67.42	73.97	63.43	70.23	75.26	34.76	64.55	9.47	68.67	69.78	16.75	72.68	72.14	70.67
Kfs	1.53	1.46	0.35	36.11	0.45	0.96	-	0.47	90.06	1.15	1.06	81.01	0.41	0.91	0.40

Table 6: Representative amphibole analyses

Rock	Mafic Granulite					Impure Marble		
Sample	F16/9	F16/9	F16/9	F16/9	F16/9	F72/6	F72/6	F72/6
Texture	Coarse Grained (Amp$_I$)	Fine Grained (Amp$_{II}$)	Amp$_I$	Amp$_{II}$	Amp$_{III}$			
Position	Core	Core	Core	Rim	Rim	Core	Core	Rim
SiO$_2$	38.41	39.84	40.21	39.28	38.78	42.78	47.52	55.32
TiO$_2$	1.71	1.89	1.66	0.27	0.38	1.39	0.25	
Al$_2$O$_3$	12.56	11.68	11.69	14.98	15.22	15.10	10.73	3.03
FeO	22.43	20.04	20.64	20.00	20.61	1.47	1.17	1.28
MnO	0.17	0.13	0.10	0.20	0.14			
MgO	6.36	7.94	7.45	7.56	7.19	18.99	20.73	22.22
CaO	10.94	11.33	11.64	11.16	11.40	13.39	13.53	13.69
Na$_2$O	1.62	1.38	1.36	1.73	1.73	2.76	2.50	0.74
K$_2$O	2.17	2.06	2.15	1.57	1.73	0.91	0.47	
Cl	1.80	1.04	1.03	0.69	0.80	0.63	0.92	0.78
Total	97.77	97.09	97.69	97.28	97.79	97.41	97.81	97.06
Oxygen	23	23	23	23	23	23	23	23
Si	6.057	6.210	6.260	6.022	5.953	6.083	6.679	7.701
Ti	0.203	0.221	0.194	0.031	0.044	0.149	0.026	
Al	2.335	2.145	2.145	2.706	2.753	2.530	1.777	0.497
Fe^{3+}	0.375	0.279	0.173	0.543	0.531	0.083	0.048	
Fe^{2+}	2.583	2.334	2.513	2.021	2.114	0.092	0.090	0.150
Mn	0.022	0.017	0.013	0.026	0.018			
Mg	1.496	1.844	1.729	1.729	1.644	4.025	4.343	4.611
Ca	1.848	1.893	1.941	1.833	1.875	2.039	2.037	2.042
Na	0.495	0.418	0.412	0.516	0.517	0.760	0.681	0.200
K	0.437	0.410	0.426	0.307	0.338	0.165	0.085	
X_{Mg}	0.371	0.445	0.409	0.468	0.442	0.978	0.980	0.969
	Potassic-Ferro-Pargasite	Potassic-Ferro-Pargasite	Potassic-Ferro-Pargasite	Ferro-Pargasite	Ferro-Pargasite	Pargasite	Edenitic hbl	Tremolite

X_{Mg} = Mg/(Mg + Fe^{2+}); Amphibole names after Hawthorne et al. (2012)

Table 7: Representative mineral analyses from the Impure Marble

Rock	Impure Marble							
Sample	F72/6	F72/6	C8/12	C8/12	C8/12	F72/6	F72/6	C8/12
Mineral	Ol	Ol	Ol	Chu	Chu	Phl	Phl	Phl
Texture	Core	Rim	Core	Core	Rim	Core	Core	Core
SiO_2	41.91	41.78	41.90	37.51	37.78	39.27	39.67	40.52
TiO_2			0.09	3.34	2.84	0.75	0.76	0.71
Al_2O_3						15.60	15.17	15.26
FeO	2.67	2.73	3.00	2.35	2.30	0.83	0.69	0.89
MnO			0.26	0.09	0.21	0.05	0.04	
MgO	55.25	55.10	55.00	53.65	53.68	26.76	26.72	26.17
CaO						0.06	0.09	
Na_2O						1.05	1.20	0.37
K_2O						9.54	9.54	10.31
F^-				1.64	1.96	1.12	0.99	1.04
Cl^-						0.11	0.09	0.07
Total	99.83	99.61	100.26	98.59	98.77	95.13	94.97	95.34
Oxygens	4	4	4	18	18	22	22	22
Si	0.994	0.993	0.994	4.037	4.044	5.572	5.627	5.722
Ti			0.002	0.270	0.288	0.080	0.082	0.075
Al						2.610	2.536	2.541
Fe	0.053	0.054	0.060	0.212	0.206	0.098	0.082	0.106
Mn			0.005	0.008	0.019	0.006	0.005	
Mg	1.953	1.952	1.945	8.607	8.565	5.661	5.650	5.510
Ca						0.009	0.013	
Na						0.289	0.331	0.101
K						1.726	1.727	1.857
Total	3.000	3.000	3.005	13.693	13.727	20.051	20.052	19.911
X_{Mg}	0.974	0.973	0.968	0.975	0.974	0.983	0.986	0.981
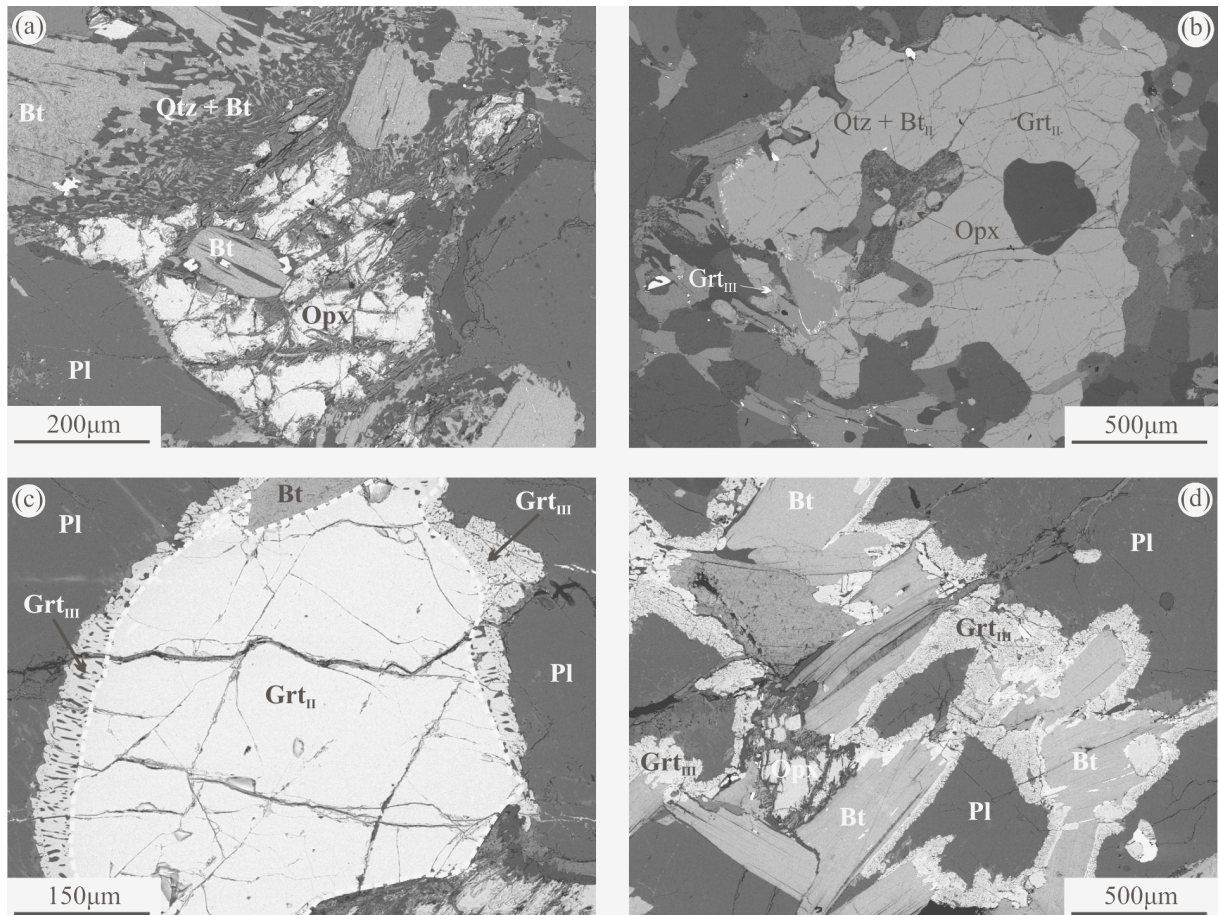
Figure 3: Back Scattered Electron (BSE) images of the felsic granulite. (a) Orthopyroxene grain, with inclusion of biotite and partly replaced by fine-grained intergrowth of biotite and quartz (af159c). (b) Xenoblastic grain of garnet (Grt$_{II}$) containing inclusion of orthopyroxene which is partly replaced by fine grained biotite and quartz (af159c). (c) Fine-grained garnet (Grt$_{III}$) with quartz, overgrowing porphyroblastic garnet (Grt$_{II}$) (F74/6). (d) Fine-grained garnet (Grt$_{III}$) overgrowing tabular biotite at contact with plagioclase (F74/6)

tine content is comparatively low (< 3.5 mol%). They usually indicate a rimwards decrease in X_{Mg} = 0.21 (core) to 0.16 (rim) and a slight increase in grossular. A third variety (Grt_{III}) occurs as fine grained masses intergrown with quartz and ilmenite (Fig. 3c and 3d). The fine grained garnet develops predominantly between biotite and plagioclase but can also be observed overgrowing Grt_{II} (Fig. 3c). This garnet is considerably more calcium rich, with the most grossular rich containing up to 21.5 mol%, has comparatively lower X_{Mg} ratios (0.12 – 0.15) with low spessartine component similar to that in porphyroblastic garnet (< 3 mol%).

Biotite has three textural and compositional forms in the felsic granulites. Inclusions within orthopyroxene and garnet (Bt_I) have X_{Mg} ratios of 0.43–0.49, are rich in titanium (up to 0.32 a.f.u.) and comparatively poor in fluorine and chlorine (up to 0.60 wt. %). Fine-grained biotite with quartz which replace orthopyroxene (Bt_{II}) has slightly higher X_{Mg} (0.47–0.52), similar TiO_2 (~ 0.3 a.f.u.), and considerably higher fluorine (up to 1.15 wt. %) and chlorine (up to 0.95 wt. %) concentrations. The coarse grained biotite (Bt_{III}) which composes the matrix and defines foliation has X_{Mg} in the range of 0.44–0.56, with moderate titanium (Ti up to 0.2 a.f.u.) and low fluorine (~ 0.5 wt. %) and chlorine (~ 0.3 wt. %) contents.

The K-feldspar is often perthitic and plagioclase grains may also exhibit anti-perthitic textures with exsolved K-feldspar. Matrix plagioclase from the felsic granulite is largely in the andesine field with compositions between An_{29-40}, grains usually exhibit a slightly more calcium rich core with albite content increasing gradually towards the rim. A small number of grains at contact with Grt_{III} develop a thin (<0.05 mm) rim (Pl_{II}) of more albitic plagioclase (An_{24}).

Mafic granulite

Mafic granulite (F16/9) occurs as a thin (c. 25 cm) lens within the felsic granulite. The sample is coarse grained and consists of a sub-granoblastic assemblage of orthopyroxene (10–15 %), amphibole (35–45 %), plagioclase (20–30 %), biotite (~5 %), and ilmenite (<5 %). Fine grained amphibole with quartz is present around orthopyroxene at contact with plagioclase (Fig. 4a). Garnet is present as highly irregular xenomorphic overgrowths, sometimes observed with fine grained ilmenite, which develops at plagioclase and orthopyroxene grain boundaries (Fig. 4b).
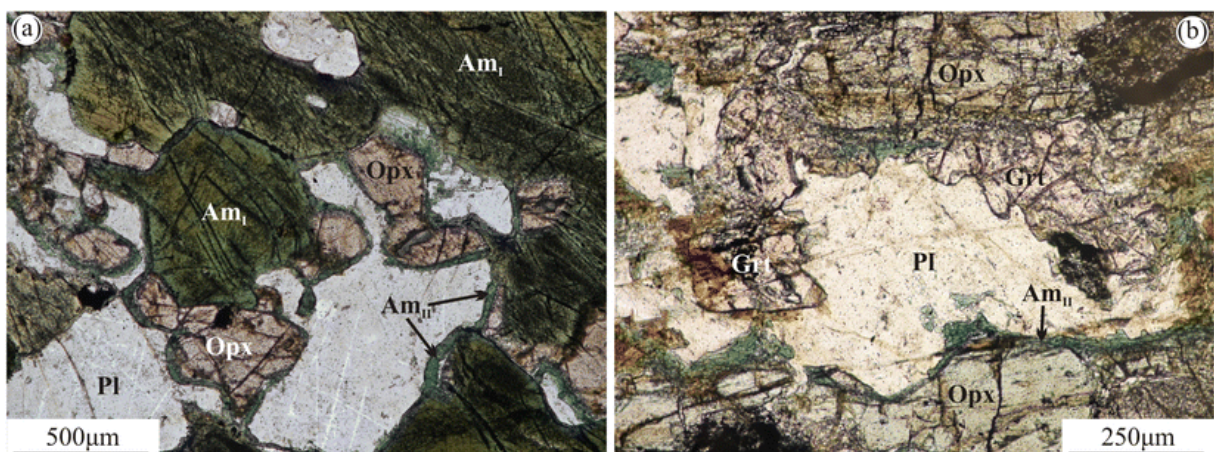
Figure 4: Photomicrographs of mafic granulite (F16/9). (a) Coarse grained orthopyroxene, amphibole (Amp_I) and plagioclase with fine-grained amphibole (Amp_{II}) developing at grain boundaries. (b) Fine-grained and xenomorphous garnet intergrown with ilmenite developing at plagioclase and orthopyroxene grain boundary

The orthopyroxene grains are typically xenoblastic and highly fractured, individual grains are up to 2 mm in diameter, and amphibole and biotite are observed as rare inclusions. Compositionally the

orthopyroxene is largely homogenous exhibiting a small range of X_{Mg} (0.43–0.47) and typically low Al concentrations (~ 0.08 a.f.u.) increasing slightly (up to 0.12 a.f.u.) towards the rim of grains.

Two varieties of amphibole are present. The first (Amp_I) variety occurs as porphyroblastic grains and the second (Amp_{II}) develops as fine grained masses with quartz often following grain boundaries between plagioclase and orthopyroxene (Fig. 4a). Amp_I is Ti (up to 0.25 a.f.u.) and K (up to 0.50 a.f.u.) rich, has a range of X_{Mg} between 0.35–0.45 and Al concentrations of around 2.3–2.4 a.f.u. In contrast Amp_{II} has higher Al (~ 2.75 a.f.u.), and X_{Mg} (0.44–0.48) and significantly lower K (~ 0.30 a.f.u.) and Ti (~ 0.05 a.f.u.).

Plagioclase is irregularly shaped and contains micro-inclusions of quartz, amphibole and rare zoisite. Plagioclase exhibits strong chemical variation with sodium content varying between a calcium rich core (An_{65}) and a more sodium rich rim (An_{35-50}). The most sodium rich rims are adjacent to garnet.

The xenomorphous garnet overgrowths exhibit fairly constant X_{Mg} ratios of around 0.17 but shows a variable grossular content increasing towards plagioclase (13.5–17.5 mol%). As in the felsic samples spessartine component is fairly low (< 4 mol%).

Impure marble

The granulite facies impure marble is characterized by the presence of olivine (F72/6) and/or clino-humite (C8/12), with porphyroblastic flakes of phlogopite and grains of amphibole (Fig. 5 a, b). The matrix is composed of fine grained calcite and dolomite in an approximate ratio of 4:1. Most of the calcite from the marble is relatively Mg (< 0.05 a.f.u.) and Fe poor (< 0.01 a.f.u.), however small calcite grains with substantially higher magnesium concentrations, up to 0.13 a.f.u., were found as inclusions in clinohumite and olivine.
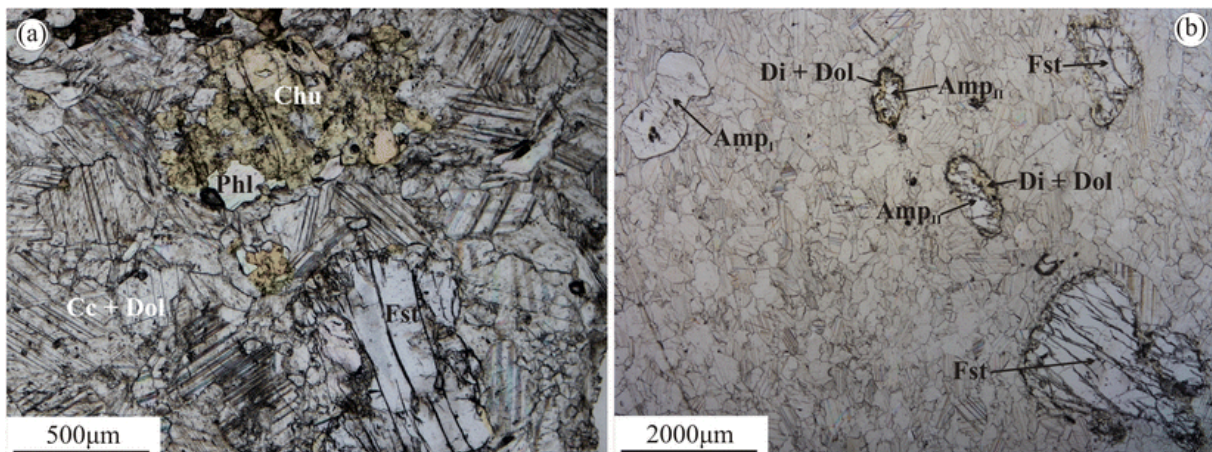
Figure 5: Photomicrographs of the impure marble (C8/12). (a) Xenomorphous clinohumite and olivine within a calcite and dolomite matrix. (b) Grains of amphibole and olivine in a calcite and dolomite matrix, Amp_I in the top left forms a larger unaltered xenoblast, Amp_{II} is partly replace by intergrown diopside and dolomite that appears yellow in color. Olivine is fractured with fractures infilled by Amp_{III} (F72/6)

Olivine (< 2 vol. %) with X_{Mg} ratios > 0.96, forms coarse (up to 2 mm diameter) highly fractured grains. The fractures are typically in filled by antigorite; while, fine grained tremolite with dolomite is observed developing around grain margins. The olivine sometimes contains small inclusions of calcite, dolomite, and diopside.

Clinohumite (2–4 %), forms fine-medium grained irregular shaped clusters and contains small rounded inclusions of calcite, dolomite, and diopside. Clinohumite in sample C8-12 has an X_{Mg} > 0.97, as well as TiO_2 content up to 3.34 wt. %, and fluorine up to 2.05 wt. %.

Phlogopite (c. 5–10 %), forms large subhedral flakes up to 1 cm in length that occur with amphibole, apatite, and rarely with clinohumite and titanite. It contains exsolution lamellae of rutile and is partly replaced by chlorite. The phlogopite has X_{Mg} ratios > 0.97, TiO_2 concentrations are very low (< 0.04 a.f.u.), fluorine concentrations are generally high (~ 1.05 wt. %) while chlorine concentrations are negligible (< 0.07 wt. %). In addition the phlogopite contains appreciable amounts of Na_2O (~ 0.55 wt. %).

In sample F72/6, amphibole takes three forms; Amp_I occurs as large, unaltered porphyroblasts of pargasitic composition, with X_{Mg} ratio > 0.95; NaK(A) = 0.88 – 0.94 and Si = 6.04 – 6.35 a.f.u. Amp_{II} forms smaller xenoblastic grains of edenitic composition (NaK(A) ~ 0.74; Si ~ 6.75 a.f.u.) partly replaced by fine-grained diopside and dolomite (Fig. 5b). Amp_{III} is observed in both samples as a replacement phase around olivine and is tremolite in composition (X_{Mg} = 0.97; Si = 7.71 a.f.u.).

Titanite occurs in sample C8/12 as fine grained masses often containing a core composed of an ilmenite-geikielite solid solution. Clinopyroxene is observed forming as small rounded inclusions in clinohumite and olivine and in fine grained intergrowths with dolomite around Amp_{II}. Large apatite grains (up to 3 mm in size) are also present.

Orthogneiss

The orthogneisses (C44/12, C47/12, and C3/13, Table 1) were sampled from a separate locality nearby to Kabul airport and approximately 8 km east of the granulite locality. They consist of a medium to coarse grained assemblage consisting of: garnet (up to 15 %), plagioclase (35–50 %), K-feldspar (10–15 %), quartz (20–30 %), biotite (5–10 %), and minor amounts of sillimanite, ilmenite, and apatite. The rocks have a weak foliation which is defined by the biotite and variations in grain size.

Garnet is observed in two textural settings. Grt_I forms as large (up to 4 mm diameter) often highly fractured porphyroblasts containing rounded inclusions of quartz, feldspar, and biotite as well as small needles of sillimanite (Fig. 6a). The fractures are commonly filled by fine-grained biotite and minor sillimanite with quartz. The garnet porphyroblasts exhibit fairly simple zoning, with a relatively pyrope rich core (X_{Mg} = 0.35), an initial gradual decrease towards the rim, is followed by a sharp drop to X_{Mg} = 0.27 at the garnet rim. A similar drop in X_{Mg} is also recorded at the fractures indicating possible diffusion with the infilling biotite. The garnets are manganese and calcium poor with both grossular and spessartine < 4 mol%, although a slight increase in grossular content is seen at the rim. In some instances a fine-grained Grt_{II} inter-grown with quartz develops between the Grt_I porphyroblasts and plagioclase. The fine-grained garnet (Grt_{II}) has a lower X_{Mg} of around 0.18 but considerably higher calcium content with grossular concentrations of up to 9.50 mol%.

In addition to the biotite inclusions in garnet (Bt_I), biotite also forms as large tabular grains (Bt_{II}) with exsolution lamellae of rutile/ilmenite and in fine grained domains (Bt_{III}) inter-grown with sillimanite and quartz (Fig. 6b). The fine grained biotite usually forms after tabular biotite or garnet. The inclusions in garnet (Bt_I) exhibit the lowest X_{Mg} ratios of around 0.57, while both the large tabular biotite (Bt_{II}) and the fine grained symplectic biotite (Bt_{III}) have similar values of X_{Mg} = 0.60–0.66. In terms of TiO_2, the inclusions in garnet (Bt_I) and matrix biotite (Bt_{II}) have similar concentrations (2.25–2.95 wt. %), while the symplectite biotite (Bt_{III}) has substantially lower TiO_2 (< 1.50 wt. %).

The feldspars are both antiperthitic, exhibiting exsolved alkali feldspar blebs within plagioclase and perthitic with fine grained lamellae of plagioclase within K-feldspar. The plagioclase host for the antiperthite has a composition of between An_{27-32} while the K-feldspar blebs are Or_{80-84}; the K-feldspar accounts for < 10 % of the antiperthite grain. The K-feldspar host for the perthite grains is slightly more
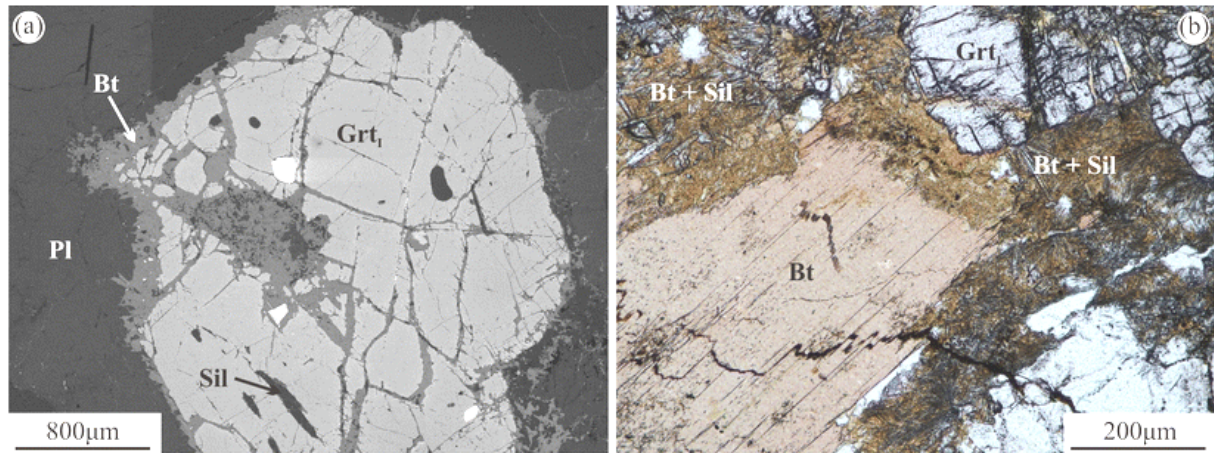
Figure 6: BSE image (a) and photomicrograph (b) from sample of orthogneiss (C44/12). (a) Garnet porphyroblast (Grt$_I$) with inclusions of sillimanite, partly replaced by fine-grained biotite (Bt$_{III}$). (b) Tabular biotite (Bt$_{II}$) and porphyroblastic garnet partly replace by intergrown biotite (Bt$_{III}$) and sillimanite

potassium rich (Or$_{87-91}$) while the fine plagioclase lamellae have similar compositions to the antiperthitic plagioclase (~ An$_{28}$) and constitute < 5 % of the perthite grain.

Needles of sillimanite occur within plagioclase and partly rim grain boundary of plagioclase with quartz. While a small number of kyanite grains were also observed in the matrix with plagioclase.

5   Metamorphism of the Sherdarwaza Formation

Based on textural relations and chemical variations among minerals in the investigated samples, two distinct metamorphic mineral assemblages indicating granulite-facies (M1) and subsequent amphibolite-facies conditions (M2) are inferred (Table 8). The granulite-facies assemblages are characterized by orthopyroxene and Ti-rich biotite in the felsic granulite; coarse grained amphibole and orthopyroxene in the mafic granulite; olivine, clinohumite and phlogopite in the impure marble; and Mg-rich garnet (Grt$_I$) in the orthogneiss. In addition to feldspars and ilmenite, the relict grains of garnet (Grt$_I$) within plagioclase from felsic granulite are assumed to be part of granulite-facies assemblage. This garnet is rich in X_{Mg} = 0.24 with high spessartine = 7.5 mol% content that is probably the result of back diffusion of Mn during garnet consumption. Post M1 rehydration results in the development of fine grained replacement of granulite-facies phases. This is evidenced by intergrown biotite (Bt$_{II}$) and quartz in the felsic granulite after orthopyroxene (Fig. 3a), and by the biotite, sillimanite and quartz symplectites seen in the orthogneiss (Fig. 6b).

Table 8: Metamorphic mineral assemblages as distinguished by textural relations

	Granulite-facies event	Amphibolite-facies event
Lithology	M1	M2
Felsic granulite	(Bt$_I$) + Opx + Grt$_I$ + Pl + Kfs + Ilm + Qtz + *Bt$_{II}$*	Grt$_{II}$ + Bt$_{III}$ + Pl$_{II}$ + Ilm + Qtz + *Grt$_{III}$*
Mafic granulite	(Bt$_I$) + Opx + Amp$_I$ + Pl$_C$ + Ilm	Grt + Bt$_{II}$ + Amp$_{II}$ + Pl$_R$ + Ilm + Qtz
Impure marble	(Di + Dol) + Ol + Chu + Phl + Amp$_I$ + Cc	Amp$_{II}$ + Di + Cc + Dol
Orthogneiss	(Bt$_I$) + Sil + Grt$_I$ + Bt$_{II}$ + Pl + Kfs + Ilm + Qtz + *Bt$_{III}$*	Grt$_{II}$ + Ky + Pl + Qtz

Minerals in brackets only present as inclusions, *italics* indicates not considered part of the peak assemblage

The amphibolite-facies overprint is evidenced by garnet (Grt$_{II}$) growth in the felsic granulite, the garnet clearly post-dates both the granulite-facies assemblage and the post-peak rehydration as it is seen to

enclose both orthopyroxene and the fine grained biotite (Bt_{II}) - quartz intergrowth (Fig. 3b). The overprint can be also recognized in the mafic granulite by the growth of fine grained xenomorphous garnet, with fine grained amphibole (Amp_{II}) and quartz that develop at the interface between granulite-facies minerals (Fig. 4b). Likewise in the orthogneiss, the fine grained garnet (Grt_{II}) is considered part of the amphibolite-facies overprint as it also overgrows the granulite-facies assemblage. Based on these inferred assemblages the pressure-temperature (P-T) conditions for the granulite-facies metamorphism, subsequent retrogression and overprint are constrained through the use of a variety of geothermobarometers as outlined below and summarized in Table 9.

PT conditions of the granulite-facies assemblages (M1)

Conventional thermombarometry

The garnet-orthopyroxene Fe-Mg exchange thermometer was applied to the Mg-rich garnet inclusions in plagioclase (Grt_I) and large unaltered orthopyroxene in the felsic granulite (sample af101) using the calibrations of Lee and Ganguly (1988) and Bhattacharya et al. (1991). The calibration of Lee and Ganguly (1988) yielded a mean temperature of 864 °C (σ-22 °C). While, slightly lower temperatures of 832 °C (σ-26 °C) were calculated using the calibration of Bhattacharya et al. (1991). It should be noted that these results and those of the garnet-biotite thermometer (see below) may not represent the peak temperatures owing to potential retrograde Fe-Mg exchange (Fitzsimmons and Harley 1994), and therefore are taken only as a guide to peak metamorphic temperatures.

The Garnet-biotite thermometer was applied to the Mg-rich cores of the garnet porphyroblasts (Grt_I) and the unaltered core composition of enclosed biotite (Bt_I) in the orthogneiss. The calculations yielded a mean temperature of 734 °C (σ-19 °C) and 800 °C (σ-13 °C) for the calibrations of Bhattacharya et al. (1992) and Holdaway (2000) respectively. As this is an inclusion assemblage, in addition to the potential for retrograde Fe-Mg exchange, the lower temperature likely reflects the temperature of entrapment of the biotite inclusions and not peak conditions (Spear and Peacock 1989). The matrix biotite (Bt_{II}) is in equilibrium with the rims of the garnet porphyroblasts and therefore an estimate for the cooling history is conducted by applying the garnet-biotite thermometer to the rim composition of the garnet (Grt_I) and the adjacent matrix biotite (Bt_{II}). A total of 10 mineral pairs were analyzed yielding a mean temperature of 606 °C (σ-13 °C) using the calibration of Bhattacharya et al. (1991) and a slightly higher temperature of 646 °C (σ-17 °C) using the calibration of Holdaway (2000).

The garnet-orthopyroxene-plagioclase-quartz barometer was applied to felsic granulite with garnet inclusions in plagioclase (Grt_I), core composition of plagioclase, and unaltered orthopyroxene. Pressures were estimated using the calibrations of Newton and Perkins (1982) and Bhattacharya et al. (1991) which yielded mean pressures of 5.51 kbar (σ-0.26) and 5.09 kbar (σ-0.28) respectively at 850 °C.

As sillimanite is present as an inclusion phase in the porphyroblastic garnet (Grt_I), it is possible to apply the garnet-aluminosilicate-quartz-plagioclase (GASP) barometer to the granulite-facies (M1) assemblage in the orthogneiss. Pressures were calculated using the calibrations of Hodges and Crowley (1985) and Koziol and Newton (1988) applied to the core composition of garnet and re-integrated antiperthite compositions, at temperatures of 800 °C. The resulting pressures are estimated to be 5.98 kbar (σ-0.23) and 6.39 (σ-0.29) for the Hodges and Crowley (1985) and Koziol and Newton (1988) calibrations respectively. Additionally the post-M1 evolution was examined by applying the GASP barometer to the rim composition of the garnet porphyroblast (Grt_I) at temperatures estimated from garnet-biotite thermometry. This yielded mean pressures of 5.71 kbar (σ-0.31) for the Hodges and Crowley (1985) calibration and 5.92

Table 9: Summary of calculated thermobarometric data

Sample	P ref kbar	Grt-Opx LG	σ	B	σ	Grt-Bt Hy	σ	Grt-Amp P	σ	T ref °C	Grt-Opx-Pl-Qtz NP	σ	Grt-Als-Qtz-Pl HC	σ	KN	σ	Grt-Bt-Pl-Qtz Ho	σ	W	σ	Grt-Amp-Pl-Qtz KS	σ
											Granulite Facies Event											
Felsic Granulite (Grt$_I$-Opx-Pl$_C$-Qtz)																						
af101	6	864	22							850	5.51	0.26										
Orthogneiss (Grt$_{IC}$-Bt$_I$-AP-Sil-Qtz)																						
C44/12	6			731	16	799	11			800			5.85	0.22	6.18	0.09	5.87	0.16	5.49	0.36		
C47/12	6			739	26	802	17			800			6.28	0.04	5.83	0.13	6.16	0.08	6.69	0.10		
Orthogneiss (Grt$_{IR}$-Bt$_{II}$-Pl$_C$-Sil-Qtz)																						
C44/12	6			609	14	656	14			625			5.44	0.18	5.67	0.17	5.22	0.14	5.33	0.10		
C47/12	6			603	12	636	15			625			5.97	0.09	6.17	0.16	5.78	0.08	5.96	0.09		
											Amphibolite Facies Event											
Felsic Granulite (Grt$_{IIR}$-Bt$_{III}$-Pl$_R$-Qtz)																						
F74/6	7.5			592	10	627	21			600							7.42	0.07	7.03	0.07		
af159c	7.5			573	15	609	14			600							7.48	0.09	6.95	0.05		
af101	7.5			584	11	619	10			600							7.24	0.10	6.91	0.08		
Orthogneiss (Grt$_{II}$-Bt$_{III}$-Pl$_R$-Ky-Qtz)																						
C44/12	7.5			527	17	569	20			550			7.3	0.32	7.87	0.22	7.56	0.20	6.94	0.36		
C47/12	7.5			512	4	549	23			550			7.3	0.50	7.84	0.42	7.50	0.38	6.72	0.43		
Mafic Granulite (Grt-Bt$_{II}$-Amp$_{II}$-Pl$_R$-Qtz)																						
F16/9	8.5			598	24	633	27	621	21	600							8.43	0.35	8.67	0.15	8.54	0.24

LG: Lee & Ganguly (1988); B: Bhattacharya et al. 1992; Hy: Holdaway (2000); P: Perchuk et al. (1985); NP: Newton & Perkins (1982); HC: Hodges & Crowley (1985); KN: Koziol & Newton (1988); Ho: Hoisch et al. (1990); W: Wu et al. (2004); KS: Kohn & Spear (1990)

Grt$_{IC}$ - Garnet 1 core; Pl$_R$ - Plagioclase rim; AP - Anti-perthite

kbar (σ-0.31) for the Koziol and Newton (1988) calibration. Indicating only marginally lower pressures than those calculated for the peak conditions.

Pressures conditions were also calculated in the orthogneiss using the garnet-biotite-plagioclase-quartz (GBPQ) barometer and the calibrations of Hoisch (1990) and Wu et al. (2004). A pressure estimate for the granulite-facies metamorphism (M1) was calculated using the core composition of the garnet porphyroblasts (Grt$_I$), the biotite inclusions in garnet (Bt$_I$) and the re-integrated antiperthite composition. Using the calibration of Hoisch (1990)yielded a mean pressure of 6.02 kbar (σ-0.12). Similar pressures of 6.09 kbar (σ-0.23) were calculated with the calibration of Wu et al. (2004). As with the GASP barometer (see above) pressures were also estimated for the garnet porphyroblast (Grt$_I$) rim in order to investigate the post-peak evolution. By taking the garnet (Grt$_I$) rim composition in conjunction with the rim composition of matrix biotite (Bt$_{II}$) and plagioclase yielded a mean pressure 5.50 kbar (σ-0.32) using the calibration of Hoisch (1990) while the calibration of Wu et al. (2004) yielded 5.65 kbar (σ-0.35).

P-T pseudosection modeling

In order to further constrain the peak metamorphic conditions P-T pseudosections have been computed for representative samples of felsic granulite (af159c, af101) and orthogneiss (C44/12). While P-T pseudosections do provide useful tools in constraining metamorphic evolution, there are certain limitations associated with the modeling of high-grade, granulite-facies rocks. Notably, melt loss is a common phenomenon during the prograde evolution; this will introduce uncertainties that can preclude definition of the prograde path. Additionally, retrograde reactions typically involve hydration; therefore, peak conditions and retrograde evolution cannot be precisely modeled using the same water content. Hence the pseudosection modeling is only used to constrain the peak granulite-facies metamorphism.

The pseudosections presented in this study were calculated using the Perple_X software package (v.6.6.8) (Connolly 2005) in conjunction with the internally consistent thermodynamic database of Holland and Powell (1998: 2004 update). The pseudosections were calculated in the NCKFMASHTO system. MnO was excluded in the calculation due to low abundances (< 0.1 wt. %) and the propensity to increase the stability of garnet to all but the most extreme conditions. This system includes TiO$_2$ and O$_2$ which allow the consideration of ilmenite within the peak assemblages and have been shown to affect the stability of biotite at high temperatures (Tajčmanová et al. 2009). The solution models used for these calculations were: orthopyroxene, clinopyroxene (Powell and Holland 1999) garnet, cordierite (Holland and Powell 1998), feldspar (Benisek et al. 2010), white mica (Auzanneau et al. 2010 and Coggon and Holland 2002), ilmenite (White et al. 2000), biotite (Tajčmanová et al. 2009), and silicate-melt (White et al. 2007).

An important criterion in the calculation of pseudosections is the estimation of an effective chemical composition for the rocks being studied. In heterogeneous samples or rocks with strong mineral zonation and poly-phase reaction domains a bulk rock analysis may not be applicable to the thin section level mineral concentrations and compositions. Therefore compositions used in these calculations were determined on the basis of molecular abundances and mineral compositions on the thin section scale. This data was then checked against whole rock analyses using wet chemical techniques at the Laboratories of the Geological Institutes at Charles University in Prague. As chemical analyses of minerals point to fairly low Fe3+ (Table 2, 3, 4, 5, 6, and 7) only small amounts of O$_2$ were incorporated in the chemical system. H$_2$O concentrations were estimated from modal abundances of hydrous phases and confirmed on T-X diagrams. The chemical compositions used in the pseudosection analysis are given in Fig. 7.

Pseudosections calculated for two samples of felsic granulite with and without granulite-facies garnet (Grt$_I$) are shown in Fig. 7a and b. For the garnet absent sample (af159c) the peak assemblage consists of:
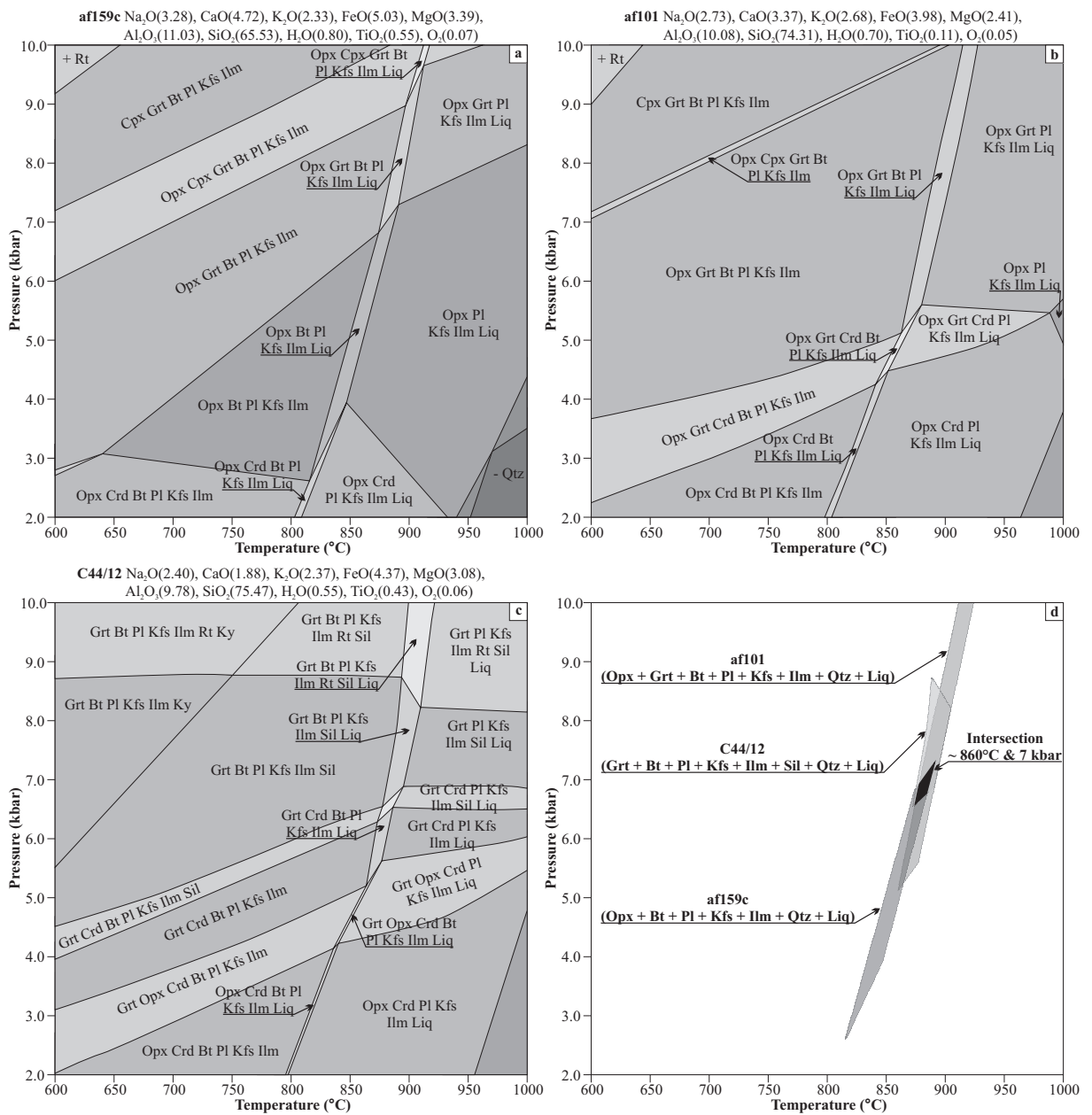
Figure 7: P-T pseudosections in the NCKFMASHTO system for samples of felsic granulite: (a) af159c, (b) af101 and orthogneiss: (c) C44/12. The P-T stability of the peak assemblage in each sample is superposed in (d) and the inferred peak conditions indicated by the dark area

opx-bt-pl.-kfs-qtz-ilm±liq, this assemblage is stable in a narrow band defined by the relative stabilities of garnet and cordierite (Fig. 7a). At the onset of melting, at approximately 850 °C, garnet is stable in excess of 6 kbar, while cordierite is stable at around 2.6 kbar increasing to 3.6 kbar at the dehydration of biotite. As biotite persists into granulite-facies assemblage the upper temperature limit is defined by the position of the biotite dehydration reaction. At the stability of cordierite this reaction occurs at approximately 850 °C increasing to 870 °C at the upper pressure limit.

In the garnet (Grt_I) bearing sample (af101) the computed pseudosection (Fig. 7b) indicates that garnet is stable at lower pressures of around 2.3 kbar at 600 °C increasing up to 5.4 kbar at higher temperatures. Once again cordierite, which is absent in the samples, provides a lower pressure bound. Cordierite is stable at less than 3.6 kbar at lower temperatures and up to 5.2 kbar at higher temperatures. At lower temperatures the relative stability of clino- and orthopyroxene provides an upper pressure bound at around 7 kbar at 600 °C increasing to above 10 kbar at 860 °C. The upper temperature limit is defined by the biotite dehydration reaction which occurs around 860 °C at the lower pressure bound increasing to almost 900 °C at 10 kbar.

In the orthogneiss (C44/12), the peak conditions are defined by the assemblage of grt-bt-pl-kfs-sil-ilm-qz±liq. This assemblage has a lower pressure bound defined by the stability of cordierite, stable at ~4.6 kbar at 600 °C increasing to 6.4 kbar at supra-solidus conditions (> 850 °C). The upper pressure limit is defined by rutile, which is stable above 8.6 kbar at lower temperatures dropping to around 8 kbar above 850 °C. Furthermore, as coarse grained tabular biotite (Bt_{II}) is considered part of the peak assemblage, an upper temperature limit is defined by the stability of biotite. At the pressure conditions defined by cordierite and rutile stability the biotite dehydration reaction occurs around 880 °C.

The inferred P-T stability of the different lithologies overlap at around 860 °C and 7 kbar (Fig. 7d), as the rocks are expected to have experienced a similar P-T history, these are interpreted to represent peak metamorphic conditions. The estimated temperature is around the same as that recorded from the garnet-orthopyroxene thermometer; however, the pressure is moderately higher than those calculated from conventional methods.

Amphibolite facies overprint (M2)

Both the felsic and mafic granulites (F74/6, af159c, af101, F16/9) and the orthogneiss (C44/12, C47/12) record textures consistent with a subsequent metamorphic overprint (M2), these consist of garnet overgrowing the granulite-facies assemblages.

The Garnet-biotite thermometry was applied to garnet xenoblasts (Grt_{II}) enclosing orthopyroxene and Ti-rich biotite in felsic granulite (Fig. 3b). Temperatures, calculated for the garnet and adjacent matrix biotite (Bt_{III}), yielded 586 °C (σ-22 °C) and 621 °C (σ-18 °C) using the calibrations of Bhattacharya et al. (1991) and Holdaway (2000) respectively. Similarly temperatures were estimated for the orthogneiss using the fine grained garnet (Grt_{II}) and adjacent biotite. A mean temperature of 521 °C (σ-15 °C) was recorded using the calibration of Bhattacharya et al. (1991), while a slightly higher temperature of 561 °C (σ-21 °C) was calculated with the calibration of Holdaway (2000).

In the mafic granulite both garnet-biotite thermometry and garnet-amphibole thermometry have been applied to the amphibolite-facies overprint. For the garnet-biotite thermometer the calibration of Bhattacharya et al. (1992) yielded temperatures of 598 °C (σ-24 °C), while higher temperatures of 633 °C (σ-27 °C) were recorded from the calibration of Holdaway (2000). The garnet-amphibole thermometer was applied to the xenomorphous garnet and fine grained amphibole (Amp_{II}) using the calibration of Perchuk et al. (1985). The calculations yielded a mean pressure of 621 °C (σ-21 °C).

In order to calculate pressures the garnet-aluminosilicate-quartz-plagioclase (GASP) barometer was applied to the fine grained garnet (Grt_{II}), biotite and plagioclase and accessory kyanite in the matrix in the orthogneiss The resulting calculation using the calibration of Hodges and Crowley (1985) yielded a mean pressure of 7.30 kbar (σ-0.34), while the calibration of Koziol and Newton (1988) yielded a slightly higher pressure of 7.86 kbar (σ-0.26).

The garnet-biotite-plagioclase-quartz (GBPQ) barometer was used in felsic granulite and the orthogneiss. In the felsic granulite, the calculation for garnet (Grt_{II}) and matrix biotite (Bt_{III}) at 600 °C yielded a mean pressure of 7.41 kbar (σ-0.15) using the calibration of Hoisch et al. (1990) and 6.94 kbar (σ-0.18) with the calibration of Wu et al. 2004. In the orthogneiss calculations were carried out on the garnet overgrowth (Grt_{II}) and adjacent plagioclase and biotite, this yielded a mean pressure of 7.54 kbar (σ-0.24) with the Hoisch (1990) calibration and 6.85 kbar (σ-0.36) with the calibration of Wu et al. (2004).

Two barometers of garnet-amphibole-plagioclase-quartz (GAPQ) and garnet-biotite-plagioclase-quartz (GBPQ) were used in mafic granulite. The former with the calibration of Kohn and Spear (1990) gave a mean pressure of 8.54 kbar (σ-0.24). While the latter using the calibration of Hoisch (1990) yielded a mean pressure of 8.43 kbar (σ-0.35), and 8.67 kbar (σ-0.32) with the calibration of Wu et al. (2004).

6 Discussion

Petrographic observations, thermobarometric calculations, and P-T pseudosection analysis indicate that the lowermost basement of the Kabul Block experienced multiple phases of mineral growth. Two metamorphic assemblages, recording high-grade granulite-facies and subsequent amphibolite-facies conditions, are identified. While these results are indicative of a polyphase evolution for the Kabul Block, it is not easy to conclude from this alone as to whether the rocks were subjected to two distinct metamorphic events or underwent two phases of mineral growth during a single polyphase metamorphism. However, both the regional geology (Abdullah and Chmyriov 1977; Karapetov et al. 1981) and recent geochronological studies (Faryad et al. 2009; Bohannon 2010; Faryad et al. 2015) seem to indicate that at least two metamorphic events occurred. Possible further metamorphic overprint can be deduced from textural relations in the felsic granulite, where fine grained garnet intergrown with quartz (Grt_{III}) with higher Ca and depleted Fe and Mg content is present.

Granulite-facies event

Based on petrographic charateristics, the granulite-facies minerals are preserved only in some competent lithologies (e.g. orthogneiss) that avoided significant migmatization and deformation. In spite of strong recrystallization of the rocks, some textures from the felsic granulite show an early stage of granulite-facies metamorphism. This includes biotite and quartz inclusions within orthopyroxene, suggestive of orthopyroxene formation in response to the dehydration reaction (Bt + Qtz (+ Pl) → Opx + Kfs + Liq). A small amount of biotite and sillimanite also occur as inclusions within the porphyroblastic garnet (Grt_I) in the orthogneiss, indicating that the garnet formed after these two minerals (Bt + Sil + Qtz (+ Pl) → Grt + Kfs + Liq). Both reactions are common in granulite-facies terranes and are interpreted to signify early stage of granulite metamorphism (Patiño Douce and Johnston 1991; Graphchikov et al. 1999; Spear et al. 1999). Similar textures are present in the mafic granulite, where amphibole and/or biotite are enclosed by orthopyroxene. As garnet is not part of the equilibrium assemblage in the mafic granulite this indicates that the high-grade metamorphism occurred beneath the strongly pressure dependent reaction of: Opx + Pl → Grt + Qtz + Cpx (Pattison 2003).

Textures indicating an early stage of granulite-facies metamorphism can be observed also in the impure marbles. They involve diopside inclusions in olivine suggesting its reaction with dolomite (Di + Dol $\rightarrow$ Ol + Cc + CO_2) as described in high-grade calc-silicates by Satish-Kumar et al.Kumar et al. (2001). Clinohumite can form by a very similar reaction as produced the olivine (Di + Dol + H_2O $\rightarrow$ Chu + Cal + CO_2) or after olivine itself (Dol + Ol + H_2O $\rightarrow$ Chu + Cal + CO_2) (Satish-Kumar et al.Kumar et al. 2001; Proyer et al. 2008). However, as the clinohumite is not seen to either interact with, or overgrow the olivine it is assumed to have formed by the former rather than the latter mechanism.

Peak P-T conditions, based on conventional thermobarometry and pseudosection modeling, for the granulite facies metamorphism are summarized in Fig. 7. The pseudosection analysis provides both the highest temperatures (around 860 °C) and pressures (around 7 kbar). Whilst the garnet-orthopyroxene-plagioclase-quartz thermobarometry does record similar temperatures (~ 860 °C) to the pseudosection modeling, pressures calculated by this method are considerably lower. The thermobarometric calculations were carried out on relict garnet inclusions in plagioclase (Grt_I); these garnets likely became depleted in calcium as a result of diffusion during garnet consumption and therefore underestimate the peak pressures of the metamorphism. Likewise the lower temperatures recorded for the orthogneisses are based on inclusion assemblages, as such these likely do not record the peak conditions but rather the conditions of entrapment (Spear and Peacock 1989). Therefore, the results of the pseudosection modeling are considered the most reliable estimate for the peak granulite-facies conditions.

Geochronological data from felsic granultes as well as from orthogneiss (Faryad et al. 2015), suggests this metamorphism was Paleoproterozoic in age (~1.8–1.9 Ga). Oscillatory zoned light colored zircon cores from both the felsic granulite at Khair Khana and the orthogneiss from Kabul Airport yielded ages of 2200–2500 Ma. Additionally a small number of cores from the orthogneiss produced even older Neoarchean ages of >2700 Ma. These zircons are overprinted by a dark colored, likely metamorphic, rim which recorded late Paleoproterozoic concordant ages of 1800–1900 Ma. Similar late Paleoproterozoic ages (1800–1900 Ma) were also reported by Collett (2011) from migmatites belonging to the Sherdarwaza Formation approximately 6 km south of the Khair Khana locality. Bohannon (2010) also reports zircon ages from the Sherdarwaza Formation yielding two possible ages of ~2200–2400 Ma and 1800 Ma. Bohannon (2010) suggested that this could indicate metamorphism at around 1800 Ma of a metasedimentary rock containing a variety of inherited zircons. The evidence for a late Paleoproterozoic event is additionally supported by in-situ U-Th analysis of monazite inclusions in garnet from the orthogneiss which yielded ages of 1780–1880 Ma (Faryad et al. 2015).

The retrograde evolution is primarily controlled by rehydration reactions. In the felsic granulite this is evidenced by the fine grained biotite and quartz domains that develop around orthopyroxene (Fig. 3a), a texture which is common to many granulite-facies terranes (Timmermann et al. 2002). Similar textures are also observed in the orthogneiss where fine grained biotite, sillimanite and quartz develop as symplectite structures at porphyroblastic garnet (Grt_I) and biotite (Bt_{II}) grain boundaries (Fig. 6b). Thermobarometric calculations carried out on the rim of porphyroblastic garnet (Grt_I) in the orthogneiss indicate that the rocks underwent significant cooling with only limited decompression. This is further supported by the absence of cordierite within the retrograde mineral assemblage as the computed P-T pseudosection indicates that cordierite bearing assemblages would form at pressures below 5 kbar (Fig. 7c).

Amphibolite-facies event

The key evidence for amphibolite-facies metamorphism is provided by the garnet growth in the felsic granulites. Garnet porphyroblasts (Grt_{II}) contain inclusions, not just of the granulite-facies minerals

(orthopyroxene, high-Ti biotite), but also the fine-grained biotite (Bt_{II}) and quartz intergrowth that are interpreted as retrograde phases after granulite-facies peak. P-T calculations on the garnet porphyroblasts indicate formation at slightly higher pressures (up to 7.5 kbar) than those estimated for the granulite-facies event. This overprint can also be observed in the orthogneiss with the development of fine-grained garnet (Grt_{II}) which overgrows the granulite-facies minerals. Pressure estimates for this garnet is similar to the porphyroblasts (Grt_{II}) in the felsic granulite; however, calculated temperatures were marginally lower. This could be a product of either local dis-equilibrium or post-peak cation exchange (Fitzsimons and Harley 1994). Moderately higher pressures of around 8.5 kbar, obtained for new garnet overgrowing both the orthopyroxene and coarse grained amphibole (Amp_I) with plagioclase and fine-grained amphibole (Amp_{II}) can be difficult to explain by isobaric cooling from granulite facies conditions. Therefore we assume that the prophyroblastic garnet (Grt_{II}) in felsic granulite as well as garnet and amphibole (Amp_{II}) in mafic granulite signify an amphibolite-facies event.

U-Th age dating of monazite from the matrix of the orthogneiss recorded Neoproterozoic ages of ~820 Ma (Faryad et al. 2015). Neoproterozoic ages are also reported from Ar-Ar dating of mica (Faryad et al. 2015) and K-Ar dating of mica (Andritzky 1971). The dating of mica yielded a range of ages between 920 and 670 Ma, with the younger data in particular likely recording metamorphic cooling ages. Neoproterozoic age data are recorded in both the Sherdarwaza and overlying Welayati Formation. This supports the geological relations; whereby, the Welayati Formation shows no paragenetic evidence for a preceding granulite-facies overprint. Assemblages present in the Welayati Formation are indicative of the staurolite-almandine, and kyanite-almandine-muscovite sub-facies of the amphibolite-facies; conditions equivalent to those seen in the amphibolite-facies overprint in the granulites (Abdullah and Chmyriov 1977; Faryad et al. 2009).

The relations of the fine grained garnet (Grt_{III}) in the felsic granulite and the metamorphic overprint are not clear. Its formation clearly post-dates the garnet porphyroblasts (Grt_{II}) as it can be seen overgrowing these grains (Fig. 3c). Some authors (e.g. Faryad and Hoinkes 2003; Godard 2009; Sarkar and Schenk 2014) have interpreted similar garnet as indicating a distinct higher-pressure metamorphic process; while, others (e.g. Sommer and Kröner 2013) have confined such garnet to a late stage of a singular P-T-t path. If we assume that the garnet belongs to a new metamorphic process, it might relate to Alpine events that resulted in very low-degrees of metamorphism in the Upper Paleozoic series (Mennessier 1976; Abdullah and Chmyriov 1977).

7   Conclusions

The results of this study indicated that the Proterozoic basement rocks of the Kabul Block experienced a polymetamorphic evolution with a granulite-facies metamorphism followed by a subsequent amphibolite-facies overprint. It was also shown that the granulite facies rocks have larger extent then it was previously assumed. They occur within a migmatite and gneiss complex that shows an upwards decreasing degree of migmatization. In addition to small bodies of felsic and mafic granulites and granulite-facies marble, the granulite-facies metamorphism is evidenced in some large orthogneiss bodies. The granulite-facies event is characterized by the presence of orthopyroxene that forms at the expense of biotite and/or amphibole in felsic and mafic lithologies and by olivine and clinohumite in marble. This metamorphism reached peak temperatures of around 850 °C at pressures of ca. 5–7 kbar (Fig. 8). This metamorphism was coincident with the formation of zircon rims that give a Paleoproterozoic age of 1.9–1.8 Ga. The granulite-facies mineral assemblages have been overgrown by amphibolite-facies phases that occurred at lower temperature (around 600 °C) but higher pressures of up to 8.5 kbar

(Fig. 8). The amphibolite-facies overprint likely correlates with the dominant regional metamorphism elsewhere in the Kabul Block. Based on geochronological data, obtained mainly by Ar-Ar methods in micas, this metamorphism occurred during Neoproterozoic period of 0.8–0.9 Ga.
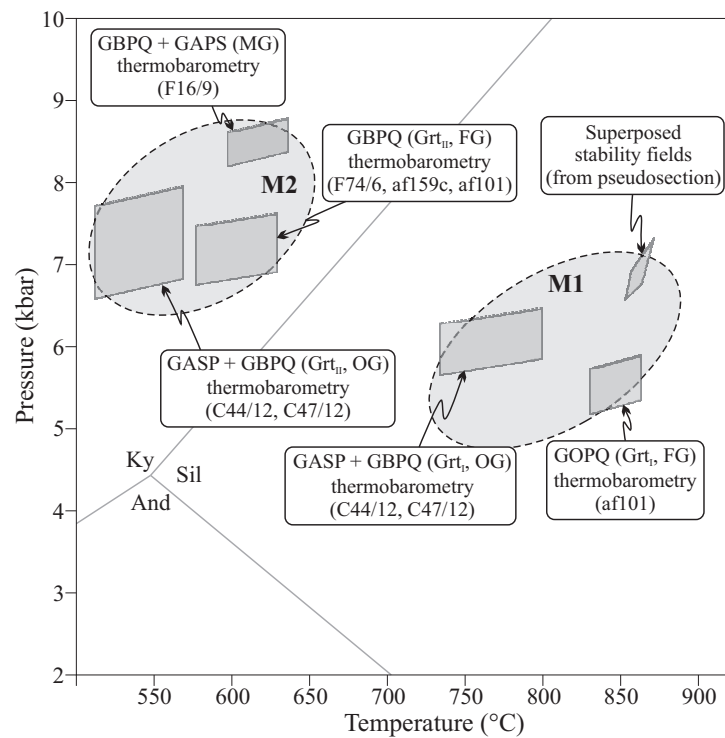
Figure 8: Summary of the P-T results for the different lithologies and the two metamorphic processes. FG: Felsic granulite, MG: Mafic granulite, OG: Orthogneiss. GOPQ: Grt-Opx-Pl-Qtz thermobarometry, GBPQ: Grt-Bt-Pl-Qtz thermobarometry, GASP: Grt-Als-Qtz-Pl barometry, GAPS: Grt-Amp-Pl-Qtz thermobarometry

8   Acknowledgments

Part III

Pressure-temperature evolution of Neoproterozoic metamorphism in the Welayati Formation (Kabul Block), Afghanistan

Stephen Collett[1*] & Shah Wali Faryad[1]

[1]Institute of Petrology and Structural Geology, Charles University, Prague, Albertov 6, 12843 Prague 2, Czech Republic

[*]Corresponding author e-mail: colletts@natur.cuni.cz

Abstract

The Welayati Formation, consisting of alternating layers of mica-schist and quartzite with lenses of amphibolite, unconformably overlies the Neoarchean Sherdarwaza Formation of the Kabul Block that underwent Paleoproterozoic granulite-facies and Neoproterozoic amphibolite-facies metamorphic events. To analyze metamorphic history of the Welayati Formation and its relations to the underlying Sherdarwaza Formation, petrographic study and pressure-temperature (P-T) pseudosection modeling were applied to staurolite- and kyanite-bearing mica-schists, which crop out to the south Kabul City. Prograde metamorphism, identified by inclusion trails and chemical zonation in garnet from the micaschists indicates that the rocks underwent burial from around 6.2 kbar at 525 °C to maximum pressure conditions of around 9.5 kbar at temperatures of around 650 °C. Decompression from peak pressures under isothermal or moderate heating conditions are indicated by formation of biotite and plagioclase porphyroblasts which cross-cut and overgrow the dominant foliation. The lack of sillimanite and/or andalusite suggests that cooling and further decompression occurred in the kyanite stability field. The results of this study indicate a single amphibolite-facies metamorphism that based on P-T conditions and age dating correlates well with the Neoproterozoic metamorphism in the underlying Sherdarwaza Formation. The rocks lack any paragenetic evidence for a preceding granulite-facies overprint or subsequent Paleozoic metamorphism. Owing to the position of the Kabul Block, within the India-Eurasia collision zone, partial replacement of the amphibolite-facies minerals in the micaschist could, in addition to retrogression of the Neoproterozoic metamorphism, relate to deformation associated with the Alpine orogeny.

Keywords

Metamorphism; amphibolite-facies; Neoproterozoic; Kabul Block; Afghanistan.

1   Introduction

The Kabul Block is a tectonic fragment that occurs at the juncture between the Indian and Eurasian continents (Fig 1a). Along with the Farah and Helmand Blocks, it is part of a series of NE-SW aligned terranes that comprise the Afghan Central Blocks. Thick Phanerozoic sedimentary sequences are prevalent in all of the Afghan Central Blocks (Abdullah and Chmyriov, 1977); however, basement rocks are

exposed in the central part of the Kabul Block (Fig 1b). This is thought to be the result of an apparent dome like structure (Andritzky, 1967; Karapetov et al. 1981). The basement rocks are represented by two, three or four superposed units, called the Khair Khana, Sherdarwaza, Kharog and Welayati Formations (Abdullah and Chmyriov, 1977; Karapetov et al. 1981; Bohannon, 2010). Recent results of extensive geochronological dating by U/Pb SHRIMP (zircon), Ar-Ar (micas) and U/Th (monazite) (Faryad et al. 2015) indicate that the oldest rocks, belonging to the Sherdarwaza (or Khair Khana) Formation(s), consist of migmatites with Neoarchean orthogneiss that show a Paleoproterozoic granulite-facies metamorphism. A subsequent Neoproterozoic amphibolite-facies event is recorded throughout both the Sherdarwaza and overlying Welayati Formation. Detailed petrological study by Collett et al. (2015) confirmed the granulite and subsequent amphibolite-facies events in the Khair Khana or Sherdarwaza Formation. However, the relations and degree of metamorphism in the Welayati Formation remains unclear. This is because of differing interpretation regarding the superposition with other formations and the lack of detailed petrological data.

This paper aims to verify metamorphic characteristics of the Welayati Formation and its relations to the polymetamorphic events recorded in the underlying Sherdarwaza Formation. The most prominent and characteristic rock sequences with coarse-grained garnetiferous mica-schists from the Welayati Formation were selected for this study. The samples come from the Chehel Sotoon area (Fig. 1b, c) in the southern part of Kabul City, where both the Sherdarwaza and Welayati formations are exposed. We apply phase-equilibria (pseudosection) modeling in combination with mineral textural relations and major element zonation in garnet to constrain pressure-temperature (P-T) evolution for the Welayati mica-schists. The new data presented here adds to the overall understanding of the tectono-thermal evolution of the Kabul Block as well as examining the utility of phase equilibria modeling to understanding petrographical and mineral-chemical observations.

2 Geological background

The Afghan Central Blocks (the Farah, Helmand and Kabul Blocks, Fig. 1a) form a set of NE-SW aligned crustal fragments that adjoin the Indian and Eurasian continental masses. They are separated from the Eurasian continent by the Herat-Panjshir Suture Zone and Hindu Kush Mountains in the north. To the south east the Katawaz Basin (a flexural basin) and Waziristan ophiolite complex represent the join to the Indian Continent (Treloar and Izatt, 1993). The Kabul Block is separated from the other Afghan Central Blocks by the Chaman fault and it is variably described as the easternmost of the Afghan Central Blocks (Andritzky, 1967; Abdullah and Chmyriov, 1977; Şengör, 1984; Faryad et al. 2015) or as a leading edge of India, detached prior to collision with Eurasia (Tapponnier et al. 1981; Treloar and Izatt, 1993).

Although rare within the other Afghan Central Blocks, high-grade basement rocks crop out in the central part of the Kabul Block. They are overlain by un-metamorphosed to low-grade late Paleozoic to Mesozoic sedimentary sequences (Fesefeldt, 1964; Andritzky, 1967; Fischer, 1971; Abdullah and Chmyriov, 1977). Peridotite sheets underlain by Jurassic volcano-sedimentary melange are thrust onto the sedimentary sequences along both the eastern and western margins of the block (Mennessier, 1976; Abdullah and Chmyriov, 1977). The south of the Kabul Block is intruded by a series of plutonic rocks of Eocene age that continue through the Afghan Central Blocks and eastwards to the Nuristan Block. They are related to continental collision subsequent to oceanic subduction between the Indian and Eurasian plates (Debon et al. 1987; Faryad et al. 2013). Much of the block is covered by a thick layer of unconsolidated Cenozoic sediments (Abdullah and Chmyriov 1977).

The basement rocks, exposed in the hills around Kabul city, are assumed to be the result of a dome-like
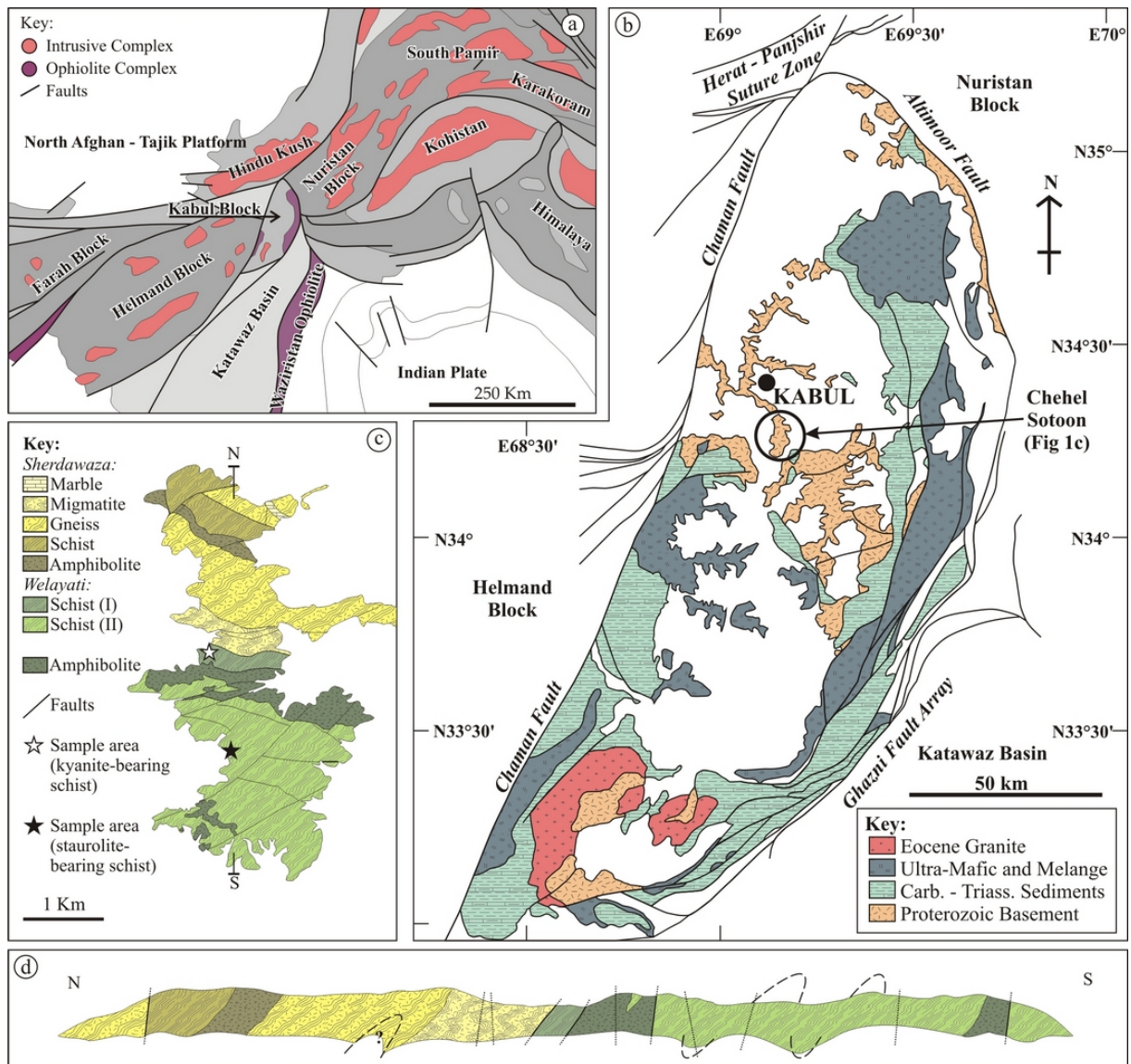
Figure 1: (a) Tectonic Map of the Afghan region after Stöcklin (1977), the Kabul Block is surrounded by the Helmand Block to the west, Hindu Kush Mountains to the North, Nuristan Block to the North-East and Katawaz Basin to the South East. (b) Schematic geological map of the Kabul Block after Kafarsky et al., (1975) and Bohannon and Turner (2005). Proterozoic basement crops out extensively around the Kabul City area. (c) Detailed geological map of the sample area after Karapetov et al., (1981). Welayati micaschist labelled (I) interpreted as belonging to the Kharog Formation by Karapetov et al., (1981); however, here and in geological maps by Kafarsky et al., (1975) and Bohannon (2010) considered part of the Welayati Formation. Stars indicate sample locations of kyanite-bearing schist (white star) and staurolite-bearing schist (black star). (d) Cross-section along boundary of the Sherdarwaza and Welayati Formation adapted from structural data in Karapetov et al (1981) and cross-section of Andritzky (1967).

structure (Andritzky 1967; Karapetov et al. 1981). They are variably classified into two, three, or four formations (the Khair Khana, Sherdarwaza, Kharog, and Welayati) with upward decreasing age and degree of metamorphism (Abdullah and Chmyriov, 1977; Karapetov et al. 1981). Archean age of the granulite-facies Khair Khana rocks in the core of the dome (Karapetov et al. 1981) was recently confirmed by SHRIMP data on zircon (Faryad et al. 2015). The overlying Sherdarwaza Formation with original thickness of approximately 5.5 km is composed predominantly of gneiss and migmatite with minor marble, amphibolite, and quartzite (Abdullah and Chmyriov, 1977; Karapetov et al. 1981; Collett et al. 2015). The rocks are folded isoclinally with fold axes almost vertical or plunging at a high angle towards the south and southeast (Fig 1d). Geochronological data obtained using SHRIMP on zircon, Ar-Ar on mica and U-Th-Pb on monazite (Faryad et al. 2015) indicated Paleoproterozoic and Neoproterozoic ages for granulite and amphibolite-facies metamorphism, respectively. The extent and distribution of the Kharog Formation, is poorly understood. It consists of metaquartzite, schist, gneiss, amphibolite, and marble (Abdullah and Chmyriov, 1977) and was defined based on stratigraphical relations in the Kharog Mountains, south of Kabul. It overlies the Sherdarwaza Formation with an apparent disconformity (but with no pronounced angular unconformity).

The Welayati Formation crops-out to the south and north east of Kabul. It consists of schist at the base, amphibolite in the middle part, and alternating amphibolite and schist at the top. A Neoproterozoic age of metamorphism (800-900 Ma) in the Welayati Formation was recently constrained by Ar-Ar data on mica and U-Th-Pb on Monazite (Faryad et al., 2015). No Paleoproterozoic age was obtained for the Welayati Formation; however, zircon from an amphibolite body, marked on figure 1c, which cuts the Welayati Formation indicated a Paleoproterozoic age of 1.8 Ga (Faryad et al. 2015). According to Abdullah and Chmyriov (1977), the Welayati formation unconformably overlies the Sherdarwaza Formation; however, in the studied area it has tectonic contact with the Sherdarwaza (Kharog?) Formation. The rocks show strong foliation that dips towards the south-southeast at a high angle (Andritzky, 1967, Karapetov et al. 1981).

Samples for this study were collected from the Chehel Sotoon area to the south of Kabul City. They come from an approximately 2 km long area marking the transition from the Sherdarwaza to Welayati Formations (Fig. 1c). North from the amphibolite body is identified by Karapetov et al. (1981) as the Kharog Formation; however, on the geological maps of Kafarsky et al. (1975) and Bohannon (2010) it is interpreted as part of the Welayati Formation. The relations of the amphibolite to the surrounding rocks is not clear, on the different geological maps of Kabul it is regarded variably as part of the Welayati (Bohannon, 2010), or as a separate Precambrian intrusive body (Karapetov et al. 1981). The southern sampling area is universally regarded as part of the Welayati Formation.

3   Sampling and petrography

In total 40 samples of micaschist, amphibolite and quartzite were collected across lithological boundaries along the S-N directed profile near contact with the Sherdarwaza Formation. This area is dominated by the occurrence of garnet-biotite micaschist that alternate with layers or lenses of quartzite and amphibolite. All rock varieties, including amphibolite show E-W trending foliation that steeply plunges to the north or south. The amphibolite consists of amphibole, plagioclase, quartz, and rarely may contain garnet. Detailed petrography is given for relatively well-preserved kyanite-bearing and the staurolite-bearing schists as these contain mineral assemblages suitable for P-T calculations and pseudosection analysis. Mineral assemblages and approximate modal abundances are listed in table 1.

Mineral compositions were analyzed using an electron microprobe at the Institute of Earth Sciences

Table 1: Mineral assemblages and modal abundances of the principal lithologies at Chehel Sotoon. All mineral abbreviations presented in this paper are after Whitney and Evans (2010).

Sample No.	Grt	Ky	St	Qtz	Pl	Bt	Ms	Pg	Rt	Ilm	Ep
Staurolite-bearing micaschist (34°27′30″N 69°10′30″)											
cl4	++		++	+++"	+	+++	+++	+		+"	+"
cl5	++		+++	++"	++	++	+++	+		+"	+"
cl6a	+++	+	+++	++"	+	+++"	+++	+		+"	+"
cl7	+++		++	+++"	++	+++"	+++	+		+"	+"
Kyanite-bearing micaschist (34°28′15″N 69°10′45″)											
C31-12	++	++		+++"	++	+++"	++		+"	+"	+"
C33-12	+++	+++		+++"	++	++"	+++		+"	+"	+"
C36-12	++	+++		++"	+++	+++"	+		+"	+"	+"

+++, abundant; ++, moderate; +, rare; ", inclusion in garnet

of the University of Graz, which is equipped with wavelength- and energy-dispersive spectrometers. Standards were pyrope (Mg, Al), adularia (K), rutile (Ti), tephroite (Mn), jadeite (Na, Si), and andradite (Fe, Ca). Na and F were measured with a Microspec wavelength-dispersive spectrometer, and operating conditions were 15 kV and 10 or 15 nA, with 20 s counting time on peak and 10 s on each background. Supplementary data was collected using EDX-SEM analysis at Charles University in Prague. Representative mineral analyses of garnet, staurolite, biotite, white mica, and plagioclase are given in tables 2-6.

Staurolite-bearing schist

Four samples (cl4, cl5, cl6a, cl7) of staurolite-bearing schist from the southern portion of the study area were analyzed for textural and compositional relations among minerals. The samples are characterized by the presence of garnet (Fig. 2a) and staurolite (Fig. 2b) porphyroblasts wrapped by a continuous foliation defined by white mica and minor biotite (Bt_I). The matrix is dominated by quartz with accessory amounts of apatite, ilmenite, monazite, and zircon. Porphyroblasts of plagioclase and biotite (Bt_{II}) are observed overgrowing the foliation (Figs. 2c, d). Epidote is present exclusively as an inclusion phase in garnet and replacing plagioclase.

The staurolite grains are often poikiloblastic, with inclusions consisting almost exclusively of quartz and ilmenite and show little or no orientation. Compositionally the staurolite shows little chemical variation, with consistent Fe-rich compositions (X_{Fe} = 0.78 - 0.82) and up to 0.07 a.f.u. Ti and 0.05 a.f.u. Zn.

Garnet porphyroblasts are up to 5 mm in diameter and exhibit well defined textural (Fig. 2a) and compositional (Figs. 3a-e, 4a) core and rim relationships. The cores of the garnet grains are typically rich in inclusions of quartz, ilmenite, apatite, and epidote. The inclusions show orientation roughly perpendicular to the main foliation and a small rotational component. Chemically the cores are rich in Mn and Ca, with a composition corresponding to approximately $Alm_{69}Sps_7Prp_4Grs_{20}$. Moving away from the core the Mn concentrations decrease rapidly, compensated by a rise in Fe, while both Mg and Ca remain relatively flat (Fig. 4a). In contrast, the rim portions of garnets are usually inclusion poor and characterized by a strong increase in Mg, and decrease in Ca concentrations. Compositionally, the rim corresponds to roughly $Alm_{76}Sps_{<1}Prp_{18}Grs_6$. A spike or annulus in Y content approximately 300 μm wide is observed occurring at the very rim of the garnet grains (Fig. 3e).

The main foliation is defined by elongate, tabular grains of muscovite and paragonite. The muscovite has low ferro-magnesian (FeO + MgO) contents (up to 0.42 a.f.u.), Al^{VI} of around 1.80 a.f.u. and

Table 2: Representative analyses of garnet composition from the Welayati micaschists, Fe^{3+} estimated based on the scheme of Droop (1987).

	cl4 core	cl4 rim	cl5 core	cl5 rim	cl6a core	cl6a rim	cl7 core	cl7 rim	C31/12 core	C31/12 rim	C33/12 core	C33/12 rim	C36/12 core	C36/12 rim
SiO_2	37.31	37.34	37.30	37.44	37.45	37.55	36.71	37.24	37.36	37.87	36.45	38.04	37.42	37.82
TiO_2	0.08	0.04	0.05	0.01	0.08	0.02	0.00	0.00	0.06	0.01	0.09	0.00	0.12	0.08
Al_2O_3	21.00	21.20	20.77	21.42	20.70	21.26	20.87	21.24	21.18	21.44	20.93	21.67	20.9	21.22
FeO	31.52	34.57	30.46	34.25	30.42	34.08	30.63	34.73	29.91	31.35	29.72	31.64	29.58	31.65
MnO	2.86	0.03	3.34	0.04	2.91	0.02	3.29	0.15	2.54	0.16	2.62	0.09	3.51	0.11
MgO	1.02	4.25	1.10	4.67	1.02	4.56	0.85	4.43	1.12	4.91	1.05	5.02	1.06	4.80
CaO	6.42	2.64	6.94	2.28	7.49	2.47	7.52	2.26	7.81	4.00	8.53	3.66	7.49	4.16
Total	100.21	100.07	99.96	100.11	100.07	99.96	99.87	100.05	99.98	99.74	99.39	100.12	100.08	99.84
Si	3.003	2.978	3.007	2.977	3.013	2.989	2.972	2.971	2.998	2.997	2.955	2.995	3.007	2.994
Ti	0.005	0.002	0.003	0.001	0.005	0.001	0.000	0.000	0.004	0.001	0.005	0.000	0.007	0.005
Al	1.993	1.995	1.975	2.008	1.964	1.996	1.994	2.000	2.004	2.000	2.003	2.012	1.980	1.982
Fe^{3+}	0.000	0.022	0.014	0.013	0.016	0.013	0.031	0.026	0.000	0.002	0.033	0.000	0.005	0.017
Fe^{2+}	2.123	2.284	2.040	2.265	2.030	2.256	2.043	2.292	2.015	2.073	1.982	2.091	1.983	2.079
Mn	0.195	0.002	0.228	0.003	0.198	0.001	0.226	0.010	0.173	0.011	0.180	0.006	0.239	0.007
Mg	0.122	0.505	0.132	0.553	0.122	0.541	0.103	0.527	0.134	0.579	0.127	0.589	0.127	0.567
Ca	0.554	0.226	0.599	0.194	0.646	0.211	0.652	0.193	0.671	0.339	0.741	0.309	0.645	0.353
Total	7.996	8.014	7.998	8.014	7.994	8.007	8.020	8.019	7.998	8.002	8.026	8.002	7.994	8.004
X_{Mg}	0.05	0.18	0.06	0.20	0.06	0.19	0.05	0.19	0.06	0.22	0.06	0.22	0.06	0.21
Andr	0.00	1.11	0.70	0.64	0.83	0.64	1.54	1.29	0.00	0.11	1.66	0.00	0.24	0.85
Alm	70.85	75.39	67.81	74.79	67.45	74.80	67.01	75.42	67.32	69.00	64.54	69.82	66.04	69.04
Sps	6.52	0.07	7.65	0.09	6.68	0.05	7.59	0.34	5.77	0.36	6.09	0.20	8.03	0.25
Prp	4.10	16.97	4.43	18.59	4.12	18.10	3.45	17.73	4.48	19.33	4.29	19.67	4.27	18.93
Grs	18.53	6.46	19.41	5.89	20.92	6.41	20.41	5.21	22.44	11.21	23.41	10.31	21.43	10.93

Table 3: Representative staurolite analyses

	cl4	cl4	cl5	cl5	cl6a	cl6a	cl7	cl7
	core	rim	core	rim	core	rim	core	rim
SiO_2	26.60	26.84	28.19	28.26	28.31	27.99	28.41	28.73
TiO_2	0.64	0.68	0.61	0.52	0.59	0.49	0.69	0.67
Al_2O_3	53.22	53.22	51.43	51.59	51.75	51.93	51.43	51.93
FeO	13.79	13.80	14.07	13.96	13.65	13.64	13.58	13.44
MnO	0.01	0.04	0.03	0.01	0.00	0.06	0.08	0.02
MgO	1.65	1.55	2.13	1.88	1.81	1.84	1.83	1.68
CaO	0.00	0.00	0.03	0.04	0.03	0.03	0.01	0.06
Na_2O	0.00	0.00	0.00	0.01	0.01	0.00	0.00	0.03
ZnO	0.30	0.33	0.22	0.25	0.39	0.48	0.33	0.17
Total	96.21	96.46	96.74	96.54	96.64	96.51	96.35	96.73
Si	3.766	3.789	3.967	3.981	3.981	3.945	4.004	4.023
Ti	0.068	0.073	0.064	0.056	0.062	0.052	0.073	0.071
Al	8.879	8.855	8.531	8.566	8.577	8.628	8.544	8.570
Fe^{2+}	1.633	1.629	1.656	1.645	1.606	1.608	1.600	1.574
Mn	0.001	0.005	0.004	0.001	0.000	0.007	0.010	0.002
Mg	0.347	0.327	0.447	0.396	0.380	0.386	0.384	0.351
Ca	0.000	0.000	0.004	0.006	0.004	0.005	0.001	0.009
Na	0.000	0.000	0.000	0.002	0.004	0.000	0.000	0.007
Zn	0.032	0.034	0.023	0.026	0.041	0.050	0.034	0.017
Total	14.726	14.711	14.701	14.680	14.665	14.686	14.651	14.625
X_{Fe}	0.811	0.817	0.777	0.796	0.792	0.784	0.789	0.809

Table 4: Representative biotite analyses, (Bt_I) indicates foliated biotite, (Bt_{II}) indicates porphyroblastic biotite.

	cl4	cl4	cl5	cl5	cl6a	cl6a	cl7	cl7	C31/12	C31/12	C33/12	C33/12	C36/12	C36/12
	Bt_I	Bt_{II}	Bt_I	Bt_{II}	Bt_I	Bt_{II}	Bt_I	Bt_{II}	Bt_I	Bt_{II}	Bt_I	Bt_{II}	Bt_I	Bt_{II}
SiO_2	36.39	36.95	37.19	37.60	37.14	37.12	35.78	37.44	37.51	37.88	37.51	37.53	37.54	37.54
TiO_2	1.56	1.59	1.54	1.54	1.56	1.58	1.41	1.45	1.63	1.62	1.64	1.67	1.64	1.67
Al_2O_3	18.40	19.40	17.32	19.04	17.86	19.44	18.38	18.36	18.11	18.98	17.80	19.14	17.97	19.06
FeO	16.28	14.52	16.51	14.33	15.99	14.32	17.40	15.22	14.67	13.72	14.78	13.55	14.68	13.53
MnO	0.08	0.03	0.12	0.04	0.12	0.00	0.17	0.03	0.05	0.08	0.14	0.17	0.08	0.06
MgO	13.00	13.15	12.79	12.85	12.88	13.00	12.89	12.82	13.32	13.24	13.04	13.06	13.09	12.97
CaO	0.21	0.22	0.06	0.09	0.09	0.00	0.00	0.00	0.05	0.00	0.06	0.08	0.05	0.06
Na_2O	0.45	0.41	0.42	0.36	0.19	0.29	0.24	0.29	0.29	0.21	0.17	0.29	0.34	0.18
K_2O	8.84	9.08	9.04	9.30	9.26	9.32	8.74	9.08	9.16	9.45	9.38	9.40	9.24	9.43
BaO	0.09	0.15	0.00	0.00	0.00	0.00	0.00	0.00	0.11	0.08	0.00	0.00	0.16	0.24
Total	95.31	95.50	94.98	95.15	95.09	95.07	95.00	94.68	94.89	95.27	94.51	94.89	94.79	94.73
Si	5.444	5.461	5.584	5.561	5.556	5.497	5.396	5.586	5.580	5.582	5.611	5.552	5.598	5.567
Ti	0.176	0.177	0.174	0.171	0.176	0.176	0.160	0.163	0.182	0.180	0.185	0.186	0.184	0.186
Al^{IV}	2.556	2.539	2.416	2.439	2.444	2.503	2.604	2.414	2.420	2.418	2.389	2.448	2.402	2.433
Al^{VI}	0.688	0.841	0.650	0.880	0.704	0.890	0.663	0.815	0.756	0.878	0.749	0.889	0.757	0.900
Fe	2.037	1.795	2.073	1.772	2.001	1.774	2.195	1.899	1.825	1.691	1.848	1.676	1.831	1.678
Mn	0.010	0.004	0.015	0.005	0.015	0.000	0.022	0.004	0.006	0.010	0.018	0.021	0.010	0.008
Mg	2.900	2.897	2.862	2.835	2.872	2.869	2.897	2.851	2.954	2.908	2.908	2.880	2.910	2.867
Ca	0.033	0.035	0.009	0.015	0.014	0.000	0.000	0.000	0.009	0.000	0.009	0.013	0.009	0.010
Na	0.130	0.118	0.121	0.105	0.055	0.082	0.070	0.084	0.084	0.060	0.050	0.082	0.098	0.052
K	1.687	1.712	1.731	1.755	1.767	1.761	1.682	1.727	1.738	1.777	1.789	1.774	1.757	1.784
Ba	0.005	0.009	0.000	0.000	0.000	0.000	0.000	0.000	0.006	0.005	0.000	0.000	0.009	0.014
Total	19.666	19.587	19.635	19.538	19.605	19.553	19.687	19.542	19.561	19.509	19.555	19.521	19.566	19.498
X_{Mg}	0.587	0.617	0.580	0.615	0.589	0.618	0.569	0.600	0.618	0.632	0.611	0.632	0.614	0.631

Table 5: Representative white mica analyses

	cl4	cl4	cl5	cl5	cl6a	cl6a	cl7	cl7	C31/12	C33/12	C36/12
	Ms	Pg	Ms	Pg	Ms	Pg	Ms	Pg	Ms	Ms	Ms
SiO_2	46.04	47.16	47.33	46.76	46.74	47.44	47.30	47.37	46.24	46.33	46.37
TiO_2	0.53	0.15	0.49	0.12	0.62	0.15	0.51	0.16	0.34	0.5	0.51
Al_2O_3	36.20	38.75	34.13	38.34	34.9	38.98	34.49	38.21	33.97	34.04	34.07
FeO	1.33	0.86	2.31	0.70	1.82	0.86	1.96	0.78	1.87	1.94	1.94
MnO	0.00	0.06	0.05	0.00	0.09	0.06	0.02	0.00	0.06	0.00	0.03
MgO	0.86	0.07	0.82	0.00	0.39	0.07	0.82	0.04	0.85	0.94	0.94
CaO	0.03	0.44	0.07	0.34	0.08	0.44	0.02	0.45	0.12	0.08	0.09
Na_2O	2.09	5.94	2.25	7.64	2.37	5.97	2.70	6.56	1.12	1.43	1.43
K_2O	7.95	1.31	7.73	1.19	7.57	1.31	7.47	1.36	9.66	9.41	9.41
BaO	0.19	0.00	0.00	0.00	0.00	0.00	0.00	0.00	0.21	0.00	0.24
Total	95.23	94.73	95.19	95.09	94.58	95.28	95.28	94.93	94.44	94.67	95.02
Si	6.084	6.068	6.268	6.029	6.213	6.068	6.245	6.096	6.226	6.211	6.207
Ti	0.053	0.015	0.049	0.012	0.062	0.014	0.051	0.015	0.035	0.050	0.051
Al^{IV}	1.916	1.932	1.732	1.971	1.787	1.932	1.755	1.904	1.774	1.789	1.793
Al^{VI}	3.722	3.944	3.595	3.857	3.681	3.945	3.613	3.892	3.617	3.591	3.582
Fe	0.147	0.092	0.256	0.076	0.202	0.092	0.216	0.084	0.210	0.218	0.217
Mn	0.000	0.007	0.006	0.000	0.010	0.007	0.002	0.000	0.007	0.000	0.003
Mg	0.169	0.013	0.162	0.000	0.077	0.013	0.161	0.007	0.170	0.188	0.187
Ca	0.004	0.060	0.010	0.047	0.011	0.060	0.002	0.062	0.017	0.011	0.012
Na	0.536	1.482	0.578	1.911	0.611	1.481	0.692	1.638	0.293	0.372	0.371
K	1.341	0.215	1.305	0.195	1.283	0.214	1.257	0.224	1.660	1.609	1.607
Ba	0.010	0.000	0.000	0.000	0.000	0.000	0.000	0.000	0.011	0.000	0.012
Total	17.982	17.827	17.961	18.098	17.938	17.826	17.995	17.922	18.020	18.039	18.044
X_{Fe}	0.465	0.877	0.612	1.000	0.724	0.873	0.573	0.918	0.554	0.537	0.537
Na/Na+K	0.285	0.874	0.307	0.907	0.322	0.874	0.355	0.880	0.150	0.188	0.188
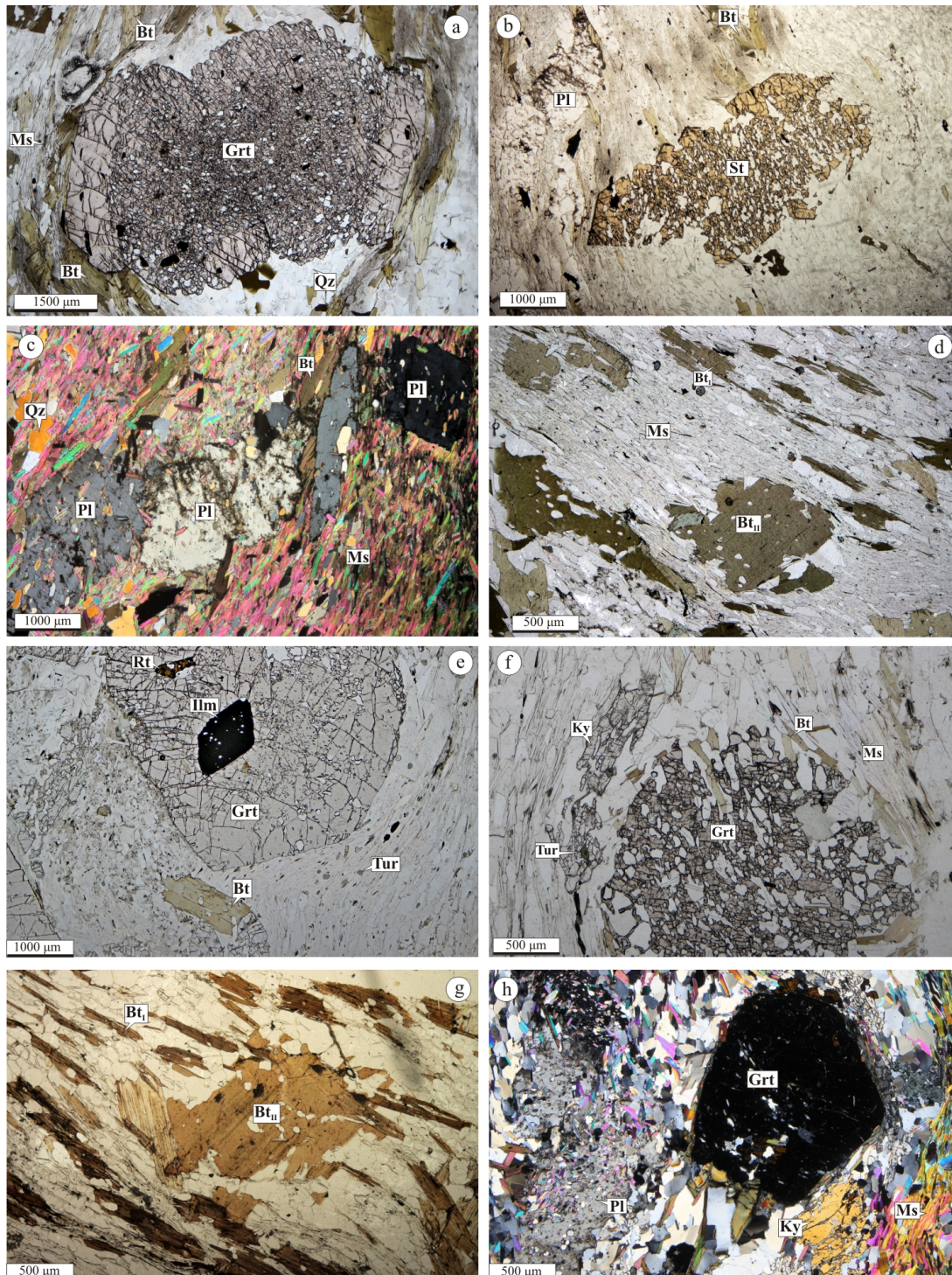
Figure 2: Photomicrographs of the staurolite-bearing (a-d) and kyanite-bearing (e-h) micaschists. (a) Garnet porphyroblast with an inclusion rich core, wrapped by foliation of biotite, muscovite, paragonite and quartz (cl5). (b) Highly poikiolitic staurolite grain with inclusions of quartz and minor ilmenite (cl7). (c) Plagioclase porphyroblasts overgrowing the main, white mica rich foliation (cl7). (d) Biotite porphyroblast growing opposed to the main foliation (cl6a). (e) Inclusions of rutile and ilmenite in garnet porphyroblast, small green rounded tourmaline grains to the bottom right of the garnet (C33/12). (f) Skeletal garnet grain wrapped by a continuous foliation including muscovite, biotite, and kyanite (C31/12). (g) Biotite porphyroblast (Bt$_{II}$) overgrowing the main foliation defined by elongate biotite (Bt$_I$) and minor muscovite (C36/12). (h) Garnet porphyroblast wrapped by continuous foliation of muscovite and kyanite, highly irregular and inclusion rich plagioclase to the left of the garnet (C33/12).
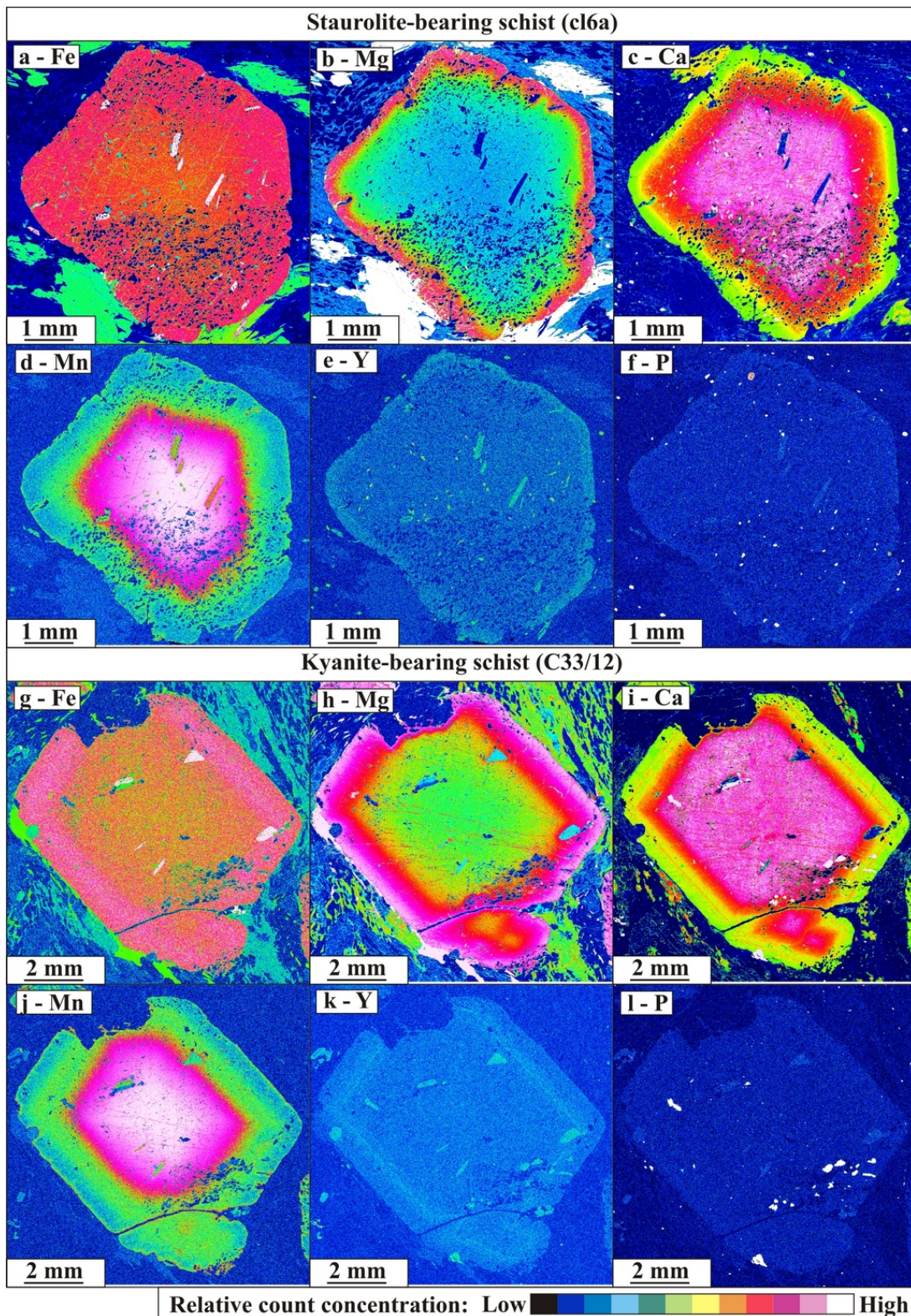
Figure 3: Compositional maps of garnet from the staurolite-bearing (a-f, cl6a) and kyanite- bearing (g-l, C33/12) micaschist calculated using the electron microprobe. The color scale of relative counts is not comparable between images.

Table 6: Representative feldspar analyses

	cl4	cl5	cl6a	cl7	C31/12	C33/12	C36/12
SiO_2	64.57	64.11	63.64	63.87	60.45	60.48	61.13
TiO_2	0.00	0.10	0.00	0.00	0.00	0.00	0.00
Al_2O_3	22.32	22.40	22.89	22.14	24.63	25.12	24.50
Fe_2O_3	0.00	0.00	0.05	0.08	0.11	0.07	0.09
Mn_2O_3	0.08	0.00	0.00	0.05	0.04	0.01	0.00
CaO	3.88	3.91	4.11	4.01	6.28	6.12	5.91
Na_2O	9.19	9.62	9.22	9.51	8.23	8.26	8.35
K_2O	0.06	0.04	0.14	0.03	0.09	0.04	0.04
BaO	0.04	0.00	0.00	0.06	0.04	0.00	0.02
Total	100.13	100.18	100.03	99.75	99.87	100.11	100.04
Si	2.841	2.825	2.810	2.830	2.696	2.687	2.715
Al	0.000	0.003	0.000	0.000	0.000	0.000	0.000
Ti	1.158	1.164	1.191	1.156	1.295	1.316	1.283
Fe	0.000	0.000	0.002	0.003	0.004	0.003	0.003
Mn	0.003	0.000	0.000	0.002	0.002	0.000	0.000
Ca	0.183	0.185	0.194	0.190	0.300	0.292	0.281
Na	0.784	0.822	0.789	0.817	0.712	0.711	0.719
K	0.003	0.002	0.008	0.002	0.005	0.002	0.002
Ba	0.001	0.000	0.000	0.001	0.001	0.000	0.000
Total	4.973	5.002	4.993	5.001	5.015	5.011	5.004
An	18.84	18.30	19.60	18.87	29.51	29.01	28.06
Ab	80.82	81.46	79.61	80.94	69.99	70.77	71.71
Or	0.34	0.24	0.79	0.19	0.50	0.23	0.23
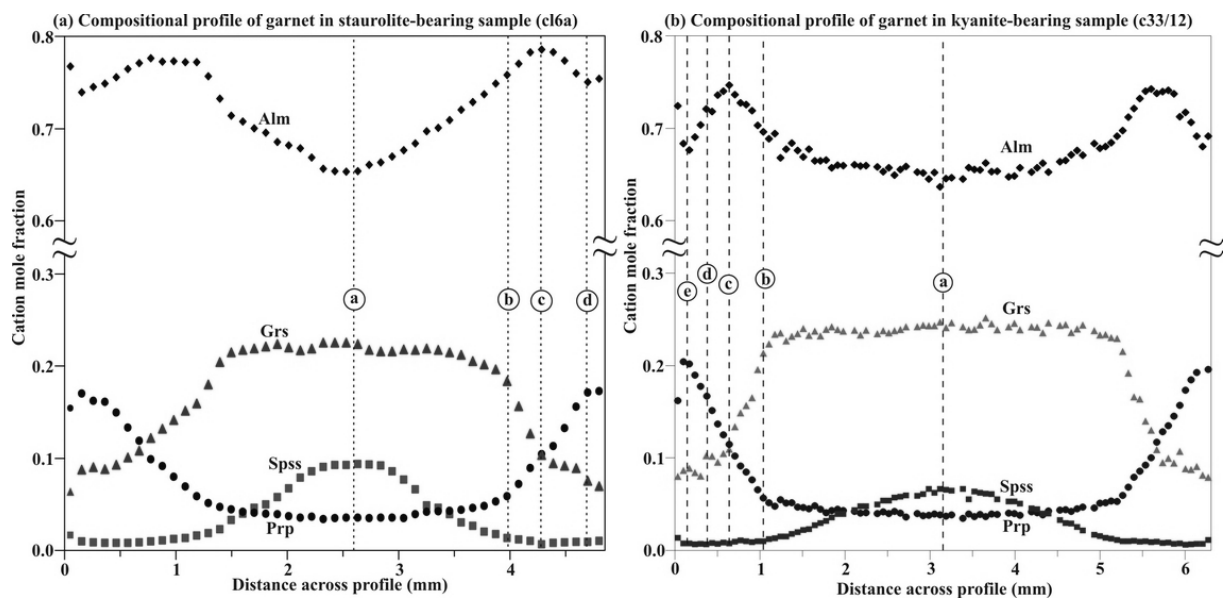
Figure 4: Compositional profiles through garnet porphyroblasts mapped in Fig. 3. Circled letters correspond to the compositional isopleth intersections used to reconstruct prograde growth history in Fig 5 b, d.

Na/(Na+K) of 0.28 - 0.36. Paragonite has FeO + MgO < 0.11 a.f.u. Al^{VI} of up to 1.98 a.f.u. and Na/(Na+K) of 0.85 - 0.91.

Biotite occurs within the foliation (Bt_I) and as tabular porphyroblasts (Bt_{II}) cross-cutting the main foliation and overgrowing muscovite. Compositionally both varieties of biotite exhibit similar Ti concentrations (0.16-0.18 a.f.u.), X_{Mg} ratios vary slightly from ~0.58 in the foliated grains to ~0.62 in the porphyroblastic grains; and they differ significantly in Al^{VI} components with ~0.65 a.f.u. in the foliated grains (Bt_I) and up to 0.90 a.f.u. in the porphyroblastic grains (Bt_{II}).

The plagioclase porphyroblasts occur as xenomorphous growths that contain inclusions of paragonite, muscovite, and quartz. Unlike the garnet porphyroblasts where the main foliation wraps around the porphyroblastic grains (Fig. 2a), the foliation is continuous either side of the plagioclase and biotite porphyroblasts (Figs 2c, d). Compositionally the plagioclase is oligoclase (An_{17-21}) and exhibits little chemical variation.

Kyanite is usually absent from these samples, but one sub-idiomorphic grain is observed in sample cl6a.

Kyanite-bearing schist

Three samples of kyanite-bearing schist were selected for detailed study; these consist of porphyroblastic garnet and kyanite wrapped by a continuous foliation defined predominantly by white mica (C33-12) or biotite (C31-12, C36-12). The matrix consists of quartz and plagioclase with accessory amounts of rutile, ilmenite, apatite and tourmaline.

Garnet porphyroblasts are up to 6 mm in diameter, are sub-idiomorphic, and poikiolitic (Figs. 2e, f), inclusions are mostly micro grains of quartz but also include epidote and larger (up to 0.5 mm across) ilmenite and rutile (Fig. 2e). The inclusions have an alignment approximately perpendicular to the main foliation and show some evidence for rotation. Compositionally the garnet exhibits similar chemical zonation to that recorded in the staurolite-bearing schist with a Ca and Mn rich core and rimwards enrichment in Mg (Figs. 3g-l, 4b). The composition of the core is approximately $Alm_{66}Sps_7Prp_4Grs_{23}$, moving rimwards Mn content drops rapidly compensated by small increases in Mg and Fe. Ca levels are relatively stable throughout the core of the garnet grains before dropping rapidly towards the rim, where the garnet has an approximate composition of $Alm_{70}Sps_{<1}Prp_{19}Grs_{11}$. A slight spike in Ca content can be observed in the garnet compositional map (Fig. 3i) approximately 400 μm from the rim of the grain. This spike in Ca occurs in close proximity to an approximately 100μm wide annulus in Y content (Fig. 3k).

Kyanite forms as elongate grains often mantled by muscovite, and can be seen to follow the foliation around garnet grains (fig. 2f).

Muscovite along with biotite defines the main foliation. The muscovite has Si content of up to 6.22 a.f.u., Al^{IV} up to 1.80 a.f.u., low ferro-magnesium levels (Fe + Mg $\approx$ 0.40 a.f.u.) and low Na/(Na+K) ratios (~0.18). Two varieties of biotite are observed, as elongate grains with the long axis parallel to the main foliation (Bt_I), and as tabular porphyroblasts (Bt_{II}) seen to cut or overgrow the white mica (Fig. 2g). Foliated biotite has an X_{Mg} ratio of 0.59 - 0.63 and Ti up to 0.19 a.f.u. As in the staurolite-bearing schist the porphyroblastic grains differ most prominently from the foliated grains in Al^{VI} component, ~0.70 a.f.u. and ~0.90 a.f.u. in the foliated and porphyroblastic grains respectively.

Plagioclase forms as highly irregular grains, which overgrows the main foliation and contains abundant inclusions of muscovite and minor quartz and epidote (Fig. 2h). Plagioclase is more calcic (An_{24-32}) than in the staurolite-bearing schist samples.

Rutile is observed as both inclusions in garnet and within the matrix and is often intergrown with or enclosed by ilmenite.

4   Thermo-barometry and phase diagram modeling

In order to constrain P-T conditions conventional geothermobarometry, multi-equilibrium reaction analysis and phase equilibria (pseudosection) modeling were combined. The multi-equilibrium reaction analysis was carried out using THERMOCALC v.3.33 and thermodynamic dataset ds55 (Powell and Holland, 1988; Holland and Powell, 1998; updated to August, 2004) in avPT mode. End-member activities for phases considered in the reactions were calculated using the software AX (Holland, 2014). Following the methodology of Dale and Holland (2003) if the fit indices exceeded the maximum allowable value for 95 % confidence then the most suspect end-member activity was removed from the system before re-running the calculation. Pressures and temperatures calculated using this approach were then checked against conventional geothermobarometers between mineral pairs. Temperature was estimated using the garnet-biotite (GB) thermometer of Holdaway (2000), calculating at pressures estimated from the avPT calculations. Pressures were checked against the garnet-Al_2SiO_5-silica-plagioclase (GASP) barometer of Koziol (1989). The results of the avPT calculations and conventional geothermobarometry are presented in Table 7.

P-T pseudosections were created using the Perple_X software packages (Connolly, 2005) and the thermodynamic data file hp04ver.dat (Holland and Powell, 1998; updated to August, 2004). Modeling was carried out in the 11 component system MnO-Na_2O-CaO-K_2O-FeO-MgO-Al_2O_3-SiO_2-H_2O-TiO_2-O_2 (MnNCKFMASHTO) considering the solid solution models for: silicate melt (Holland and Powell, 2001; White et al., 2001; White et al., 2007); chlorite (Holland et al., 1998); feldspar (Fuhrman and Lindsley, 1988); garnet (White et al. 2005); biotite and ilmenite (White et al. 2000); white mica and chloritoid (Smye et al. 2010); and cordierite, epidote, and staurolite (Holland and Powell, 1998). Chemical compositions used in these calculations were analyzed using wet chemical techniques at the Laboratories of the Geological Institutes at Charles University in Prague. Proportional adjustments were made to account for major elements in accessory phases (e.g. CaO in apatite). Fe^{3+}, recast as O_2 in the model system, was set below the stability of magnetite (calculated on T-X(O_2) diagrams) because ilmenite is present as the only oxide indicating highly reducing conditions. The fluid phase was set to be in excess with an activity of H_2O (aH_2O) set to 1.

AvPT calculations

The AvPT conditions were calculated for the staurolite-bearing micaschist (samples cl4, cl5, cl6a, and cl7) with the assemblage of Grt-St-Bt-Ms-Pg-Pl-Qtz-H_2O. As kyanite is present in sample cl6a it was additionally considered in the calculation. Ilmenite and the spessartine end-member of garnet were not considered in the calculations owing to them being the only Ti- and Mn- bearing phases respectively. The calculated temperatures range between 615-628 °C with a standard deviation of approximately 20 °C. These values are marginally higher but within error of those estimated using the garnet-biotite thermometer of Holdaway (2000), which yielded temperatures of 604-620 °C (± 25 °C). Pressure estimates for each of the samples were consistent at 8.7-8.8 kbar but show significant uncertainty with a standard deviation of up to 1.1 kbar. As kyanite is only present in sample cl6a, the GASP barometer of Koziol (1989) was only applied to this sample, this predicted pressure conditions similar to the avPT calculations of 8.8 kbar (± 0.5 kbar).

Table 7: Results of conventional geothermobarometry and multi-equilibrium reaction analysis

Sample	Calculation Assemblage	GB[a] (°C)	T (°C)	1σ	GASP[b] (kbar)	P (kbar)	1σ	Corr.	Sig. Fit.	Reactions*
Staurolite-bearing micaschist										
cl4	Grt, St, Bt, Ms, Pg, Pl, Qtz, H_2O	605	617	20	n/a	8.7	1.0	0.848	0.54	1, 2, 3, 4, 6, 7, 8, 9
cl5	Grt, St, Bt, Ms, Pg, Pl, Qtz, H_2O	611	615	20	n/a	8.7	1.0	0.862	0.61	1, 2, 5, 6, 9, 10
cl6a	Grt, St, Bt, Ms, Pg, Pl, Ky, Qtz, H_2O	604	628	16	8.8	8.8	0.9	0.685	0.88	1, 2, 3, 4, 11, 15, 16, 17
cl7	Grt, St, Bt, Ms, Pg, Pl, Qtz, H_2O	620	621	22	n/a	8.8	1.1	0.874	0.33	1, 2, 12, 13, 14
Kyanite-bearing micaschist										
C31/12	Grt, Bt, Ms, Pl, Ky, Ilm, Rt, Qtz, H_2O	622	648	15	9.1	9.3	0.8	0.798	0.92	3, 4, 15, 17, 18, 19, 20
C33/12	Grt, Bt, Ms, Pl, Ky, Ilm, Rt, Qtz, H_2O	626	641	19	9.3	9.0	1.1	0.790	0.81	3, 4, 15, 17, 18, 19, 20
C36/12	Grt, Bt, Ms, Pl, Ky, Ilm, Rt, Qtz, H_2O	620	642	17	9.1	9.3	1.0	0.845	0.55	5, 11, 15, 16, 21

[a]: Holdaway (2000), [b]: Koziol (1989)

*(1) 23Grs + 6Mst + 48Qtz = 8Prp + 69An + 12H_2O; (2) 23Grs + 6Fst + 48Qtz = 8Alm + 69An + 12H_2O; (3) Ms + 2Phl + 6Qtz = Prp + Ms + Cel; (4) 2Eas + 6Qtz = Prp + 3Cel; (5) 3East + 6Qtz = Prp + 2Ms + Phl; (6) 23Eas + 2Mst + 62Qtz = 18Prp + 23Ms + 4H_2O; (7) Ms + 2Ann + 6Qtz = Alm + 3Fcel; (8) 23Fcel + 4Fst = 13Alm + 23Ms + 14Qtz + 8H_2O; (9) 22Phl + 12Ab + 6Mst = 20Prp + 7Ms + 12Pg + 15Eas; (10) Ann + 3An = Grs + Alm + Ms; (11) Prp + Ann = Alm + Phl; (12) Phl + 3An = Prp + Grs + Ms; (13) Ann + 3An = Grs + Alm + Ms; (14) 17Phl + 12Ab + 6Mst = 25Prp + 17Ms + 12Pg; (15) Grs + Qtz + 2Ky = 3An; (16) Pg + 3An = Grs + Ab + 3Ky + H_2O; (17) 3Cel + 4Ky = Prp + 3Ms + 4Qtz; (18) Ann + Qtz + 2Ky = Alm + Ms; (19) Alm + 3Rt = 3Ilm + 2Qtz + Ky; (20) Prp + Ms + Pg = Phl + Ab + 3Ky + H_2O; (21) Phl + Qtz + 2Ky = Prp + Ms

For the samples of kyanite-bearing micaschist (C31/12, C33/12, and C36/12) an assemblage of Grt-Bt-Ms-Pl-Ky-Ilm-Rt-H_2O was considered and spessartine end-member was ignored as the only Mn-bearing phase. Temperatures estimated using the AvPT method were 641-648 °C for the three samples with uncertainties of up to 19 °C. These values are slightly higher than those estimated using the garnet-biotite thermometer (Holdaway, 2000) which yielded a range of 620-626 °C (± 25 °C). The avPT calculations yielded pressures of 9.0-9.3 kbar with a maximum uncertainty of 1.1 kbar, these values compare favorably to those estimated using the GASP barometer (Koziol, 1989), which yielded pressures of 9.1-9.3 kbar (± 0.5 kbar).

Pseudosection modeling

Pseudosections were constructed for both the staurolite-bearing (cl6a) and kyanite-bearing (C33/12) micaschist, the results of the pseudosection modeling are presented in Fig. 5. The general topology of the two pseudosections is broadly similar with first garnet, then staurolite, plagioclase, and finally alumino-silicate stabilizing at progressively higher temperatures. Pressure variations are characterized by the transition from ilmenite to rutile stability. Compositional isopleths for the pyrope, grossular, and spessartine components in garnet are provided for both pseudosections (Fig 5b, d). An approximation of the prograde evolution of the samples is made by matching the calculated compositional isopleths to segments on the measured garnet compositional profiles as highlighted by the circled letters (Figs. 4 & 5b, d).

Staurolite-bearing schist (cl6a)

In the staurolite-bearing schist the garnet-in reaction occurs at around 460 °C at the higher pressure limit of the diagram, increasing to 545 °C at the lower pressure bound, while staurolite is stable within a zone of approximately 550 to 640 °C and up to 9.5 kbar. The core composition of the garnet (approximately $Sps_7Prp_4Grs_{21}$) intersects at around 530 °C and 6.3 kbar, in close proximity to the garnet-in reaction. From here the proposed P-T path is steep and clockwise, passing the staurolite-in/chlorite-out reactions and reaching the kyanite stability field at intersect of the garnet rim compositional isopleths. The isopleths for the garnet rim composition (~$Sps_{<1}Prp_{18}Grs_7$) intersect at around 640 °C and 8.4 kbar, moderately higher temperature conditions than those estimated using conventional geothermobarometry and multi-equilibrium reaction analysis.

Kyanite-bearing schist (C33/12)

The inferred peak assemblage in the kyanite-bearing schist [Grt-Bt-Ms-Pl-Ky-Rt-Ilm-Qtz] occurs in a zone in excess of 645 °C and 8 kbar up to the solidus. The garnet-in reaction occurs between 480 and 530 °C with varying pressure. The intersection of the compositional isopleths for the garnet core (approximately $Sps_8Prp_4Grs_{24}$) occurs at around 520 °C and 6.1 kbar, close to both the biotite-in and epidote-out reactions. A notable difference between the two samples is that biotite is stabilized at higher temperatures than in the kyanite-bearing schist. This sample is more aluminous which Tinkham et al. (2001) showed reduces biotite stability relative to chlorite. As was the case in the staurolite-bearing schist, the initial part of the prograde path involves significant pressure increase, before flattening out as it approaches T_{Max}. The inferred prograde path largely passes above the upper pressure limit (~9.2 kbar) of the staurolite stability field. The garnet rim composition (~$Sps_{<1}Prp_{20}Grs_{10}$) intersects at around 670 °C and 8.8 kbar, within the stability field of the inferred peak assemblage, but at significantly higher temperature than that predicted using the conventional methods.
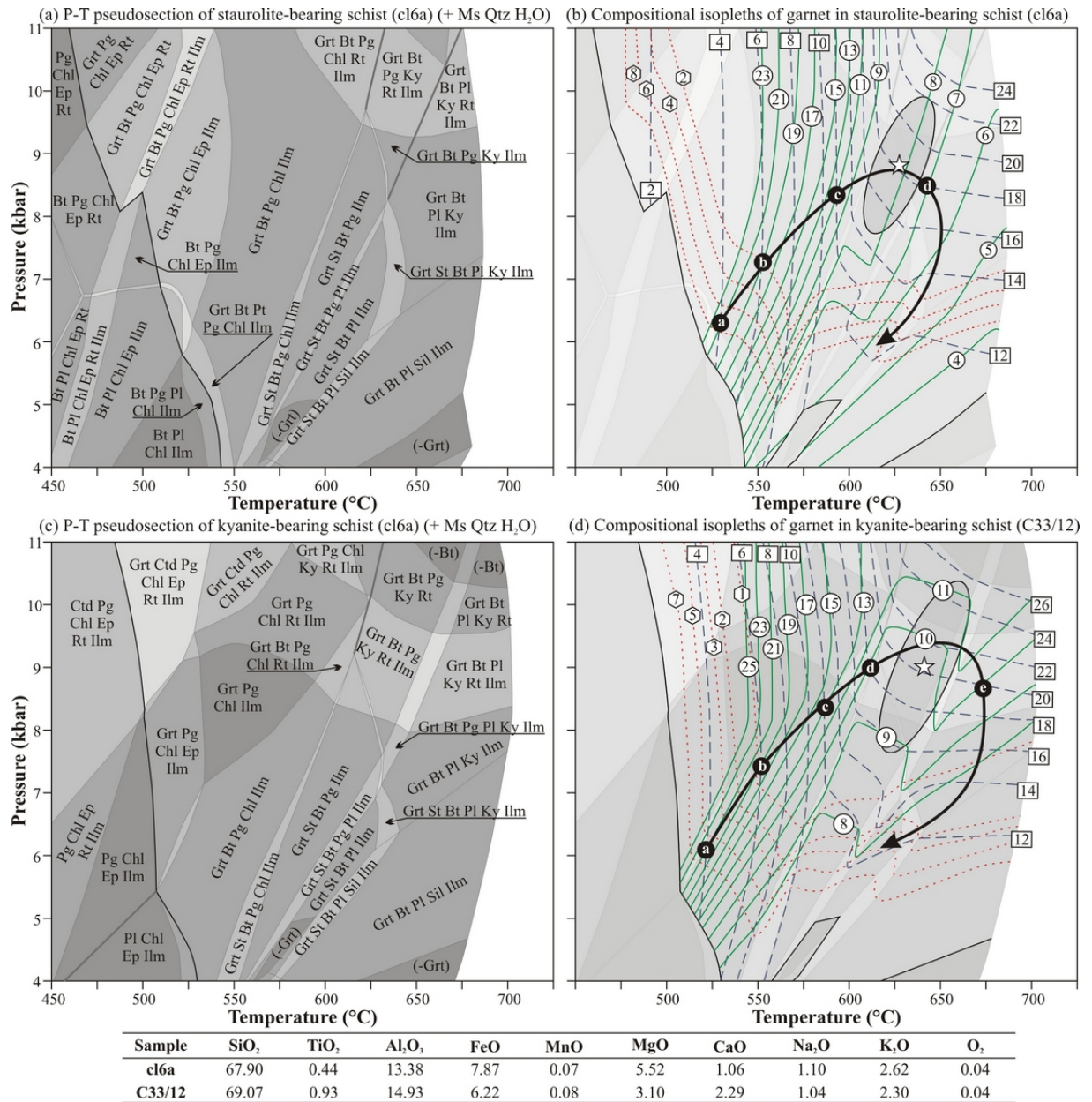
Figure 5: Pseudosection analysis for samples cl6a (staurolite-bearing schist) and C33/12 (kyanite bearing schist. Supra-solidus regions are not shown for clarity. Compositional isopleths of spessartine (short dashed red lines, values in hexagons), pyrope (long dashed blue lines, values in rectangles), and grossular (solid green lines, values in circles) plotted in b and d. Stars in b and d represent the results of avPT calculations and ellipses the 1σ P-T uncertainties. Garnet compositions from Fig. 4 used to draw an approximate P-T path based on intersection marked by circled letters. Compositions used in the calculations are given in mol %.

Formation of biotite and plagioclase porphyroblasts

A striking feature of both varieties of mica-schist is the presence of biotite and plagioclase porphyro-blasts which cross-cut and overgrows the matrix phases (Figs. 2c, d, g, h). These porphyroblasts clearly overprint the dominant foliation and suggest that they formed at a late stage in the metamorphic evolution. Plagioclase is stabilized in both the staurolite- and kyanite-bearing micaschists at approximately 560 °C at 4 kbar increasing to over 670 °C at 11 kbar (Fig. 5). Calculated modal abundances of biotite and plagioclase (Fig. 6) indicate that both phases become increasingly abundant with decreasing pressure from peak conditions. This suggests that in order to stabilize plagioclase and biotite the rocks must have undergone decompression from peak pressures either isothermally or with a small heating component. This decompression path can be partly constrained in the kyanite-bearing schist by the lack of sillimanite; considering an isothermal decompression path, had decompression from peak conditions exceeded 2 kbar the rocks would pass into the stability field of sillimanite.
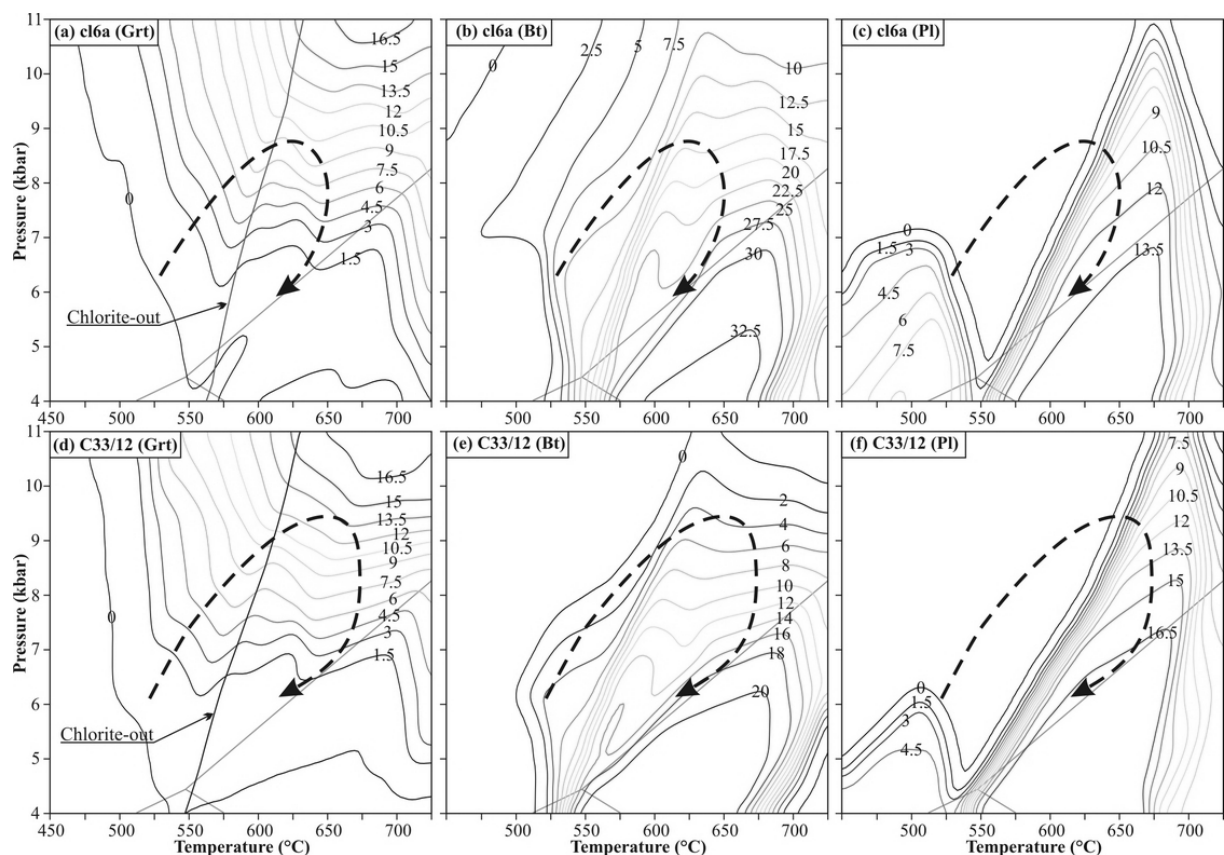
Figure 6: Modal abundances of garnet (a, d), biotite (b, e), and plagioclase (c, f) calculated from the pseudosection analysis for the staurolite- (a, b, c) and kyanite-bearing (d, e, f) micaschists. Arrows indicate inferred P-T path based on chemical zoning in garnet and textural relations.

5   Discussion

Metamorphic PT path of the Welayati micaschists

Textural and compositional relations among minerals were used to constrain metamorphic history of the Welayati Formation of the Kabul Block. The P-T paths have a clockwise sense with T_{Max} reached during decompression. Geotherms for 66 °C kbar^{-1}, 75 °C kbar^{-1}, and 100°C kbar^{-1} are given in Fig.

7. The inferred P-T path is bracketed by the two colder geotherms, suggesting that during prograde metamorphism the geotherm evolved from 75 °C kbar-1 towards 66 °C kbar-1 before inflecting back to the hotter geotherm prior to reaching T_{Max}.
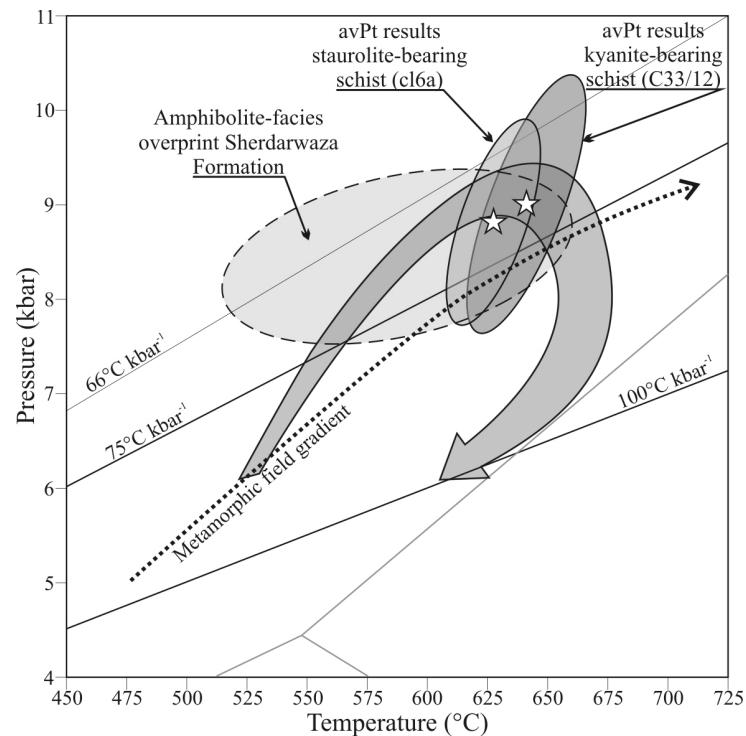
Figure 7: Amalgamated results of this study with the proposed P-T paths for staurolite-bearing and kyanite-bearing micaschist of the Welayati Formation from the Chehel Sotoon area of Kabul. Stars represent the results of avPT calculations and ellipses the 1σ P-T uncertainties. The dashed ellipse corresponds to conditions for the amphibolite-facies overprint calculated in the Sherdarwaza Formation (Collett et al., 2015). Geotherms are drawn as straight lines that go through the origin.

The prograde stage is defined by inclusion trails and chemical zoning in garnet, which shows a rimward decrease of Mn and Ca, and increase of Mg. Maximum pressure conditions of approximately 9.5 kbar are constrained in kyanite-bearing samples through GASP barometry and by multi-equilibrium reaction analysis. T_{Max} occurs on the decompression path, and is constrained by multi-equilibrium reaction analyses to around 620-650 °C. Slightly higher temperatures (up to 675 °C) are estimated from pseudosection analysis. Garnet has a high modal abundance in the samples (up to 10%) and this discrepancy may be a result of a fractionating bulk composition. However, pseudosection analysis is considered to have an approximate uncertainty of around 25 °C and 0.5 kbar (Waters and Lovegrove, 2002; Powell and Holland, 2008), and given the uncertainties associated with the multi-equilibrium reaction analysis as well the minero-chemical data, these values are considered within error of one another.

Further constraint on the P-T paths of this metamorphism can be inferred by the occurrence of biotite and plagioclase porphyroblasts which cross-cut and overgrow the foliation. Predicted modal abundances of biotite and plagioclase computed from the pseudosection analysis (Fig. 6) indicates that decompression after peak pressures likely occurred under near isothermal conditions or under slightly heating conditions. It is assumed that the continuous breakdown of matrix phyllosilicates and garnet during decompression results in the growth of biotite and plagioclase around pre-existing or newly formed nuclei (Jamieson and O'Beirne-Ryan, 1991). This is also indicated by a slight decrease of Mg at the most rim part of garnet accompanied by an increase of Mn as a result of back diffusion during partial consumption of garnet. The absence of sillimanite suggests that further decompression was associated

with cooling that occurred within the kyanite stability field.

In addition to major component zoning in garnet, important information regarding P-T path of the Welayati rocks can be deduced from yttrium (Y) annuli, observed near garnet rims in both varieties of micaschist. A relatively wide (~ 300 μm) annulus occurs at the very rim of garnet in the staurolite-bearing schist (Fig. 3e) and a thinner (~ 100 μm) annulus, but about 400 μm from the garnet rim is present in the kyanite-bearing schist (Fig. 3k). Annuli of Y and other trace elements towards the rims of garnet are fairly common in metapelitic rocks of garnet, staurolite, sillimanite and migmatite zones. Several mechanisms are proposed for the occurrence of rimwards Y annuli, these include: (1) the break-down and/or growth of trace element rich minerals such as monazite, allanite, zircon, and apatite (e.g. Hickmott and Spear, 1992; Chernoff and Carlson, 1999; Yang and Pattison, 2006; Konrad-Schmolke et al., 2008); (2) consumption and regrowth of garnet at temperatures higher than those of the staurolite zone (e.g. Pyle and Spear, 1999; Kohn and Malloy, 2004); and (3) changes in reaction kinetics (e.g. Lanzirotti, 1995; Moore et al. 2013).

In the Welayati micaschists, the Y-annuli are developed in inclusion-free rims that coincide well with the chlorite-out reaction at 550-600 °C (Fig. 5). In the staurolite-bearing sample, the chlorite-out reaction occurs just below the peak modal abundance of garnet (Fig. 6a) and the corresponding annular occurs at the rim of garnet. In the kyanite-bearing sample, where the Y annular occurs ~ 400 μm from the garnet rim, estimated garnet modal abundance at the chlorite-out reaction is roughly 10 mol % (Fig. 6d). However, garnet abundance at peak conditions is estimated to be up to 13.5 mol %, indicating continued garnet growth after the chlorite-out reaction. Textural relations indicate that initial garnet growth should have been suitably rapid in order to trap abundant inclusions within the core of the grains (Fig. 2a), while the relatively inclusion poor rim could signify a relaxation in this growth rate. As Y is strongly compatible with garnet (Hickmott et al. 1987; Hickmott and Spear, 1992; Schwandt et al. 1996), any decrease in the garnet growth rate is likely to result in enrichment of yttrium at the garnet growth interface. Considering the coincidence of the Y-annuli with the chlorite-out reaction this could signify that a relaxation of the garnet rate occurred as a result of changes to the predominant garnet-forming reaction beyond the chlorite stability field, and this relaxation in the garnet growth rate led to the formation of the Y-rich annuli.

Tectonic implications

The results of our petrological study indicate that both kyanite- and staurolite-bearing micaschists are similar in lithology and underwent a single amphibolite-facies metamorphism with retrogression in greenschist-facies conditions. Therefore, consistent with Kafarsky et al. (1975), we interpret the kyanite-bearing micaschist north of the amphibolite body as part of the Welayati Formation. We observed no paragenetic evidence of older (granulite-facies) metamorphism as seen in the Sherdarwaza Formation (Collett et al. 2015). Similarly, the amphibolite body exposed in the study area (Fig. 1c) does not contain a granulite-facies precursor assemblage (Faryad et al. 2015). It is not clear if the Paleoproterozoic U-Pb age of ~1850 Ma, obtained for zircon in amphibole gneiss within the amphibolite body (Faryad et al. 2015), comes from detrital zircon or if the amphibolite represents a tectonic slice of the Sherdarwaza Formation which was tectonically imbricated within the soft kyanite-staurolite schists. Regardless of these unclear relations, the boundary between the Sherdarwaza and Welayati Formations represents a tectonic zone (Fig. 1d), where rocks from the two formations are imbricated with each other.

The calculated P-T conditions for the Welayati Formation (Fig. 7) are comparable to the amphibolite-facies overprint recorded in the Sherdarwaza (Collett et al., 2015). This supports the interpretation that

both the Paleoproterozoic basement of the Sherdarwaza Formation and overlying volcano-sedimentary sequences of the Welayati Formation (Abdullah and Chmyriov, 1977; Karapetov et al., 1981) underwent a common Neoproterozoic amphibolite-facies metamorphism (Faryad et al., 2015). A Neoproterozoic age of around 820 Ma for this metamorphism was obtained by U-Th-Pb method in monazite from both the Sherdarwaza and Welayati Formations, and comparable ages were also obtained using Ar-Ar method on white mica and biotite (Faryad et al., 2015). As mentioned before, the amphibolite-facies minerals in the micaschist are usually replaced into greenschist-facies assemblages. Although part of this mineral transformation could occur during retrogression, an Alpine overprint is not excluded as very low-grade to greenschist-facies conditions are reported from some Permian and Triassic sediments (Mennessier, 1977; Bohannon, 2010). The lack of evidence for Pan-African orogeny within the basement formations would support the proposed link of Kabul and adjacent Afghan Central blocks to the Eurasian blocks (North Afghan-Tajik Platform) from which they were separated by the Hindu Kush Ocean during Paleozoic time (Şengör, 1984; Boulin, 1991; Faryad et al. 2015). Owing to a lack of precise data regarding metamorphism and geochronology from other basement units in Afghanistan, their correlation with the Kabul Block is difficult. Proterozoic and Archean rocks are known from north of the Herat-Panjshir Suture Zone, notably the South Badakhshan Block is assumed to be Archean in age (Khoreva et al. 1971; Abdullah and Chmyriov, 1977) with amphibolite to granulite-facies metamorphic rocks (Faryad, 1999, 2002). However, on the geological map of Kafarsky et al. (1975) Precambrian rocks are scarce south of the Eurasia-Afghan suture (Herat-Panjshir Suture Zone) and those that are known are poorly studied.

6   Conclusions

This paper presents the first modern petrological study of the Proterozoic Welayati Formation of the Kabul Block, Afghanistan. Detailed study of mineral-textural relations, combined with thermodynamic modeling and conventional geothermobarometry, was applied to kyanite- and staurolite-bearing micaschistst. The results show that the Welayati Formation underwent amphibolite-facies metamorphism of early- to mid-Neoproterozoic age. This metamorphism reached pressure and temperature conditions of up to 9.5 kbar and 650 °C and had a clockwise sense. The P-T conditions are consistent with Neoproterozoic metamorphic overprint of the underlying, granulite-facies, Sherdarwaza Formation. The Welayati rocks show mineral transformation that occurred under low-grade conditions and relate either to retrogression of the Neoproterozoic event or to an Alpine metamorphic overprint, known in the Late Paleozoic-Triassic sedimentary sequences. However, no evidence for Pre-Alpine metamorphic overprint (e.g. of Pan-African or Variscan age) was observed in the Welayati Formation.

7   Acknowledgments

Part IV

The Kabul Block (Afghanistan), a segment of the Columbia Supercontinent, with a Neoproterozoic metamorphic overprint

Shah Wali Faryad[a], Stephen Collett[a], Fritz Finger[b], Sergey A. Sergeev[c], Renata Čopjaková[d], Pavol Siman[e]

[a] Institute of Petrology and Structural Geology, Charles University, Albertov 6, 14328 Prague, Czech Republic

[b] Department of Materials Science and Physics, University of Salzburg, Hellbrunnerstraße 34, A-5020 Salzburg, Austria

[c] Centre of Isotopic Research, VSEGEI, 74 Sredny prospect, 199106 St. Petersburg, Russia

[d] Department of Geological Sciences, Masaryk University, Kotlářská 267/2, Brno, Czech Republic

[e] Geological Institute, Slovak Academy of Sciences, Dúbravská cesta 9, Bratislava, Slovak Republic

Highlights

- Neoarchean age was confirmed for the Kabul Block in Afghanistan.

- The basement rocks show two metamorphisms in granulite and amphibolite facies.

- Paleo- and Neoproterozoic ages were obtained for the two metamorphic events.

Abstract

We report field relationships, petrography and isotopic ages from two superposed basement units of the Kabul Block, the so called Lower Sherdarwaza and Upper Welayati formations. The Sherdarwaza Formation is represented mostly by migmatites and gneisses that are derived from pelitic and psammitic lithologies with lenses and layers of mafic and carbonate rocks. Several bodies of orthogneisses are also exposed in the Sherdarwaza Formation. The Upper Welayati Formation is characterized by micaschist, quartzite and amphibolites. SHRIMP U–Pb data on zircon from the orthogneiss in the Sherdarwaza Formation indicates a Neoarchean age of ca 2.5–2.8 Ga for their magmatic crystallization. The rocks exhibit granulite facies conditions of 5–7 kbar and 800 °C that are documented by the presence of orthopyroxene and Ti-rich biotite in the orthogneiss and by olivine and phlogopite in some calc-silicate rocks at contact with marble. A Paleoproterozoic age of ca. 1.85–1.80 Ga for this metamorphism was obtained using U-Pb SHRIMP dating on zircon and U-Th dating on monazite. Mineral textural relations also show a younger amphibolite facies metamorphism that is documented in both the Sherdarwaza and Welayati formations. This metamorphism occurred at relatively higher pressure conditions of up to 9 kbar at ca. 650 °C, compared to the granulite facies event. A Neoproterozoic age of ca 0.85–0.9 Ga, for this metamorphism is confirmed by Ar-Ar data on biotite and white mica as well as by U-Th data on monazite. By combining the presented results on the metamorphic petrology, geochronology and geochemistry, we conclude that: (1) The Kabul basement is a fragment of an Archean block (craton); (2) the ca. 1.85–1.8 and 0.9–0.85 Ga metamorphism marks an important orogenic events

for the basement rocks of the Kabul Block which was stabilized during the early Precambrian; (3) the two metamorphic ages correlate well with global-scale orogenies related to the assembly of the Paleoproterozoic Columbia and Neoproterozoic Rodinia supercontinents; (4) based on metamorphic characteristics and ages, the Kabul basement rocks show an affinity to the Neoarchean rocks of the Tarim and/or South China cratons.

Keywords

Kabul Block; Neoarchean orthogneiss; Paleoproterozoic and Neoproterozoic orogenies

1   Introduction

Recent progress in the definition of the Rodinia and Columbia Supercontinents has advanced the understanding of geodynamic processes during the Earth's history which enables correlation between various tectonic fragments and orogenic belts (e.g. Torsvik et al., 1996, Hoffman et al., 1998, Meert, 2002, Rogers and Santosh, 2002, Zhao et al., 2002, Condie, 2003, Pisarevsky et al., 2003, Zhao et al., 2004, Li et al., 2008 and Meert, 2014). Most information comes from the largest and best preserved cratonic relics of these supercontinents; where, sedimentary, magmatic and tectonic processes are well constrained and supported by geochronological and paleomagnetic data. In spite of their importance as paleo-plate-tectonic markers, smaller continental fragments, many of which later became incorporated in to various orogenic belts, are so far hardly included in that research.

The Kabul Block and associated Afghan Central blocks, which occur along the Hindu Kush - Himalayan belt, are an example of such smaller continental fragments. Usually interpreted as the leading edge of Gondwana, the Kabul Block, along with the Lut Block, Alborz, Sanandaj-Sirjan and others, was detached from Gondwana during opening of Neotethys. The blocks subsequently collided with Eurasia during the Late Cretaceous-Early Paleogene (Tapponnier et al., 1981, Treloar and Izatt, 1993 and Stampfli et al., 2002). As the Kabul Block occurs at the triple junction of three continental masses (Eurasia, India, and other fragments of former Gondwana), detailed information about its Precambrian basement is needed to decipher its former connection or relations to the Gondwanan or Eurasian cratons. Such data will also help to test the validity of the two available palaeogeographic models for that region (Stampfli et al., 2002 and Li et al., 2008), about the position and paleogeographical reconstruction of various continental blocks (including: Tarim, North China, South China, and Afghan) during the Cambro-Ordovician period.

In this work we present field, petrological and geochronological data for rocks from the Kabul Block. An Archean age is indicated for the tectonically deeper part of the Kabul Block. Two metamorphic events of late Paleoproterozoic and Neoproterozoic age could be identified. The first metamorphism occurred under granulite - amphibolite facies conditions and the second under amphibolite facies conditions. These two metamorphic events coincide well with those recognized in some Central Asian Archean blocks and allow discussion on the formation of the two supercontinents, Columbia and Rodinia. Based on this data we also discuss the ancestry of the Kabul Block and the other Afghan Central Blocks in relation to Gondwana fragmentation and convergence of continental blocks to the southern margin of Eurasia.

2 Geology

The Afghan Central blocks (the Farah, Helmand and Kabul blocks, Fig. 1b) form a set of continental fragments that occur at the triple junction of the Indian subcontinent (in the southeast), the North Afghan-Tajik Block to the north and the Lut Block in Iran in the west. The Afghan Central blocks are separated from the surrounding tectonic blocks by Palaeozoic and Alpine mountain belts. The border with the Indian subcontinent is represented by the Sulaiman Mountain range, a fold and thrust belt between Afghanistan and Pakistan. The Hindu Kush Mountains, along the Herat and Panjsher suture zones, separate the Afghan Central blocks from the North Afghan-Tajik Block, while the western border with the Lut Block is marked by the East Iran Range.
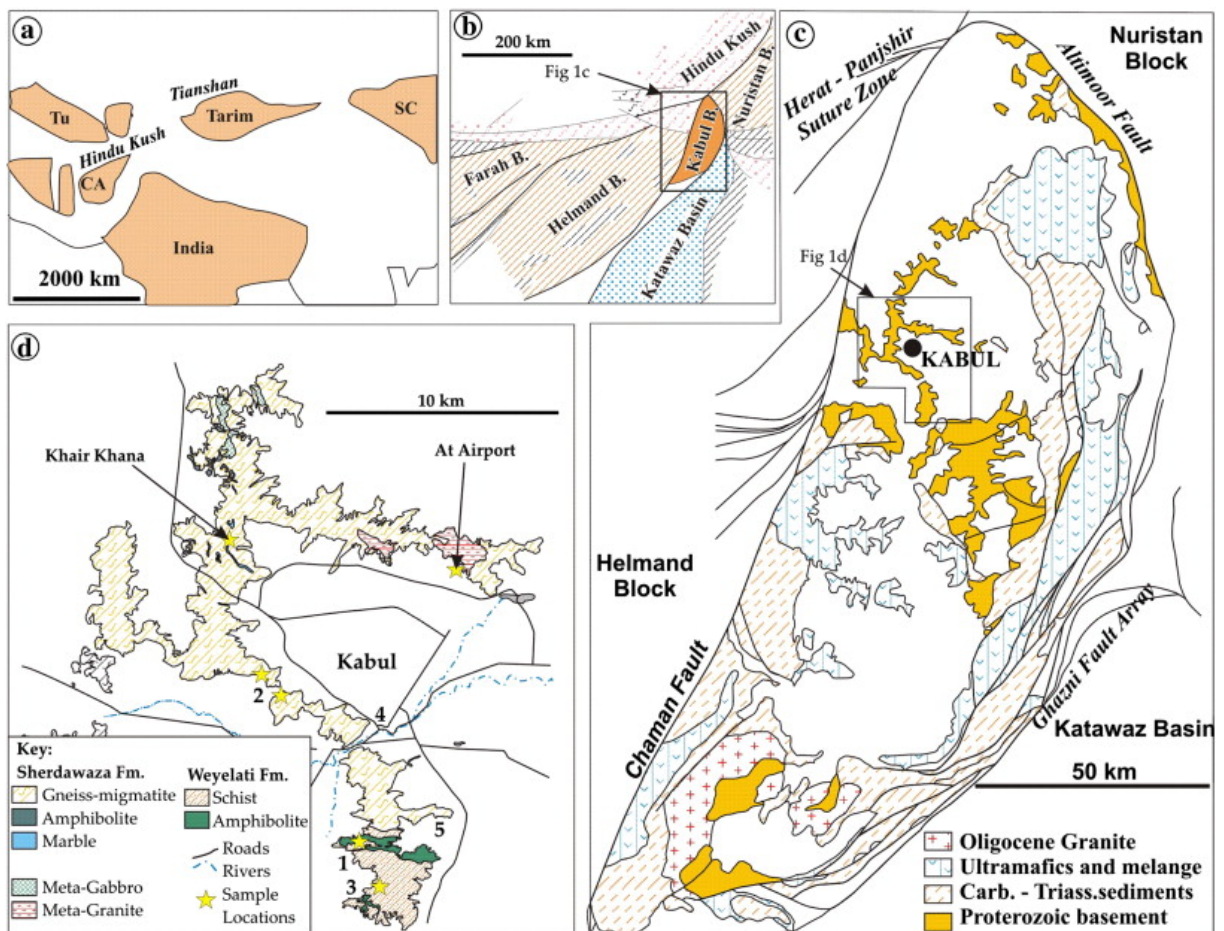
Figure 1: (a) Present position of Precambrian blocks in South Asia and (b) tectonic position of the Afghan Central Blocks (Stöcklin, 1977; Tapponnier et al, 1981 and Boulin, 1988). (c) Schematized geological map of the Kabul Block (Kafarsky et al, 1975). (d) Distribution of Proterozoic basement rocks around Kabul (Karapetov et al, 1981) with location of samples used in this study. Numbers refer to age data used in text.

Whereas the boundary between the Farah and Helmand blocks is poorly defined due to sedimentary cover sequences, the Kabul and Helmand blocks are clearly separated from each other by the Chaman strike slip Fault. Some authors (Tapponnier et al., 1981 and Treloar and Izatt, 1993) consider that the Kabul Block detached from India and collided with Eurasia along the Chaman Fault zone. Others (Andritzky, 1967 and Abdullah and Chmyriov, 1977) interpret the Kabul Block as an eastward continuation of the Afghan Central blocks. The Altimoor and Ghazni fault zones separate the Kabul Block from the Nuristan Block in the northeast and from the Katawaz Basin in the east and southeast (Fig. 1c). The Katawaz Basin is interpreted as a large flexural basin (Treloar and Izatt, 1993) representing the northern

extension of the Makran accretionary complex and therefore as the northwestern continental margin of the Indian plate. In contrast to the Helmand Block, with its thick Paleozoic sedimentary sequences, the Kabul Block exposes high-grade Proterozoic basement units. According to Andritzky (1967), the present position of the Kabul Block is the result of northwards wedge tectonics between the Nuristan and Helmand blocks.

The Kabul Block includes a strongly metamorphosed Proterozoic basement which is overlain by low-grade to un-metamorphosed Late Paleozoic to Cenozoic sequences (Fesefeldt, 1964, Andritzky, 1967, Fischer, 1971, Abdullah and Chmyriov, 1977 and Collett et al., 2015). The Late Paleozoic (Carboniferous–Permian) sequences are represented by phyllites, shales, marbles and meta-conglomerates with various amounts of volcanic material. Large peridotite sheets are thrust onto both the western and the eastern margin of the block (Abdullah and Chmyriov, 1977). According to Tapponnier et al. (1981) these sheets represent ophiolite complexes and the eastern peridotite sheets are a continuation of the Waziristan ophiolite, while those in the south and west are related to the Chaman Fault Zone. The southern part of the Kabul Block is intruded by a series of plutonic rocks of Eocene-Oligocene age that continue through the Afghan Central blocks and eastwards to the Nuristan Block. They are related to continental collision subsequent to oceanic subduction between the Indian and Eurasian plates (Debon et al., 1987). Much of the block is covered by a thick layer of Cenozoic sediments and drift deposits (Abdullah and Chmyriov, 1977).

The Proterozoic basement rocks of the Kabul Block are traditionally subdivided into three formations with upward decreasing age and metamorphic grade; these are the Sherdarwaza, Kharog and Welayati formations respectively (e.g. Abdullah and Chmyriov, 1977). The high-grade rocks of the Sherdarwaza formation are represented by granulite facies orthogneiss and migmatites. The orthogneisses are well exposed in the central part of the block in the Khair Khana Mountains (Andritzky, 1967 and Karapetov et al., 1981) and also in the foothills around Kabul airport (Fig. 1d). According to Karapetov et al. (1981) the granulite facies rocks of the Khair Khana Mountains represent an older, possibly Archean formation underlying the Sherdarwaza Formation. The largest body of orthogneiss, exposed at Kabul airport is indicated as syenite-anorthosite on the geological map of Kabul (Karapetov et al., 1981 and Bohannon, 2010). Neoproterozoic ages of 0.93 – 0.64 Ga, obtained by K-Ar and Ar-Ar dating of biotite from migmatites and schists (Andritzky, 1971 and Faryad et al., 2009) are considered to date the metamorphism of the Sherdarwaza and Khair Khana formations. Paleoproterozoic U-Pb zircon ages in the range of 1.8–2.3 Ga were recently obtained from gneisses and migmatites (Faryad et al., 2009, Bohannon, 2010 and Collett, 2011).

The Kharog Formation was defined based on stratigraphical relations in the Kharog Mountains, south of Kabul. It overlies the Sherdarwaza Formation with an apparent disconformity (but with no pronounced angular unconformity) and consists of metaquarzite crystalline schists, gneisses, amphibolites and marbles (Abdullah and Chmyriov, 1977). Within the study area a thin zone of the Kharog Formation is indicated on the Geological Map of Afghanistan (Karapetov et al., 1981) at the contact between the Sherdarwaza and the Welayati formations. Based on our field and petrological study, the rocks show similar lithology and metamorphic conditions to those exposed in the Welayati Formation.

The Welayati formation is assumed to rest conformably on the Kharog Formation. It includes crystalline schists at the base, amphibolite in the middle part and alternating crystalline schists and amphibolites at the top (Abdullah and Chmyriov, 1977). In one locality out of Kabul, metaconglomerate is reported from the base of the formation.

3   Analytical methods

Major elements were analyzed by wet chemical analyses in the Geological Laboratory at Charles University in Prague. Trace elements were determined using a modified total digestion in mineral acids (HF + HClO$_4$) and borate fusion (Na2CO3 + Na2B4O7) followed by conventional solution nebulisation of ICP-MS Thermo X-Series II. The analytical precision, calculated as one relative standard deviation RSD, ranged from 0.5 to 5 % for most elements. The QA/QC was controlled using the AGV-2 and BCR-2 (USGS) reference materials. Mineral analyses were obtained using a CAMECA SX 50 electron microprobe at the Institute of Mineralogy and Crystal Chemistry, University of Stuttgart, which is equipped with four wavelength-dispersive spectrometers and partly also by using scanning electron microscope at Charles University.

U-Pb zircon geochronological analyses of seven samples from three different rock types and localities (Table 1) were performed at the SIMS SHRIMP-II facility at the Centre of Isotopic Research (CIR) in St. Petersburg, Russia. The results were obtained with a secondary electron multiplier in peak-jumping mode following the procedure described by Williams (1998) and adapted for CIR (e.g. Schuth et al., 2012). Individual corrected ratios and ages are reported with 1y analytical errors (68% confidence), as are the error ellipses presented in the concordia diagrams. Detailed description of the analytical procedure was given in Faryad et al. (2013). Error in TEMORA zircon standard calibration was 0.37%. During the course of this study, the 91500 zircon standard yielded a ^{207}Pb/^{206}Pb age of 1066 ± 5 Ma (n = 8).

Chemical composition of monazite was investigated using a CAMECA SX100 electron microprobe in the wavelength-dispersion mode in Laboratory of the Masaryk University and at University of Salzburg. Operating conditions included an accelerating voltage of 15 kV, a beam current of 120 nA, and a beam diameter of 3 μm. Peak counting times vary from 20 to 220 s in order to optimise detection limits. Uranium was determined on the U Mβ line (counting time 80 s, detection limit 270 ppm), Th on the Th Mα line (counting time 60 s, detection limit 280 ppm) and Pb on the Pb Mα line (counting time 220 s, detection limit 150 ppm). Synthetic and natural phases (U – metallic U, Pb – vanadinite, Th – CaTh(PO$_4$)2, P – LaPO$_4$, Y – YAG, La – LaPO$_4$, Ce – CePO$_4$, Pr – PrPO$_4$, Nd – NdPO$_4$, Sm – SmPO$_4$, Eu - EuPO$_4$, Gd – GdPO$_4$, Dy – DyPO$_4$, Er – YErAG, Al – sanidine, Si – sanidine, Ca – CaTh(PO$_4$)$_2$, Fe – andradite, S – BaSO$_4$, Sr – SrSO$_4$) were used as standards. Data was reduced using the PAP matrix correction routine (Pouchou and Pichoir, 1985). Overlapping of peaks and background positions were carefully tested and chosen using detailed WDS angle scans on natural and synthetic REE-phases. The background model on PbMα according to Jercinovic and Williams (2005) using exponential interpolation was chosen. Concentrations of Pb were additionally manually corrected for YLγ$_2$, ThMζ$_1$ and ThMζ$_2$ overlap on PbMα and concentrations of U were corrected for overlapping with ThMγ. The concentration of Si (and Eu) was calculated by empirical correction for the interference of Nd (Dy respectively) on SiKα (EuLβ respectively). The monazite age was calculated using the method of Montel et al. (1996). Three monazite age-standards of known age (498 Ma, 868 Ma and 1023 Ma) were measured together with studied samples (Table 1).

Ar-Ar analyses were performed by measuring the ^{40}Ar*/^{39}Ar isotopic ratio of mica aggregates at the Central European Ar-Laboratory (CEAL) in Bratislava, equipped with VG 5400 Noble Gas Mass Spectrometer and special own built Ar gas extraction line. Parts of samples were analyzed at Lund University ^{40}Ar/^{39}Ar Geochronology Laboratory (Table 1). It is equipped with a Micromass 5400 Gas Source MS with custom designed UHV gas metal extraction line and a New-Wave Dual-Lase system – CO$_2$ and UV Laser. Step-wise progressive outgassing of the sample was done mostly in 8–10 temperature steps from 610 to 1250 °C. Each separate value on Y axis in the age plot is corresponding to single degassing

of the sample in determined temperature. The details of the method are described by Faryad and Frank (2011).

Mineral abbreviations: am = amphibole, ap = apatite, cc = calcite, do = dolomite, ep = epidote, graph = graphite grt = garnet, ilm = ilmenite, ksp = K-feldspar, ky = kyanite, mnz = monazite, ms = muscovite, ol = olivine, opx = orthopyroxene, pg = paragonite, phl = phlogopite, pl = plagioclase, q = quartz, ru = rutile, sil = sillimanite, st = stuarolite, tnt = titanite, zrn = zircon; garnet: Alm = Fe/(Ca + Fe + Mg + Mn), Prp = Mg/(Ca + Fe + Mg + Mn), Grs = Ca/(Ca + Fe + Mg + Mn), Sps = Mn/(Ca + Fe + Mg + Mn), X_{Mg} = Mg/(Fe + Mg).

4 Petrology and mineral chemistry of basement rocks

The samples, selected for geochronological dating (Table 1) come from the Sherdarwaza and Welayati formations based on the Geological Map of Afghanistan (Kafarsky et al., 1975). From the Sherdarwaza Formation, they include granulite facies orthogneiss (7 samples), calc-silicate marble (2 samples), and migmatites (4 samples). From the Welayati Formation one sample of amphibole gneiss and 3 samples from micaschist were taken.

Granulites facies orthogneisses

A detailed petrography of these granulite facies rocks has recently been reported by Collett et al. (2015). At Kabul airport (Fig. 1d), two orthogneiss bodies (the largest 1 x 3 km in size) are present. They consist of K-feldspar, quartz, plagioclase, biotite, commonly also garnet, ilmenite and rarely sillimanite and rutile. K-feldspar is usually perthitic and plagioclase with antipertite can also be observed in some samples. In addition to porphyroblastic garnet I, which contains inclusions of sillimanite, small grains of garnet II are also present in the matrix. Compared to porphyroblastic garnet (Alm62 -66, Prp30 -33, Grs3 -4), the fine-grained variety has lower pyrope and higher almandine and grossular contents (Alm70 -72, Prp20 -23, Grs5 -7). At least two textural varieties of biotite are present. The first variety with tabular grains has exsolution lamellae of rutile/ilmenite and is rich in Ti = 0.26–0.29 a.f.u. It is overgrown or replaced by a fine-grained biotite with low Ti < 0.15 a.f.u. Both varieties have similar values of X_{Mg} = 0.65–0.66. Plagioclase has composition of An27 -37 and some grains may show albite rich rims with An24. Sillimanite was observed in garnet porphyroblasts as well as in the matrix. Small grains of kyanite were also observed in the matrix. Two samples were selected for SHRIMP dating on zircon and one sample for Th-U-Pb age dating on monazite (Table 1).

The granulite facies orthogneiss at the Khair Khana Mts. (Fig. 1d) are represented mostly by felsic granulite; however, some mafic varieties of diorite or gabbro composition are also present. The granulite facies minerals are orthopyroxene (X_{Mg} = 0.45–0.41), K-feldspar, plagioclase ($An_{29 -40}$), and Ti-rich biotite (X_{Mg} = 45–49, Ti = 0.62 a.f.u.) in the felsic granulite and orthopyroxene (X_{Mg} = 43–47), plagioclase (An_{45-65}), amphibole of potassium pargasite composition (X_{Mg} = 0.32–40) and biotite (X_{Mg} = 0.56–0.59, Ti = 0.48–0.52 a.f.u.) in the mafic variety. Textural relations indicate a medium-pressure amphibolite facies overprint that is characterized by the formation of garnet (Alm_{69-76}, Prp_{11-18}, Grs_{7-9}, Sps_{1-3}), which encloses orthopyroxene and high-Ti biotite in the felsic granulite. It is associated with biotite (X_{Mg} = 0.42–0.50) of lower Ti = 0.35 a.f.u. and plagioclase with An_{8-24}. In the mafic granulite, coronitic garnet (Alm_{67-71}, Prp_{14}, Grs_{11-18}, Sps_{2-4}) with new amphibole at contact between orthopyroxene and plagioclase is present. Four samples of felsic granulite were selected for SHRIMP dating on zircon. Three of

Table 1: Minerals present in the selected samples for age dating using U-Pb (zircon- Zrn), Th-U-Pb (monazite-Mnz) and Ar-Ar (biotite- Bt, phlogopite- Phl and white mica-Wm).

Unit	Sherdarwaza Formation			Khair Khana					Calc silicate		Baghe Bala Migmatites			Welayati Formation			
Locality / Rock	Airport Orthogneiss			Khair Khana					Calc silicate		Baghe Bala Migmatites			Chehel Sotoon Gneiss	micaschists		
Sample	C5-13	C1-13	C44-12	AF59B	AF101	F70-6	AF-59A	AF102	F-6	F15-9	F12-9	F13-9	F14-9	F82-6	CL-5	CL-6	CL-7
Mineral used for age dating	Zrn	Zrn	Mnz	Zrn	Zrn Mnz	Zrn	Zrn	Mnz	Phl	Phl	Bt	Ms	Bt	Zr	Wm	Wm	Wm Bt Mnz
qtz	o	o	o	o	o	o	o	o			o	o	o	o	o	o	o
pl	o	o	o	o	o	o	o	o			o	o	o	o	o	o	o
ksp	o	o	o	o	o	o	o	o			o	o					
grt	o	o	o	o	o		o	o					o*	o	o	o	o
bt	o	o	o	o	o	o	o	o			o	o	o	o	o	o	o
opx					o			o									
st																o	
ky(sil)	o	o													o	o	o
cc			o						o	o							
do									o	o							
phl									o	o							
ms												o			o	o	o
pg									o						o	o	o
am						o				o			o	o			
ol										o							
ep						o*					o**	o		o			
tnt						o											
ap			o			o			o								
ilm	o	o	o	o	o		o	o				o			o	o	o
graph	o	o		o			o										
rt	o											o					

* Accessory, ** forms cluster (replacement product?).

them are free of orthopyroxene (Table 1), one is an orthopyroxene-bearing granulite. One sample from orthopyroxene-bearing granulite was also used for monazite dating.

Granulite facies calc-silicate rocks

The granulite facies calc-silicate rocks at the Khair Khana Mountains contain olivine ($X_{Mg} > 0.96$), clinopyroxene ($X_{Mg} > 97$), phlogopite ($X_{Mg} > 0.97$), pargasitic amphibole ($X_{Mg} > 97$), calcite and dolomite. Olivine is often highly fractured, with the fractures filled by antigorite. The phlogopite is mostly fresh, but commonly shows exsolution needles of rutile and/or ilmenite. Two samples from phlogopite-bearing marble at contact with granulite were chosen for Ar-Ar dating (Table 1).

Migmatites of the Sherdarwaza Formation

Migmatites are the most common basement rocks that are exposed around Kabul. They may contain lenses of amphibolite and locally of marble and are usually associated with micaschists that are formed by retrogression of more pelitic lithologies. The migmatites are characterized by quartz, perthitic K-feldspar, plagioclase and biotite. In some cases they may contain epidote or allanite, amphibole and accessory titanite and ilmenite. The presence of Ca-amphibole or white mica depends on the bulk rock composition, but white mica is usually present in more retrogressed types, where it may replace biotite and feldspar. Garnet is rare and forms idioblastic grains in plagioclase or in the matrix with inclusions of epidote and/or biotite. Three samples were selected for Ar-Ar age dating (location 2 in Fig. 1d and Bagh-e Bala in Table 1). In addition to biotite ($X_{Mg} = 0.58$) and plagioclase (An_{13}), they may contain white mica (sample F13-9) or amphibole of ferro-tschermakite composition (Si = 6.22 a.f.u., $X_{Mg} = 0.4$) and prograde zoning garnet (Alm_{47-58}, Prp_{2-6}, Grs_{35-45}, Sps_{1-5}) (sample F14-9) or epidote ($XAl = (Al-2)/(Al-2 + Fe) = 17–33$ (samples F12-9). The epidote forms a cluster with biotite, which seems to be pseudomorphous after garnet.

Micaschists from the Welayati Formation

The micaschist at Chehel Sotoon (location 3 in Fig. 1d, Table 1) represents a spectacular lithotype that consists of white mica, paragonite, biotite, quartz, plagioclase, and ilmenite, with large porphyroblasts of garnet, staurolite, and rarely of kyanite. Staurolite and garnet form porphyoblasts with inclusions of quartz and ilmenite; garnet may additionally contain epidote-allanite. Garnet (Alm_{66-83}, Prp_{4-19}, Grs_{7-21}, Sps_{1-9}) shows prograde zoning, and staurolite has $X_{Mg} = 19–21$. White mica is rich in $Na_2O = 2.0–2.8$ wt % and biotite has $X_{Mg} = 0.59–0.61$. Notable is the presence of plagioclase, which cuts across or has inclusions of quartz and mica that follow the main foliation. Its anorthite content is between 17 and 21 mol %.

Amphibole gneiss from the Welayati Formation

Amphibolite and amphibole gneiss are exposed within the Welayati micaschist near contact to the Sherdarwaza Formation (location 1 in Fig. 1d). In contrast to the amphibolite, the gneiss is rich in quartz and it is not clear if it represents a leucocratic variety in the amphibolite or represents a mixture of basaltic and sedimentary rocks. It consists of amphibole, garnet, plagioclase, biotite, and small, accessory amounts of epidote and ilmenite, respectively. Amphibole is tschermakite with Si = 6.3 a.f.u. and plagioclase

has anorthite content in the range of 21–28 mol %. Garnet (Alm_{65-68}, Prp_{5-15}, Grs_{16-21}) shows strong compositional zoning with increase of X_{Mg} toward the rims. Spessartine content is below 1 mol %.

5   Geochemistry of the orthogneisses

Major and trace element concentrations of the analyzed samples are given in Table 2. The orthogneisses have variable silica content, (SiO_2 = 59.67–72.86 wt %), and are generally rich in potassium (K_2O = 2.62–4.81 wt %). The samples also show considerable variation in FeO_T (3.60–6.42 wt %) and MgO (1.14–2.16 wt %); but all have a high Mg# in common (40.2 - 50.5). On primitive mantle normalized multi-element spidergram (Fig. 2a), the samples are characterized by enrichment in Rb, Ba, Th and the LREE. They show pronounced negative anomalies in Nb and Ti, as well as a small negative Sr anomaly. On a Chondrite normalized REE plot (Fig. 2b), they exhibit LREE-enrichment with $[La/Yb]_N$ ratios of 12-15 combined with weak negative to weak positive Eu anomalies (Eu* = 0.77–1.21). The chemical features of the orthogneisses are in some ways comparable to late Archean TTG´s (Condie, 2014), in particular regarding their LILE enrichment and the striking depletions in Nb and Ti. However, they do not display the very strong REE fractionation that is characteristic of Archean TTG's (Fig. 2b). Furthermore, many TTG´s have lower K_2O/Na_2O ratios (0.51) and higher Sr/Y ratios (89) than our samples (Condie, 2005a and Condie, 2005b). On the other hand the orthogneisses contrast greatly to typical calc-alkaline suites, as they lack significant depletions in Ba, Sr or Eu. Data for potassic granites (K_2O/Na_2O > 1) from the Tarim Craton (Zhang et al., 2007, Long et al., 2012 and He et al., 2013) show a good fit with the Kabul samples (Fig. 2).
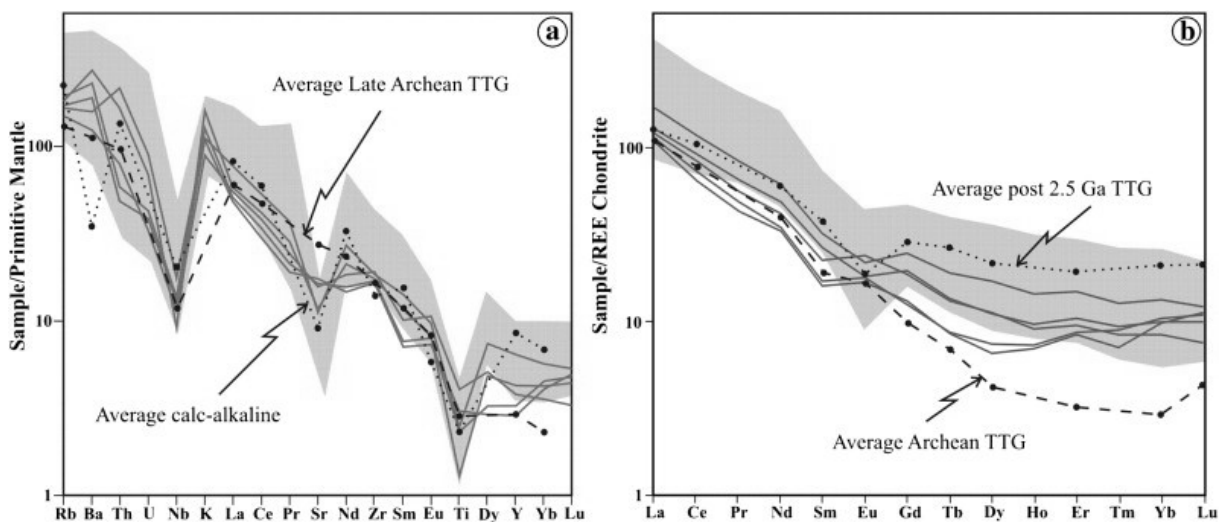
Figure 2: (a) Multi element spidergram normalized to primitive mantle after Sun and Mcdonough (1989). The solid grey lines represent the orthogneiss samples from Kabul, the dashed line is average late Archean TTG, the dotted line average calc-alkaline granite (both after Condie, 2014). The light grey field indicates the range of compositions for potassic granites in the Tarim Craton after He et al., 2013 and Long et al., 2012 and Zhang et al., 2007. (b) REE abundance normalized to chondrite after Nakamura (1974).

Table 2: Geochemical compositions of the studied samples.

Sample	Af159c	Af102	C44-12	C47-12	C3-13
Major elements (in wt. %)					
SiO_2	59.67	66.62	67.96	66.18	72.86
TiO_2	0.66	0.49	0.52	0.87	0.28
Al_2O_3	18.49	15.33	14.95	16.16	13.07
Fe_2O_3	1.04	2.42	1.67	1.23	1.41
FeO	5.48	2.98	4.06	3.77	2.33
MnO	0.1	0.09	0.09	0.06	0.06
MgO	2.07	1.45	1.86	2.16	1.14
CaO	4.26	2.88	1.58	2.23	1.04
Na_2O	3.08	2.52	2.23	2.74	1.76
K_2O	3.32	3.76	3.34	2.67	4.81
P_2O_5	0.27	0.14	0.08	0.06	0.06
Trace elements (in ppm)					
Rb	107.63	118.87	105.37	96.3	112.07
Sr	365.43	344.5	234.5	331.8	242.7
Zr	187.45	191	202.3	212.1	193
Ba	1324.3	1611.4	1089.5	868	1894.7
Y	12.79	14.6	28.85	17.2	19.07
Nb	8.64	9.3	12.3	8	6.5
Pb	67.23	78.42	53.5	25.16	74.06
Th	4.1	4.97	18.32	6.7	13.95
U	0.8	0.88	1.86	0.69	1.43
La	33.46	35.08	52.5	37.48	39.63
Ce	52.17	58.88	94.29	67.97	73.61
Pr	5.23	5.9	10.19	6.84	7.92
Nd	19.9	20.94	36.66	25.06	29.06
Sm	3.13	3.34	6.27	4.41	5.16
Eu	1.23	1.32	1.61	1.77	1.34
Gd	3.41	3.26	6.41	4.85	5.09
Tb	0.4	0.41	0.9	0.62	0.64
Dy	2.11	2.39	5.46	3.64	3.57
Ho	0.5	0.52	1.03	0.65	0.69
Er	1.75	1.81	3.12	1.99	2.17
Tm	0.23	0.29	0.41	0.27	0.3
Yb	2.04	2.18	2.78	1.74	2.08
Lu	0.36	0.35	0.39	0.24	0.32
$(La/Yb)_N$	15.46	11.75	11.55	13.55	13.67
ACNK	1.13	1.4	1.47	1.41	1.31
K_2O/Na_2O	1.08	1.49	1.5	0.97	2.73
Mg#	40.24	46.45	44.95	50.53	46.59
Eu*	1.17	1.15	1.21	0.77	0.79

$ACNK = Al_2O_3/[CaO + Na_2O + K_2O]$ (mol%); $Mg\# = MgO/[MgO + FeO + 0.79*Fe_2O_3]$; $Eu* = Eu_N/(Sm_N + Gd_N)^{0.5}$.

6   Geochronology

U-Pb Zircon dating

Orthogneiss at the Kabul airport

Zircons from samples C5-13 and C1-13 are mostly 150–250 µm long, 100–150 µm wide, brown in color, and of prismatic shape (Fig. 3a, b). CL images often reveal core–rim structures, with a dark oscillatory-zoned core of probable magmatic origin and light (low-U) overgrowths of probable metamorphic origin. A concordant cluster of data from magmatic zircon from sample C5-13 provides a ^{206}Pb/^{238}U age of 2474 ± 13 Ma (Table 3; Fig. 4a). A slightly older concordant age of 2760 ± 30 was obtained for a single zircon from this sample. Ten spots in metamorphic zircon overgrowths yielded concordant ages in the range of ca 1820 – ca 2100 Ma, the older ages of this group may be mix ages with magmatic zircon (Table 3; Fig. 4a).

Very consistent ages were obtained from sample C1-13, indicating a ca 2450 Ma magmatic crystallization stage and a precise age of 1845 ± 9 Ma for the metamorphic overgrowths (Fig. 4b). Some cores gave ages of more than 2700 Ma.

The Khair Khana orthogneiss

Zircons from this granulitic orthogneiss (samples AF159B, AF159A, F70-6 and AF-101) are mostly 200–300 µm in length, 100–150 µm wide, and pale yellow in color. They are long-prismatic with significant rounding at their ends (Fig. 3c-f) ascribed to "metamorphic" corrosion. Some grains show light oscillatory or sector zoning in CL images, suggesting a magmatic origin; the remaining grains display small cores with wide sectorial-zoned rims, indicating zircon recrystallization (Fig. 3c). Three magmatic zircon grains, each from the first three samples, yielded concordant ^{206}Pb/^{238}U ages within a 2200–2300 Ma interval (Table 3; Fig. 4c-f). The oldest mean age from three zircons in sample AF101 is 2180 ± 13 Ma. The most reliable estimation of the age of metamorphic zircon formation in all four samples is 1854 ± 8 Ma, judging from the big concordant age cluster in sample AF101 (Fig. 4d).

Amphibole gneiss from the Welayati Formation (location no. 1 in Fig. 1d)

Except for one long-prismatic zircon in sample F82-6 with an age of 500–600 Ma, the zircon ages (Fig. 3h) are similar to the metamorphic zircon ages in the granulitic orthogneisses, i.e., about 1850 Ma old (Table 3, Fig. 4g).

Monazite dating

Orthogneiss at the Kabul airport

This orthogneiss (sample C44-12) contains large, mostly elongate (up to 300 µm) monazite crystals, but isometric grains can be observed as well. Except for some small monazite in the garnet cores (Fig. 5a), most monazite crystals are enclosed in the garnet rims. BSE images reveal complex zonation in many grains, mostly defined by dark core domains and bright rim domains (Fig. 5b). Occasionally, patchy bright islands are also seen within the dark cores, possibly representing recrystallized domains. The boundaries of the dark cores towards the bright rims are sharp and embayed, indicating that a

Table 3: SHRIMP U-Th-Pb results for basement rocks of the Kabul Block.

Sample spot	$^{206}Pb_c$ %	U ppm	Th ppm	$^{232}Th/^{238}U$	$^{206}Pb^*$ ppm	$^{206}Pb/^{238}U$ age (1)	±1σ	$^{207}Pb/^{206}Pb$ age (1)	±1σ	D %	$^{207}Pb^*/^{206}Pb^*$(1)	±%	$^{207}Pb^*/^{235}U$(1)	±%	$^{206}Pb^*/^{238}U$(1)	±%	rho
C513.11.2	0.16	699	3	0.00	196	1817	27	1914	12	5	0.1172	0.7	5.26	1.8	0.3256	1.7	0.931
C513.5.2	0.04	546	21	0.04	156	1847	26	1851	16	0	0.1132	0.9	5.18	1.9	0.3318	1.6	0.881
C513.2.2	0.22	681	5	0.01	199	1882	27	1875	34	0	0.1147	1.9	5.36	2.5	0.3391	1.7	0.660
C513.10.2	0.01	1059	56	0.05	317	1926	27	1955	7	2	0.1199	0.4	5.76	1.7	0.3482	1.6	0.971
C513.8.2	0.06	545	53	0.10	166	1951	28	1875	10	-4	0.1147	0.5	5.59	1.7	0.3534	1.6	0.951
C513.5.1	0.6	183	110	0.62	57.8	2003	30	1991	26	-1	0.1224	1.5	6.15	2.3	0.3644	1.7	0.758
C513.4.1	0.02	942	108	0.12	299	2028	28	1967	9	-3	0.1207	0.5	6.15	1.7	0.3697	1.6	0.956
C513.8.1	ld	365	141	0.40	119	2077	29	2097	10	1	0.1300	0.6	6.81	1.8	0.3802	1.7	0.942
C513.9.1	ld	183	150	0.85	59.9	2082	32	2059	14	-1	0.1272	0.8	6.68	1.9	0.3812	1.8	0.910
C513.10.1	0.02	468	207	0.46	155	2098	29	2114	14	1	0.1312	0.8	6.96	1.8	0.3848	1.6	0.893
C513.7.1	0.04	1587	894	0.58	626	2435	33	2435	7	0	0.1580	0.4	10.00	1.7	0.4589	1.6	0.969
C513.6.1	0.04	237	219	0.95	94	2444	34	2465	11	1	0.1609	0.6	10.23	1.8	0.4610	1.7	0.935
C513.13.1	0.02	639	343	0.55	253	2446	33	2486	21	2	0.1629	1.2	10.36	2.0	0.4615	1.6	0.800
C513.2.1	ld	994	520	0.54	399	2470	33	2492	10	1	0.1635	0.6	10.52	1.7	0.4669	1.6	0.933
C513.3.1	0.06	600	423	0.73	244	2495	35	2467	12	-1	0.1611	0.7	10.50	1.8	0.4727	1.7	0.917
C513.12.1	ld	1015	85	0.09	432	2592	34	2452	5	-5	0.1597	0.3	10.90	1.6	0.4949	1.6	0.981
C513.1.1	ld	163	143	0.91	70.8	2633	37	2488	12	-6	0.1631	0.7	11.34	1.8	0.5046	1.7	0.925
C513.11.1	ld	64	37	0.59	29.7	2771	45	2758	16	0	0.1919	1.0	14.21	2.2	0.5370	2.0	0.902
C1-13.6.1	0.04	656	43	0.07	184	1821	12	1837	10	1	0.1123	0.6	5.05	0.9	0.3264	0.8	0.803
C1-13.8.2	0.11	515	5	0.01	143.3	1807	12	1837	12	2	0.1123	0.7	5.01	1.0	0.3236	0.8	0.752
C1-13.12.2	0.19	554	4	0.01	152	1784	9	1840	19	3	0.1125	1.0	4.94	1.2	0.3188	0.6	0.496
C1-13.10.2	0.1	508	6	0.01	142.5	1819	13	1843	17	1	0.1127	0.9	5.06	1.2	0.3260	0.8	0.651
C1-13.11.2	0.06	499	3	0.01	143.5	1861	11	1847	12	-1	0.1129	0.7	5.21	1.0	0.3346	0.7	0.727
C1-13.4.2	0.07	506	9	0.02	140	1800	12	1853	15	3	0.1133	0.8	5.03	1.1	0.3221	0.8	0.693
C1-13.5.2	0.03	732	8	0.01	206	1822	12	1853	10	2	0.1133	0.5	5.10	0.9	0.3266	0.8	0.814
C1-13.7.1	0.13	532	5	0.01	143.3	1755	12	1888	13	8	0.1155	0.7	4.98	1.1	0.3129	0.8	0.735
C1-13.4.1	0.42	113	128	1.17	38.3	2136	12	2145	26	0	0.1336	1.5	7.23	1.6	0.3927	0.6	0.402
C1-13.2.1	0.11	182	82	0.47	65	2239	18	2287	26	2	0.1449	1.5	8.30	1.8	0.4152	0.9	0.517
C1-13.1.1	1.41	12	9	0.78	4.87	2450	55	2351	140	-4	0.1500	8.1	9.59	8.5	0.4620	2.7	0.314
C1-13.9.1	0.03	1155	42	0.04	413.7	2246	14	2362	40	5	0.1514	2.3	8.70	2.4	0.4168	0.7	0.294

Table 3: Contd.

Sample spot	$^{206}Pb_c$ %	U ppm	Th ppm	$^{232}Th/^{238}U$	$^{206}Pb^*$ ppm	$^{206}Pb/^{238}U$ age (1)	± 1σ	$^{207}Pb/^{206}Pb$ age (1)	± 1σ	D %	$^{207}Pb^*/^{206}Pb^*(1)$	±%	$^{207}Pb^*/^{235}U(1)$	±%	$^{206}Pb^*/^{238}U(1)$	±%	rho
C1-13.10.1	0.01	712	384	0.56	279.6	2426	15	2464	7	2	0.1608	0.4	10.13	0.9	0.4569	0.8	0.881
C1-13.3.1	0.42	30	16	0.57	11.8	2441	27	2480	48	2	0.1623	2.9	10.30	3.2	0.4603	1.3	0.424
C1-13.8.1	0.09	103	62	0.62	39.8	2382	21	2552	26	7	0.1694	1.6	10.44	1.9	0.4471	1.1	0.563
C1-13.5.1	0.05	212	88	0.43	93	2656	31	2671	10	1	0.1820	0.6	12.80	1.5	0.5099	1.4	0.919
C1-13.11.1	0.3	114	186	1.69	50.7	2691	18	2682	16	0	0.1832	1.0	13.08	1.3	0.5180	0.8	0.646
C1-13.12.1	0.02	282	132	0.48	128.1	2737	14	2758	9	1	0.1919	0.5	13.99	0.8	0.5289	0.6	0.776
AF101-1_10.2	ld	193	62	0.33	55.1	1854	15	1837	21	-1	0.1123	1.2	5.16	1.5	0.3332	1.0	0.635
AF101-1_7.3	0.03	955	185	0.20	260.6	1777	11	1845	10	4	0.1128	0.5	4.94	0.9	0.3175	0.7	0.796
AF101-1_6.2	0.03	1698	29	0.02	475.5	1818	11	1849	8	2	0.1130	0.4	5.08	0.8	0.3258	0.7	0.842
AF101-1_9.2	0.11	216	47	0.23	62.6	1876	16	1851	23	-1	0.1131	1.3	5.27	1.6	0.3377	1.0	0.617
AF101-1_5.2	0.04	252	30	0.13	71.1	1833	14	1853	18	1	0.1133	1.0	5.14	1.4	0.3289	0.9	0.660
AF101-1_10.1	0.02	1058	165	0.16	294.1	1807	11	1856	10	3	0.1135	0.5	5.06	0.9	0.3236	0.7	0.799
AF101-1_1.2	0.06	1327	15	0.01	374.9	1831	11	1863	9	2	0.1139	0.5	5.16	0.8	0.3285	0.7	0.820
AF101-1_7.2	0.21	323	83	0.26	93.4	1865	13	1883	19	1	0.1152	1.1	5.33	1.3	0.3354	0.8	0.615
AF101-1_6.1	0.13	425	107	0.26	120.3	1834	12	1893	15	3	0.1158	0.8	5.26	1.1	0.3290	0.8	0.688
AF101-1_9.1	ld	462	123	0.28	132.8	1862	13	1900	13	2	0.1163	0.7	5.37	1.1	0.3349	0.8	0.738
AF101-1_4.1	0.07	366	97	0.27	104.2	1843	13	1927	15	5	0.1181	0.8	5.39	1.1	0.3310	0.8	0.694
AF101-1_1.1	0.02	675	94	0.14	205.7	1957	12	1930	9	-1	0.1183	0.5	5.78	0.9	0.3547	0.7	0.829
AF101-1_3.1	0.03	678	193	0.29	195.5	1865	12	1931	11	4	0.1183	0.6	5.47	0.9	0.3355	0.7	0.767
AF101-1_2.1	0.03	1125	250	0.23	345.3	1969	14	2008	9	2	0.1235	0.5	6.09	0.9	0.3573	0.8	0.849
AF101-1_7.1	0.15	697	443	0.66	219.2	2008	13	2131	11	6	0.1324	0.6	6.67	1.0	0.3654	0.7	0.772
AF101-1_5.1	0.03	799	368	0.48	268.8	2130	13	2170	9	2	0.1355	0.5	7.31	0.9	0.3916	0.7	0.816
AF101-1_8.1	0.25	178	68	0.39	59.7	2117	17	2175	19	3	0.1358	1.1	7.28	1.4	0.3888	0.9	0.646
AF101-1_11.1	ld	377	132	0.36	128.2	2150	15	2187	12	2	0.1368	0.7	7.47	1.1	0.3959	0.8	0.760
AF159B.1.1	0.01	269	43	0.16	78.8	1894	26	1855	13	-2	0.1134	0.7	5.34	1.7	0.3414	1.6	0.910
AF159B.1.2	0.02	1693	16	0.01	507	1926	26	1962	14	2	0.1204	0.8	5.78	1.7	0.3483	1.5	0.884
AF159B.2.1	0.02	1490	37	0.03	437	1893	25	1855	6	-2	0.1134	0.3	5.34	1.6	0.3414	1.5	0.980
AF159B.3.1	ld	2235	279	0.13	673	1936	26	1904	5	-2	0.1166	0.3	5.63	1.6	0.3504	1.6	0.981
AF159B.4.1	0.01	575	226	0.41	214	2326	30	2290	7	-2	0.1452	0.4	8.70	1.6	0.4345	1.5	0.970
AF159B.4.2	0.01	740	30	0.04	207	1819	24	1833	8	1	0.1121	0.4	5.04	1.6	0.3259	1.5	0.964
AF159B.5.1	ld	615	94	0.16	198	2048	29	2018	14	-1	0.1243	0.8	6.41	1.9	0.3740	1.7	0.899
AF159B.5.2	0.01	1098	91	0.09	318	1871	25	1883	12	1	0.1152	0.7	5.35	1.7	0.3367	1.5	0.915
AF159B.6.1	0.01	1182	113	0.10	354	1926	26	1917	6	0	0.1174	0.3	5.63	1.6	0.3481	1.6	0.977
AF159B.7.1	ld	231	107	0.48	66	1853	25	1830	14	-1	0.1119	0.8	5.14	1.7	0.3330	1.6	0.902

Table 3: Contd.

Sample spot	$^{206}Pb_c$ %	U ppm	Th ppm	$^{232}Th/^{238}U$	$^{206}Pb*$ ppm	$^{206}Pb/^{238}U$ age (1)	± 1σ	$^{207}Pb/^{206}Pb$ age (1)	± 1σ	D %	$^{207}Pb*/^{206}Pb*(1)$	±%	$^{207}Pb*/^{235}U(1)$	±%	$^{206}Pb*/^{238}U(1)$	±%	rho
AF159A.1.1	0.01	347	149	0.44	122	2205	29	2217	12	1	0.1392	0.7	7.83	1.7	0.4079	1.6	0.912
AF159A.2.1	0.01	2499	129	0.05	711	1845	25	1840	4	0	0.1125	0.2	5.14	1.5	0.3314	1.5	0.988
AF159A.2.2	0.02	171	92	0.56	48	1826	25	1837	16	1	0.1123	0.9	5.07	1.8	0.3275	1.6	0.873
AF159A.3.1	0.01	3924	75	0.02	1120	1855	25	1893	3	2	0.1158	0.2	5.32	1.5	0.3334	1.5	0.992
AF159A.3.2	0.01	369	125	0.35	118	2039	27	1874	14	-8	0.1146	0.8	5.88	1.7	0.3720	1.6	0.900
AF159A.4.1	0.05	1224	75	0.06	325	1735	23	1855	7	7	0.1134	0.4	4.83	1.6	0.3088	1.5	0.971
AF159A.5.1	0.02	753	64	0.09	206	1779	24	1786	8	0	0.1092	0.4	4.79	1.6	0.3178	1.5	0.962
AF159A.6.1	0.02	261	119	0.47	74.8	1853	26	1836	23	-1	0.1122	1.3	5.15	2.1	0.3330	1.6	0.777
AF159A.7.1	0.01	2349	68	0.03	671	1851	25	1832	4	-1	0.1120	0.2	5.14	1.5	0.3326	1.5	0.988
AF159A.9.1	0.06	208	85	0.42	59.3	1845	28	1844	17	0	0.1127	1.0	5.15	1.8	0.3314	1.6	0.858
F70_6.1.1	1.14	3027	80	0.03	762	1656	31	1809	20	9	0.1106	1.1	4.47	2.2	0.2929	1.9	0.871
F70_6.10.1	0.50	2550	73	0.03	702	1792	30	1855	6	4	0.1134	0.3	5.01	2.0	0.3204	2.0	0.987
F70_6.11.1	0.68	2017	24	0.01	543	1754	30	1824	8	4	0.1115	0.5	4.81	2.0	0.3127	2.0	0.973
F70_6.12.1	1.82	1631	102	0.06	413	1662	29	1887	12	14	0.1154	0.7	4.68	2.1	0.2942	2.0	0.950
F70_6.12.2	1.49	755	353	0.48	244	2058	35	2206	10	7	0.1383	0.6	7.17	2.1	0.3762	2.0	0.957
F70_6.13.1	0.75	2147	242	0.12	558	1702	29	1798	7	6	0.1099	0.4	4.58	2.0	0.3022	2.0	0.979
F70_6.14.1	0.69	1799	218	0.13	468	1706	31	1793	8	5	0.1096	0.4	4.58	2.1	0.3030	2.0	0.979
F70_6.14.2	1.83	1561	188	0.12	370	1573	27	1831	8	16	0.1119	0.4	4.26	2.0	0.2763	2.0	0.978
F70_6.15.1	0.23	1681	198	0.12	464	1795	31	1826	6	2	0.1116	0.4	4.94	2.0	0.3211	2.0	0.984
F70_6.16.1	2.17	2004	42	0.02	459	1522	26	1813	9	19	0.1108	0.5	4.07	2.0	0.2663	2.0	0.973
F70_6.16.2	0.01	208	115	0.57	75.3	2252	39	2204	37	-2	0.1381	2.1	7.96	3.0	0.4182	2.0	0.690
F70_6.17.1	1.38	2144	44	0.02	540	1657	29	1844	6	11	0.1127	0.3	4.56	2.0	0.2931	2.0	0.985
F70_6.18.1	2.09	3192	46	0.01	727	1515	27	1810	6	19	0.1107	0.4	4.04	2.0	0.2649	2.0	0.985
F70_6.18.2	0.01	153	82	0.55	53.5	2192	39	2124	33	-3	0.1319	1.9	7.37	2.8	0.4050	2.1	0.741
F70_6.18.3	1.45	823	418	0.53	259	2014	47	2162	15	7	0.1348	0.9	6.82	2.8	0.3667	2.7	0.952
F70_6.2.1	1.11	1640	13	0.01	427	1705	29	1845	9	8	0.1128	0.5	4.71	2.0	0.3028	2.0	0.972
F70_6.3.1	2.44	2028	44	0.02	438	1444	28	1800	8	25	0.1100	0.4	3.81	2.2	0.2511	2.2	0.982
F70_6.4.1	0.59	3209	16	0.01	912	1842	32	1908	7	4	0.1168	0.4	5.33	2.0	0.3307	2.0	0.982
F70_6.5.1	1.84	1631	12	0.01	390	1582	27	1829	9	16	0.1118	0.5	4.29	2.0	0.2781	2.0	0.970
F70_6.6.1	0.73	1780	86	0.05	463	1705	29	1800	7	6	0.1101	0.4	4.59	2.0	0.3027	1.9	0.982
F70_6.7.1	1.81	2146	42	0.02	527	1621	29	1863	7	15	0.1139	0.4	4.49	2.1	0.2858	2.0	0.984
F70_6.8.1	1.01	2051	227	0.11	518	1661	29	1793	7	8	0.1096	0.4	4.44	2.0	0.2940	2.0	0.983
F70_6.9.1	2.34	1934	34	0.02	420	1453	25	1789	9	23	0.1094	0.5	3.81	2.0	0.2528	2.0	0.972

Table 3: Contd.

Sample spot	$^{206}Pb_c$ %	U ppm	Th ppm	$^{232}Th/^{238}U$	$^{206}Pb^*$ ppm	$^{206}Pb/^{238}U$ age (1)	± 1σ	$^{207}Pb/^{206}Pb$ age (1)	± 1σ	D %	$^{207}Pb^*/^{206}Pb^*(1)$	±%	$^{207}Pb^*/^{235}U(1)$	±%	$^{206}Pb^*/^{238}U(1)$	±%	rho
F82_6.2.1	6.40	3172	79	0.03	224	508	10	1765	11	247	0.1079	0.6	1.22	2.1	0.0820	2.0	0.952
F82_6.2.2	6.85	2563	42	0.02	225	627	12	1870	15	198	0.1143	0.8	1.61	2.1	0.1022	2.0	0.923
F82_6.6.1	3.99	1064	56	0.05	193	1232	22	1826	21	48	0.1116	1.1	3.24	2.3	0.2105	2.0	0.866
F82_6.5.1	1.28	2298	44	0.02	595	1697	29	1859	7	10	0.1137	0.4	4.72	2.0	0.3012	1.9	0.979
F82_6.3.1	1.94	1573	82	0.05	408	1702	29	1948	7	14	0.1194	0.4	4.98	2.0	0.3021	2.0	0.982
F82_6.11.1	0.59	1148	496	0.45	305	1735	30	1806	11	4	0.1104	0.6	4.70	2.1	0.3088	2.0	0.957
F82_6.13.1	1.75	913	24	0.03	245	1754	30	1969	8	12	0.1209	0.4	5.21	2.0	0.3126	2.0	0.976
F82_6.14.1	1.67	945	91	0.10	260	1794	31	1991	11	11	0.1224	0.6	5.41	2.1	0.3208	2.0	0.953
F82_6.10.1	3.11	468	99	0.22	130	1802	36	2141	14	19	0.1332	0.8	5.93	2.4	0.3226	2.3	0.944
F82_6.8.1	3.55	725	164	0.23	201	1803	31	2186	13	21	0.1367	0.7	6.08	2.1	0.3226	2.0	0.936
F82_6.12.1	0.72	819	5	0.01	230	1822	31	1902	13	4	0.1164	0.7	5.24	2.1	0.3266	2.0	0.938
F82_6.15.1	0.94	1353	219	0.17	392	1875	32	1982	7	6	0.1217	0.4	5.67	2.0	0.3375	2.0	0.980
F82_6.1.1	2.17	1480	17	0.01	464	2003	34	2216	7	11	0.1391	0.4	6.99	2.0	0.3644	2.0	0.979
F82_6.4.1	1.24	308	126	0.42	98.2	2032	35	2144	18	5	0.1335	1.0	6.82	2.2	0.3706	2.0	0.894
F82_6.7.1	5.56	583	61	0.11	189	2065	35	2554	8	24	0.1696	0.5	8.83	2.0	0.3776	2.0	0.972
F82_6.9.1	1.93	465	360	0.80	161	2183	37	2366	12	8	0.1518	0.7	8.44	2.1	0.4030	2.0	0.947

Notes:

Errors are 1-sigma; Pb_c and Pb^* indicate the common and radiogenic portions, respectively.

ld - Limit of determination;

(1) - Common Pb corrected using measured ^{204}Pb;

D - Degree of discordance, % (D = $100 \times \{[Age(^{207}Pb/^{206}Pb)] / [Age(^{206}Pb/^{238}U)]^{-1}\}$);

rho - Correlation coefficient of U-Pb ratio errors
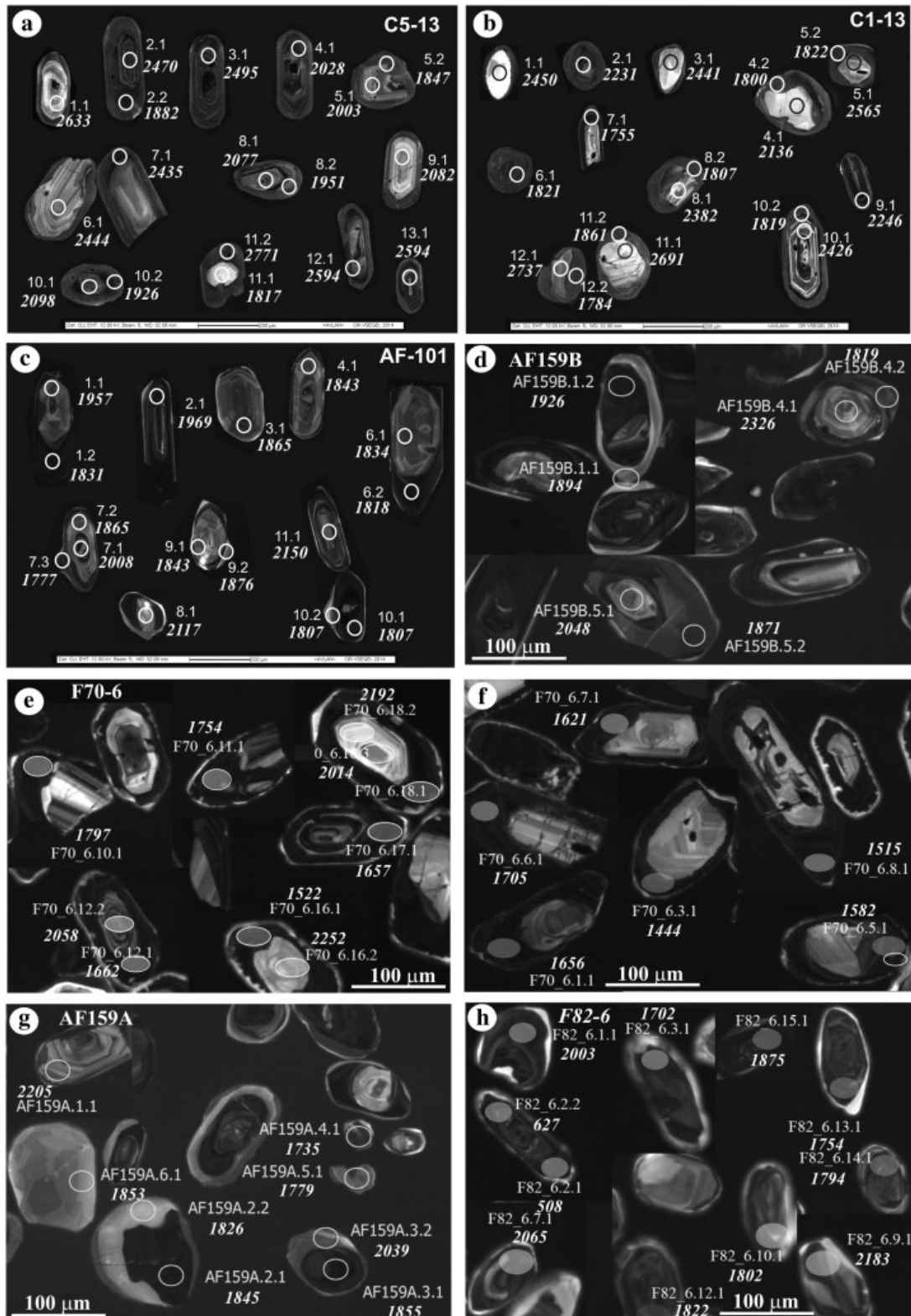
Figure 3: Cathodoluminesence (CL) images of dated zircons (a-c) orthogneiss from the Kabul airport, (d-g) granulite from the Khair Khana Formation and (e) amphibole gneiss from the Welayati Formation.
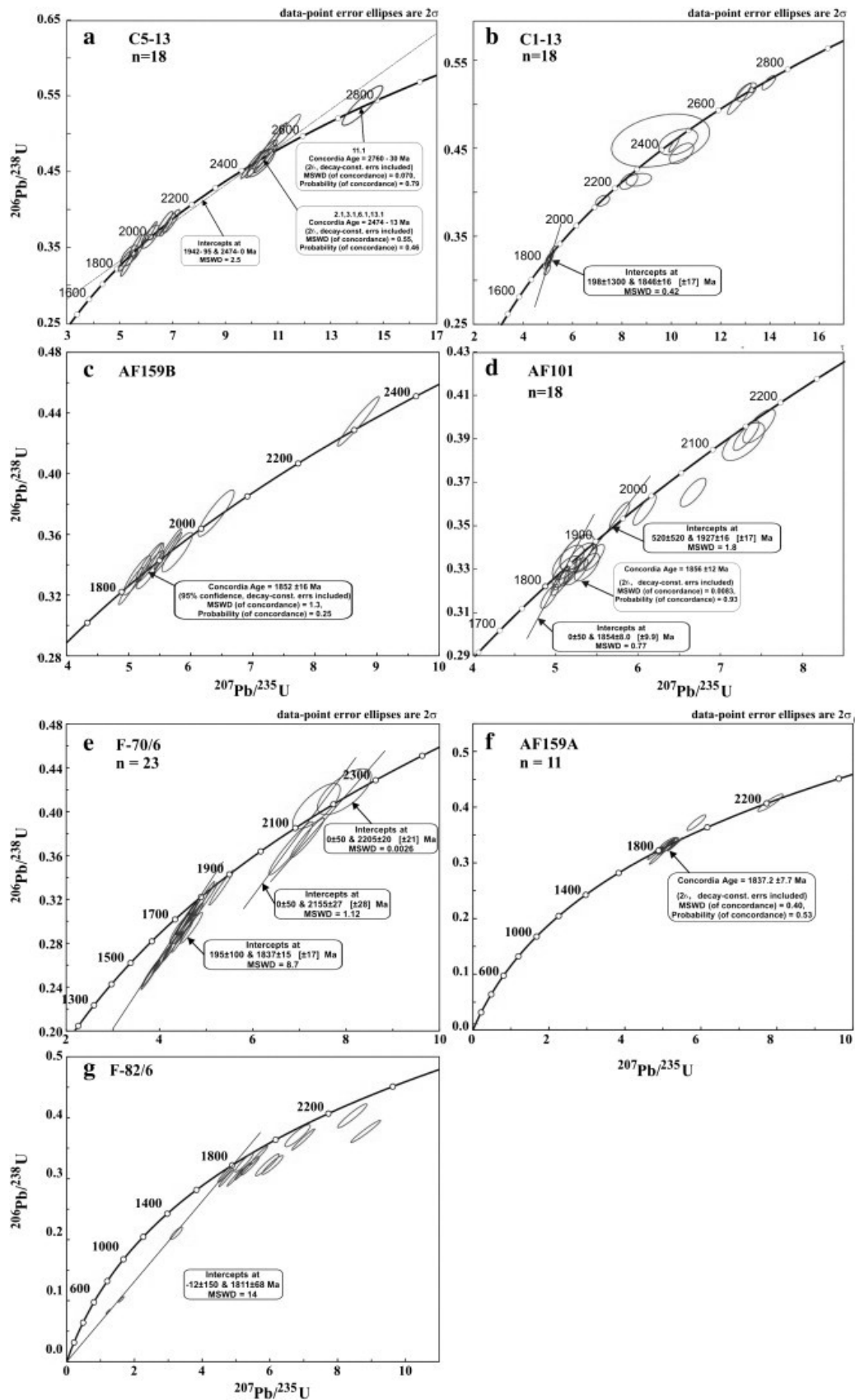
Figure 4: Wetherill (1956), Concordia diagrams of sensitive high-resolution ion microprobe (SHRIMP) U–Pb analyses of zircons from the Kabul Basement rocks. Note that the orthogneisses (a-f) exhibiting bimodal clustering of ages reflecting a magmatic and a metamorphic phase of zircon growth (b, n = 1) ages. Error ellipses shown at 1σ level of uncertainty. MSWD – mean square of weighted deviates.

dissolution-reprecipitation process may have operated. Indeed, dissolution-reprecipitation is a common feature in monazite from high-T metamorphic rocks (e.g., Finger and Krenn, 2007).
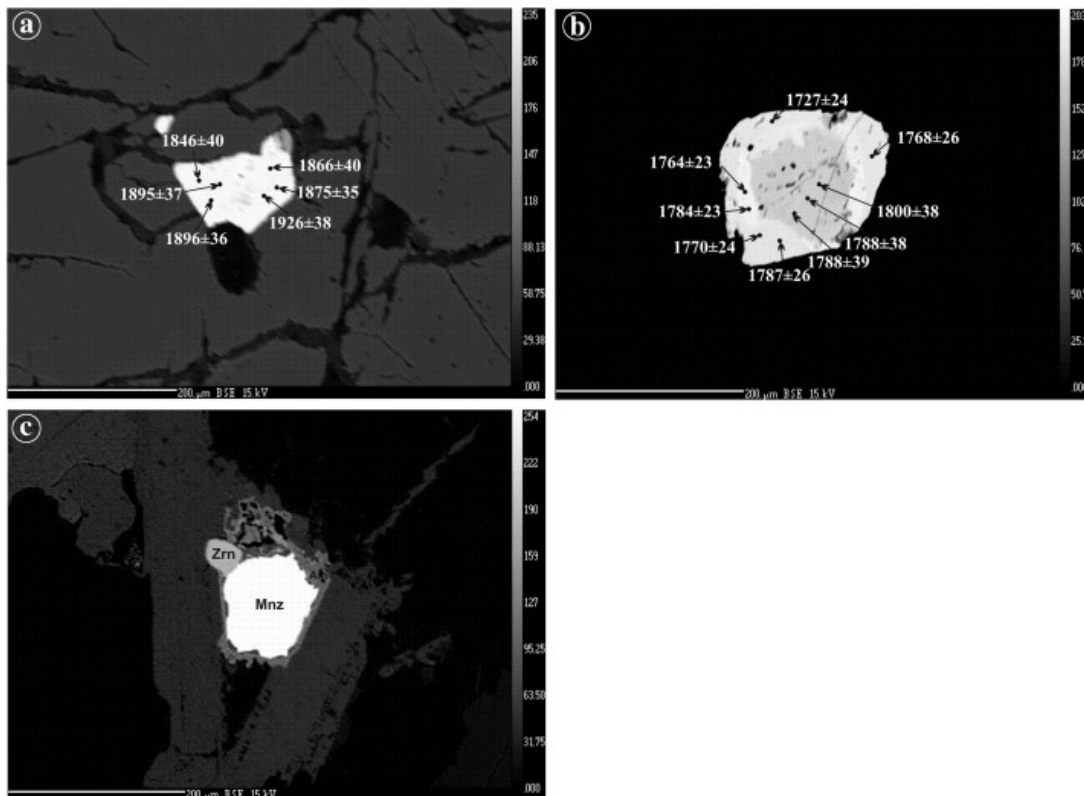
Figure 5: Backscatter electron images of monazite grains from orthogneisses in the Kabul Block. a) Small Y-rich monazite in garnet core (sample C44-12). b) Zoned monazite with dark core and bright rim (sample C44-12). c) Monazite with allanite corona (sample AF 102).

The dark cores in the BSE images have relatively low Th contents (5–6 wt. %, Table 4), accommodated mainly through the cheralite exchange reaction. They are also characterized by a moderately steep LREE distribution (La/Nd ~ 1.3), low Y contents < 0.7 wt %, and low to moderate U contents (0.3–0.8 wt %). The bright domains show high Th contents (6–16 wt. %) incorporated to a large extent via the huttonite substitution vector. The LREE distribution displays significantly lower La/Nd ratios (around 1). Y contents are extremely low (mostly < 0.1 wt. %).

The rare small monazite inclusions in the garnet cores show elevated Y contents between 1.6 and 2.5 wt. %. Their Th contents are around 4 wt. % (mainly represented by cheralite), and the Th/U ratio is significantly lower than in the other monazite grains of the sample (5–7 vs. 10 and more). The REE patterns are similar to those of the dark cores of large monazite crystals.

In total 52 microbe analyses of monazite grains from the orthogneiss were obtained in two different laboratories (Table 4). The Th-U-Pb ages are in the range of 1751 to 1825 Ma. A first set of data, mostly analysing the bright rim domains with a few dark core domains, yielded a weighted average age of 1785 ± 19 Ma (95 % confidence, MSWD 4.1, n = 10). Considering the whole data set, three monazite generations can be distinguished. The Y-rich monazite grains preserved in the garnet centers display the highest Th-U-Pb ages. The weighted average age for this monazite group is 1885 ± 28 Ma (95 % confidence, MSWD 2.1, n = 5). For the dark monazite cores a mean of 1797 ± 12 Ma can be calculated (95 % confidence, MSWD 1.3; n = 14). A slightly lower average age of 1771 ± 13 Ma (95 % confidence, MSWD 3.3; n = 15) was obtained from the bright rim domains. Two small monazite grains in the matrix, chemically fairly similar to the bright rim domains, gave significantly younger ages of ~ 820 Ma, which

Table 4: Microprobe Th-U-Pb data from Monazite of basement rocks of the Kabul Block.

Sample C44-12#						Sample C44-12##					
Grain	Th	U	Pb	Th*	Age	Grain	Th	U	Pb	Th*	Age
Monazite core domains						2.1c	4.752	0.457	0.504	6.43	1697 ± 40*
6.1	6.121	0.324	0.603	7.151	1777 ± 35	2.1	9.103	0.149	0.791	9.655	1767 ± 27
7.1	6.18	0.344	0.618	7.271	1791 ± 35	2.1r	13.06	0.721	1.281	15.727	1760 ± 16
8.1	5.359	0.292	0.539	6.287	1806 ± 40	8.1	7.391	0.607	0.78	9.635	1751 ± 27
15.1	4.687	0.597	0.575	6.582	1800 ± 38	9.1	7.567	0.111	0.297	7.943	825 ± 33*
16.1	4.645	0.607	0.57	6.573	1788 ± 38	10.1c	4.633	0.668	0.591	7.114	1798 ± 36
17.1	4.639	0.544	0.551	6.367	1788 ± 39	10.1r	9.099	0.748	0.989	11.876	1799 ± 22
20.1	5.351	0.448	0.585	6.774	1802 ± 35	11.1r	10.453	0.262	0.948	11.425	1791 ± 23
21.1	5.348	0.458	0.598	6.803	1829 ± 37	11.2	15.284	0.204	1.336	16.042	1796 ± 16
25.1	5.319	0.377	0.506	6.515	1638 ± 37*	11.3c	4.7	0.956	0.695	8.258	1820 ± 31
26.1	4.653	0.433	0.492	6.028	1706 ± 39*	13.1	3.646	1.287	0.712	8.44	1825 ± 31
24.1	4.915	0.403	0.516	6.194	1744 ± 38	14.1	7.011	0.085	0.27	7.299	821 ± 33
27.1	4.958	0.45	0.547	6.388	1783 ± 39						1785 ± 19
35.1	4.648	0.789	0.63	7.154	1798 ± 34						
54.1	4.9	0.412	0.546	6.208	1831 ± 38						
55.1	4.893	0.41	0.539	6.195	1812 ± 40	Sample AF102#					
58.1	4.736	0.453	0.536	6.175	1803 ± 38	Grain	Th	U	Pb	Th*	Age
					1797 ± 12	22.1	11.055	0.514	1.069	12.687	1782 ± 23
						23.1	10.969	0.517	1.058	12.611	1774 ± 23
Monazite rim domains						24.1	10.325	0.463	1.014	11.796	1816 ± 25
9.1	11.752	0.526	1.132	13.423	1784 ± 23	25.1	6.561	0.046	0.556	6.707	1783 ± 38
10.1	11.805	0.537	1.126	13.512	1764 ± 23	26.1	6.404	0.138	0.57	6.842	1781 ± 37
11.1	10.023	0.531	0.956	11.709	1727 ± 24	27.1	3.291	0.109	0.299	3.638	1751 ± 62
12.1	10.248	0.629	1.03	12.246	1770 ± 24	28.1	4.688	0.249	0.461	5.477	1776 ± 44
13.1	9.519	0.632	0.981	11.527	1787 ± 26	29.1	5.211	0.244	0.52	5.986	1832 ± 40
14.1	9.398	0.607	0.953	11.325	1768 ± 26	30.1	7.053	0.353	0.69	8.173	1782 ± 33
18.1	6.331	0.477	0.668	7.845	1783 ± 34	31.1	7.009	0.346	0.689	8.108	1793 ± 33
19.1	7.407	0.47	0.77	8.9	1814 ± 30	32.1	6.045	0.182	0.55	6.624	1768 ± 39
28.1	9.053	0.114	0.697	9.416	1596 ± 29*	33.1	9.315	0.35	0.645	10.426	1334 ± 25*
29.1	8.423	0.437	0.805	9.812	1735 ± 29	34.1	9.418	0.426	0.786	10.77	1558 ± 25*
30.1	12.25	0.484	1.172	13.786	1800 ± 23	35.1	5.789	0.316	0.548	6.791	1706 ± 37
31.1	6.175	0.456	0.628	7.622	1730 ± 33	36.1	5.752	0.297	0.545	6.696	1722 ± 38
32.1	12.47	0.179	1.081	13.038	1776 ± 23	51.1	6.485	0.197	0.59	7.11	1768 ± 36
33.1	16.245	0.163	1.391	16.763	1781 ± 20						1778 ± 17
34.1	13.493	0.205	1.168	14.144	1769 ± 22						
53.1	9.938	0.117	0.847	10.31	1762 ± 28	Sample CL-7#					
56.1	14.284	0.687	1.228	16.466	1588 ± 19*	Grain	Th	U	Pb	Th*	Age
57.1	8.208	0.245	0.736	8.986	1745 ± 30*	6.1	4.953	0.29	0.221	5.875	823 ± 37
					1771 ± 13	7.1	6.461	0.301	0.257	7.417	760 ± 30*
						8.1	3.874	0.31	0.191	4.858	856 ± 45
Y-rich monazite in garnet						9.1	6.693	0.313	0.297	7.688	847 ± 30
22.1	4.051	0.667	0.559	6.168	1846 ± 40	10.1	7.156	0.312	0.304	8.148	819 ± 27
23.1	3.984	0.655	0.556	6.062	1866 ± 40	11.1	7.087	0.33	0.296	8.136	798 ± 29
59.1	4.161	0.777	0.622	6.629	1895 ± 37	12.1	6.434	0.307	0.277	7.41	821 ± 30
60.1	4.074	0.829	0.631	6.708	1896 ± 36	13.1	8.6	0.314	0.347	9.597	795 ± 24
61.1	3.929	0.747	0.603	6.302	1926 ± 38	14.1	8.704	0.34	0.366	9.783	821 ± 24
62.1	4.945	0.751	0.674	7.331	1875 ± 35	15.1	8.652	0.323	0.346	9.679	786 ± 24
					1885 ± 28	16.1	4.055	0.317	0.182	5.06	788 ± 40
						17.1	7.424	0.286	0.317	8.332	836 ± 28
						19.1	6.156	0.273	0.274	7.023	854 ± 31
						20.1	7.797	0.321	0.336	8.817	837 ± 27
						21.1	9.736	0.338	0.405	10.808	824 ± 23
											820 ± 12

* Not considered for mean, # measured at Masaryk University, ## measured at Salzburg University.

fits with the monazite age obtained for the staurolite schist from the Welayati Formation (see below).

The Khair Khana orthogneiss

Monazite in sample AF-102 is up to 80 μm in size. Some crystals have isometric, some elongate shapes. They occur in the matrix or, more rarely, as inclusions in garnet, in this case generally in a near rim position. Patchy zoning is commonly seen in BSE images. Furthermore, many grains look corroded, being surrounded by a thin apatite-allanite reaction rim (Fig. 5c), a feature indicative of a retrograde metamorphic overprint (Finger et al., 1998).

In total sixteen analyses were carried out on monazite from sample AF-102. They show that the observed zoning patterns are mainly a reflection of the Th contents, which vary between 3 and 11 wt. % and are positively correlated with U (0.1–0.5 wt. %). Th substitution is dominated by huttonite component, while the cheralite end member plays a comparably minor role. The REE patterns of individual grains show little variation, with La/Nd ratios being close to 1.4. Yttrium contents are always below 1 wt. %, in most cases even below 0.3 wt. %.

Single point ages fall for their most part between 1750 and 1830 Ma, with typical errors of 20–40 Ma. Neglecting the two analyses with unusually low ages of 1334 and 1558 Ma, the data can be combined to a weighted average age of 1778 ± 17 Ma (95 % confidence, MSWD 3.3). The main stage of monazite formation should have taken place at this time.

Micaschist from the Welayati Formation (location 3 in Fig. 1d)

The monazite crystals in this rock (sample CL7-6) are small, generally less than 20 μm in diameter. They occur in the matrix and have subhedral shapes. In BSE imaging zoning is weak or absent. Fifteen grains were analyzed. The analyses show relatively little compositional spread. LREE patterns show little variation with La/Nd ratios pivoting around 1.6. Y contents are generally low, i.e., < 0.2 wt. %. Only the Th contents show an appreciable variation from grain to grain, covering a range from ~ 4 to 10 wt. %. U contents remain at a constantly low level of ~ 0.3 wt. %. The Th substitution mainly takes place via the cheralite end member $ThCa(PO_4)_2$. Th-U-Pb age dates cluster around a weighted mean of 820 ± 12 Ma (95 % confidence, MSWD 2.3). Apart from one outlier (grain 7, Table 4), all single point ages overlap within error, indicating monocyclic monazite formation. According to Wing et al. (2003), massive metamorphic monazite growth occurs in metapelites on entering the staurolite field. The age of 820 ± 12 Ma probably dates this stage of the metamorphic evolution.

Ar-Ar dating

Granulite facies calc-silicate rocks from Khair Khana

Coarse-grained (8–15 mm) phlogopite from two samples (F15-9 and F-6, Table A1 in the Supplementary data), were analysed in Bratislava and Lund University, respectively. The ^{39}Ar-^{40}Ar data yielded weighted mean age patterns of 1662 ± 5 Ma to 1519 ± 4 Ma and 1468.1 ± 16.9 Ma (Table A1 in the Supplementary data; Fig. 6a, b).
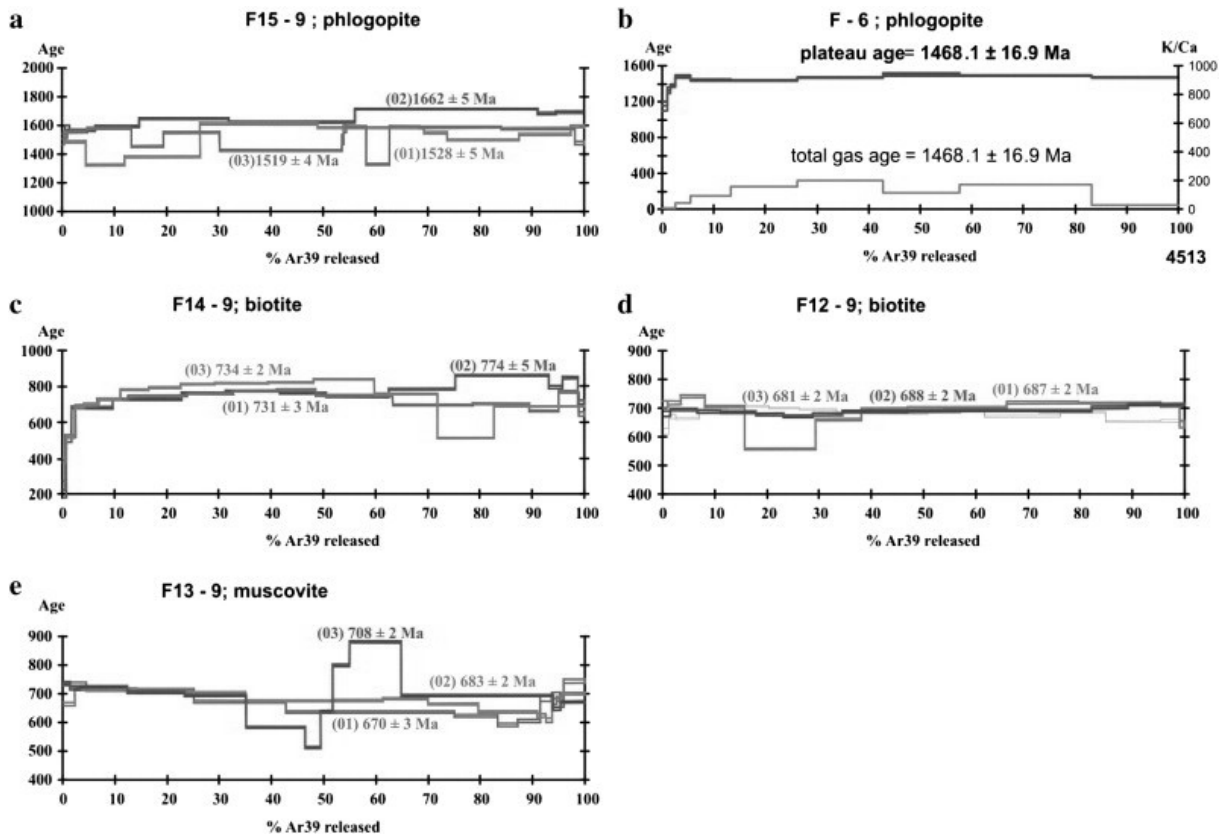
Figure 6: Ar/Ar ages for micas from Basement the Kabul basement rocks. (a, b) – Granulite facies marble, (c-e) migmatites from the Sherdarwaza Formation.

Migmatite from the Sherdarwaza Formation (location no. 2 in Fig. 1d)

Three samples, two with biotite (F12-9, F14-9) and one with white mica (F13-9) were analyzed for age dating. The ages obtained for biotite are widely distributed between 770–670 Ma (Table A1 in the Supplementary data, Fig. 6c, d). Biotite from the first sample shows a typical "staircase pattern" which indicates relics of older cores in the dated mica aggregates. Similarly to biotite, the white mica data from sample F13-9 are also strongly disturbed (Fig. 6e).

Micaschist from the Welayati Formation (location no. 3 in Fig. 1d)

^{39}Ar/^{40}Ar biotite data from of sample Cl-7 yielded a plateau age pattern of 900.9 ± 7.4 Ma (Fig. 7a). White mica from this sample shows a slightly disturbed plateau with a younger total age of 786.0 ± 9.4 Ma (Table A1 in the Supplementary data; Fig. 7b). Slightly disturbed spectra with total ages of 705 ± 8.3 and 782 ± 8.6 Ma were obtained for white mica from samples CL-5 and CL-6, respectively (Fig. 7c, d). The highest age values are 906 and 849 / 834 Ma, which are close to the biotite age in sample CL-7. The age pattern in the diagram is strongly influenced by lattice breakdown and redistribution / diffusion of argon. The oldest age domains in the mica flakes reach values higher than 850 Ma. The overprinting metamorphic event should be close to / or younger than 570 Ma. Data for CL-7, and Fa CL-5 indicate a partially reset system due to a low to intermediate temperature metamorphic overprint and lighter ^{40}Ar excess. The original age of the micas was probably between 834 Ma and 906 Ma.
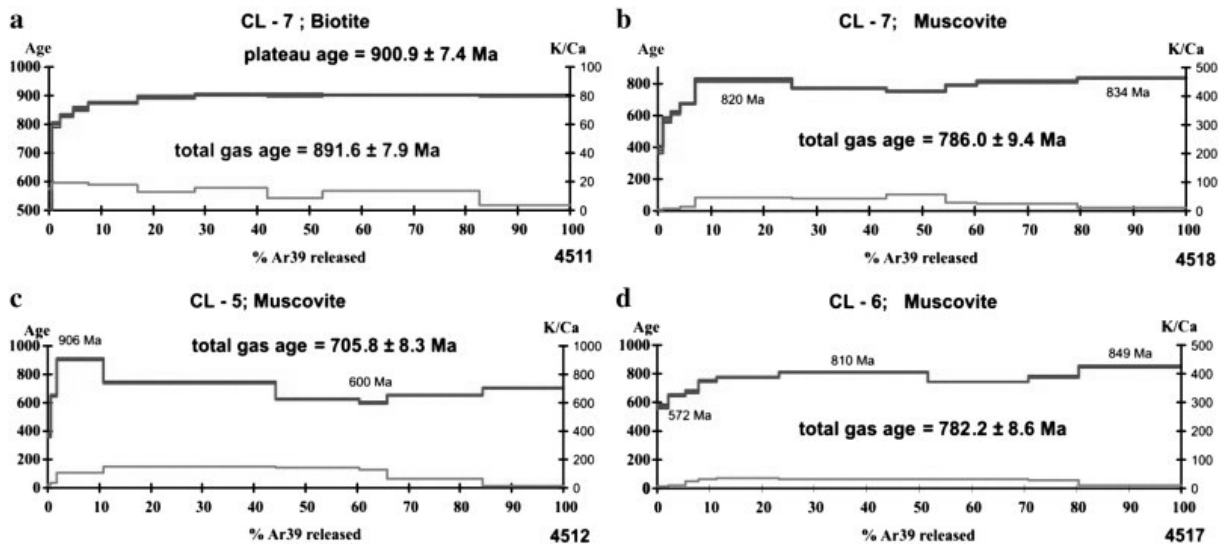
Figure 7: Ar/Ar ages for micas in micaschists from the Welayati Formation.

7   Metamorphic conditions

Based on textural relations two metamorphic events are distinguished in the orthogneisses of the Sherd-arwaza Formation (Collett et al., 2015). The first, a granulite facies metamorphism, occurred at medium pressure conditions of 5–7 kbar and reached up to 850 °C (Fig. 8). It is characterised by the formation of orthopyroxene, Ti-rich biotite, and in some cases also Mg-rich garnet in the felsic granulite, and by olivine and phlogopite in the calc-silicate rocks. A younger amphibolite facies event is recognized in the granulite, documented by the formation of new garnet, which overgrows the granulite facies minerals. PT conditions of 560–650 °C and 8–9 kbar were calculated for this second metamorphic event.
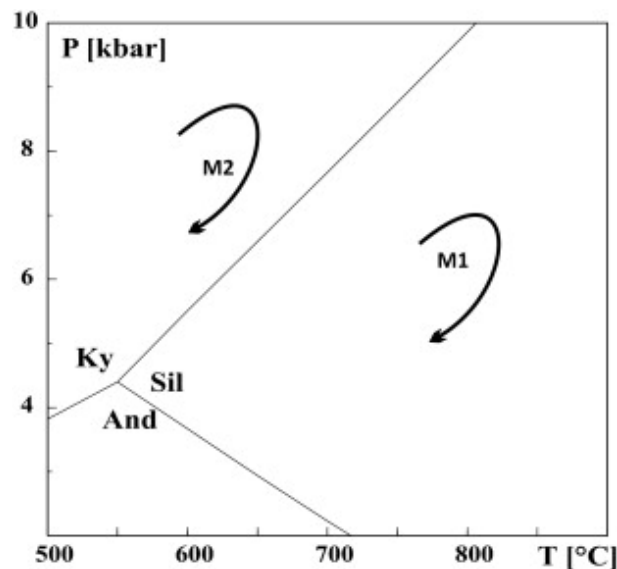
Figure 8: Metamorphic PT conditions of the granulite and amphibolite facies metamorphic events in the Kabul basement rocks (Collett et al., 2015). The granulite facies metamorphism (M1) is only recorded in the Sherdarwaza Formation and the amphibolite facies metamorphism (M2) in both in the Sherdarwaza and Welayati formations.

No granulite facies index phase was observed in the migmatites. Pressure and temperature conditions of 560–650 °C and 8–9 kbar were estimated using garnet + amphibole + plagioclase + quartz thermo-barometry (Dale et al., 2000) and garnet biotite thermometry (Bhattacharya et al., 1992). Mineral com-

positions and calculated pressure and temperature conditions for migmatites (sample F14-9) are listed in Table 5. The metamorphic grade corresponds well to the amphibolites facies overprint in the granulite gneisses.

Table 5: Selected mineral analyses used for geothermobarometry in migmatites (sample F14-9) from the Sherdarwaza Formation.

	Am*	Gr*	Pl*	gr-c	gr-r**	Bt**
SiO_2	40.15	38.17	64.11	38.12	38.68	35.63
TiO_2	0.58	0.07	0.02	0.00	0.04	2.63
Al_2O_3	13.57	20.69	22.42	20.92	20.92	15.55
FeO	21.77	22.83	0.00	22.34	22.27	23.62
MnO	0.26	0.96	0.00	1.54	0.55	0.24
MgO	5.81	0.85	0.00	1.44	1.04	6.95
CaO	11.24	15.67	4.27	15.30	16.27	0.03
Na_2O	1.21	0.09	8.78	0.06	0.00	0.57
K_2O	1.95	0.06	0.20	0.00	0.08	9.85
Total	96.53	99.43	99.82	99.71	99.86	95.10
per	23(O)	12(O)	8(O)	12(O)	12(O)	11(O)
Si	6.239	3.028	2.852	3.007	3.048	2.851
Ti	0.067	0.004	0.001	0.000	0.002	0.159
Al	2.485	1.934	1.175	1.945	1.942	1.466
Fe^{3+}	0.411	0.019	0.000	0.050	0.000	0.000
Fe^{2+}	2.418	1.495	0.000	1.424	1.467	1.580
Mn	0.034	0.065	0.000	0.103	0.036	0.016
Mg	1.346	0.101	0.000	0.169	0.122	0.829
Ca	1.871	1.332	0.203	1.293	1.373	0.002
Na	0.363	0.014	0.757	0.009	0.000	0.088
K	0.386	0.006	0.011	0.000	0.008	1.006
T [°C]	640 ± 30				634 ± 23	
P [Kbar]	8.6					

*Amphibole-garnet-plagioclase-quartz thermobarometry (Dale et al., 2000); **Garnet-biotite thermometry (Bhattacharya et al.,1992)

The Welayati micaschist shows only one metamorphic event with PT conditions of 600–640 °C and 8.5–9.5 kbar. This is again similar to the amphibolite facies overprint recorded in the granulite facies rocks and the metamorphism in the migmatites, respectively. The micaschists are characterized by the presence of prograde zoned garnet, staurolite and kyanite and also by plagioclase, which contains inclusions of white mica and biotite. The plagioclase forms at the expense of paragonite and overgrows the foliation of the rock. Both the Welayati rocks and migmatites of the Sherdarwaza Formation show various degrees of retrogression, expressed by chloritization.

8   Discussion

Mineral textures in combination with geochronological and geochemical data from basement rocks of the Kabul Block allow constraint of its geodynamic evolution during the Archean and Proterozoic periods. The oldest inherited zircon cores with SHRIMP ages of 2.5–2.8 Ga observed in the orthogneisses indicate the presence of Neoarchean crustal material in the Kabul Block. The age of 2474 ± 13 Ma for sample C5-13 from the Kabul airport probably indicates the lower limit of the magmatic event recognized in these rocks. A zircon age of 2.4 Ga, obtained using the Laser ablation method, was also reported by Bohannon (2010) from amphibole schist (intermediate igneous rocks) of the Sherdarwaza Formation south of Kabul (locality no. 5, Fig. 1d). The real geological meaning of younger zircon ages (< 2.4 Ga) is

less clear, whether they represent another magmatic stage or these ages are due to a partial metamorphic resetting of the isotopic system.

The SHRIMP dating of ca. 1.8–1.9 Ma from zircon rims in all of these rocks is a strong evidence for a metamorphic event. Various stages of monazite growth are documented at 1885 ± 28 Ma, 1797 ± 12 Ma and 1771 ± 13 Ma, implying a long-lived metamorphic process. Similar ages by U-Pb (SHRIMP) dating on zircon were reported from migmatite nearby to localities 2 and 4 (Fig. 1d) by Collett (2011). We interpret all these ages to date granulite facies metamorphism and migmatization in the Sherdarwaza Formation. These events are approximately coeval with the formation of the supercontinent Columbia (Meert, 2002, Rogers and Santosh, 2002 and Zhao et al., 2003).

The amphibolite facies metamorphism which is seen throughout the Kabul Block most likely occurred around 900–800 Ma, as suggested by the monazite and Ar-Ar ages for the Welayati micaschists. Single monazite ages close to 820 Ma were also measured in the orthogneiss from the Kabul airport and are interpreted to mark the amphibolite facies overprint seen in this rock. However the Ar-Ar spectra from migmatite generally show a strong disturbance that could be the result of reequilibration or redistribution of radiogenic isotopes during retrogression or younger (Alpine?) metamorphic overprints. The degree of Alpine metamorphism within the Kabul basement units has yet to be properly investigated; however, low-grade conditions are reported elsewhere from the Paleozoic cover sequences in the Kabul Block (Abdullah and Chmyriov, 1977). The age of the amphibolite facies metamorphism in the Kabul basement falls in the period when the Rodinia supercontinent formed. Noteworthy are the older ages of 1.6–1.4 Ga from phlogopite in the granulite facies calc-silicate rocks at the Khair Khana locality. They could be interpreted as a result of excess Ar or as mixed ages between the Paleoproterozoic and Neoproterozoic granulite and amphibolite facies metamorphic events, respectively. As mentioned before, phlogopite is mostly fresh, but contains numerous exsolution lamellae of rutile and/or ilmenite, indicating significant post-crystalline reequilibration.

The Paleoproterozoic U-Pb ages from zircon in the amphibole gneiss of the Welayati Formation that is exposed near contact to the Sherdarwaza rocks also remains unclear. Two alternative interpretations are possible: 1) the amphibolite body is part of the Sherdarwaza Formation and it was tectonically emplaced within the Welayati rocks or 2) the amphibole gneiss represents a clastic sediment, comparable to volcanosedimentary sequences of the Welayati Formation (Abdullah and Chmyriov, 1977). Therefore, the detrital zircon could come from the underlying Sherdarwaza basement rocks. Notably, we did not observe evidence for older granulite facies metamorphism in the amphibole gneiss or in the surrounding amphibolite.

In order to analyze the magmatic and metamorphic events, recognized in the Kabul Block, a short summary on global-scale processes about the amalgamation or destruction of the present day exposed Archean-Proterozoic blocks is given below. This is aimed to discuss possible correlation of the aforementioned magmatic and metamorphic events with particular focus on potential parent cratons from which the Kabul Block could potentially have derived.

The Archean-Paleoproterozoic basements of continental crust

In order to make a comparison between Archean and/or Proterozoic blocks exposed in present day continents (Fig. 9), various criteria, including magmatic and metamorphic events of similar ages are used (Martin, 1999, Kamber and Collerson, 2000, Smithies, 2000, Bindeman et al., 2005, Condie, 2005a, Condie, 2005b, Martin et al., 2005, Naqvi and Rana Prathap, 2007 and Zhang et al., 2012). The Archean – Paleoproterozoic cratons of South America are correlated with those of West Africa on the basis of

3.4–2.9 Ga old TTG gneisses/migmatite complexes and voluminous 2.8–2.6 Ga greenstones (Bullard et al., 1965, Barbosa, 1990 and Alkmim and Marshak, 1998). TTG orthogneisses of Paleoarchean (3.5–3.2 Ga) and Neoarchean (2.7–2.4 Ga) ages are known from South Africa and southern India (Mohan et al., 2012, Bhattacharya et al., 2014, Brandt et al., 2014, Glorie et al., 2014, Samuel et al., 2014, Shaji et al., 2014 and Yang et al., 2014). A Neoarchean-Paleoproterozoic (2.8–2.1 Ga) link between South Africa and Western Australia has been proposed, based on similar stratigraphy with banded iron formations (Button, 1976, Cheney, 1996 and Zegers et al., 1998). On the other hand, connections between Laurentia (North America and Greenland) and Baltica during the Paleoproterozoic are constrained by paleomagnetic, iso-topic, lithological, structural, and geochronological data (Hoffman, 1988, Hoffman, 1989 and Gower et al., 1990). A large number of SHRIMP and U-Pb zircon age data and geochemical data were recently obtained from both the Tarim and China blocks and they indicated the presence of Archean basement with Neoarchean (2.7–2.4 Ga) magmatism (for ref. see Shi et al., 2012, Wang and Liu, 2012, Wang et al., 2012, Zhang et al., 2012, Ge et al., 2013, Ge et al., 2014b and Ge et al., 2014a).
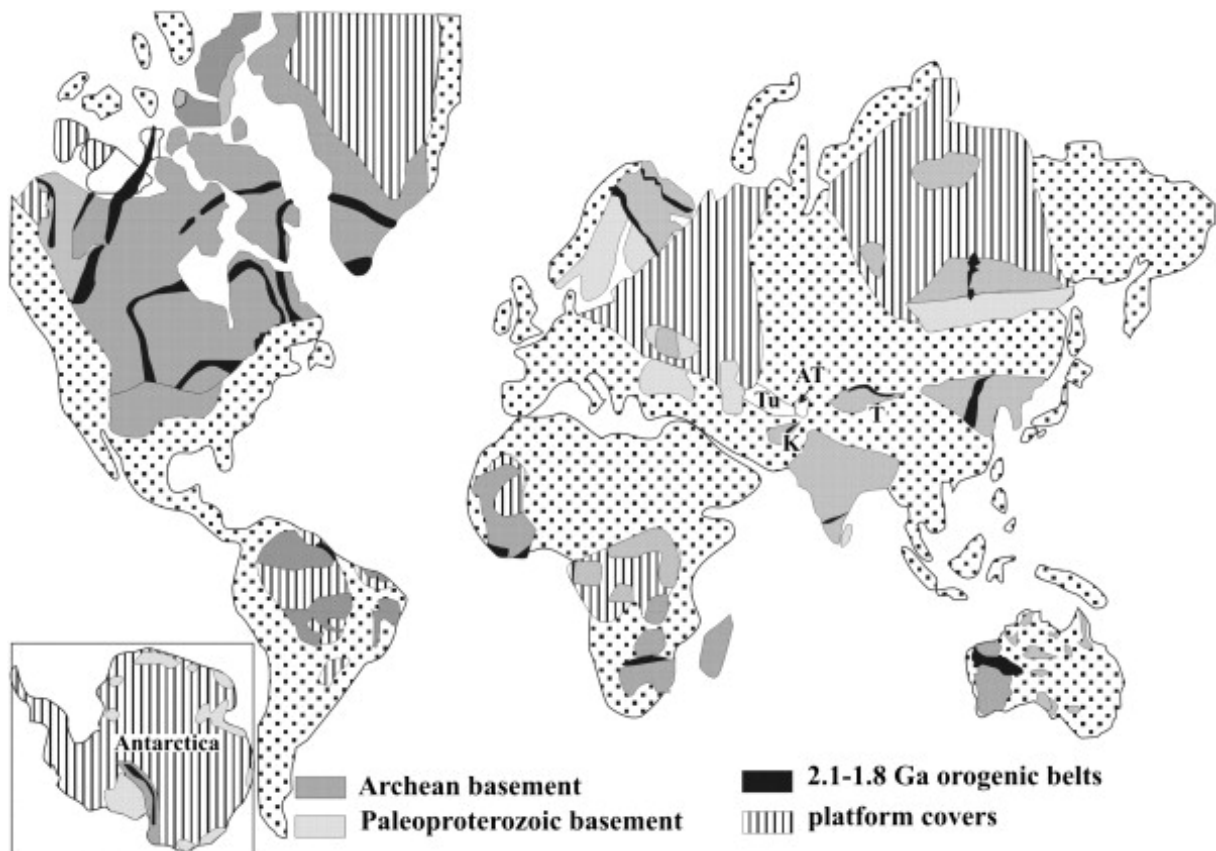
Figure 9: Spatial distribution of 2.1–1.8 Ga orogens and associated Archean cratons (Zhao et al., 2002, modified). A-Afghan Central blocks with position of Neoarchean of Kabul Block, AT-Afghan-Tajik Block, T-Tarim Block and Tu-Turan Block.

The assembly of Columbia was completed during a sequence of global-scale 2.1–1.8 Ga collisional events (Rogers and Santosh, 2002, Zhao et al., 2003 and Meert, 2014). Evidence for these events has been recog-nized in most Archean blocks (Fig. 9). In many cases, possible connections between various continental blocks or their orogenic belts have been well established. Some authors (Hoffman, 1991, Condie and Rosen, 1994, Frost et al., 1998, Smethurst et al., 1998, Ernst et al., 2000, Piper, 2000 and Sears and Price, 2000) correlate the Paleoproterozoic orogens and cratonic blocks in Laurentia with those in Siberia. A connection of Central Australia with northwestern Laurentia and East Antarctica is also considered (Dalziel, 1991, Hoffman, 1991, Moores, 1991, Ross et al., 1992, Borg and DePaolo, 1994 and Burrett and

Berry, 2000). According to Chen et al (2013) the Tarim Craton shared a similar tectonic history with the North China Craton. It is thus likely that these two cratons converged during the Paleoproterozoic, co-inciding with the global assembly of the Columbia supercontinent. The age of amphibolite to granulite facies metamorphism of about 1.9 Ga was established by SHRIMP and Laser ablation ICPMS technique both in the North China and Tarim cratons (Hu et al., 2000, Zhang et al., 2007, Liu et al., 2009, Wang et al., 2009, Long et al., 2010, Long et al., 2012, Chen et al., 2013, He et al., 2013, Zhang et al., 2013, Ge et al., 2014b and Ge et al., 2014a).

Rodinia and the Grenvillian Orogeny

There is a broad agreement that the amalgamation of Rodinia was completed at about 1.0 Ga (Dalziel et al., 2000). However, many parts of Rodinia (Fig. 10) had collided earlier (Torsvik et al., 1996, Meert et al., 2004 and Li et al., 2008). Collision zones with an age around 1100 Ma are known along the southwestern margin of Laurentia, in parts of Cathaysia, Central Australia and at the western margin of Baltica. At 1050 Ma the Kalahari collided with the SW margin of Laurentia and collision started along the western margin of Australia, the eastern margin of India, and the northern margin of Congo-Sao Francisco. These orogenic zones remained active until 1000 Ma. At 900 Ma (Fig. 10), India collided along its eastern margin with Eastern Antarctica and Australia. Like the Tarim Block, the North China Block was surrounded by collision zones during this time. The period of 850 Ma is characterized by the formation of continental rifts, spreading ridges and superplumes that continued to ~ 720 Ma. As suggested by Hoffman (1991), the break-up of the Rodinia supercontinent involved fragmentation around Laurentia with continental pieces moving away from Laurentia and colliding on the other side of the Earth to form Gondwana. The collision between Laurentia–Cathaysia and Yangtze started after ca.1140 Ma and lasted to ca. 900 Ma (Li et al., 2003 and Ling et al., 2003).
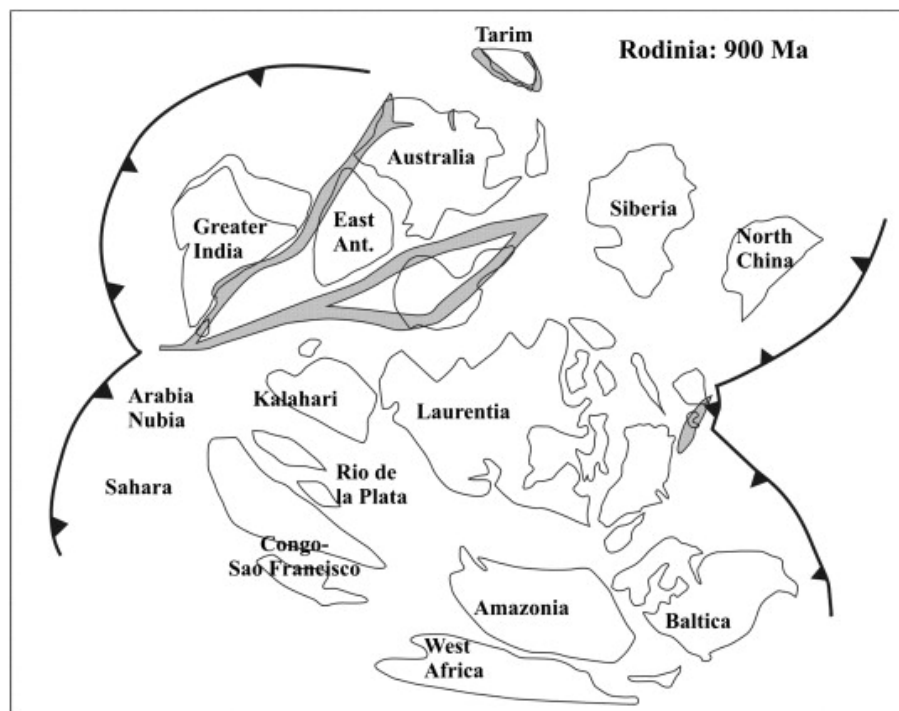

Figure 10: Cartoon showing orogenic events and active margins (shaded area) in Rodinia at 900 Ma (Li et al., 2008).

In the Tarim Craton, magmatic and metamorphic ages of 1002–907 Ma and 950–910 Ma respectively,

were reported from granitic gneiss and metapelites in the Qaidam-Qilian Block (Song et al., 2012). The authors interpret these ages as a direct evidence of the Grenvillian age orogeny that extended northwestward from the Yangtze Block to the Qaidam-Qilian Block in the Tarim Craton. According to R. Ge et al. (2014) and R.F. Ge et al. (2014) the Neoproterozoic tectonothermal events in the northern Tarim Craton were not related to the assembly of Rodinia, but a long-lived subduction-accretionary orogeny in central Asia. However, a continental rift setting associated with the break-up of the Rodinia supercontinent has been proposed based on the 820–735 Ma magmatic pulses along the northern margin of the Tarim Craton, which include ultramafic–mafic–carbonatite complex and adakitic granitoids with bimodal intrusive and volcanic rocks (Xu et al., 2005, Zhang et al., 2007, Zhu et al., 2008, Zhang et al., 2009a, Zhang et al., 2009b, Zhang et al., 2010, Long et al., 2011, Zhang et al., 2011 and Zhu et al., 2011). He et al. (2012) reported metamorphic ages of ca. 790–820 Ma also for HP granulites in the northern margin of the Tarim Craton.

Gondwana and the Pan-African Orogeny

The period between 630 and 530 Ma is characterized by the formation of Gondwana (Meert, 2003 and Meert and Lieberman, 2008). This was accompanied by collision zone processes that started with the accretion of Amazonia-West Africa with the Sahara-Congo-Sao Francisco cratons and ended by collision with India, East Antarctica and Australia (Fig. 11). Gondwana amalgamated through the closure of the so-called "Mozambique Ocean", (Meert, 2003, Jacobs and Thomas, 2004 and Collins and Pisarevsky, 2005). The North China and Tarim blocks with other Asian fragments were located on the northern passive margin of the Proto-Tethys Ocean (Kusky et al., 2003) and they were not affected by Mozambique or Panafrican Orogenies. However, Stampfli and Borel (2004) consider that the Tarim Block was part of Gondwana and attached to the southern margin of Asia during the closure of the Asiatic Ocean in the Devonian. The Paleotethys (or a branch of this ocean) is assumed to have separated Gondwana from the body of Eurasian blocks during the Middle Paleozoic to Lower Permian times (Stöcklin, 1974, Stöcklin, 1977, Boulin, 1990 and Stampfli et al., 2011). In this interpretation, the Iranian and Afghan blocks are interpreted as part of northeastern margin of Gondwana at the contact with the Arabian plate (Kroener and Stern, 2005). According to Boulin (1990), this part of the Paleotethys coexisted at that time with the Turkestan Ocean, the present suture of which separates the Turan-Turkestan-Tarim blocks from the northernmost Eurasian blocks and probably finds its prolongation in the Uralian suture.

Summary of Precambrian events in the Kabul Block and its relation to other continental blocks

The results of this study show that the Kabul Block represents a fragment of an Archean craton which was affected by two 1.9–1.8 Ga and 0.9–0.8 Ga orogenic events. As mentioned above, the position of Archean blocks, exposed around the present day continents (Fig. 9), are the results of multiple rotations and displacements during geological history (e.g. Pesonen et al., 2003, Pisarevsky et al., 2003 and Li and Peng, 2010). The presence of Neoarchean magmatism, followed by metamorphism during Paleoproterozoic and Neoproterozoic orogenies in the Kabul Block reduces the criteria to be used for its correlation with similar blocks or potential parent cratons. The Precambrian history of the Kabul Block indicates several comparable features with the Tarim or South China cratons. This includes the Neoarchean TTG-like magmatism and the Paleoproterozoic granulite facies and Neoproterozoic amphibolite facies metamorphism as reported from these two cratons (Hu et al., 2000, Li et al., 2003, Ling et al., 2003, Wang et al., 2009, Long et al., 2010, Long et al., 2012, Song et al., 2012, Chen et al., 2013, He
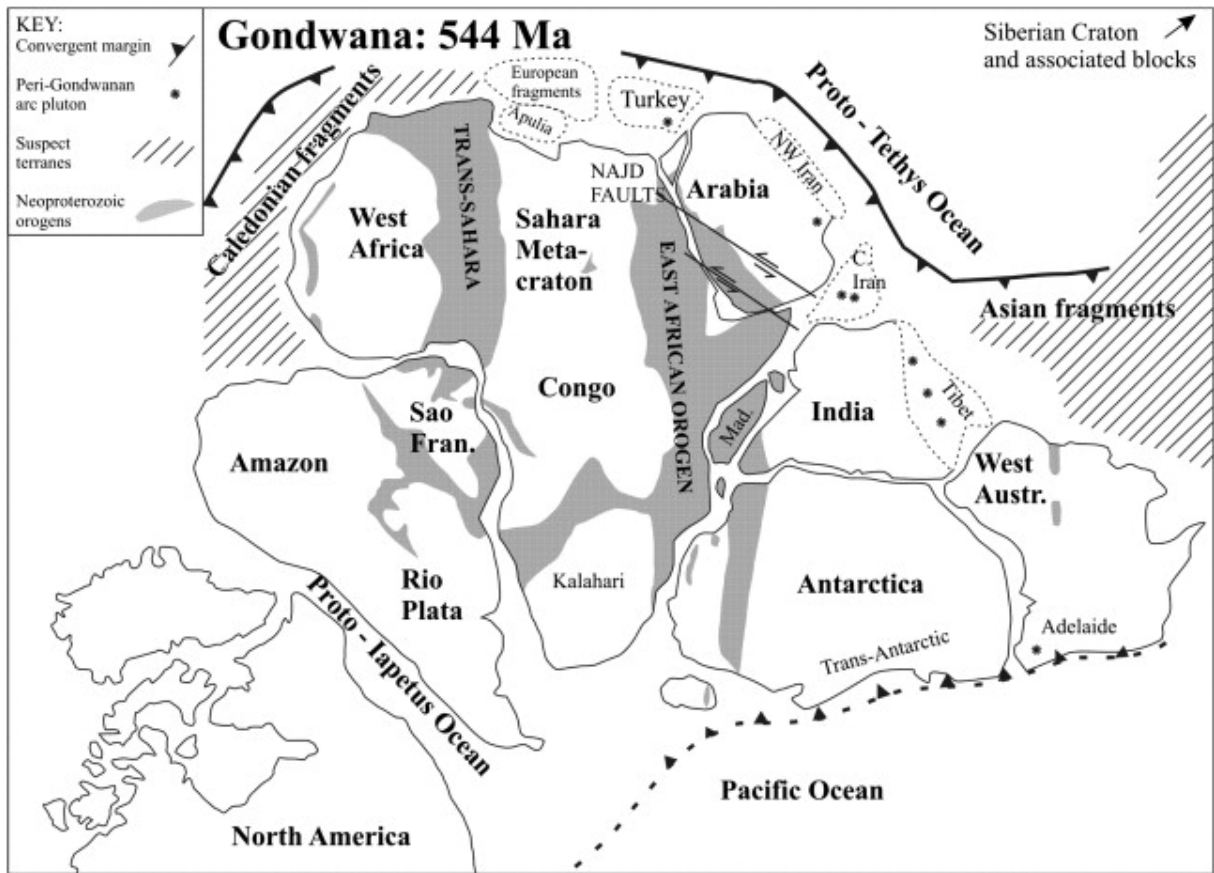
Figure 11: Map of Gondwana at the end of Neoproterozoic time (ca 540 Ma) showing general arrangement of continental blocks and of Pan-African Belt (Kusky et al., 2003).

et al., 2013 and Zhang et al., 2013). However, this interpretation does not fit well with the Paleozoic and Mesozoic configuration as assumed by some authors for the Afghan Central blocks. According to Treloar and Izatt (1993) and Tapponnier et al. (1981), the Farah, Helmand and Kabul blocks were separated from the northern margin of Gondwana and subsequently joined the southern Asian margin during two or three subduction events of upper Triassic, lower Cretaceous and Paleocene age. Stampfli and Borel (2004) consider that the Afghan Central blocks have close affinity with the Iran Central blocks and they were detached from eastern part of the Arabian plate or northern part of India during the closure of Paleotethys in the Triassic. Detachment of Tarim and North China cratons from Gondwana in this model is assumed to have occurred by the opening of the Asiatic Ocean during the Cambrian and the cratons attached to the southern margin of Asia in the Late Paleozoic. As there is no information regarding Archean or Paleoproterozoic orogenies in the Iran Central blocks, it is difficult to correlate it with the Afghan Central blocks. Conversely, no evidence of the Proto-Tethyan related magmatic arc (0.52–0.55 Ga), which is known from the Iran Central blocks (Ramezani and Tucker, 2003 and Rahmati-Ilkhchi et al., 2011), have been reported from the Afghan Central Blocks yet. According to the Cambrian (530 Ma) configuration of Li et al (2008), the Tarim Craton was next to Australia, and the North China Craton occurred as a separate block, so that both could have escaped the Pan-African Orogeny.

Based on the Paleozoic evolution of Central Asia (Boulin, 1991 and Sengör et al., 1993); Xiao et al., 2013, Xia et al., 2014 and Biske and Seltmann, 2010), the North China, Tarim and Karakoram blocks were separated by two east-west trending oceans during the early Paleozoic, the Tethys Ocean in the south and the Tianshan Ocean in the north. In this model, the Afghan-Tajik Block was part of the Tarim or Karakoram blocks. Connection of the Afghan-Tajik and Turan blocks (Fig. 1a) and their relations to the Belomorians were assumed by Abdullah and Chmyriov (1977). The Archean and Paleoproterozoic ages of 2.4–2.7 Ga and 1.75 Ga for the Afghan-Tajik Block were confirmed by lead isochrones and by K-Ar for phlogopite in marble from Pamir (Khoreva et al., 1971). These rocks are compared with those in the Sare Sang series with Lapis-Lazuli deposit (Faryad, 1999 and Faryad, 2002). According to Boulin (1991) the Hindu Kush mountain belt is a multiple suture zone that separated the Afghan Tajik blocks from the Afghan Central blocks (Fig. 1a). The closure of the Paleozoic Hindu Kush Ocean is documented by the presence of Devonian blueschist facies rocks in the Western Hindu Kush (Bouyx and Collomb, 1985 and Blaise et al., 1993; see also Faryad et al., 2013). Reopening of this ocean during the Permian and its closure in the early Triassic is documented by the Triassic plutonic arc in the western Hindu Kush and Pamir (Debon et al., 1987). In the present configuration, the Hindu Kush Devonian Ocean could be the continuation of the South Tianshan Ocean (Xiao et al., 2013 and Xia et al., 2014) and the Tarim, Karakoram and Afghan blocks occurred south of this ocean (Fig. 1a) during the period from the Devonian to the Late Carboniferous. To confirm the Paleozoic evolution of the Afghan Central blocks and Hindu Kush Ocean and correlate them with Iran Central blocks and South Tianshan Ocean, respectively, detailed petrology, geochemistry and geochronological data from the other Afghan blocks are needed.

9   Acknowledgments

10   Supplementary material

Table A: $^{40}Ar/^{39}Ar$ isotopic ratios and ages of micas from the Kabul basement rocks

Release T (°C)	39%	40*(mV)	%rad	39/37	%36Ca	40*/39	Age (Ma)	± Age
Sample Cl- 5; Muscovite, cg., 15 mgJ =0.014500 0.4%								
635	0.60%	11.93	73.70%	81	0.02%	15.76	371.2	11.5
710	1.10%	43.94	84.80%	157	0.01%	29.86	649.1	8.7
760	9.10%	547.21	99.10%	433	0.05%	45.00	906.1	5.2
810	33.50%	1573.29	99.50%	598	0.10%	35.15	743.0	4.8
880	16.20%	620.99	98.90%	579	0.05%	28.65	626.8	5.3
940	5.40%	195.36	97.20%	511	0.02%	27.21	599.9	5.4
1070	18.60%	747.57	99.20%	265	0.13%	30.14	654.1	3.8
1260	15.60%	685.6	98.90%	44	0.54%	2.98	705.1	5.2
					total gas age:		705.8	8.3
					[1]plateau age:		705.8	8.3
Sample F- 6; Phlogopite, 15.2 mgJ =0.014500 0.4%								
600	0.90%	127.38	93.00%	22	0.08%	61.43	1149.1	49.9
635	0.60%	104.28	92.10%	15	0.09%	75.02	1328.0	34.2
670	1.10%	209.96	95.00%	28	0.07%	79.25	1380.1	16.5
710	2.80%	572	97.30%	170	0.02%	88.09	1484.7	18
760	7.80%	1530.08	99.10%	381	0.03%	84.07	1437.9	8.8
810	13.00%	2534.14	99.80%	632	0.07%	84.00	1437.0	5.7
880	16.50%	3325.71	99.40%	804	0.02%	86.69	1468.5	11.2
940	14.80%	3090.04	99.10%	452	0.02%	89.59	1501.9	17.1
1070	25.70%	5276.05	98.80%	694	0.01%	88.47	1489.1	8.3
1260	16.80%	3377.61	99.10%	102	0.10%	86.75	1469.2	9.1
					total gas age:		1468.1	16.9
					[1]plateau age:		1468.1	16.9
Sample Cl - 6; Muscovite, 14 mgJ =0.014880 0.4%								
610	2.10%	62.1	88.20%	25	0.09%	25.05	571.5	11.9
655	3.20%	111.28	94.20%	39	0.12%	29.07	648.4	8.4
680	2.60%	93.61	93.50%	101	0.04%	30.65	677.8	11.4
725	3.40%	137.96	94.80%	132	0.03%	34.51	747.7	7.7
765	11.90%	506.7	98.10%	144	0.08%	36.12	775.9	3.3
810	28.40%	1280.49	99.10%	128	0.20%	8.10	810.1	4.7
870	19.20%	779.47	99.00%	123	0.20%	34.27	743.4	2.8
920	9.60%	410.38	97.60%	116	0.08%	36.29	779.0	4.2
1040	19.60%	938	99.00%	47	0.44%	40.41	849.3	5
					total gas age:		782.2	8.6
Sample Cl - 7; Biotite, 15 mgJ =0.014880 0.4%								
600	0.50%	23.25	71.30%	61	0.02%	20.64	483.1	20.2
635	1.70%	134.6	92.80%	78	0.04%	37.46	799.2	9.4
670	2.40%	197.53	95.80%	78	0.06%	39.34	831.4	5.9
710	3.00%	259.05	96.60%	77	0.07%	40.71	854.4	6.6
760	9.40%	848.08	98.70%	73	0.21%	42.02	876.2	3.9
810	11.10%	1019.55	98.90%	51	0.35%	43.15	894.8	4.3
880	13.90%	1300.43	99.10%	65	0.35%	43.71	903.9	4.5
940	10.50%	980.25	99.00%	35	0.58%	43.60	902.1	5.5
1070	30.10%	2799.21	99.60%	54	1.01%	43.61	902.2	2.9
1260	17.40%	1617.61	99.30%	14	2.12%	43.43	899.3	2.5
					total gas age:		891.6	7.9
					[1]plateau age:		900.9	7.4
Sample Cl - 7; Muscovite, 17.6 mgJ =0.014880 0.4%								
610	1.00%	30.53	65.80%	19	0.05%	15.87	382.5	22.3
655	1.50%	72.21	79.30%	29	0.04%	24.87	568.1	16.4
680	1.80%	96.69	93.70%	36	0.13%	27.20	613.1	11
725	2.80%	172.1	96.30%	57	0.12%	30.31	671.6	4.6
765	18.40%	1423.64	99.10%	185	0.14%	38.68	820.1	9.9
810	17.80%	1270.56	99.20%	179	0.18%	35.68	768.3	4.2
870	11.30%	775.79	99.10%	227	0.12%	34.43	746.2	2.9
920	6.00%	441.07	98.00%	121	0.09%	36.80	787.7	4.1
1040	18.90%	1444.56	99.40%	95	0.43%	38.11	810.3	5
1250	20.60%	1629.48	99.20%	42	0.63%	39.52	834.4	3
					total gas age:		786.0	9.4

Table A: Ar/Ar data Lund

Watts	Ca/K	Cl/K	%36Ca	40*/39	Mol 39	% Step	%40*	Age (Ma)	± Age
Sample F15-9, Run ID# 2157-01, Muscovite (J = 0.004339 ± 7.400000e-6), 99.5 %Rad										
1.8	236011	0.001	0.20	296.0	0.012	0.40	89.9	1490.4	11.4
1.9	178286	0.015	0.80	312.3	0.015	0.40	97.6	1545.4	8.4
2.0	0.144	0.001	0.30	296.1	0.126	3.70	99.5	1490.6	3.9
2.1	0.024	0.001	0.10	251.0	0.255	7.50	99.7	1329.0	3.3
2.2	0.077	0.004	0.30	266.5	0.490	14.40	99.7	1386.4	2.6
2.3	0.658	0.019	0.80	334.9	0.761	22.40	99.2	1618.9	4.3
2.4	0.002	0.002	0.00	325.7	0.692	20.40	99.6	1589.3	2.6
2.5	0.168	0.002	0.60	315.1	0.153	4.50	99.7	1554.5	3.8
2.7	0.024	0.001	0.10	299.7	0.467	13.70	99.7	1502.8	2.4
2.9	0.030	0.001	0.30	311.7	0.337	9.90	99.9	1543.5	3.2
3.2	0.059	0.011	0.10	329.1	0.087	2.60	99.4	1600.4	4.2
3.5	0.369	0.029	0.10	226.1	0.006	0.20	93.3	1233.3	22.7
4.0	-341365	0.018	-1.50	169.5	0.007	0.20	95.5	994.4	16.7
								1528.0	5.0
Sample F15-9, Run ID# 2157-02, Muscovite (J = 0.004339 ± 7.400000e-6), 99.6 %Rad										
2.0	108015.0	0.021	0.10	307.3	0.013	0.50	88.2	1528.5	11.4
2.1	0.1	0.001	0.10	325.3	0.021	0.80	98.9	1588.1	8.1
2.2	0.3	0.006	0.40	319.1	0.139	5.00	99.2	1567.9	3.3
2.3	0.2	0.006	0.30	327.5	0.231	8.40	99.4	1595.0	3.3
2.4	0.0	0.004	0.10	344.7	0.476	17.20	99.6	1649.9	2.5
2.5	0.0	0.003	0.00	336.9	0.668	24.20	99.6	1625.1	2.5
2.7	0.0	0.002	0.00	366.1	0.972	35.20	99.9	1715.8	2.2
2.9	0.1	0.000	1.00	356.2	0.097	3.50	99.9	1685.5	3.9
3.2	0.1	0.003	0.10	359.3	0.148	5.30	99.0	1695.2	4.0
3.5	2079	0.022	0.50	295.2	0.004	0.10	95.7	1487.6	31.3
4.0	392191	0.393	0.30	202.8	0.001	0.00	79.4	1138.8	129.2
5.0	-654282	-24156	1.20	749.1	0.000	0.00	133.8	2610.6	348.4
								1662.0	5.0
Sample F15-9, Run ID# 2157-03, Muscovite (J = 0.004339 ± 7.400000e-6), 99.6 %Rad										
1.8	172743	0.016	0.40	305.9	0.023	1.20	95.0	1523.9	7.1
1.9	0.12	0.002	0.10	314.9	0.074	3.80	98.4	1554.0	3.9
2.0	0.06	0.002	0.10	321.8	0.165	8.50	98.8	1576.6	3.0
2.1	0.33	0.001	0.40	284.4	0.121	6.20	99.1	1450.2	3.1
2.2	0.16	0.002	0.40	312.8	0.211	10.80	99.5	1547.1	2.7
2.3	0.07	0.003	0.40	276.6	0.455	23.30	99.8	1422.6	2.1
2.4	0.11	0.031	0.30	298.2	0.008	0.40	99.6	1497.7	17.1
2.5	104067	0.019	3.40	322.0	0.009	0.40	99.7	1577.3	15.6
2.7	0.24	0.002	0.80	325.0	0.075	3.80	99.7	1587.1	3.9
2.9	0.07	0.000	0.40	250.6	0.086	4.40	99.7	1327.7	3.6
3.2	0.06	0.006	0.10	324.3	0.113	5.80	99.6	1584.6	4.4
3.5	0.09	0.002	0.20	324.5	0.305	15.60	99.5	1585.5	2.8
4.0	0.01	0.004	0.00	320.9	0.275	14.10	99.8	1573.6	2.9
5.0	0.15	0.009	1.60	291.4	0.034	1.80	99.9	1474.4	5.1
								1519.0	4.0

Table A: Ar/Ar data Lund (contd.)

Watts	Ca/K	Cl/K	%36Ca	40*/39	Mol 39	% Step	%40*	Age (Ma)	± Age
Sample F13-9, Run ID# 2158-01, Muscovite (J = 0.004339 ± 7.400000e-6), 99.5 %Rad									
1.8	136075	0.015	0.20	64.3	0.005	0.30	69.1	443.9	27.8
1.9	172727	0.006	1.00	77.9	0.010	0.50	93.3	525.3	14.2
2.0	0.02	0.003	0.00	116.6	0.075	4.20	97.3	738.7	3.0
2.1	0.01	0.001	0.10	112.8	0.365	20.60	99.7	718.5	2.0
2.2	0.01	0.000	0.00	104.7	0.309	17.40	98.7	675.9	2.0
2.3	0.01	0.000	0.10	98.3	0.570	32.10	99.7	640.8	2.0
2.4	0.04	0.002	0.20	95.9	0.149	8.40	99.2	627.8	2.1
2.5	0.07	0.003	1.00	90.1	0.066	3.70	99.8	595.4	2.9
2.7	0.16	0.001	0.50	92.7	0.075	4.20	98.8	609.7	2.6
2.9	0.83	0.024	1.30	107.0	0.040	2.30	98.1	688.0	4.7
3.2	0.82	0.026	0.60	108.9	0.027	1.50	95.8	698.4	5.5
3.5	159731	0.051	0.60	105.7	0.013	0.70	92.1	681.2	11.5
4.0	0.06	0.001	0.10	118.5	0.068	3.80	98.8	748.6	3.1
5.0	144909	0.022	0.20	144.5	0.007	0.40	85.9	878.3	17.9
								670.0	3.0
Sample F13-9, Run ID# 2158-02, Muscovite (J = 0.004339 ± 7.400000e-6), 99 %Rad									
1.8	242548	0.016	0.30	69.1	0.012	0.40	72.9	473.4	12.3
1.9	0.16	0.002	0.10	103.1	0.073	2.30	95.2	667.2	2.7
2.0	0.01	0.001	0.00	112.6	0.378	11.80	98.1	717.9	1.7
2.1	0.03	0.000	0.20	110.5	0.671	20.90	99.4	706.8	1.4
2.2	0.02	0.000	0.00	105.3	0.531	16.50	98.6	678.8	1.4
2.3	0.00	0.000	0.00	105.5	0.307	9.60	99.4	679.8	1.5
2.4	0.01	0.001	0.30	106.6	0.278	8.70	99.9	685.9	1.6
2.5	0.02	0.001	2.60	103.3	0.307	9.50	100.0	668.0	1.5
2.7	0.03	0.001	2.30	98.5	0.364	11.30	100.0	641.7	1.5
2.9	0.26	0.011	0.70	96.3	0.054	1.70	98.6	629.6	3.1
3.2	0.50	0.017	1.40	93.4	0.036	1.10	98.7	613.6	3.7
3.5	0.54	0.005	1.20	104.9	0.027	0.80	98.5	677.0	4.9
4.0	0.84	0.019	1.60	106.6	0.033	1.00	98.3	686.0	4.3
5.0	0.05	0.000	0.50	109.9	0.144	4.50	99.6	703.3	1.9
								683.0	2.0
Sample F13-9, Run ID# 2158-03, Muscovite (J = 0.004339 ± 7.400000e-6), 99.3 %Rad									
1.8	169475	0.005	0.40	80.7	0.007	0.20	85.7	541.4	15.7
1.9	0.30	0.002	0.50	116.8	0.067	1.50	98.4	739.6	2.4
2.0	0.07	0.002	0.30	113.1	0.087	2.00	99.3	720.3	2.1
2.1	0.00	0.000	0.00	114.2	0.399	9.00	98.4	726.0	1.5
2.2	0.03	0.001	0.20	110.3	0.480	10.90	99.6	705.7	1.5
2.3	0.01	0.001	0.00	108.3	0.521	11.80	99.3	695.2	1.4
2.4	0.06	0.000	1.50	88.1	0.504	11.40	99.9	584.3	1.2
2.5	0.24	0.001	5.40	75.8	0.127	2.90	99.8	512.9	1.6
2.7	0.12	0.002	0.80	97.9	0.101	2.30	99.5	638.6	1.8
2.9	0.13	0.000	2.00	128.8	0.142	3.20	99.8	800.8	2.1
3.2	0.03	0.001	0.10	145.5	0.441	10.00	99.1	883.1	1.8
3.5	0.02	0.001	0.10	108.3	1.283	29.00	99.5	695.1	1.2
4.0	0.43	0.001	7.40	99.9	0.063	1.40	99.8	649.4	2.7
5.0	0.08	0.001	5.50	104.2	0.209	4.70	100.0	672.8	1.6
								703.0	2.0

Table A: Ar/Ar data Lund (contd.)

Watts	Ca/K	Cl/K	%36Ca	40*/39	Mol 39	% Step	%40*	Age (Ma)	± Age
Sample F14-9, Run ID# 2164-02,biotite(J = 0.004339 ± 7.400000e-6), 99.4 %Rad									
1.8	0.07	0.033	0.00	26.5	0.012	0.60	56.4	196.6	10.7
1.9	0.39	0.028	0.20	74.4	0.020	1.00	90.4	505.0	6.8
2.0	0.22	0.002	0.30	106.6	0.052	2.60	97.3	685.8	3.2
2.1	0.12	0.002	0.40	105.9	0.109	5.40	99.1	682.3	2.2
2.2	0.07	0.003	0.40	115.3	0.264	13.10	99.6	732.1	1.6
2.3	0.06	0.002	0.50	121.8	0.171	8.50	99.7	765.5	1.9
2.4	0.20	0.002	1.40	124.7	0.209	10.40	99.6	780.0	1.9
2.5	0.08	0.000	0.90	122.1	0.182	9.00	99.7	766.8	1.9
2.7	0.10	0.001	0.60	118.2	0.242	12.00	99.5	746.9	1.8
2.9	0.04	0.002	0.40	126.7	0.258	12.80	99.7	790.1	1.8
3.2	0.00	0.001	0.00	142.3	0.363	18.00	99.7	867.4	1.9
3.5	0.36	0.001	0.70	128.9	0.053	2.60	98.7	801.3	3.7
4.0	0.15	0.001	0.30	139.7	0.060	3.00	98.7	854.6	3.3
5.0	0.20	0.010	3.10	112.3	0.019	0.90	99.8	716.0	6.2
								774.0	3.0
Sample F14-9, Run ID# 2164-03, biotite (J = 0.004339 ± 7.400000e-6), 99.3 %Rad									
1.8	0.22	0.010	0.10	55.3	0.026	0.90	79.3	388.2	5.0
1.9	126614	0.021	0.60	76.7	0.045	1.50	91.3	518.3	3.5
2.0	132326	0.018	1.20	105.3	0.054	1.80	96.6	678.7	3.2
2.1	106859	0.011	1.70	108.5	0.080	2.70	98.1	696.2	2.7
2.2	0.19	0.005	0.60	113.7	0.126	4.30	99.1	723.6	2.3
2.3	0.18	0.006	1.00	123.8	0.155	5.30	99.5	775.8	1.8
2.4	0.04	0.004	0.40	125.9	0.177	6.00	99.7	786.5	2.1
2.5	0.11	0.002	0.40	129.8	0.192	6.60	99.4	805.7	1.7
2.7	0.06	0.003	0.40	130.9	0.299	10.20	99.7	811.4	1.6
2.9	0.02	0.001	0.30	131.6	0.254	8.70	99.8	814.7	1.8
3.2	0.03	0.001	0.20	135.2	0.336	11.40	99.7	832.6	1.4
3.5	0.01	0.001	0.10	119.4	0.354	12.10	99.7	753.1	1.5
4.0	0.49	0.001	3.20	75.3	0.320	10.90	99.3	509.9	1.1
5.0	0.44	0.003	3.30	106.5	0.515	17.60	99.6	685.3	1.3
								734.0	2.0
Sample F12-9, Run ID# 2156-01, biotite (J = 0.004339 ± 7.400000e-6), 99.5 %Rad									
1.8	0.24	0.009	0.20	112.2	0.021	1.00	95.8	715.7	5.9
1.9	0.01	0.000	0.00	113.0	0.053	2.50	98.8	719.6	3.1
2.0	0.02	0.001	0.00	117.5	0.101	4.70	98.2	743.5	2.4
2.1	0.03	0.001	0.10	110.5	0.162	7.50	98.9	706.6	1.7
2.2	0.01	0.002	0.10	83.5	0.296	13.60	99.4	557.7	1.5
2.3	0.04	0.002	0.70	101.9	0.189	8.70	99.8	660.5	1.6
2.4	0.07	0.003	1.60	108.9	0.193	8.90	99.9	698.2	1.8
2.5	0.00	0.003	0.00	109.6	0.153	7.10	99.6	701.6	2.1
2.7	0.00	0.002	0.00	109.8	0.260	12.00	99.7	703.1	1.8
2.9	0.00	0.003	0.10	113.3	0.299	13.80	99.8	721.4	2.3
3.2	0.00	0.001	0.00	113.0	0.341	15.70	99.9	719.9	1.5
3.5	0.02	0.001	0.30	111.4	0.077	3.50	99.8	711.2	2.6
4.0	0.16	0.011	0.40	98.9	0.024	1.10	98.6	644.1	5.6
5.0	0.91	0.002	0.70	79.9	0.008	0.40	94.9	537.2	16.0
								687.0	2.0

Table A: Ar/Ar data Lund (contd.)

Watts	Ca/K	Cl/K	%36Ca	40*/39	Mol 39	% Step	%40*	Age (Ma)	± Age
Sample F12-9, Run ID# 2156-02, biotite (J = 0.004339 ± 7.400000e-6), 99.5 %Rad									
1.8	0.16	0.006	0.10	98.0	0.010	0.50	92.4	639.1	13.0
1.9	0.34	0.025	0.20	105.1	0.029	1.50	95.4	677.8	4.5
2.0	0.01	0.005	0.00	107.8	0.100	5.00	98.7	692.0	2.0
2.1	0.01	0.003	0.10	106.4	0.090	4.50	99.7	684.8	2.4
2.2	0.08	0.000	1.00	106.1	0.136	6.80	99.8	683.0	2.0
2.3	0.16	0.004	2.90	104.7	0.107	5.40	99.8	675.7	2.1
2.4	0.17	0.005	0.50	103.5	0.113	5.70	98.8	669.4	2.0
2.5	0.11	0.004	0.50	104.8	0.110	5.50	99.3	676.5	2.1
2.7	0.03	0.004	0.10	106.6	0.248	12.40	99.4	685.9	1.7
2.9	0.03	0.002	0.80	106.9	0.203	10.10	99.9	687.3	1.8
3.2	0.02	0.002	0.30	107.1	0.305	15.20	99.8	688.8	1.4
3.5	0.10	0.002	6.30	106.9	0.199	9.90	100.0	687.6	1.9
4.0	0.05	0.001	0.70	109.0	0.140	7.00	99.7	698.8	2.0
5.0	0.04	0.001	0.20	110.9	0.222	11.10	99.3	708.7	1.7
								688.0	2.0
Sample F12-9, Run ID# 2156-03, biotite (J = 0.004339 ± 7.400000e-6), 99.5 %Rad									
1.8	0.56	0.015	0.40	94.1	0.023	1.00	95.2	617.6	5.3
1.9	0.43	0.003	3.10	103.8	0.032	1.40	99.6	671.0	4.2
2.0	0.06	0.004	0.20	102.3	0.100	4.40	99.1	662.7	1.9
2.1	0.09	0.001	1.80	108.5	0.124	5.40	99.8	695.8	1.6
2.2	0.01	0.004	0.10	110.3	0.183	8.00	99.7	705.6	1.7
2.3	0.23	0.008	1.50	109.2	0.134	5.90	99.5	699.7	1.8
2.4	0.11	0.006	1.70	108.5	0.162	7.10	99.8	696.2	1.6
2.5	0.19	0.010	3.40	106.0	0.141	6.20	99.8	682.5	1.9
2.7	0.02	0.004	0.40	105.7	0.257	11.30	99.8	681.0	1.6
2.9	0.03	0.004	1.10	108.1	0.247	10.80	99.9	693.7	1.4
3.2	0.01	0.004	0.10	103.8	0.332	14.60	99.7	670.7	1.5
3.5	0.00	0.002	0.00	106.5	0.197	8.60	99.5	685.5	1.6
4.0	0.05	0.004	0.20	100.5	0.239	10.50	99.1	652.7	1.3
5.0	0.07	0.005	0.10	100.9	0.108	4.80	97.5	655.0	2.2
								681.0	2.0

Samples F-6, Cl-5, Cl-6 and Cl-7 were measured in CEAL Bratislava and samples F12-15-9 were measured at Lund University.

Part V

Magmatism and metamorphism linked to the accretion of continental blocks south of the Hindu Kush, Afghanistan

Shah Wali Faryad[a], Stephen Collett[a], Mike Petterson[b], Sergey A. Sergeev[c]

[a]Institute of Petrology and Structural Geology, Charles University in Prague, Albertov 6, 128 43 Prague, Czech Republic

[b]Applied & Environmental Geoscience, Department of Geology, University of Leicester, LE1 7RH, UK

[c]Centre of Isotopic Research, VSEGEI, 74 Sredny prospect, 199106 St. Petersburg, Russia

Highlights

- Three metamorphic events were distinguished in the Western Hindu Kush.

- The younger Eocene metamorphism was coincided with the collision of western margin of Indian plate.

- Age dating showed that some orthogneisses within the Proterozoic basement formed from Cretaceous granite.

Abstract

Metamorphic basement rocks in the southern part of the Western Hindu Kush at contact with the Kabul and Helmand crustal blocks were investigated to elucidate pressure–temperature variation and relative time relations among different metamorphic rocks. The rocks are represented by Proterozoic amphibolite facies para-/orthogneisses and migmatites with low-grade Paleozoic volcano-sedimentary sequences. Major- and trace-element geochemistry from two orthogneiss bodies and geochronological data, including new SHRIMP analyses on zircon from one of these bodies shows that they are derived from granitic rocks that related to two different magmatic arcs of Triassic and Cretaceous ages. The Triassic granites are common in the Western Hindu Kush where they intrude basement units; the Cretaceous granitic belt crosses the Afghan Central blocks south of the Hindu Kush Mountains. Three different metamorphic events have been distinguished in the southern part of Western Hindu Kush. Based on an unconformity between basement units and Carboniferous cover sequences, the first two amphibolite and greenschist facies metamorphic events are Proterozoic and Pre-Carboniferous in age respectively. The third metamorphism was recognized in Triassic and Cretaceous granitic rocks near to contact with the Kabul Block. It is of Eocene age and reached medium pressure amphibolite facies conditions. This event is genetically linked to the collision of India and Eurasia which produced a series of trans-Afghan Central block magmatic arcs and crustal scale deformation.

Keywords

Western Hindu Kush; Polymetamorphic evolution; Accretion tectonics; Eocene collisional processes

1   Introduction

Recent progress in geological and geophysical research along the Himalayan Orogenic Zone has significantly improved our knowledge on the plate convergence and geodynamic processes in collision zones. It was also shown that accretion of the Indian continent to the southern margin of Eurasia was a stepwise process, which involved separation of small blocks from India and the formation of magmatic arcs prior to continental collision between India and Eurasia (e.g. Beck et al., 1996, Coward et al., 1987, Khan et al., 2009, Petterson and Windley, 1985, Rehman et al., 2011, Şengör, 1984, Tapponnier et al., 1981 and Treloar and Izatt, 1993). The western segment of this collision zone is best exposed in eastern Afghanistan, where several continental blocks with associated ophiolites are present. The accretionary events began in the Paleozoic and have continued until recent times. However much of the tectonic evolution of Afghanistan is related to the closure of Paleozoic and Mesozoic Tethys. The eastern margin, adjacent to the Chaman Fault and Hindu Kush (Fig. 1) records geochronological, magmatic, and metamorphic-tectonic events linked to the final docking of terranes during the Himalayan orogeny and its preceding active Andean-type continental margin environment.
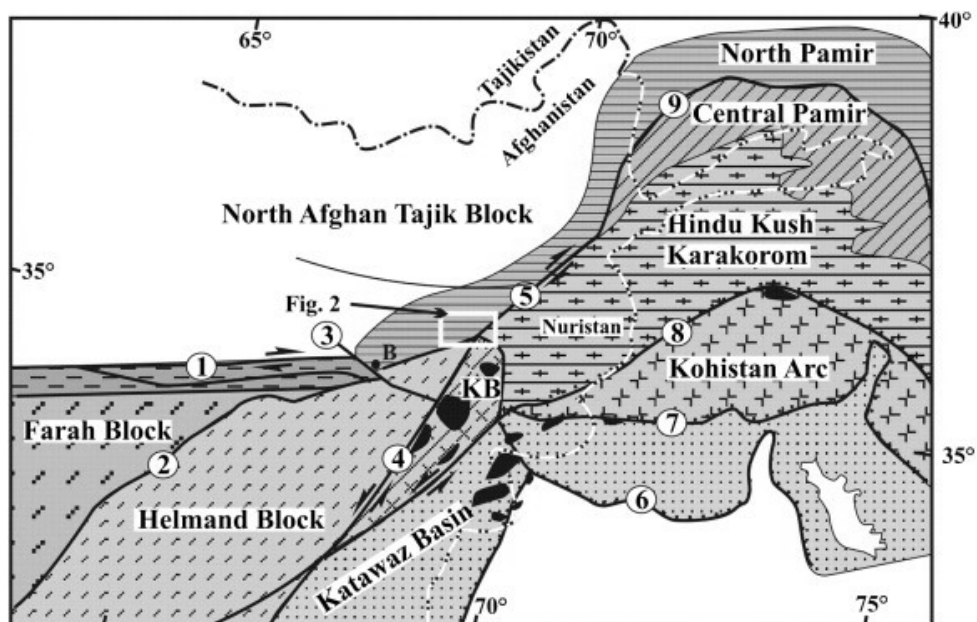
Figure 1: Simplified tectonic map of Afghanistan and western Himalaya–Karakoram–Hindu Kush region (modified from Beck et al., 1996, Boulin, 1988, Lawrence et al., 1992 and Tapponnier et al., 1981). Black fields in the Kabul Block (KB) are ophiolite occurrences. 1-Harirod Fault (Paleozoic suture), 2-Helmand Fault (Mesozoic suture), 3-Bamiyan-Shibar Fault, 4-Chaman Fault, 5-Panjshir Fault, 6-Main Boundary Thrust,7-Main Central Trust (Indus-Tsangpo Suture), 8-Shyok Suture, 9-Mesozoic Suture. B-Bamiyan Town.

The terranes, exposed in Afghanistan, include the North Afghanistan or Tajik block, the Afghan Central blocks (the Farah and Helmand blocks, Fig. 1) and the Frontal fold and thrust belts (the Katawaz Basin), which represent the northwestern continental margin of the Indian plate. The North Afghanistan-Tajik Block lies north of the Harirod–Panjshir fault system and has been part of the Asian plate since before the Permo-Triassic. The Afghan Central Blocks occur west from the Chaman Fault and they were once part of Gondwanaland, but separated prior to the separation of the Indian continent and its accretion to southern margin of Eurasia (Boulin, 1988, Boulin, 1991, Şengör, 1984 and Treloar and Izatt, 1993). The Kabul block occurs in the triple junction of these three terranes and has been interpreted as either the eastern most part of the Afghan Central blocks (Andritzky, 1967) or a distinct separate terrane that was accreted against the Afghan Central blocks prior to the India collision with Eurasia (Tapponnier et al.,

1981 and Treloar and Izatt, 1993).

Some key questions remain concerning the position and accretion of the Kabul block during Himalayan and pre-Himalayan orogenic times (c. 80 Ma–40 Ma). There is only scarce information about the timing and character of the Himalayan-Alpine metamorphism and convergence of the Kabul Block within the Western Hindu Kush. The Kabul Block is formed by Proterozoic basement with Upper Paleozoic cover that is, locally, and tectonically overlain by ophiolite complexes. The best markers of the Himalayan-Alpine convergence in Afghanistan are several intrusive belts that are formed as a result of subduction and crustal thickening during various periods of the Himalayan-Alpine orogeny (Debon et al., 1978). In order to decipher the character and timing of Himalayan-Alpine metamorphic events along the southern border of the Hindu Kush around the margins of the Kabul Block, a carefully collected suite of granitoid and related lithologies were selected for geochronology, geochemical analysis, and metamorphic petrology. The aim of this study is to analyze: 1) metamorphism in the Western Hindu Kush, particularly around the contact zones of the Kabul and Helmand blocks; 2) the relationship and significance of metamorphosed Cretaceous granitoids in this area to other granitic rock in the Western Hindu Kush; and 3) the timing of metamorphism and convergence of the Kabul Block with the Hindu Kush during the Alpine Orogeny.

2   Geological setting

The Western Hindu Kush refers to a ca 220 km long segment of nearly east–west trending high mountains which continue eastward through the Central and Eastern Hindu Kush to the Karakoram. It is bounded by Panjshir fault in the east and the Bamiyan–Shibar fault in the west (Fig. 1). The geology of the Hindu Kush is dominated by medium-grade Proterozoic and low-grade Early Paleozoic rocks that are intruded by granite–granodiorite plutons. In contrast to the northern long and gentle slopes, the southern slopes of the Hindu Kush are steep with east–west striking thrust slices that dip almost vertically southward at the contact with the Kabul Block and northward with the Helmand Block (Fig. 1).

The study area (Fig. 2) was mapped in detail by Boulin (1971), Boulin and Bouyx (1977), Wallbrecher (1974), Resch (1971), and compiled within the geological map of Afghanistan (1:2,000,000, Kafarsky et al., 1975). The Proterozoic basement and the Paleozoic low-grade rocks are strikingly co-parallel and generally follow an east–west to northeast direction. The Proterozoic basement, exposed in the eastern part of the study area (Fig. 2), comprise of migmatites, various kinds of gneisses, (garnet-biotite gneiss ± sillimanite ± staurolite, plagioclase-biotite gneiss, and orthoclase orthogneisses) and quartzite (Wallbrecher, 1974). Along the Panjshir tectonic zone (Panjshir Valley in Fig. 2), they are thrusted and tectonically imbricated by relatively low-grade Paleozoic rocks. Continuation of the Proterozoic basement rocks is assumed along the north-western border of the Kabul Block. Proterozoic age for the basement rocks is based on their higher grade of metamorphism in relation to the overlying Paleozoic rocks (Abdullah and Chmyriov, 1977) however this has not been confirmed by geochronological data. According to Andritzky (1967) the Proterozoic basement represents the northern sector of the Kabul Block. However, Boulin (1971) compares them to the Nuristan Proterozoic basement (Fig. 1).

The low-grade early Paleozoic sequences consist primarily of phyllites, mica-schists and marble. Also present in the western part of the study area are small bodies of serpentinite and two thin belts of metabasite and meta-andesite (Fig. 2) that continue about 150 km westward along the Ghorband Valley to Bamiyan (Fig. 1). The geological map published by Kafarsky et al. (1975) interprets these mafic–ultramafic bodies as Lower Carboniferous in age; however Devonian ages for these rocks were
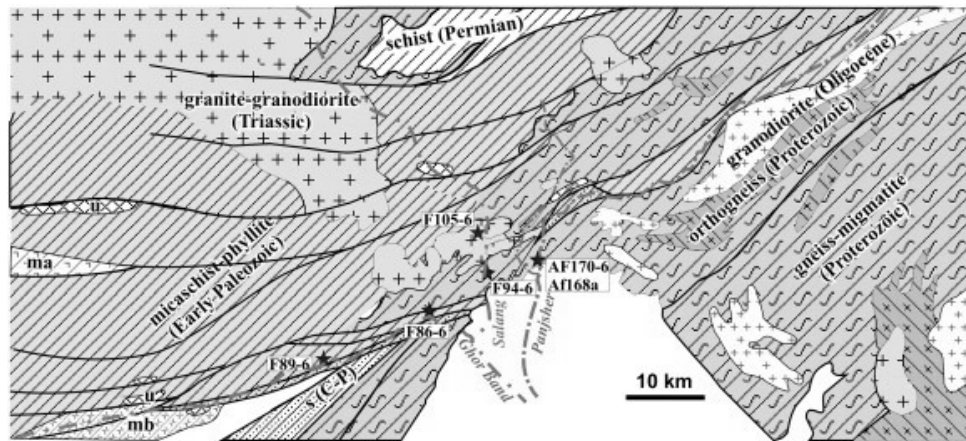
Figure 2: Simplified geological map of southern slopes of the Western Hindu Kush (modified from Kafarsky et al., 1975). Symbols ma, mb and u are metaandesite, metabasite, and ultramafic rocks (serpentinite) respectively. s(C-P) is schist (Upper Carboniferous-Lower Permian). Stars indicate locations of the studied samples. The Panjshir tectonic zone is represented by a series parallel faults, where Paleozoic phyllites and schists are imbricated within the Proterozoic basement.

confirmed by conodonts from radiolarite associated with serpentinite and metabasite (Bouyx et al., 1993). Blue amphibole from these metabasites was reported by Bouyx and Collomb (1985) from Bamiyan. Based on an unconformity between basement rocks and Late Paleozoic sedimentary sequences in Bamiyan, two metamorphic events: the first HP pressure (older than Late Devonian) and the second very low-grade (older than Middle Namurian) are considered for the Paleozoic sequences in the Western Hindu Kush (Blaise et al., 1993 and Boulin and Bouyx, 1977). A Lower Eocene age of 49 Ma was obtained by K–Ar whole-rock method for the Proterozoic orthogneiss in the mouth of Panjshir Valley (Ilavsky and Kantor, 1965).

Both the Proterozoic and Paleozoic metamorphic rocks are intruded by granitoid bodies of different ages. In the studied area, one large pluton (the Central Salang batholith upper-left corner in Fig. 2) and several small bodies of granite–granodiorite rocks are exposed. According to Debon et al., 1983 and Debon et al., 1987, all these granite bodies belong to the Western Hindu Kush Badakhshan plutonic belt, and exhibit a calc-alkaline affinity (Debon et al., 1978). Whole rock Rb–Sr and biotite Rb–Sr Triassic ages of 230 and 210 Ma for this magmatic belt are reported by (Debon et al., 1983) and Desio et al. (1964), respectively. Part of the granitic rocks, exposed in the southern part of the Salang Valley, are deformed and, based on geological map of Afghanistan (Kafarsky et al., 1975), they are interpreted as a composite of Proterozoic orthogneiss and Triassic granite–granodiorite. Together with the surrounding rocks, these granitic bodies and orthogneiss are intruded by a series of pegmatite veins. Ilavsky and Kantor (1965) reported a 190 Ma age for muscovite in beryl-bearing pegmatite from Ruka, about 30 NE from the mouth of the Panjshir Valley (Fig. 2).

3   Samples and petrography

Samples selected for detailed study come from the Proterozoic migmatite, Paleozoic garnet-bearing phyllite and mica-schist and Alpine metagranitoids, Based on the geogical map (Kafarsky et al., 1975), the migmatite (F86-6) comes from nearby to the contact between the Proterozoic and Paleozoic basement in the Ghorband Valley (Fig. 2). Relatively massif white color migmatite forms a thin (2–5 m) and about 200 m long crest striking parallel to the Panjshir fault zone (SW–NE). It consists of K-feldspar, quartz, plagioclase, sillimanite and small amounts of garnet and accessory biotite (Table 1). Sillimanite defines

the foliation in the rocks. Backscatter images show that sillimanite together with K-feldspar forms thin bands in quartz aggregate (Fig. 3a), suggesting dehydration melting of former muscovite. K-feldspar encloses plagioclase. Garnet has inclusions of quartz and sillimanite. It contains accessory muscovite, replacing K-feldspar.

Table 1: Investigated samples and their metamorphic minerals.

Sample	GPS location	pl	bt	ms	hbl	grt	st	sill	ksp	ep	tnt	ilm
Proterozoic (?) migmatite												
F86-6	35°05′51.76″N 69°10′57.87″E	+	+			+		+	+			+
Paleozoic phyllite (*) and micaschist (#)												
F94-6*	35°08′31.00″N 69°13′20.54″E		+	+		+						+
F89-6#	35°05′32.69″N 69°08′55.92″E	+	+	+		+	+					
Alpine metagranitoids												
F105-6	35°11′48.10″N 69°12′56.05″E	+	+	+		+				+		
F104-6	35°09′17.17″N 69°13′15.78″E	+	+	+		+						
AF-170	35°10′09.31″N 69°17′04.19″E	+	+		+						+	
AF-168a	35°10′09.31″N 69°17′04.19″E									+ al		

All samples contain quartz.
Mineral abbreviations: pl-plagioclase, bt-biotite, ms-muscovite, hbl-hornblende, grt-garnet, st-staurolite, sill-sillimanite, ksp-K-feldspar, ep-epidote, tnt-titanite, ilm-ilmenite, al-alanite.

The Paleozoic phyllitic rocks are usually fine-grained and some from the lower Salang Valley (F100-6) or middle part of the hill (F94-6) between the Ghorband and Salang valleys may contain small garnet, biotite and in some case also staurolite (Table 1). Garnet contains inclusions of quartz, ilmenite and, rarely, staurolite (F94-6). The selected two mica-schist samples (F89-6, F90-6) from the Ghorband Valley contain garnet, muscovite, biotite, staurolite and plagioclase. Some large garnet porphyroblasts may have two different inclusion patterns and their backscatter images indicate that they represent two generations of garnet growth (Fig. 3b). Garnet (I) has irregular shapes and its boundary with garnet (II) is followed by opaque minerals. Staurolite crystals enclose small grains of garnet. No garnet was found in amphibolite and amphibole gneisses in the study area.

Most samples of metagranite–metagranodiorite are from the South Salang granitic bodies (Fig. 2). The rocks show weak foliation in the central part of bodies, but strong foliation at contact with surrounding phyllites. The foliation strikes SW–NE almost vertical and parallel to the thrust faults of the Panjshir and Ghrband valleys. These rocks preserve igneous textures with zoned plagioclase and K-feldspar porphyroclasts, but they also show various degrees of recrystallization and deformation. In addition to garnet porphyroblasts (up to 1 cm, sample F105-6), metamorphic minerals are biotite, titanite and epidote (Table 1). Biotite along with quartz aggregates defines the foliation in this sample. Garnet crystals contain inclusions of biotite, quartz, plagioclase and apatite. Some large plagioclase grains exhibit oscillatory zoning that is visible in back scattered electron (BSE) images with anorthite-rich cores (Fig. 3c). Accessory allanite, rimmed by epidote, is also present. The metagranite sample F104-6 contains white mica in addition to garnet and biotite (Fig. 3d) and shows no foliation. The sample exhibits a low-degree of recrystallization with the exception of garnet grains that form at contact with biotite (Fig. 3d). Some mafic varieties may contain brown hornblende which is replaced or rimmed by actinolite. If the rock is foliated, the foliation is defined by biotite, white mica and aggregates of quartz.

Metagranite–metagranodiorites from the Panjshir Valley (Fig. 2) are strongly foliated with characteristic augen texture that is represented by porphyroclasts of feldspar in a fine-grained matrix. In the geological map, they are indicated as part of the Proterozoic basement. These rocks are mostly free of garnet, but contain biotite and hornblende (Table 1), depending on their composition. The metagranodiorite (sample AF-170) contains plagioclase porphyroclasts which are surrounded by a medium-grained foli-
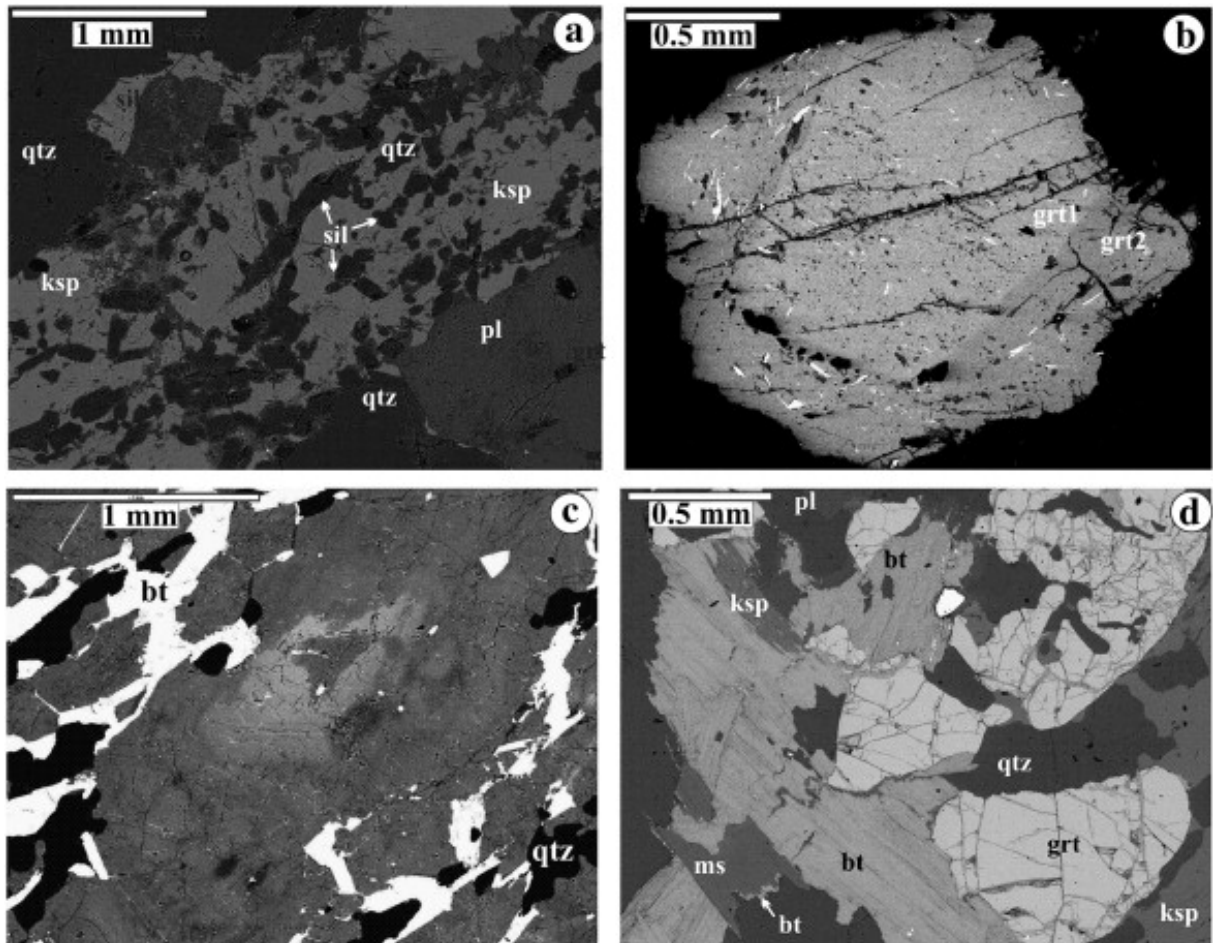
Figure 3: Backscatter electron images showing textural relations of minerals: (a) Migmatite with K-feldspar enclosing plagioclase. Sillimanite follows foliation of the rock and may form thin strips with K-feldspar, enclosed by quartz. (b) Garnet from micaschist shows two generations deferring from each other by their composition and orientation of ilmenite inclusion in the light core and dark rim. Note that the interface of two garnets is featured by quartz inclusions. (c) Metagranodiorite with relict (igneous) plagioclase showing compositional zoning with high Ca (light gray) in the core and dark-gray rim. The dark-gray domains in the central part are due to partial replacement and formation of small grains of zoisite–clinozoiste and albite-rich plagioclase. Biotite follows foliation around plagioclase grain. (d) Metagranite with garnet, biotite and muscovite.

ated matrix, consisting of quartz, plagioclase, biotite, hornblende and titanite. Sample AF-168a consists of plagioclase and biotite with porphyroblasts of garnet and allanite. Both garnet and allanite contain inclusions of biotite, apatite and garnet in addition to quartz.

A few samples were investigated for comparison from the Central Salang batholith (C14-12 & C16-12). In contrast to the South Salang batholith, they show only brittle deformation with new chlorite, prehnite and white mica.

4 Analytical methods

Minerals were studied using a scanning electron microscope at Charles University and a CAMECA SX 50 electron microprobe at the Institute of Mineralogy and Crystal Chemistry, University of Stuttgart, which is equipped with four wavelength-dispersive spectrometers. The following standards were used: pyrope (Si, Al, Mg), andradite (Ca, Fe), jadeite (Na), spessartine (Mn), K-silicate glass (K), Ba-silicate glass (Ba), NaCl (Cl), as well as natural rutile (Ti) and topaz (F). The operating voltage was 15 kV using a beam current between 10 and 15 nA, and the beam was focused to a 1- to 2-μm diameter except for micas, for which an 8- to 10-μm beam was used. Representative mineral analyses are listed in Table 2. Proportions of Fe^{2+} and Fe^{3+} were calculated by cation and charge balance. Whole rock geochemistry was undertaken at Laboratories of Geological Institutes, Charles University in Prague. Major oxides were analyzed by XRF and trace elements by ICP-MS.

U–Pb zircon geochronology analyses for sample AF-170 (Panjshir Valley) were performed at the SIMS SHRIMP-II facility at the Centre of Isotopic Research (CIR) in St Petersburg, Russia. The results were obtained with a secondary electron multiplier in peak-jumping mode following the procedure described by Williams (1998) and adapted for CIR (e.g. Schuth et al., 2012). Individual corrected ratios and ages are reported with 1σ analytical errors (68% confidence), as are the error ellipses presented in the concordia diagrams. The associated plots show concordant data points (insets to concordia diagrams). The Pb/U ratios have been normalized relative to a value of 0.0668 for the $^{206}Pb/^{238}U$ ratio of the TEMORA reference zircons (Black et al., 2003). The second, 91,500 zircon standard, with U concentration of 81.2 ppm (Wiedenbeck et al., 1995) was applied as the "U-concentration" standard. Error in TEMORA standard calibration was 0.68%. During the course of this study, the 91,500 standard yielded a $^{207}Pb/^{206}Pb$ age of 1063 ± 7 Ma (n = 7). The data collected were processed with the SQUID 1.02 (Ludwig, 2001) and Isoplot/Ex 3.00 (Ludwig, 2003) software, using the decay constants of Steiger and Jäger (1977). Uncertainties given for individual analyses (ratios and ages) are at the one σ level, however the uncertainties in calculated concordia ages are reported at two σ level. The common lead correction was done on the basis of measured $^{204}Pb/^{206}Pb$ and modern (i.e. 0 Ma) Pb isotope composition, according to the model of Stacey and Kramers (1975).

5 Mineral composition

Garnet

Garnet from migmatite is relatively rich in pyrope (Table 2, Fig. 4) content with almost homogenous composition, but at the rim shows retrograde zoning with back diffusion of Mn. The rim part of garnet has inclusions of sillimanite. Garnet from phyllite (sample F94-6) is rich in almandine component and shows prograde zoning with a decrease of Sps towards the rims. It has a very low Grs content and X_{Fe}

Table 2: Microprobe analyses of minerals from the studied rock in Western Hindu Kush.

Mineral	Garnet											Staurolite		
Sample	F86-6	F94-6	F90-6	F89-6	F-89-6	F105-6	F105-6	F105-6	F104-6	AF-168a	AF-168a	F89-6	F94-6	F90-6
Position	r	r	r	Ic	IIr	r	r	c	r	r	c	st	st	st
SiO_2	37.77	36.90	37.65	37.29	37.24	36.98	36.80	36.62	35.84	36.91	37.00	28.12	28.31	28.07
TiO_2	0.00	0.04	0.00	0.10	0.01	0.04	0.05	0.14	0.02	0.00	0.04	0.51	0.55	0.74
Al_2O_3	21.08	20.93	21.18	20.29	20.23	20.92	21.00	20.78	20.26	21.00	21.02	53.35	55.48	55.58
FeO	31.54	38.80	34.49	24.32	35.97	24.79	26.98	29.44	34.52	33.61	34.91	13.90	14.45	13.99
MnO	3.66	1.17	3.23	14.00	0.09	5.94	5.94	7.42	7.11	1.27	2.02	0.20	0.13	0.36
MgO	4.90	2.21	3.11	0.81	2.21	0.70	1.06	1.68	0.72	1.17	1.14	1.28	1.06	1.98
CaO	1.04	0.25	1.72	2.79	2.94	10.89	8.14	4.42	1.04	6.07	4.67	0.04	0.00	0.01
ZnO												0.46	0.20	0.26
Total	99.99	100.30	101.39	99.60	98.68	100.25	99.96	100.50	99.51	100.11	100.80	97.85	100.19	101.00
(O) per	12											47		
Si	3.004	2.993	2.996	3.052	3.043	2.954	2.970	2.962	2.963	2.976	2.976	7.994	7.850	7.699
Ti	0.000	0.002	0.000	0.006	0.001	0.002	0.003	0.009	0.001	0.000	0.002	0.109	0.115	0.152
Al	1.976	2.000	1.979	1.958	1.972	1.970	1.998	1.981	1.972	2.003	1.993	17.877	18.130	17.968
Fe^{3+}	0.016	0.015	0.059	0.000	0.062	0.117	0.085	0.114	0.099	0.048	0.054	0.000	0.000	0.000
Fe^{2+}	2.082	2.616	2.229	1.666	2.426	1.539	1.730	1.868	2.286	2.217	2.295	3.304	3.350	3.210
Mn	0.247	0.081	0.217	0.971	0.006	0.402	0.406	0.508	0.498	0.087	0.138	0.047	0.030	0.083
Mg	0.581	0.267	0.368	0.098	0.273	0.084	0.127	0.203	0.089	0.141	0.136	0.542	0.440	0.809
Ca	0.089	0.022	0.146	0.245	0.261	0.932	0.704	0.383	0.092	0.525	0.403	0.011	0.000	0.003
Zn												0.097	0.042	0.054
Alm	0.69	0.88	0.75	0.56	0.82	0.52	0.58	0.63	0.77	0.73	0.76			
Prp	0.19	0.09	0.12	0.03	0.09	0.03	0.04	0.07	0.03	0.05	0.04			
Grs + Adr	0.03	0.01	0.05	0.08	0.09	0.32	0.24	0.13	0.03	0.19	0.15			
Sps	0.08	0.03	0.07	0.32	0.00	0.14	0.14	0.17	0.17	0.03	0.05			
X_{Fe}	0.78	0.91	0.86	0.94	0.90	0.95	0.93	0.90	0.96	0.94	0.94	0.86	0.88	0.80

c and r are refer to core and rim respectively, I and II are garnets I and II in sample F89-6.

Table 2: Microprobe analyses of minerals from the studied rock in Western Hindu Kush.

Mineral	Biotite								Muscovite			ma	amph
Sample	F86-6	F94-6	F89-6	F90-6	F105-6	F104-6	AF-170	AF-168a	F89-6	F94-6	F90-6	F90-6	AF-170
Position												In grt	
SiO_2	36.46	35.51	36.63	36.99	35.66	34.13	36.27	33.47	48.48	46.55	47.33	31.86	40.45
TiO_2	1.66	1.65	1.71	1.80	3.19	1.62	2.61	2.58	0.49	0.32	0.41	0.26	1.16
Al_2O_3	20.73	19.96	19.26	19.39	17.95	18.24	15.67	18.80	36.30	36.99	37.29	51.17	12.41
FeO	16.40	21.45	18.78	18.82	23.06	27.74	21.32	28.33	0.66	0.94	0.80	1.35	19.92
MnO	0.17	0.06	0.08	0.05	0.17	0.46	0.24	0.10	0.00	0.00	0.00	0.24	0.41
MgO	11.23	8.31	10.16	11.43	6.69	3.66	10.04	4.06	0.21	0.22	0.44	0.00	7.86
CaO	0.02	0.02	0.05	0.02	0.15	0.00	0.00	0.02	0.00	0.01	0.02	10.93	11.65
Na_2O	0.13	0.25	0.27	0.38	0.06	0.10	0.19	0.09	1.19	1.75	1.55	1.44	1.39
K_2O	9.89	8.79	8.37	8.76	9.39	9.11	9.52	9.39	8.78	8.30	8.62	0.05	1.36
Total	96.68	96.00	95.31	97.64	96.33	95.06	95.84	96.85	96.11	95.07	96.46	97.30	96.62
O per	22												23
Si	2.762	2.774	2.848	2.793	2.827	2.795	2.839	2.630	3.200	3.086	3.099	2.060	6.210
Ti	0.094	0.097	0.100	0.102	0.190	0.100	0.154	0.153	0.025	0.016	0.020	0.012	0.134
Al	1.851	1.837	1.765	1.725	1.678	1.760	1.445	1.741	2.824	2.890	2.877	3.899	2.245
Fe^{3+}	0.000	0.000	0.000	0.000	0.000	0.000	0.000		0.000	0.000	0.000	0.073	0.552
Fe^{2+}	1.038	1.401	1.221	1.188	1.529	1.899	1.396	1.862	0.037	0.052	0.044	0.000	2.005
Mn	0.011	0.004	0.005	0.003	0.011	0.032	0.016	0.007	0.000	0.000	0.000	0.013	0.054
Mg	1.267	0.967	1.178	1.287	0.790	0.446	1.172	0.476	0.021	0.022	0.043	0.000	1.799
Ca	0.001	0.001	0.004	0.002	0.013	0.000	0.000	0.002	0.000	0.001	0.001	0.757	1.917
Na	0.018	0.038	0.041	0.055	0.010	0.015	0.028	0.013	0.152	0.225	0.197	0.181	0.414
K	0.955	0.876	0.830	0.844	0.950	0.951	0.950	0.941	0.739	0.702	0.720	0.004	0.265
X_{Fe}	0.45	0.59	0.51	0.48	0.66	0.81	0.54	0.80					

ma — margarite, amph — amphibole.

Table 2: Microprobe analyses of minerals from the studied rock in Western Hindu Kush.

Mineral	Plagioclase					
Sample	F86-6	F89-6	F105-6	F104-6	AF-170	AF-168a
Position			c	c	In grt	
SiO_2	61.51	62.90	58.20	64.13	60.19	61.00
Al_2O_3	24.10	24.94	26.49	23.06	25.59	25.55
CaO	5.40	6.06	7.92	3.90	6.88	5.64
Na_2O	8.87	7.57	6.81	9.34	7.60	8.38
K_2O	0.27	0.11	0.11	0.13	0.30	0.41
Total	100.14	101.57	99.53	100.55	100.56	100.97
O per	8					
Si	2.715	2.762	2.614	2.819	2.667	2.687
Al	1.254	1.291	1.402	1.194	1.336	1.326
Ca	0.255	0.285	0.381	0.184	0.327	0.266
Na	0.759	0.645	0.593	0.796	0.653	0.716
K	0.015	0.006	0.006	0.007	0.017	0.023

decreases slightly towards the rims of grains. Garnet may contain inclusions of staurolite. Two generations of garnet growth (sample F89-6), recognized by the inclusion patterns and backscatter images (Fig. 5a), show prograde zoning with decrease of X_{Fe} and Sps towards the rims (Fig. 5b). Garnet (I) has relatively low but homogenous Grs content. In contrast, garnet (II) indicates compositional jump with high Grs content that decrease towards the rims.
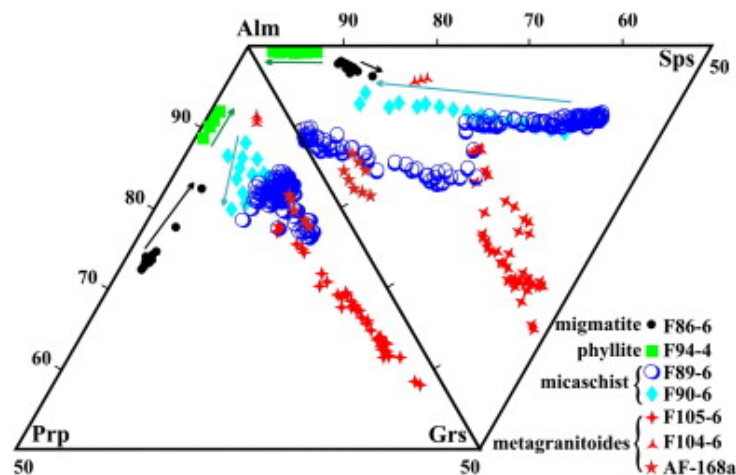
Figure 4: Composition of garnet from metagranite and metapelites in the southern part of the Western Hindu Kush. The arrows indicate compositional zoning from core to rim of grains in samples F90-6, F94-6 and F86-6.

Garnet from metagranodiorite in the Salang Valley (sample F105-6) has a relatively high grossular content with complex zoning (Fig. 5c, d). The trend from core to rim is characterized by an initial increase in Grs content, followed by a decrease and finally an increase at the crystal rim. Changes in the Grs content are compensated by variations in the Alm content, which shows opposite zoning from core to the rim. Pyrope content generally decreases towards the rim. Garnet from metagranite (sample F104-6) does not show pronounced zoning. Similar to the other metagranitoids, sample AF-168a from the Panjshir Valley has low pyrope and spessartine content. It is fairly homogenous in the central part with increasing Ca and decreasing Mn and Fe at the rim.
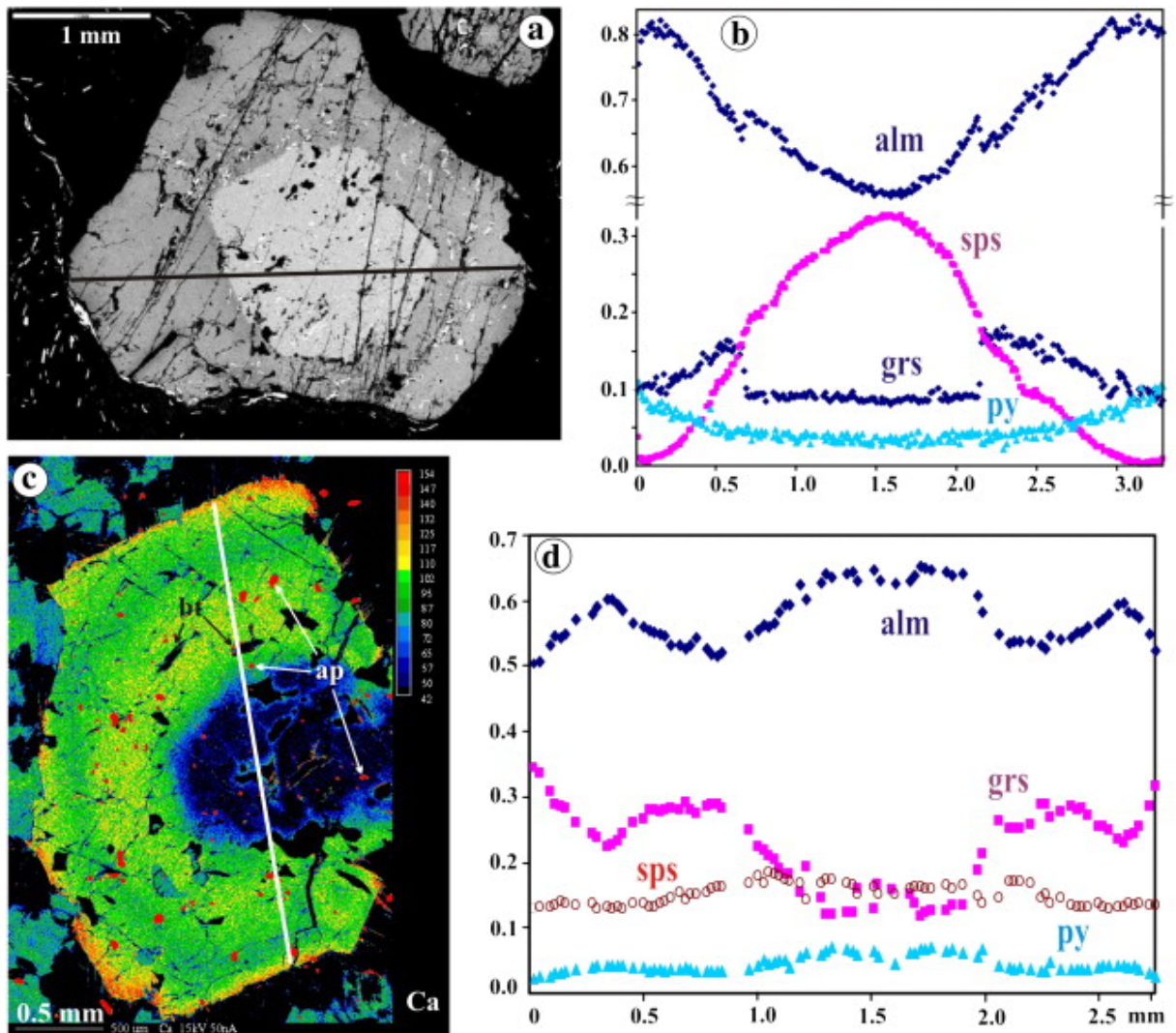
Figure 5: Compositional maps (a) and profiles (b) of two garnets: (I) in the core and (II) at the rim from micaschist (sample F89-6). Note that garnet (I) has irregular or rounded forms. Both garnets indicate prograde zoning with Mn decrease, but they show compositional jump with lower Ca in garnet (I) and higher in garnet (II). (c) and (d) show garnet porphyroblast from metagranodiorite in the Salang Valley (F105-6). The isometric inclusions with high Ca are apatite (ap) and dark long grains are biotite.

Micas

Biotite composition ranges from X_{Fe} 0.46–0.51 in phyllite and micaschist to 0.68–0.81 in metagranitoid (Table 2). Ti content is below 0.1 a.p.f.u., except for biotite in metagranodiorite with Ti = 0.15–0.19 a.p.f.u. Biotite associated with hornblende from the garnet-free sample (AF-170) has X_{Fe} = 0.52–0.54 with Ti = 0.15–0.17 a.p.f.u. and that with (AF-168a) has X_{Fe} = 0.8. Accessory biotite in migmatite occurs in the quartz and K-feldspar matrix and doesn't form in contact with garnet. Muscovite has Si = 3.0–3.1 a.p.f.u. (sample, F94-6, F90-6, F104-6) to Si = 3.2 a.p.f.u (F89-6). Margarite was found as inclusions in garnet from sample F90-6.

Staurolite

Staurolite has X_{Fe} = 0.8 in sample F90-6 and X_{Fe} = 0.88 in phyllite and micaschists (samples F94-6 and F-89-6). In all three samples it has low (< 0.6 a.p.f.u) Zn content.

Plagioclase

Plagioclase has An = 30 mol% in micaschist and 25 mol% in metagranodiorite. Plagioclase in metagranodiorite (sample F105-6) preserves magmatic zoning with high An = 0.39 mol%. The An content decreases towards the rims and albite is present at contact with garnet and/or epidote. Plagioclase from sample AF-170 and AF-168a has almost homogenous composition with An = 0.34 and 0.28 mol% respectively.

Amphibole

Amphibole analyzed in sample AF-170 is pargasitic with Si = 6.2 a.p.f.u. and X_{Mg} = 0.59.

6   Pressure—temperature conditions

To calculate peak PT conditions and a possible polymetamorphic history of the rocks, the available themobarometers, based on the ion exchange reactions, and pseudosection method were used. This includes garnet–biotite thermometry (calibrations of Hodges and Spear, 1982 and Perchuk and Lavrent'eva, 1983 and Ganguly et al., 1996), GASP barometry (Koziol, 1989) and garnet–muscovite–plagioclase–quartz (GMPQ) barometry (Wu and Zhao, 2006). The pressure–temperature (PT)-sections for the three samples (F86, F94-6, and F89-6) were constrained based on Gibbs free energy minimization using Perplex 6.6.6 (Connolly, 2009) with the internally consistent thermodynamic data set of Holland and Powell (1998: 2004 upgrade). Mixing models for garnet, chlorite, staurolite, plagioclase and melt following Holland and Powell (2003), mica following Coggon and Holland (2002) and biotite following Tajcmanová et al. (2009) were used. Two pseudosections were constructed for garnet (I) and (II) in sample F89-6 (Fig. 6c and d). The pseudosection constructed for garnet (I) was based on the whole-rock composition and that for garnet (II) was on the basis of effective bulk-rock composition, which was obtained by extracting the garnet (I) from the whole-rock composition. The modal proportion of garnet (I) in the rock was determined by image analysis from several BSE images of the studied thin section. The average composition of garnet (I) was calculated using compositional profiles analyzed in several grains.
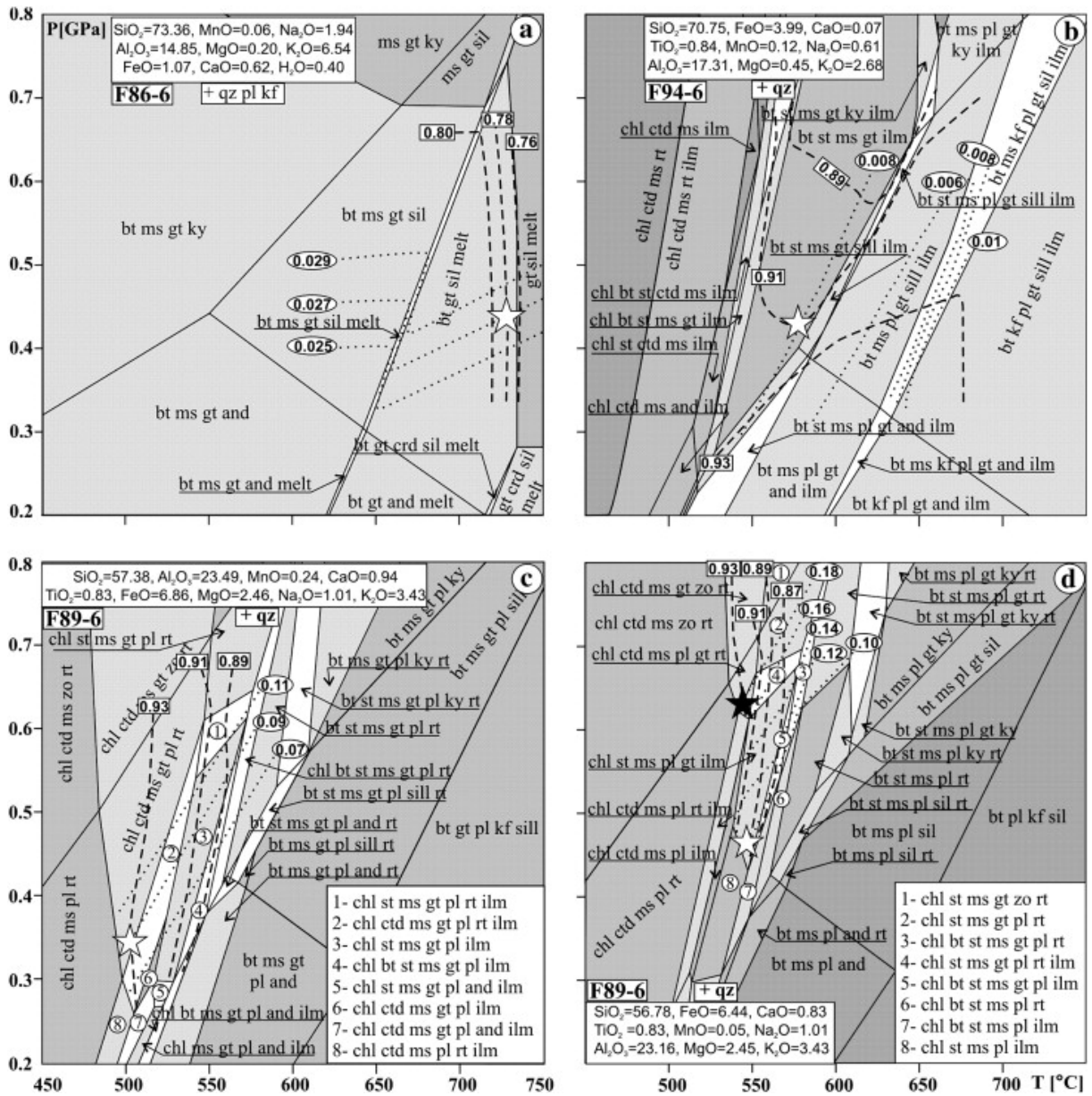
Figure 6: PT sections for migmatite (a), garnet–staurolite phyllite (b), and micaschist (c—garnet I), (d—garnet II) with isopleths of X_{Fe} = Fe / (Fe + Mg) (rectangles) and X_{Ca} = Ca / (Fe + Mg + Mn + Ca) (ellipses) for garnet. Phase abbreviations are as follows: and-andalusite, bt—biotite, chl—chlorite, ctd—chloritoid, gt—garnet, ilm—ilmenite, kf—K-feldspar, ky—kyanite, ms—mica, pl—plagioclase, qz—quartz, rt—rutile, sil—sillimanite, st—staurolite, zo—zoisite. Open stars represent the intersections of mineral isopleths for rim composition and solid star in (d) is core of garnet II.

Except for the mica-schist with two different garnets, no clear evidence of multistage or polymeta-morphic history was observed in the other samples. The temperature calculated using garnet–biotite thermometry for migmatite (sample F86-6, Table 3) is about 70–130 °C lower than that obtained by the pseudosection method (Fig. 6a). As mentioned before, mineral textural relations in this sample show complete dehydration reaction of muscovite and it is not clear if the lower temperature by garnet–biotite thermometry is due to reequilibration or new formation of biotite during younger events. Pressure conditions of 0.428 ± 0.036 GPa obtained by the GASP method fit well with those in the pseudosec-tion. For the garnet–staurolite-bearing phyllite (sample F94-6), the calculated temperatures of 447–565 °C (Table 3) are comparable to those obtained by the pseudosection method (Fig. 6b) and know for similar assemblages in pelitic rocks elsewhere (Faryad and Hoinkes, 2003 and Jeřábek et al., 2008). In the micaschist (sample F89-6) two different temperature/pressure conditions of 500 °C/0.35 GPa and 540 °C/0.65 GPa were obtained using garnet isopleths for garnet I and II, respectively (Fig. 6c and d). Garnet–biotite thermometry and GMPQ barometry for garnet II in this sample yield PT conditions of 514–568 °C/0.6 ± 0.05 GPa (Table 3), which are close to that in the pseudosection (Fig. 6d).

Table 3: Results of calculated temperature and pressure for the studied rocks.

Rock	Migmatite	Phyllite	Micaschist				Metagranitoid	
Sample	F86-6	F94-6	F89-6	F90-6	F105-6	F104-6		AF-168a
Minerals	grt + bt + sil + qtz	grt + bt	grt + bt + ms + pl	grt + bt	grt + bt	grt + bt + ms + pl		grt + bt
Calibration	Temperature (°C)							
HS 82	681	519	547	523	565	563		537
PL 83	649	565	568	558	534	585		563
G 96	638	466	514	447	545	546		535
Calibration	Pressure (GPa)							
GASP	0.428 ± 0.036							
GBPQ			0.6 ± 0.05				0.45 ± 0.06	

HS 82 - Hodges and Spear (1982); PL 83 - Perchuk and Lavrent'eva (1983); G 96 - Ganguly et al. (1996)

Metagranite and metagranodiorite still preserve igneous minerals, mainly feldspars, which form por-phyroclasts. Large plagioclase grains preserve magmatic zoning with high anorthite content in the core. Because of incomplete recrystallization and equilibration of these rocks, the pseudosection method was not applied to these samples. The garnet–biotite thermometry used for sample F105-6 and F104-6 gave temperatures in the range of 534–585 °C. The GMPQ barometer used for sample F104-6 with new mus-covite yield pressure of 0.4 to 0.5 GPa regarding plagioclase composition from An18 to An15. A certain level of caution should be noted for this pressure and temperature estimate as the minerals are in local equilibrium, in addition the GMPQ barometer was empirically tested for metapelitic rocks with high amounts of muscovite.

7   Whole rock geochemistry

As mentioned in the introduction, the granitoid rocks in the southern part of the Salang Valley were mapped as a single body (the South Salang batholith, Wallbrecher, 1974) and based on their geochem-istry of calc-alkine composition they were assumed to be part of the Triassic Central Salang batholith (Debon et al., 1983). To assess the relationship between the Salang batholiths and meta-granodiorite in the Panjshir Valley, two samples of granite from the Central Salang batholith (C14/12 & C16/12), one sample (F105-6) from the South Salang batholith and one sample of the Panjshir meta-granodiorite (AF-170) were selected for geochemical analysis. A primitive mantle normalized multi-element plot (Fig. 7a) displays many of the typical patterns of an arc-subduction zone setting, with LFSE/HFSE ratio > 1, strong negative Nb anomaly as well as relative enrichment in elements such as Rb and Ba. Although

all four samples show a similar trend, slight variations can be seen in the meta-granodiorite sample (AF-170), which shows comparatively less enrichment in the radioactive elements (U & Th), as well as a larger depletion in Nb and slight enrichment in Sr. On the Pearce et al. (1984) tectonic discrimination, (Y + Nb) vs Rb diagram (Fig. 7b), all four samples plot around the same place, comfortably within the volcanic arc granite field. Meanwhile on the Nb and Y vs Rb/Zr binary plots (Fig. 7c) the samples from the Salang batholiths all plot within the normal continental arc field defined by Brown et al. (1984) while the Panjshir meta-granodiorite (AF-170) plots in the more primitive island arc setting. For the purposes of comparison geochemical data has also been plotted for granitoids from the Karakoram–Pamir region that Debon et al. (1987) consider as continuations of the Afghan belts. The selected data comes from: Triassic granitoids from the western Kunlun terrane (Jiang et al., 2013), Cretaceous intrusives in the Karakoram Batholith (Rex et al., 1988) and Cretaceous intrusives from the Kohistan island arc (Bignold et al., 2006).
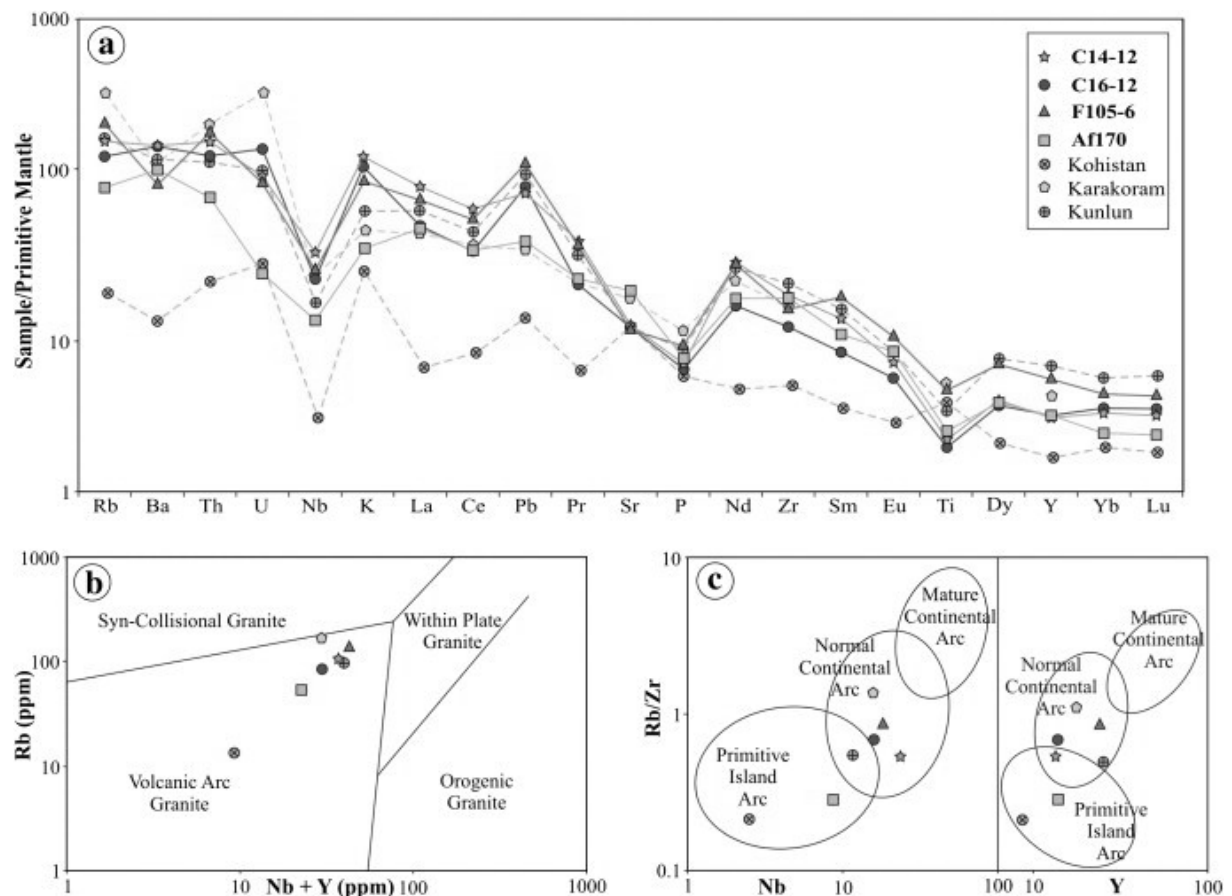
Figure 7: (a) Multi element plot normalized to primitive mantle values of McDonough and Sun (1995), Panjshir meta-granodiorite (170) shows higher depletion in radioactive elements and Nb and a smaller depletion in Sr. (b) Tectonic discrimination diagram of Rb ppm vs Nb + Y ppm shows all four samples fit comfortably in the Volcanic arc field defined by Pearce et al. (1984). (c) Tectonic variation diagrams of Nb ppm and Y ppm vs Rb/Zr, fields after Brown et al. (1984) show Panjshir meta-granodiorite from a more primitive island arc setting than the Salang granites.

8   SHRIMP U–Pb zircon geochronology

Fig. 8 illustrates an abundance of large (200–300 μm), prismatic zircons within metagranodiorite (sample AF-170). Cathodoluminescence (CL) imaging shows oscillatory growth structures and heterogeneous

rims (Fig. 8). Euhedral zircon grains are interpreted as igneous in origin, whereas rounded-irregular shaped grains and unzoned overgrowths most likely result from metamorphic growth, and may be older relict zircons that have survived magmatic processes. This distinction is corroborated by generally high Th/U for 'igneous' zircons (average = 0.30) compared with lower Th/U (average = 0.09) for 'metamorphic' zircons in this sample (Table 4). Results of SHRIMP analyses are shown in a concordia diagram in Fig. 9. The concordant, clustered SHRIMP ages from unambiguous igneous grains, define the Campanian (Late Cretaceous) age of magmatic crystallization event of 74 ± 1 Ma (Fig. 9a), whereas ages for metamorphic rim of zircon indicate Cenozoic (46 ± 3 Ma) overprint (Fig. 9b; Table 4). A few intermediate data points (Fig. 9a) reflect incomplete re-crystallization of magmatic zircon matrix.
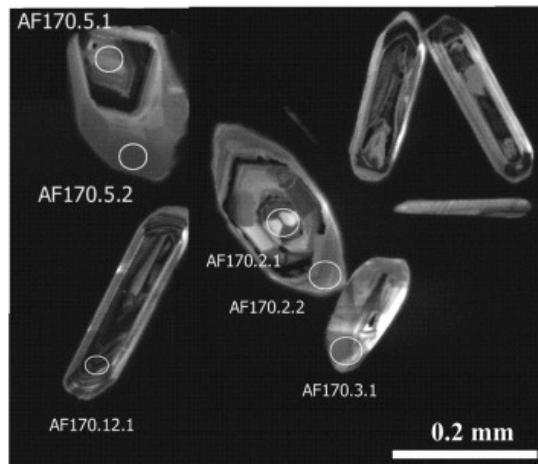
Figure 8: Cathodoluminesence (CL) images of representative zircons from the Panjshir metagranodiorite (AF-170) with analytical points. The prismatic grains represent igneous zircon and the rounded grains indicate metamorphic overgrowth.
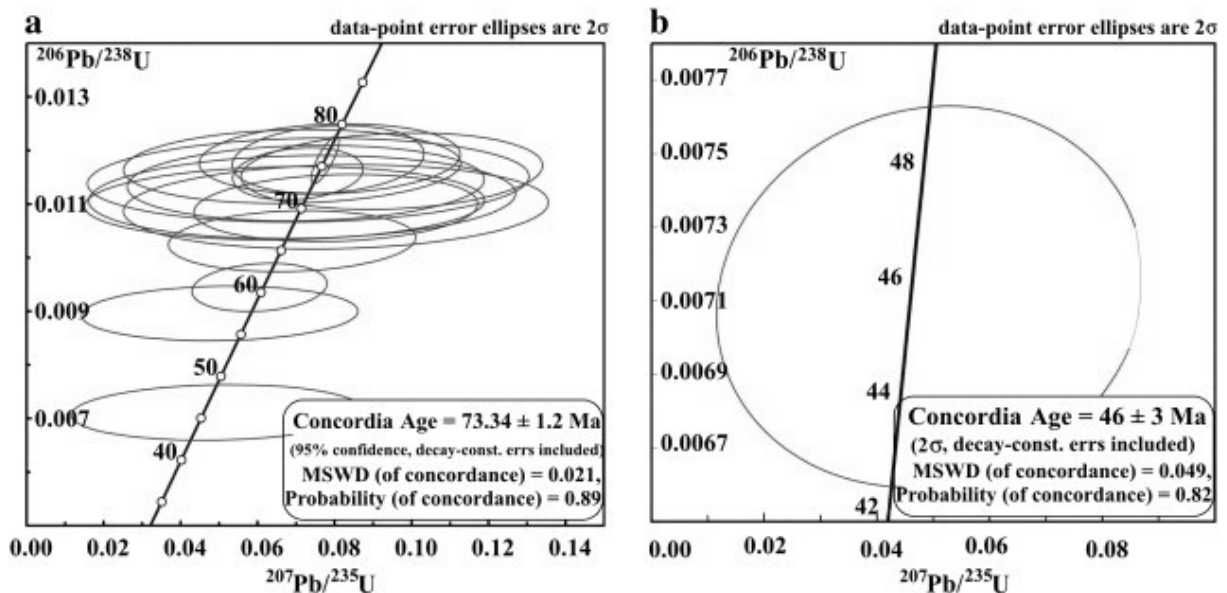
Figure 9: Wetherill (1956), Concordia diagrams of sensitive high-resolution ion microprobe (SHRIMP) U–Pb analyses (a, n = 16) of zircons from the Panjshir metagranodiorite (AF-170) exhibiting bimodal clustering of ages into an igneous and a metamorphic (b, n = 1) ages. Error ellipses shown at 1σ level of uncertainty. MSWD—mean square of weighted deviates.

Table 4: SHRIMP U-TH-PB results for the Hindu Kush metagranite (sample AF-170).

Spot	% $^{206}Pb_c$	ppm U	ppm Th	$^{232}Th/^{238}U$	ppm $^{206}Pb^*$	$(1)^{206}Pb/^{238}U$ Age	±	$(1)^{238}U/^{206}Pb^*$	±%	$(1)^{207}Pb^*/^{206}Pb^*$	±%	$(1)^{207}Pb^*/^{235}U$	±%	$(1)^{206}Pb^*/^{238}U$	±%	Err corr
AF170.4.2	1.87	241	10	0.04	1.50	45.7	± 1.4	140.6	3.0	0.05	31	0.049	31	0.00711	3	0.095
AF170.5.2	1.46	545	52	0.10	4.26	57.5	± 1.3	111.6	2.3	0.041	29	0.05	29	0.00896	2.3	0.079
AF170.8.1	0.63	462	53	0.12	3.77	60.6	± 1.2	105.9	1.9	0.0465	12	0.0605	12	0.00944	1.9	0.164
AF170.9.1	1.55	293	33	0.12	2.64	66.1	± 1.5	97.0	2.3	0.0485	19	0.069	19	0.01031	2.3	0.119
AF170.2.2	1.14	242	67	0.29	2.30	70.1	± 1.6	91.5	2.3	0.0533	19	0.08	19	0.01093	2.3	0.125
AF170.6.1	1.74	141	37	0.27	1.35	70.2	± 2.0	91.3	2.9	0.053	28	0.08	28	0.01095	2.9	0.105
AF170.5.1	1.72	379	128	0.35	3.65	70.6	± 1.8	90.8	2.5	0.044	32	0.067	32	0.01102	2.5	0.080
AF170.3.1	1.77	168	36	0.22	1.64	71.4	± 2.0	89.8	2.8	0.047	32	0.072	32	0.01113	2.8	0.090
AF170.13.1	1.48	284	68	0.25	2.82	73.0	± 1.8	87.8	2.5	0.046	26	0.073	26	0.01139	2.5	0.097
AF170.7.1	1.80	186	33	0.18	1.86	73.4	± 2.0	87.4	2.8	0.046	32	0.073	32	0.01145	2.8	0.087
AF170.12.1	0.53	1469	489	0.34	14.70	74.1	± 1.3	86.5	1.7	0.0442	9.7	0.0705	9.8	0.01156	1.7	0.175
AF170.2.1	1.06	156	54	0.36	1.57	74.4	± 1.9	86.1	2.5	0.0593	17	0.095	17	0.01161	2.5	0.149
AF170.10.1	1.36	325	97	0.31	3.32	75	± 1.8	85.5	2.4	0.043	26	0.069	26	0.01170	2.4	0.093
AF170.4.1	0.04	6345	1928	0.31	64.50	75.8	± 1.2	84.6	1.5	0.04756	1.1	0.0775	1.9	0.01182	1.5	0.802
AF170.1.1	0.7	387	225	0.60	3.96	75.8	± 1.6	84.5	2.2	0.048	13	0.078	13	0.01183	2.2	0.168
AF170.11.1	0.99	225	29	0.13	2.31	75.9	± 1.7	84.4	2.3	0.0482	17	0.079	18	0.01184	2.3	0.128

Errors are 1-sigma; Pbc and Pb* indicate the common and radiogenic portions, respectively.
Error in Standard calibration was 0.68% (not included in above errors but required when comparing data from different mounts).
(1) Common Pb corrected using measured ^{204}Pb.

9   Discussion

To analyze the results of petrological and geochronological study in the Western Hindu Kush, two points should be addressed. The first is about the origin of the studied granitoids and their relationship to the major magmatic events in Afghanistan (Debon et al., 1983) (Fig. 10) and the second question is to address the age of metamorphism and possible polymetamorphic history of the surrounding basement rocks. In the following we discuss our observations in relation to available tectonic models in this part of the collisional orogeny.
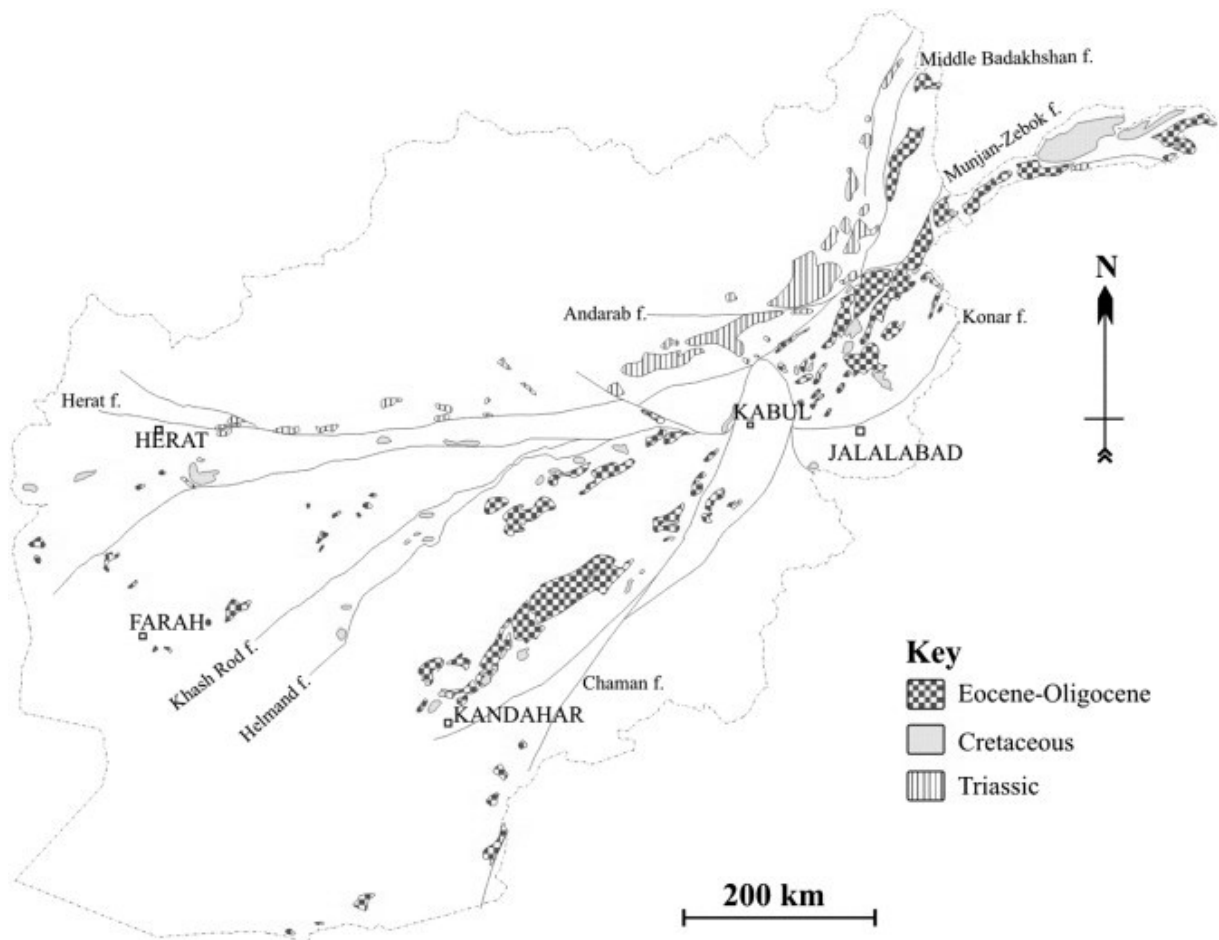
Figure 10: Magmatic belts of Afghanistan after Debon et al. (1978) using data from Stazhilo-Alekseev et al. (1973) and Chmyriov and Salah (1973).

Main features of Mesozoic intrusives in the Western Hindu Kush

The Mesozoic and Cenozoic evolution of the Hindu Kush and Afghan Central blocks, and the formation of plutonic belts in Afghanistan are constrained by three major magmatic stages of Triassic, Cretaceous and Eocene—Oligocene ages (Debon et al., 1987): (i) Triassic (210 Ma) intrusives of sub-alkaline to calc-alkaline geochemistry occur north of the Harirod–Panjshir fault system within the Western Hindu Kush–Badakhshan belt (Fig. 10). These were formed by subduction of oceanic crust beneath the region, the direction of which is the subject of controversy. Debon et al. (1987) suggest south-dipping subduction beneath a strip of continental crust detached from the Eurasian margin, while Boulin (1988) assumes north-dipping subduction of the Hindu Kush oceanic basin beneath the Turkestan–Tarim continental

blocks. (ii) Cretaceous (100–110 Ma) calc-alkaline volcanic rocks in the Kandahar arc and intrusive gran-itic rocks within southern central Afghanistan testify to a newly initiated subduction of oceanic crust beneath the recently accreted terranes of the Asian continent (Debon et al., 1987). This several hundred km long plutonic belt was emplaced along the Asian continental margin (comprising a range of terranes including Helmand, Arghandab, Western Nuristan, Safed Koh and Wakhan or Eastern Nuristan). (iii) Continental collision subsequent to oceanic subduction between the Indian and Eurasian plates, which began during the Lower Eocene, played a major role in the genesis of granitoids in Afghanistan (Debon et al., 1987). It resulted in the formation of numerous subalkaline, alkaline granite–trondhejmite intrus-ives of Upper Eocene and/or Oligocene (ca 30 Ma) ages. In Afghanistan, they form ca. 1000 km long belt crossing the Helmand, Kabul and Nuristan blocks (Fig. 10).

The results of our petrological study in combination with REE and trace elements data from metagranite bodies exposed in the Salang Valley indicate that the south Salang granitic bodies are not part of Protero-zoic basement as assumed by Kafarsky et al. (1975), but rather they belong to the Triassic intrusives in the Western Hindu Kush (Debon et al., 1987). The trace element geochemical signature of these rocks is comparable to granites from the western Kunlun region (Jiang et al., 2013). Consistent with the sugges-tion of Debon et al. (1987) that the Triassic granitoids of the Hindukush represent the western edge of an intrusive belt stretching from Afghanistan through the Northern Pamir to Kunlun, Northwest China.

Fig. 10 shows the distribution of Cretaceous intrusives that are restricted to the Afghan Central and Nuristan blocks. The Cretaceous age for the protolith of the orthogniesses in the Panjshir Valley raises a question, as to whether the Cretaceous magmatism also occurred in the Western Hindu Kush, or if it originates from the Afghan blocks and has been tectonically emplaced in the southern part of the Western Hindu Kush. According to Debon et al. (1987) the Cretaceous granitoids of Afghanistan are the direct continuation of the large Kohistan–Ladakh–TransHimalaya batholith.

Metamorphism in the Western Hindu Kush

Textural relations and mineral compositions of the studied samples enable us to distinguish at least three sets of rocks that possibly experienced different metamorphic events. The first set is represented by mig-matite (sample F86-6). Rocks of a similar mineral assemblage (feldspars, biotite, garnet, sillimanite) are described by Wallbrecher (1974) from gneisses northwest of the Panjshir Valley. Although high-pressure amphibolite facies rocks are reported from the Sare-Sang area north from the Panjshir Valley (Faryad, 1999 and Faryad, 2002), these are part of the Meso-archaen Badakhshan Block. Instead the gneisses and migmatites southeast of the Panjshir Valley are compared with the Western Nuristan Blocks, which are considered to have been metamorphosed in the Proterozoic (Boulin, 1988).

The second set of rocks is mica-schist, phyllite with marbles and quartzite that are, based on the geolo-gical map of Afghanistan (Kafarsky et al., 1975), assumed to be early Paleozoic (Ordovician, Silurian) in age. These contain tectonic bodies of serpentinites and at least two east–west trending belts of am-phibolites (Fig. 2) which are also assigned to the Early Paleozoic basement (Boulin, 1988). Our data from the area around Salang indicates upper greenschist to amphibolite facies conditions; this is consistent with available information about mineral assemblages in the Paleozoic basement rocks (Resch, 1971 and Wallbrecher, 1974). According to Boulin (1988) and Blaise et al. (1993) blueschist facies metamorphism, is recognized in the western part of metabasite belt near Bamiyan (Bouyx and Collomb, 1985), this pred-ated the greenschist facies event in the Western Hindu Kush. However, we observed no evidence for blueschist facies metamorphism in the area around Salang Valley.

The third set of rocks is the metagranite–metagranitoid, which based on geochronological data under-

went metamorphism of middle Eocene age. Preservation of relict igneous textures and minerals suggest that this metamorphism was a short-lived process and its effects in the surrounding phyllitic rocks are difficult to distinguish. Although it was not possible to accurately attain PT conditions for the Middle Eocene event in metagranite due to the lack equilibrium and index phases; pressure dominated amphibolite facies conditions (~ 500 °C) could be considered based on stability of garnet instead of epidote in these rocks. As the whole traverse along the southern slopes of the Western Hindu Kush is represented by south-verging slices with a fan like structure that shows a southward increase in deformation and degrees of recrystallization and mineral formation, the amphibolite facies metagranite could have been exhumed by an extrusion wedge.

As no geochronological data is available from the migmatite and phyllites, the relationship of garnet I and II in micaschist (sample F89-6) to the above metamorphic events can only be discussed based on the estimated PT conditions. Considering the Proterozoic age of relatively high-grade basement rocks east from the Panjshir fault zone (Kafarsky et al., 1975) and its continuation to the mouth of the Ghorband Valley (Fig. 2) represented by migmatite shows ~ 225 °C higher temperature than that recorded for the micaschist and total dehydration of muscovite in the migmatites, then garnet I and II in the micaschist reflect the, Paleozoic and Eocene events, respectively in the Western Hindu Kush.

Eocene metamorphism and the role of Kabul-Afghan blocks

The crustal blocks south of the Harirod and Panjshir faults (the Afghan Central blocks) are considered as part of Gondwanaland that were accreted to Eurasian continent prior to the collision of India with the southern margin of Eurasia (Boulin, 1988, Boulin, 1991, Şengör, 1984 and Treloar and Izatt, 1993). This includes the Helmand and Nuristan blocks, which based on the similarity of their rock assemblages are assumed to be related with each other (e.g. Karapetov et al., 1975 and Stöcklin, 1977). These two blocks are separated by the Kabul Block, the relations of which to the neighboring blocks and the origin of the overlying Eocene ophiolites are the subject of some discussion. Several authors (e.g. Tapponnier et al., 1981 and Treloar and Izatt, 1993) assume that the Kabul-Altimur and Khost Waziristen ophiolites are related to the closure of two distinct oceanic basins, the first between the Helmand and Kabul blocks and the second related to the accretion of Indian plate to the Afghan blocks. This interpretation is based on the vergence of folds, stretching lineation, and fabrics that suggest the direction of transport of the Kabul ophiolite nappes is roughly to the southeast from the Chaman fault. However, Andritzky (1967) interprets the Kabul Block as the eastern most part of the Afghan Central blocks that was wedged between the Helmand and Nuristan blocks along the Chaman and Altimur fault, respectively. The limited occurrence of Paleozoic strata in the Kabul Block in comparison with that in the Helmand Block is interpreted as a result of erosion and uplift tectonics during Pre-Permian time. According to Badshah et al. (2000) the Kabul–Altimur ophiolite complex represents a deformed and metamorphosed equivalent of the Waziristan–Khost ophiolite complex that was obducted. The fabrics showing SE direction of transport may not indicate the original direction of obduction, because the folds may have been rotated in a counter-clockwise sense during the southwestward extrusion of the Afghan Central blocks and formation of the Katawaz basin (Beck et al., 1996 and Cassaigneau, 1979).

The presence of the Eocene intrusive belt crossing the Helmand, Kabul and Nuristan blocks (Fig. 10) suggests that all three blocks were contiguous within the same structural zone during the convergence of India and Eurasia. If the Cretaceous granitoids in the Panjshir Valley represent a tectonic fragment which was tectonically emplaced in the southern margin of Western Hindu Kush during the northward indentation of the Kabul Block, then the present position of the Kabul Block in relation to the Helmand and Nuristan Blocks has changed greatly since the Cretaceous. This would seem to support the inter-

pretation of Andritzky (1967) and Badshah et al. (2000) and fill the gap in continuity of Cretaceous magmatic arc from Helmand through Kabul to Kohistan blocks.

On the basis of palaeomagnetic data, Klootwijk et al. (1991), place the collision of India to the southern margin of Asia as occurring at about 55 Ma, with the possibility that collision was earlier in the northwest than further east (Treloar and Izatt, 1993). The metamorphic peak of the Indian plate rocks in the northwestern Pakistan was attained at about 50 Ma ago (Chamberlain et al., 1991 and Treloar and Rex, 1990). In Afghanistan, this process resulted in crustal thickening leading to the formation of some aluminous granitoid rocks in Western Nuristan, Safed Koh, Wakhan, northern part of Arghandab belt (Debon et al., 1978).

We interpret the Eocene age of 45–50 Ma for metamorphism in Western Hindu Kush as indicating a major geotectonic processes that resulted in the formation of a magmatic arc crossing the Helmand, Kabul and Nuristan blocks and reached amphibolite facies metamorphism (c. 550 °C, and 15–20 km depth) in the Western Hindu Kush. This event appears to fit well with collision of India with Asia about 50 Ma (Beck et al., 1996) and it was either coincident with or postdated the Kabul–Altimur ophiolite obduction (Mennessier, 1972). The extent of this metamorphism in the basement rocks of the Western Hindu Kush is difficult to distinguish, while these rocks had already undergone Paleozoic metamorphism of similar PT conditions. Variations in PT conditions from low-grade to greenschist/amphibolite facies across the different tectonic slices in the southern part of Western Hindu Kush are probably the result of tectonic emplacement and extrusion of deep seated rocks along the east–west trending slices. This is in agreement with previous interpretation of Tapponnier et al. (1981) who assumed that large-scale tectonics resulting in crustal thickening of the Eurasian plate margin was accompanied by lateral extrusion of continental blocks along strike-slip faults (e.g. westward extrusion of Central Afghan blocks along the Harirod dextral wrench fault). Wedging of the Kabul Block between the Helmand and Nuristan blocks is indicative of the effects of indentation style tectonics as the Kabul Block pushed northwards and resulted in exhumation of Eocene metamorphic rocks around the Salang–Panjshir valleys.

10   Acknowledgments

Part VI

Conclusions

The lowermost basement of the Kabul Block has undergone multiple metamorphic and deformation events (Fig. 1). This is best preserved in orthogneiss from the Khair Khana Mountains in the north west of Kabul and the mountains adjacent to Kabul Airport in the north of the city. These rocks were identified as containing granulite-facies assemblages and suggested to belong to a possible Archean Formation (the Khair Khana Formation) by Karapetov et al. (1981). Our results confirm a Neoarchean age based on U/Pb dating of selected zircon cores from the orthogneiss at Kabul Airport. However, the majority of magmatic zircon cores yield early Paleoproterozoic ages of 2100 - 2400 Ma. The spread of age data could indicate that the rocks were emplaced as a result of multiple magmatic pulses or could represent partial resetting of the geochronological system during subsequent metamorphism and deformation. Mid- to Late-Paleoproterozoic ages of 1800 - 1900 Ma are calculated for metamorphic zircon rims. These ages are considered to correlate with granulite-facies metamorphism recorded by orthopyroxene in felsic and mafic granulites and olivine in calc-silicate at Khair Khana and by Mg-rich garnet in orthogneiss at Kabul Airport. Pressure-Temperature (P-T) conditions of up to 850 °C at around 7 kbar are confirmed through the use of conventional thermobarometry and P-T pseudosection modelling. The absence of cordierite in the orthogneiss and rare occurence of granulite-facies garnet in the felsic granulite suggests that this was a temperature dominated metamorphism with limited pressure variations. The Mid- to Late-Paeloproterozoic timing of this metamorphic event is further confirmed by U-Th-Pb dating of monazite from the Kabul Airport orthogneiss. Y-rich monazite grains in the Mg-rich garnet cores yield an average age of around 1885 Ma, while younger ages of 1750 - 1830 Ma were calculated for monazite in the garnet rim domains. Coarse-grained phlogopite in the calc-silicate thought to also belong to the granulite-facies assemblage was also analysed using the Ar/Ar geochronological technique. This yielded younger ages than the other methods of around 1450 - 1660 Ma; however, these are almost certainly the product of Ar loss during subsequent deformation.

Karapetov et al. (1981) suggested that the granulite-facies assemblages and the garnet-biotite gneiss and migmatite host rocks represent two distinct formations; the Khair Khana and Sherdarwaza respectively. However, similar Paleoproterozoic ages (1800 - 1900 Ma) have also been calculated using U/Pb zircon analysis for migmatite of the Sherdarwaza Formation that hosts granulite-facies assemblages. Additionally some zircon grains from the migmatite yield older ages of 2100 - 2250 Ma. Migmatization of the Sherdarwaza Formation is therefore considered to be coeval with the granulite-facies metamorphism and the distinction between the Khair Khana and Sherdarwaza Formations is an arbitrary construct defined purely on the strength of retrogression and preservation of granulite-facies phases.

Mid- to Early-Paleoproterozoic age metamorphism is widespread throughout Archean terranes. This is a function of global scale collisional events associated with the formation of the Columbia supercontinent. We identified rocks from the Tarim and South China Cratons that have a similar age and geochemical signatures to the basement of the Kabul Block and underwent metamorphism up to granulite-facies conditions at 1800 - 1900 Ma. On this basis we propose a possible early affinity between the Kabul Block and these two cratons.

The granulite-facies assemblages are additionally overprinted by amphibolite-facies phases that include the growth of garnet porphyroblasts in the felsic granulite and fine-grained garnet overgrowths in the mafic granulite and orthogneiss. P-T estimates for this overprint, calculated using conventional geothermobarometry, indicates conditions of around 550 - 650 °C and 7.5 - 9 kbar. Similar, amphibolite-facies,

Figure 1: Summary of the different events recorded within the basement of the Kabul Block
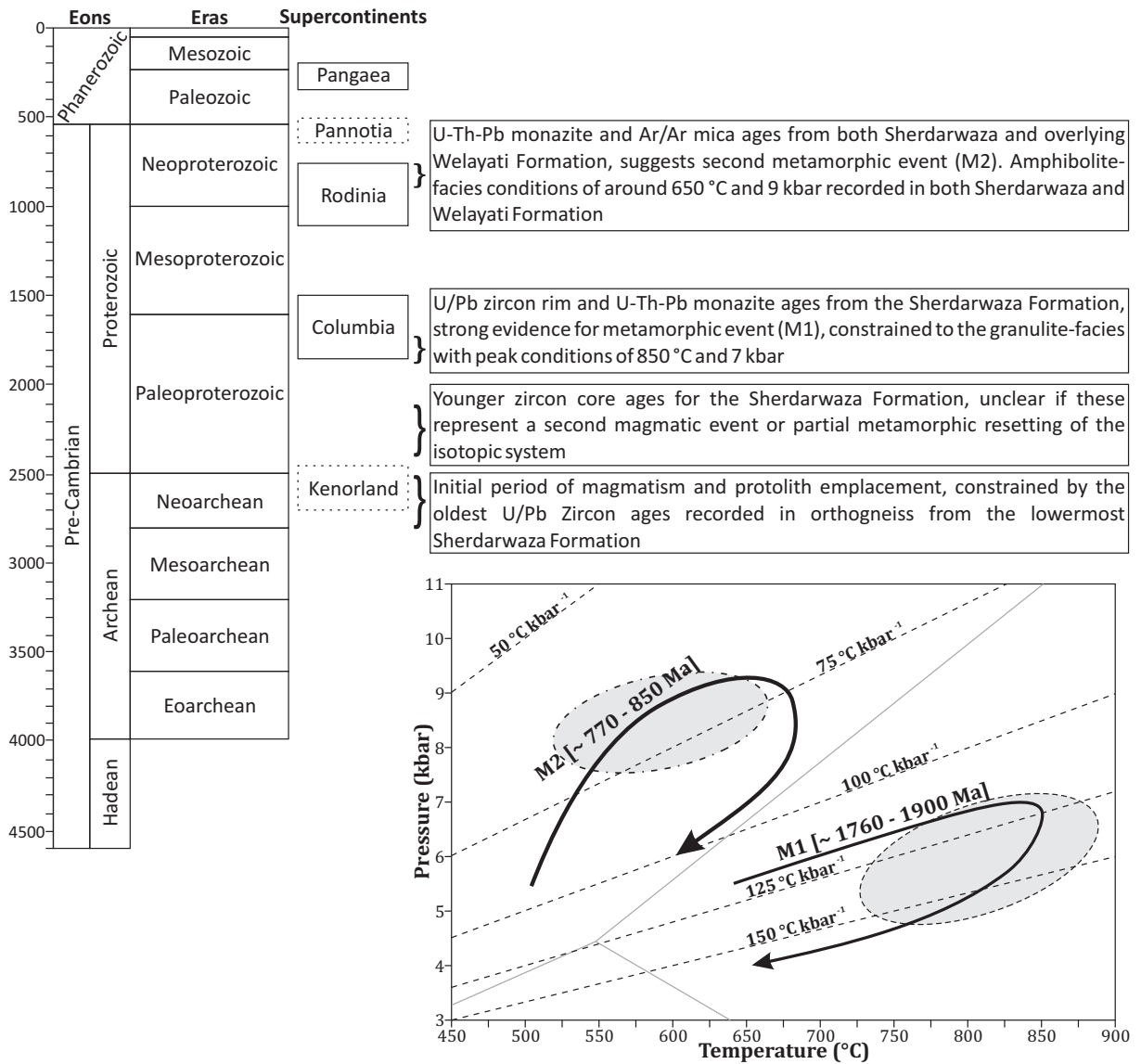
P-T conditions are also estimated for the overlying Welayati Formation, which crops-out in the south of Kabul. Micaschists from the Welayati Formation contain garnet porphyroblasts that preserve prograde zoning. P-T pseudosection modelling for the Welayati micaschists indicate that the rocks underwent burial from around 6 kbar at 525 °C up to 9.5 kbar at 650 °C. Textural relations, including biotite and plagioclase porphyroblasts overgrowing the main foliation, indicate that the rocks were initially decompressed (up to 2 kbar) under isothermal or moderate heating conditions. However, the lack of sillimanite in the micaschists suggests that further decompression and cooling occurred within the kyanite stability-field. Timing of this event has been constrained through U-Th-Pb dating of monazite and Ar/Ar dating of mica. The monazite dating produced a robust dataset with all single points overlapping within error and yielding a mean age of around 820 Ma. The argon-argon dating yielded a range of ages between around 700 and 900 Ma. The age calculated using the Ar/Ar technique usually reflects the time at which a mineral cooled through its closure temperature (~ 400 °C for muscovite and ~ 300 °C for biotite); therefore, the 900 Ma age, calculated from biotite, is anomalous as it is significantly older than the monazite age. Furthermore, the younger ages are produced on disturbed spectra indicating that they have likely undergone argon loss during a subsequent deformation event.

An approximately 820 Ma age is also calculated for matrix monazite in the orthogneiss from Kabul Airport. Ar/Ar dating was also undertaken for the Sherdarwaza Formation which yielded ages of 670 - 780 Ma. As in the Welayati samples the spectra indicate significant disruption as a result of lattice breakdown and redistribution of argon during a later deformation event. Overall the similarity between the P-T conditions and the age dating indicates probable correlation between the amphibolite-facies metamorphism in the Welayati Formation and the metamorphic overprint in the granulites and orthogneiss.

Late Mesoproterozoic to Early Neoproterozoic global scale orogenies are recorded as a result of the amalgamation of the Rodinia supercontinent. Within the Tarim Craton widespread magmatic ages of 1000 - 900 Ma and metamorphic ages of 950 - 910 Ma are reported. The culmination of collisional events associated with the assembly of Rodinia is usually proposed to have occured around 900 Ma (e.g. Li et al. 2008). However, younger metamorphic ages of ca. 790 - 820, consistent with those calculated for the Kabul Block, are reported from the northern Tarim margin (He et al., 2012). If this metamorphism represents a collisional event the timing is broadly consistent with the proposed 800 Ma convergence between Tarim, South China and India in paleogeographic reconstructions for Rodinia proposed by Evans (2009).

In addition to the disruption in the Ar/Ar spectra evidence for a younger metamorphic event in the basement of the Kabul Block is exhibited by the presence of fine grained garnet in the felsic granulite which overgrows both the granulite-facies assemblage and the amphibolite-facies overprint. Owing to the lack of equilibrium it is not possible to constrain either the P-T conditions or the exact timing of this garnet formation. However, given the position of the Kabul Block within the Cimmerian and Alpine collision belts (for reference see Part I Fig. 3) it would seem likely that it was involved in one or both of these events. Alpine age metamorphism is confirmed north from the Kabul Block in the Western Hindu Kush. Our investigations in the Western Hindu Kush identified three metamorphic processes the first of which relates to migmatization of possible Proterozoic age. A second event reaching upper greenschist to amphibolite-facies is recorded in Paleozoic micaschist and phyllite. Eocene, Alpine, metamorphism is recorded as an overprint in the Paleozoic micaschist and phyllite and in Cretaceous age meta-granitoids. Within the meta-granitoids the presence of garnet indicates that this was a pressure dominated amphibolite-facies event. Weakly deformed Triassic age granite north from the meta-granitoids indicates that the degree of metamorphism increases southwards towards the Kabul Block. An Eocene age intrusive belt crosses the Helmand, Kabul, and Nuristan Blocks this would appear to indicate that these blocks were contiguous at this time and the metamorphism relates to the closure of

the Tethys Ocean and India - Eurasia collision. This would appear to support the interpretations of An-dtizky (1971) and Şengör, (1984) that suggested the Kabul Block has affinity to the other Afghan Central Blocks, rather than representing an exotic terrane or a fragment of the Indian continent.

1   Outstanding issues

Overall much progress has been made in regards to the understanding of the evolution of the Kabul Block and many of the original objectives of this project have been accomplished. However, there are still significant gaps in our knowledge and issues that need to be resolved; a selection of which are provided below:

- Clarification of the relations of each of the basement formations is still required. In particular the extent and distribution of granulite-facies assemblages beyond the Khair Khana Mountains and the Kabul Airport are unclear, the maps of these areas produced by Karapteov et al., (1981) have been lost and our fieldwork in these areas was limited by time constraints and safety concerns. Additionally, the relations of the Kharog Formation remain unresolved, it was mapped in the Chehel Sotoon area by Karapetov et al., (1981); however, our studies suggest this area actually belongs to the Welayati Formation. Karapetov et al., (1981) also mapped the Kharog to west of Kabul, and it was defined in the Kharog Mountains further south from Kabul.

- The timing and P-T conditions of the fine-grained garnet in the felsic granulites should be ana-lysed. In the above conclusions it is suggested that this garnet could be related to Alpine events; however, there is limited petrographic evidence for Alpine metamorphism in the other lithologies and it could therefore be associated with retrogression after the amphibolite-facies event.

- The effects of Alpine events on the Kabul Block still need to be fully resolved within both the basement formations and the overlying Phanerozoic sequences. Low degrees of metamorphism and deformation are reported from the Vendian-Cambrian and Carboniferous-Permian sequences; however, this has not been constrained.

- Furthermore, the relationship between the Kotagai Mélange, Peridotite thrust sheets and the rest of the Kabul Block needs to be resolved. In particular clarification of the observation of Bohannon (2010) that the mélange underlies the Proterozoic basement should be confirmed and explained.

- Finally, age relations and metamorphic history from the neighbouring Nuristan and Helmand Blocks would be particularly useful for understanding the affinity between the Kabul Block and the Afghan Central Blocks. On the geological map of Kafarsky et al. (1975) large swathes of the Nuristan Block are mapped as Proterozoic gneiss, similarly Proterozoic rocks are mapped in the Paghman Mountains to the west of the Kabul Block. However, the ages were assigned based on metamorphic grade and pseudostratigraphy and have not been confirmed through geochronolo-gical dating. This is particularly egregious in the case of the Nuristan Block, where similar gneisses to those assigned a Proterozoic age within Afghanistan are given Paleozoic and Mesozoic age on the Pakistan side of the border (e.g. Calkins et al., 1981).

Part VII

Bibliography

Abdullah, S., Chmyriov, V.M., 1977. Geologiya I poleznye iskopaemye Afganistana, Kniga 1, Geologiy. Moscow, Nedra, 535 p.

Abdullah, S., Chmyriov, V.M., 2008. Geology and Mineral Resources of Afghanistan. 2 Volumes. British Geological Survey-Occasional Publication No. 15. (Reprint of the 1980 English translation of the 1977 Russian publication).

Alkmim, F.F., Marshak, S., 1998. Transamazonian orogeny in the Southern Sao Francisco craton region, Minas Gerais, Brazil: evidence for Paleoproterozoic collision and collapse in the Quadrilátero Ferrifero. Precambrian Research 90 (1), 29 – 58.

Andritzky, G., 1967. Bau und Entstehungsgeschichte des Altkristallin-Keils von Kabul (Afghanistan) und seiner Rendzonen. Geologisches Jahrbuch 84, 617 – 636.

Andritzky, G., 1971. Das Kristallin im Gebiet Panjao-Kabul-Jalalabad (Zentral- und Ost-Afghanistan). Niedersachsische Landesamt fur Bodenforschung, Geologisches Jahrbuch 96, 5 – 77.

Auzanneau, E., Schmidt, M.W., Vielzeuf, D., Connolly, J.D., 2010. Titanium in phengite: a geobarometer for high temperature eclogites. Contributions to Mineralogy and Petrology 159(1), 1–24.

Badshah, M.S., Gnos, E., Jan, M.Q., Afridi, M.I., 2000. Stratigraphic and tectonic evolution of the northwestern Indian plate and Kabul Block. Geological Society London Special Publications 170(1), 467-476.

Barbosa, J.S.F., 1990. The granulites of the Jequié Complex and Atlantic Coast Mobile Belt, southern Bahia, Brazil - An expression of Archean/Early Proterozoic plate convergence. Granulites and crustal evolution. Springer, Netherlands, pp. 195 – 221.

Beck, R.A., Burbank, D.W., Sercombe, W.J., Khan, M.A., Lawrence, R.D., 1996. Late Cretaceous ophiolite obduction and Paleocene India-Asia collision in the westernmost Himalaya. Geodinamica Acta 9, 114-144.

Benham, A.J., Kováč, P., Petterson, M.G., Rojkovic, I., Styles, M.T., Gunn, A.G., McKervey, J.A., Wasy, A., 2009. Chromite and PGE in the Logar Ophiolite Complex, Afghanistan. Applied Earth Science: Transactions of the Institutions of Mining and Metallurgy: Section B 118(2), 45-58.

Benisek, A., Dachs, E., Kroll, H., 2010. A ternary feldspar-mixing model based on calorimetric data: development and application. Contributions to Mineralogy and Petrology 160(3), 327–337.

Bhattacharya, A., Krishnakumar, K.R., Raith, M., Sen, S.K., 1991. An Improved Set of a-X Parameters for Fe-Mg-Ca Garnets and Refinements of the Orthopyroxene-Garnet Thermometer and the Orthopyroxene-Garnet-Plagioclase-Quartz Barometer. Journal of Petrology 32(3), 629–656.

Bhattacharya, A., Mohanty, L., Maji, A., Sen, S.K., Raith, M., 1992. Non-ideal mixing in the phlogopite-annite binary: constraints from experimental data on Mg-Fe partitioning and a reformulation of the biotite-garnet ge othermometer. Contributions to Mineralogy and Petrology 111, 87 – 93.

Bhattacharya, S., Santosh, M., Zhang, Z., Huang, H., Banerjee, A., George, P.M., Sajeev, K., 2014. Imprints of Archean to Neoproterozoic crustal processes in the Madurai Block, Southern India. Journal of Asian Earth Sciences 88, 1 – 10.

Bignold, S.M., Treloar, P.J., Petford, N., 2006. Changing sources of magma generation beneath intra-oceanic island arcs: An insight from the juvenile Kohistan island arc, Pakistan Himalaya. Chemical Geology 233, 46-74.

Bindeman, I.N., Eiler, J.M., Yogodzinski, G.M., Tatsumi, Y., Stern, C.R., Grove, T.L., Portnyagin, M., Hoernle, K., Danyushevsky, L.V., 2005. Oxygen isotope evidence for slab melting in modern and ancient subduction zones. Earth and Planetary Science Letters 235 (3), 480 – 496.

Biske, Y.S., Seltmann, R., 2010. Paleozoic Tian-Shan as a transitional region between the Rheic and Urals-Turkestan oceans. Gondwana Research 17 (2), 602 – 613.

Black, L.P., Kamo, S.L., Allen, C.M., Aleinikoff, J.N., Davis, D.W., Korsch R.J., Foudoulis, C., 2003. TEMORA 1: a new zircon standard for Phanerozoic U–Pb geochronology, Chemical Geology 200, 155-170.

Blaise, J., Desparmet, R., de Lapparent, A.F., 1971. Stratigraphie et structure du Paléozoïque de la région de Wardak, en Afghanistan. Bulletin de la Societe Geologique de France 3-4, 420-429.

Blaise, J., Boulin, J., Bouyx, E., Lardeux, H., Vachard, D., 1993. Identification de faunes dévoniennes dans les formations métamorphiques de l'Hindou Kouch occidental, en Afghanistan: implications. Comptes rendus de l'Académie des sciences. Série 2, Mécanique, Physique, Chimie, Sciences de l'univers, Sciences de la Terre 317 (7), 963 – 969.

Bohannon, R.G., 2010. Geologic and topographic maps of the Kabul North 30′ × 60′ quadrangle, Afghanistan: U.S. Geological Survey Scientific Investigations Map 3120, 34 p. pamphlet, 2 map sheets, scale 1:100,000. [Available at: http://pubs.usgs.gov/sim/3120]

Bohannon, R.G., 2010. Geologic and topographic maps of the Kabul South 30′ × 60′ quadrangle, Afghanistan: U.S. Geological Survey Scientific Investigations Map 3137, 34 p. pamphlet, 2 map sheets, scale 1:100,000. [Available at: http://pubs.usgs.gov/sim/3137]

Bohannon, R.G., Turner, K.J., 2005. Geological map of quadrangle 3468, Chak Wardak-Syahgerd (509) and Kabul (510) quadrangles, Afghanistan. USGS open file report 2005-1107-A

Bordet, P., 1969. Le volcanisme récent de la région de Zardalou (province de Ghazni, Afghanistan). Bulletin de la Societe Geologique de France, Paris 11, 810-815.

Borg, S.G., DePaolo, D.J., 1994. Laurentia, Australia, and Antarctica as a Late Proterozoic supercontinent: constraints from isotopic mapping. Geology 22 (4), 307 – 310.

Boros, È., Earle, M.J., Gîlea, M.A., Metlen, A., Mudring, A.V., Rieger, F., Robertson, A.J., Seddon, K.R., Tomaszowska, A.A., Trusov, L., Vyle, J.S., 2010. On the dissolution of non-metallic solid elements (sulfur, selenium, tellurium and phosphorus) in ionic liquids. Chemical Communications 46(5), 716-718.

Boulin, J., 1971. Remarques sur la structure de l'Hindou-Kouch, en Afghanistan, d'apres la transversale du Salang. Comptes Rendus de l'Académie des Sciences Paris Série D 273, 1903-1906.

Boulin, J., 1972. L'évolution stratigraphique et structurale de l'Hindou Kouch central, en Afghanistan, d'après la transversale du Salang. Revue de Geologie Dynamique et de Geographie Physique 14(4), 371-382.

Boulin, J., 1988. Hercynian and Eocimmerian events in Afghanistan and adjoining regions. Tectonophysics 148 (3), 253 – 278.

Boulin, J., 1990. Neocimmerian events incentral and western Afghanistan. Tectonophysics 175 (4), 285 – 315.

Boulin, J., 1991. Structures in Southwest Asia and evolution of the eastern Tethys. Tectonopysics 196 (3), 211 – 268.

Boulin, J., Bouyx, E., 1977. Sutures peri-indiennes successives et structures d'Afghanistan. Comptes Rendus de l'Académie des Sciences Paris Série B 284, 795-8.

Bouyx, E., Collomb, P., 1985. Les schistes cristallins à amphiboles bleues du massif du Sang-e-Caspan, à l'extrémité occidentale de l'Hindou Kouch (Afghanistan). Comptes-rendus des séances de l'Académie des sciences. Série 2, Mécanique-physique, chimie, sciences de l'univers, sciences de la terre 300 (6), 213 – 216.

Bouyx, E., Caridroit, M., Degardin, J.M., 1993. Découverte de radiolairés et conodontés du devonien supérieur dans l'éxtrémité occidentale de l'hindou kouch (afghanistan). Implications sur l'évolution téctonométamorphiqué de la chainé. Annales de la société géologique du nord 2, 189.

Brandt, S., Raith, M., Schenk, S., Sengupta, P., Srikantappa, C., Gerdes, A., 2014. Crustal evolution of the Southern Granulite Terrane, south India: New geochronological and geochemical data for felsic orthogneisses and granites. Precambrian Research 246, 91 – 122.

Bratash, V.I., Egupov, S.V., Pechnikov, V.V., Shelomentsev, A.I., 1970. Geology and petroleum potential of northern Afghanistan. Proceedings of VNIGNI 80.

British Geological Survey, 2005. Aynak information package—Part II, Geological setting of Aynak and summary of exploration, Afghanistan Geological Survey and the British Geological Survey, compilers, Kabul, Ministry of Mines, Department of Mines Affairs.

Brookfield, M.E., Hashmat, A., 2001. The geology and petroleum potential of the North Afghan platform and adjacent areas (northern Afghanistan, with parts of southern Turkmenistan, Uzbekistan and Tajikistan). Earth Science Reviews 55(1), 41–71.

Brown, G.C., Thorpe, R.S., Webb, P.C., 1984. The geochemical characteristics of granitoids arcs and comments on magma sources. Journal of the Geological Society of London 141, 413-426.

Bullard, E., Everett, J.E., Smith, A.G., 1965. The fit of the continents around the Atlantic. Philosophical Transactions of the Royal Society of London. Series A, Mathematical and Physical Sciences 258 (1088), 41 – 51.

Burrett, C., Berry, R., 2000. Proterozoic Australia – Western United States (AUSWUS) fit between Laurentia and Australia. Geology 28 (2), 103 – 106.

Button, A., 1976. Iron-formation as an end member incarbonate sedimentary cyclesinthe Transvaal Supergroup, South Africa. Economic Geology 71 (1), 193 – 201.

Calkins J.A., Jamiluddin, S., Kamaluddin, B., Hussain, A., 1981. Geology and mineral resources of the Chitral- Partsan area, Hindu Kush Range, Northern Pakistan: United States Geological Survey Professional Paper 716–G, 33 p.

Cassaigneau, C., 1979. Contribution dt l'Otude des structures Inde-Eurasie. La zone de suture de Khost dans le Sud-Est de l'Afghanistan, l'obduction Paleocene et la tectonique Tertiaire. PhD thesis, Université des Sciences et Techniques du Langue-doc, Montpellier, France.

Chamberlain, C.P., Zeitler, P.K., Erickson, E., 1991. Constraints on the tectonic evolution of the northwestern Himalaya from geochronologic and petrologic studies of Babusar Pass, Pakistan. The Journal of Geology, 829-849.

Chen, N.,Liao, F.,Wang, L.,Santosh, M.,Sun, M.,Wang, Q.,Mustafa, H.A., 2013. Late Paleoproterozoic multiple metamorphic events in the Quanji Massif: Links with Tarim and North China Cratons and implications for assembly of the Columbia super- continent. Precambrian Research 228, 102 – 116.

Cheney, E.S., 1996. Sequence stratigraphy and plate tectonic signi fi cance of the Transvaal succession of southern Africa and its equivalent in Western Australia. Precambrian Research 79 (1), 3 – 24.

Chernoff, C.B., Carlson, W.D., 1999. Trace element zoning as a record of chemical disequilibrium during garnet growth. Geology 27(6), 555-558.

Chmyriov, V.M., Salah, A.S., 1973. Tectonic map of central and south-western Afghanistan. Kabul, Kabul Times.

Coggon, R., Holland, T.J.B., 2002. Mixing properties of phengitic micas and revised garnet-phengite thermobarometers. Journal of Metamorphic Geology 20, 683-96.

Collett, S., 2011. Crustal evolution in the Paleoproterozoic of Afghanistan: Insights from the Sherdarwaza gneiss of the Kabul Block. Masters Dissertation, University of Leicester (74 pp.).

Collett, S., Faryad, S.W., Mosazai, A.M., 2015. Polymetamorphic evolution of the granulite-facies Paleoproterozoic basement of the Kabul Block, Afghanistan. Mineralogy and Petrology, doi: 10.1007/s00710-015-0371-9.

Collins, A.S., Pisarevsky, S.A., 2005. Amalgamating eastern Gondwana: the evolution of the Circum-Indian Orogens. Earth-Science Reviews 71 (3), 229 – 270.

Condie, K.C., 2003. Supercontinents, superplumes and continental growth: the Neoproterozoic record. Geological Society, London, Special Publications 206 (1), 1 – 21.

Condie, K.C., 2005a. TTGs and adakites: are they both slab melts? Lithos 80 (1), 33 – 44.

Condie, K.C., 2005b. High fi eld strength element ratios in Archean basalts: a window to evolving sources of mantle plumes? Lithos 79 (3), 491 – 504.

Condie, K.C., 2014. How to Make a Continent: Thirty-five Years of TTG Research. Evolution of Archean Crust and Early Life. Springer, Netherlands, pp. 179 – 193.

Condie, K.C., Rosen, O.M., 1994. Laurentia-Siberia connection revisited. Geology 22 (2), 168 – 170.

Connolly, J.A.D., 2005. Computation of phase equilibria by linear programming: a tool for geodynamic modeling and its application to subduction zone decarbonation. Earth and Planetary Science Letters 236, 524-541.

Connolly, J.A.D. 2009. The geodynamic equation of state: what and how. Geochemistry, Geophysics, Geosystems, 10

Coward, M.P., Butler, R.W.H., Khan, M.A., Knipe, R.J., 1987. The tectonic history of Kohistan and its implications for Himalayan structure. Journal of the Geological Society of London 144, 377-391.

Dale, J., Holland, T.J.B., 2003. Geothermobarometry, P–T paths and metamorphic field gradients of high-pressure rocks from the Adula Nappe, Central Alps. Journal of Metamorphic Geology 21(8), 813-829.

Dale, J., Holland, T.J.B., Powell, R., 2000. Hornblende – garnet – plagioclase thermobarometry: a natural assemblage calibration of the thermodynamics of hornblende. Contributions to Mineralogy and Petrology 140, 353 – 362.

Dalziel, I.W., 1991. Pacific margins of Laurentia and East Antarctica-Australia as a conjugate rift pair: Evidence and implications for an Eocambrian supercontinent. Geology 19 (6), 598 – 601.

Dalziel, I.W., Mosher, S., Gahagan, L.M., 2000. Laurentia-Kalahari collision and the assembly of Rodinia. The Journal of Geology 108 (5), 499 – 513.

Debon, F., Le Fort, P., Sonet, J., 1978. Des caracteres geochimiques de deux provinces plutoniques d'Afghanistan: Hindou-Kouch et Montagnes Centrales, 6eme Reunion Ann. Sci. Terr, Orsay, 135p.

Debon, F., Le Fort, P., Sonet, J. 1983. Chemical-mineralogical typology, chronology and geodynamic setting of the western Hindu Kush-Badakhshan plutonic belt (Afghanistan). In: Shams, F.A., (Ed.), Granites of Himalayas, Karakorum and Hindu Kush: Institute of Geology, Punjab University, Lahore, Pakistan, 407-423p.

Debon, F., Afzali, H., Le-Fort, P., Sonet, J., 1987. Major intrusive stages in Afghanistan; typology, age and geodynamic setting. Geologische Rundschau 76, 245 – 264.

Desio, A., Martina, E., Pasquarè, G., 1964. On the geology of central Badakhshan (north-east Afghanistan). Quarterly Journal of the Geological Society 120, 127-151.

Desio, A., Cita, M.B., Premoli Silva, I., 1965. The Jurassic Karkar Formation in North-East Afghanistan. Revista Italiana di Paleontologia 41(4), 1181-1222.

Desio, A., Guj, P., Pasquarè, G., 1968. Notes on the Geology of Wakhan, North-east Afghanistan. Accademia Nazionale dei Lincei.

Doebrich, J.L., Wahl, R.R., 2006. Geologic and mineral resource map of Afghanistan: U.S. Geological Survey Open-File Report 2006–1038, version 2.0, scale 1:850,000. (Available at: http://pubs.er.usgs.gov/ usgspubs/ofr/ofr20061038)

Droop, G.T.R., 1987. A general equation for estimating Fe^{3+} concentrations in ferromagnesian silicates and oxides from microprobe analyses, using stoichiometric criteria. Mineralogical magazine, 51(361), 431-435.

Ernst, R.E., Buchan, K.L., Hamilton, M.A., Okrugin, A.V., Tomshin, M.D., 2000. Integrated Paleomagnetism and U/Pb Geochronology of Mafic Dikes of the Eastern Anabar Shield Region, Siberia: Implications for Mesoproterozoic Paleolatitude of Siberia and Comparison with Laurentia. The Journal of Geology 108 (4), 381 – 401.

Evans, D.A.D., 2009. The palaeomagnetically viable, long-lived and all-inclusive Rodinia supercontinent reconstruction. Geological Society Special Publication 327, 371-404.

Fabries, J., Lang, J., 1970. Quelques remarques sur les formations ante-neogenes de la region de Bamian (Afghanistan central). Bulletin de la Societe Geologique de France (1), 108-113.

Faryad, S.W., 1999. Metamorphic evolution of the Precambrian South Badakhshan block, based on mineral reactions in metapelites and metabasites associated with whiteschists from Sare Sang (Western Hindu Kush, Afghanistan). Precambrian Research 98, 223-241.

Faryad, S.W., 2002. Metamorphic conditions and fluid compositions of scapolite-bearing rocks from the lapis lazuli deposit at Sare Sang, Afghanistan. Journal of Petrology 43, 725-747.

Faryad, S.W., Hoinkes, G., 2003. P–T gradient of Eo-Alpine metamorphism within the Austroalpine basement units east of the Tauern Window (Austria). Mineralogy and Petrology 77(1–2),129–159.

Faryad, S.W., Frank, W., 2011. Textural and age relations of polymetamorphic rocks in the HP Meliata Unit (Western Carpathians). Journal of Asian Earth Sciences 42 (1), 111 – 122.

Faryad, S.W., Mosazai, A. M., Sergeev,S., Wasay,A., 2009. Metamorphism and age relations in the Proterozoic Kabul Block; PT conditions and new SHRIMP dating. Abstract volume, 2nd International Hindu Kush Geoscience Conference, September, 27-29. 2009, Kabul.

Faryad, S.W., Collett, S., Petterson, M., Sergeev, S.A., 2013. Magmatism and metamorphism linked to the accretion of continental blocks south of the Hindu Kush, Afghanistan. Lithos 175, 302-314.

Faryad, S.W., Collett, S., Finger, F., Sergeev, S.V., Čopjaková, R., Simon, P., 2015. The Kabul Block (Afghanistan), a segment of the Columbia Supercontinent, with a Neoproterozoic metamorphic overprint. Gondwana Research. doi:10.1016/j.gr.2015.02.019

Fesefeldt, K., 1964. Das Palaozoikum in Gebiet der oberen Logar und im ostlichen Hazarajat sudwestlich Kabul, Afghanistan. Geologisches Jahrbuch 70, 185 – 228.

Finger, F., Broska, I., Roberts, M.P., Schermaier, A., 1998. Replacement of primary monazite by apatite-allanite-epidote coronas in an amphibolite facies granite gneiss from the eastern Alps. American Mineralogist 83 (3), 248 – 258.

Finger, F., Krenn, E., 2007. Three metamorphic monazite generations in a high-pressure rock from the Bohemian Massif and the potentially important role of apatite in stimulating polyphase monazite growth along a PT loop. Lithos 95 (1), 103 – 115.

Fischer, J., 1971. Zur Geologie des Kohe Safi bei Kabul (Afghanistan) (Doctoral dissertation).

Fitzsimons, I.C.W., Harley, S,L., 1994. The influence of retrograde cation exchange on granulite PT estimates and a convergence technique for the recovery of peak metamorphic conditions. Journal of Petrology 35(2), 543–576.

Frost, B.R., Avchenko, O.V., Chamberlain, K.R., Frost, C.D., 1998. Evidence for extensive Proterozoic remobilization of the Aldan shield and implications for Proterozoic plate tectonic reconstructions of Siberia and Laurentia. Precambrian Research 89 (1), 1 – 23.

Fuhrman, M.L., Lindsley, D.H., 1988. Ternary-feldspar modeling and thermometry. American Mineralogist 73(3-4), 201-215.

Gaina, C., Hinsbergen, D.J., Spakman, W., 2015. Tectonic interactions between India and Arabia since the Jurassic reconstructed from marine geophysics, ophiolite geology, and seismic tomography. Tectonics doi:10.1002/2014TC003780.

Ganguly, J., Cheng, W., Tirone, M., 1996. Thermodynamics of aluminosilicate garnet solid solution: new experimental data, an optimized model, and thermometric applications. Contributions to Mineralogy and Petrology 126, 137-151.

Ge, R.F., Zhu, W.B., Wu, H.L., He, J.W., Zheng, B.H., 2013. Zircon U-Pb ages and Lu-Hf isotopes of Paleoproterozoic metasedimentary rocks in the Korla Complex, NW China: Implications for metamorphic zircon formation and geological evolution of the Tarim Craton. Precambrian Research 231, 1 - 18.

Ge, R.F., Zhu, W.B., Wilde, S.A., Wu, H., He, J., Zheng, B., 2014a. Archeanmagmatismandcrustal evolution in the northern Tarim Craton: insights from zircon U-Pb-Hf-O isotopes and geochemistry of ~ 2.7 Gaorthogneiss and amphibolite inthe Korla Complex. Precambrian Research 252, 145 – 165.

Ge, R.F., Zhu, W.B., Wilde, S.A., He, J.W., Cui, X., Wang, X., Bihai, Z., 2014b. Neoproterozoic to Paleozoic long-lived accretionary orogeny i n the northern Tarim Craton. Tectonics 33, 302 – 329.

Glorie, S., De Grave, J., Buslov, M.M. , Zhimulev, F.I., Safonova, I.Y., 2014. Detrital zircon prov- enance of early Palaeozoic sediments at the southwestern margin of the Siberian Cra- ton: Insights from U – Pb geochronology. Journal of Asian Earth Sciences 82, 115 – 123.

Godard, G., 2009. Two orogenic cycles recorded in eclogite-facies gneiss from the southern Armorican Massif (France). European Journal of Mineralogy 21(6), 1173–1190.

Gower, C.F., Ryan, A.B., Rivers, T., 1990. Mid-Proterozoic Laurentia-Baltica: an overview of its geological evolution and a summary of the contributions made by this volume. Mid-Proterozoic Laurentia-Baltica 38, 1 – 20.

Graphchikov AA, Konilov AN, Clemens JD (1999) Biotite dehydration, partial melting, and fluid composition: Experiments in the system $KAlO_2$-FeOMgO-SiO_2-H_2O-CO_2. American Mineralogist 84, 15–26.

Griesbach, C.L., 1885. Afghan field notes. Records of the Geological Survey of India 18, 57-64.

Hawthorne, F.C., Oberti, R., Harlow, G.E., Maresch, W.V., Martin, R.F., Schumacher, J.C., Welch, M.D., 2012. Nomenclature of the amphibole supergroup. American Mineralogist 97(11–12), 2031–2048.

Hayden, S.H.H., 1911. The geology of northern Afghanistan. Office of the Geological Survey of India.

He, Z.Y., Zhang, Z.M., Zong, K.Q., Wang, W., Santosh, M., 2012. Neoproterozoic granulites from the northeastern margin of the Tarim Craton: petrology, zircon U - Pb ages and implications for the Rodinia assembly. Precambrian Research 212, 21 - 33.

He, Z.Y., Zhang, Z.M., Zong, K.Q., Dong, X., 2013. Paleoproterozoic crustal evolution of the Tarim Craton: constrained by zircon U - Pb and Hf isotopes of meta-igneous rocks from Korla and Dunhuang. Journal of Asian Earth Sciences 78, 54 – 70.

Hickmott, D., Spear, F.S., 1992. Major-and trace-element zoning in garnets from calcareous pelites in the NW Shelburne Falls Quadrangle, Massachusetts: Garnet growth histories in retrograded rocks. Journal of Petrology 33(5), 965-1005.

Hickmott, D.D., Shimizu, N., Spear, F.S., Selverstone, J., 1987. Trace-element zoning in a metamorphic garnet. Geology 15(6), 573-576.

Hodges, K.V., Crowley, P.D., 1985. Error estimation and empirical geothermobarometry for pelitic systems. American Mineralogist 70(7–8), 702–709.

Hodges, K.V., Spear, F.S., 1982, Geothermometry, geobarometry and the Al2SiO5 triple point at Mt. Moosilauke, New Hampshire. American Mineralogist 67, 1118-1134.

Hoffman, P.F., 1988. United Plates of America, the birth of a craton-Early Proterozoic assembly and growth of Laurentia. Annual Review of Earth and Planetary Sciences 16, 543 – 603.

Hoffman, P.F., 1989. Speculations on Laurentia's first gigayear (2.0 to 1.0 Ga). Geology 17 (2), 135 – 138.

Hoffman, P.F., 1991. Did the break out of Laurentia turn Gondwanaland inside-out? Science 252 (5011), 1409 – 1412.

Hoffman, P.F., Kaufman, A.J., Halverson, G.P., Schrag, D.P., 1998. A Neoproterozoic snowball earth. Science 281 (5381), 1342 – 1346.

Hoisch, T.D., 1990. Empirical calibration of six geobarometers for the mineral assemblage quartz + muscovite + biotite + plagioclase + garnet. Contributions to Mineralogy and Petrology 104(2), 225–234.

Holdaway, M.J., 2000. Application of new experimental and garnet Margules data to the garnet-biotite geothermometer. American Mineralogist 85, 881-892.

Holland, T.J.B., 2014. AX: A program to calculate activities of mineral end-members from chemical analyses. http://www.esc.cam.ac.uk/research/research-groups/holland/ax last accessed on 13 May 2015.

Holland, T.J.B., Baker, J., Powell, R., 1998. Mixing properties and activity-composition relationships of chlorites in the system MgO-FeO-Al2O3-SiO2-H2O. European Journal of Mineralogy 10, 395-406.

Holland, T.J.B., Powell R., 1998. An internally consistent thermodynamic data set for phases of petrological interest. Journal of Metamorphic Geology 16, 309-343.

Holland, T.J.B., Powell, R., 2001. Calculation of phase relations involving haplogranitic melts using an internally consistent thermodynamic dataset. Journal of Petrology 42(4), 673-683.

Holland, T.J.B., Powell, R., 2003. Activity-composition relations for phases in petrological calculations: an asymmetric multicomponent formulation. Contributions to Mineralogy and Petrology 145, 492-501.

Hu, A., Jahn, B.M., Zhang, G., Chen, Y., Zhang, Q., 2000. Crustal evolution and Phanerozoic crustal growth in northern Xinjiang: Nd isotopic evidence. Part I. Isotopic characterization of basement rocks. Tectonophysics 328 (1), 15 – 51.

Ilavsky, J., Kantor, J., 1965. Prispevok ku geochronologii sirsieho okolia kabulu (afghanistan). Geol. Prace 37, 65-90.

Jacobs, J., Thomas, R.J., 2004. Himalayan-type indenter-escape tectonics model for the southern part of the late Neoproterozoic – early Paleozoic East African – Antarctic orogen. Geology 32 (8), 721 – 724.

Jamieson, R.A., O'Beirne-Ryan, A.M., 1991. Decompression-induced growth of albite porphyroblasts, Fleur de Lys Supergroup, western Newfoundland. Journal of Metamorphic Geology 9(4), 433-439.

Jercinovic, M.J., Williams, M.L., 2005. Analytical perils (and progress) in electron micro-probe trace element analysis applied to geochronology: background acquisition, interferences, and beam irradiation effects. American Mineralogist 90 (4), 526 – 546.

Jiang, Y.H., Jia, R.-Y., Liu, Z., Liao, S.Y., Zhao, P., Zhou, Q., 2013. Origin of Middle Triassic high-K calc-alkaline granitoids and their potassic microgranular enclaves from the western Kunlun orogen, northwest China: A record of the closure of Paleo-Tethys. Lithos 156-159, 13-30.

Kafarsky, A.Kh., Chmyriov, V.M., Stazhilo-Alekseev, K.F., Abdullah, Sh., Saikovsky, V.S., 1975. Geological map of Afghanistan, scale 1:2,500,000

Kamber, B., Collerson, K.D., 2000. The role of slab melting in continental crustal growth: traceelement constraints from Archean TTG Gneiss complexesand models of oceanic crust production. American Geophysical Union 2000 Fall Meeting Vol. 81, No. 48. American Geophysical Union.

Karapetov, S.S., Sonin, J.J., Khain, V.E., 1975. Some major properties of the structure and development of the Afghan-Pamir segment of the Eurasian Alpine folding belt. Vestnik Moskovskogo Universiteta, Geologiya 30, 38-46.

Karapetov, S.S., Sorokin, Yu.A., Sytov, Yu.N., Chepela, V.F., Abdullah, Sh., Ashmat, A., 1981. Geological structure of Kabul town region (Report of Logar and Helmand prospecting-mapping group in 1979-1981). Unpublished report, Afghan Geological Survey.

Khan, S.D., Walker, D.J., Hall, S.A., Burke, K.C., Shah, M.T., Stockli, L., 2009. Did the Kohistan-Ladakh island arc collide first with India?. Geological Society of America Bulletin 121, 366-384.

Khoreva, B.Y., Iskanderova, A.D., Chukhonin, A.P., 1971. On the age of the most ancient carbonate rocks in the Southern Altai and the Central Kyzyl-kums according to the data of the lead isochronous mehtod. Izvestiya Akademii Nauk SSSR, Seriya Geologicheskaya 11, 3 – 8.

Khoreva, B.Ya., Iskanderova, A.D., Shergina, Yu.P., 1971. Lead-isotope dating of the substratum of the metamorphic series in the South-Western Pamirs. Izvestiya of the Academy of Sciences of the U.S.S.R. 8, 40-46.

Klootwijk, C.T., Gee, J.S., Peirce, J.W. Smith, G.M., 1991. Constraints on the India-Asia convergence: paleomagnetic results from Ninetyeast Ridge. Proceedings of the ODP Scientific Results 121, 777-882.

Kohn, M.J., Spear, F.S., 1990. Two new geobarometers for garnet amphibolites, with applications to southeastern Vermont. American Mineralogist 75(1–2), 89–96.

Kohn, M.J., Malloy, M.A. 2004. Formation of monazite via prograde metamorphic reactions among common silicates: implications for age determinations. Geochimica et Cosmochimica Acta 68(1), 101-113.

Konrad-Schmolke, M., Zack, T., O'Brien, P.J., Jacob, D.E., 2008. Combined thermodynamic and rare earth element modelling of garnet growth during subduction: examples from ultrahigh-pressure eclogite of the Western Gneiss Region, Norway. Earth and Planetary Science Letters 272(1), 488-498.

Koziol, A.M., 1989. Recalibration of the garnet–plagioclase–Al_2SiO_5–quartz (GASP) geobarometer and applications to natural parageneses. Eos, Transactions American Geophysical Union 70(15), 493.

Koziol, A.M., Newton, R.C., 1988. Redetermination of the anorthite breakdown reaction and improvement of the plagioclase-garnet-Al_2SiO_5-quartz geobarometer. American Mineralogist 73(3–4), 216–223.

Kroener, A., Stern, R.J., 2005. Africa; Pan-African Orogeny. In: Selley, R.C., Cocks, L.R.M., Plimer, I.R. (Eds.), Encyclopedia of geology. Elsevier Academic Press, Oxford, 1 – 12p.

Kusky, T.M., Abdelsalam, M., Tucker, R.D., Stern, R.J., 2003. Evolution of the East African and related orogens, and the assembly of Gondwana. Precambrian Research 123 (2), 81 – 85.

Lanzirotti, A., 1995. Yttrium zoning in metamorphic garnets. Geochimica et Cosmochimica Acta 59(19), 4105-4110.

Lapparent, A.F., Bordet, P., 1963. Du volcanisme en Afghanistan central. Bulletin de la Societe Geologique de France, Paris 7, 214-217.

Lapparent, A.F., Mennessier, G., 1962. Observations stratigraphiques sur les séries précambriennes de l'Afghanistan. Comptes Rendus de l'Académie des Sciences Paris 254, 1834-1836.

Lawrence, R.D., Khan, S.H., Nakata, T., 1992. Chaman Fault, Pakistan-Afghanistan. Annales Tectonicae 6, 196-223.

Lee, H.Y., Ganguly, J., 1988. Equilibrium compositions of coexisting garnet and orthopyroxene: experimental determinations in the system FeO-MgO-Al$_2$O$_3$-SiO$_2$, and applications. Journal of Petrology 29(1), 93–113.

Leven, E.J., 1971. Lee gisements permiens et los Fusulinides de l'Afghanistan du Nord. Notes et Mémoir Moyen-Orient, Paris 12,

Leven, E.J., 1997. Permian stratigraphy and fusulinida of Afghanistan with their paleogeographic and paleotectonic implications, Stevens, C.H., and Baars, D.L., eds: Geological Society of America Special Paper 316, 134 p.

Li, Z.X., Bogdanova, S.V., Collins, A.S., Davidson, A., De Waele, B., Ernst, R.E., Fitzsimons, I.C.W., Fuck, R.A., Gladkochub, D.P., Jacobs, J., Karlstrom, K.E., Lu, S., Natapov, L.M., Pease, V., Pisarevsky, S.A., Thrane, K., Vernikovsky, V., 2008. Assembly, configuration, and break-up history of Rodinia: a synthesis. Precambrian Research 160(1), 179 – 210.

Li, Z.X., Li, X.H., Kinny, P.D., Wang, J., Zhang, S., Zhou, H., 2003. Geochronology of Neoproterozoic syn-rift magmatism in the Yangtze Craton, South China and correlations with other continents: evidence for a mantle superplume that broke up Rodinia. Precambrian Research 122(1), 85 – 109.

Li, Z.X., Peng, S., 2010. Detrital zircon geochronology and its provenance implications: responses to Jurassic through Neogene basin-range interactions along northern margin of the Tarim Basin, Northwest China. Basin Research 22(1), 126 – 138.

Lindsay, C.R., Snee, L.W., Bohannon, R.G., Wahl, R.R., Sawyer, D.A., 2005. Geologic map of quadrangle 3568, Polekhomri (503) and Charikar (504) quadrangles, Afghanistan. USGS Open-File Report 2005-1101-A.

Ling, W., Gao, S., Zhang, B., Li, H., Liu, Y., Cheng, J., 2003. Neoproterozoic tectonic evolution of the northwestern Yangtze craton, South China: implications for amalgamation and break-up of the Rodinia Supercontinent. Precambrian Research 122 (1), 111 – 140.

Liu, Y.C., Wang, A., Rolfo, F., Groppo, C., Gu, X., Song, B., 2009. Geochronological and petrological constraints on Palaeoproterozoic granulite facies metamorphism in southeastern margin of the North China Craton. Journal of Metamorphic Geology 27, 125 – 138.

Locock, A.J., 2014. An Excel spreadsheet to classify chemical analyses of amphiboles following the IMA 2012 recommendations. Computers & Geosciences 62, 1–11.

Long, X., Yuan, C., Sun, M., Zhao, G., Xiao, W., Wang, Y., Yang, Y., Hu, A., 2010. Archean crustal evolution of the northern Tarim craton, NW China: Zircon U – Pb and Hf isotopic constraints. Precambrian Research 180(3), 272 – 284.

Long, X., Yuan, C., Sun, M., Kröner, A., Zhao, G., Wilde, S., Hu, A., 2011. Reworking of the Tarim Craton by underplating of mantle plume-derived magmas: evidence from Neoproterozoic granitoids in the Kuluketage area, NW China. Precambrian Research 187(1), 1 – 14.

Long, X., Sun, M., Yuan, C., Kröner, A., Hu, A., 2012. Zircon REE patterns and geochemical characteristics of Paleoproterozoic anatectic granite in the northern Tarim Craton, NW China: implications for the reconstruction of the Columbia supercontinent. Precambrian Research 222, 474 – 487.

Ludwig, K.R., 2001. SQUID 1.02, A User Manual, A Geochronological Toolkit for Microsoft Excel. Berkeley Geochronology Center Special Publication, Berkeley, USA.

Ludwig, K.R., 2003. User's Manual for Isoplot/Ex, Version 3.00, A Geochronological Toolkit for Microsoft Excel. Berkeley Geochronology Center Special Publication, Berkeley, USA.

Maldonado, F., Turner, K.J., 2005. Geologic map of quadrangle 3368 and part of quadrangle 3370, Ghazni (515), Gardez (516), and part of Jaji-Maydan (517) quadrangles, Afghanistan. USGS Open-File Report 2005-1112-A.

Martin, H., 1999. Adakitic magmas: modern analogues of the Archean continental crust, comparison with modern processes. Lithos 30, 373 – 388.

Martin, H., Smithies, R.H., Rapp, R., Moyen, J.F., Champion, D., 2005. An overview of adakite, tonalite – trondhjemite – granodiorite (TTG), and sanukitoid: relationships and some implications for crustal evolution. Lithos 79(1), 1 – 24.

McDonough, W.F., Sun, S.-S., 1995. The composition of the Earth. Chemical Geology 120, 223–253.

Meert, J.G., 2002. Paleomagnetic Evidence for a Paleo-Mesoproterozoic Supercontinent Columbia. Gondwana Research 5, 207 – 215.

Meert, J.G., 2003. A synopsis of events related to the assembly of eastern Gondwana. Tectonophysics 362 (1), 1 – 40.

Meert, J.G., 2014. Strange attractors, spiritual interlopers and lonely wanderers: The search for pre-Pangean supercontinents. Geoscience Frontiers 5, 155 – 166.

Meert, J.G., Torsvik, T.H., 2004. Paleomagnetic constraints on Neoproterozoic 'Snowball Earth' continental reconstructions. In: Jenkins, et al. (Eds.), The Extreme Proterozoic: Geology, Geochemistry and Climate. ADU Geophysical Monograph Series 146, pp. 5 – 12.

Meert, J.G., Lieberman, B.S., 2008. The Neoproterozoic assembly of Gondwana and its relationship to the Ediacaran-Cambrian Radiation. Gondwana Research 14, 5 – 21.

Mennessier, G., 1963. Afghanistan. Lexique Stratigraphique International, 3, Asie, 9a.

Mennessier, G., 1968. Contributions à la géologie et à la paleontologie de l'Afghanistan. Etude tectonique des montanges du la région de Kaboul. Notes et Mèmoir Moyen-Orient, Paris 9, 1-185.

Mennessier, G., 1972. Presentation des recherches geologiques en Afghanistan. Revue de Geographie Physique et de Geologie Dynamique 14, 323-325.

Mennessier, G., 1976. Nouvelles observations sur l'âge de la série de Kotagaé et les ultrabasites qui la surmontent; incidence sur la structure du fossé de Kaboul (Afghanistan occidental), Comptes rendus hebdomadaires des séances de l'Académie des sciences, Série D: Sciences naturelles 282(17), 1581–1583.

Mennessier, G., 1977. Stratigraphie, tectonique et evolution du fossé de Kaboul (Afghanistan). Mémoires hors série Société géologique de France 8, 153-168.

Mohan, M.R., Singh, S.P., Santosh, M., Siddiqui, M.A., Balaram, V., 2012. TTG suite from the Bundelkhand Craton, Central India: Geochemistry, petrogenesis and implications for Archean crustal evolution. Journal of Asian Earth Science 58, 38-5.

Molnar, P., Tapponnier, P., 1975. Cenozoic tectonics of Asia: effects of a continental collision. Science 189(4201), 419-426.

Montel, J.M., Foret, S., Veschambre, M., Nicollet, C., Provost, A., 1996. Electron microprobe dating of monazite. Chemical Geology 131 (1), 37 – 53.

Moore, S.J., Carlson, W.D., Hesse, M.A., 2013. Origins of yttrium and rare earth element distributions in metamorphic garnet. Journal of Metamorphic Geology 31(6), 663-689.

Moores, E.M., 1991. Southwest US-East Antarctic (SWEAT) connection: a hypothesis. Geology 19 (5), 425 – 428.

Nakamura, N., 1974. Determination of REE, Ba, Fe, Mg, Na and K in carbonaceous and ordinary chondrites. Geochimica et Cosmochimica Acta 38 (5), 757 – 775.

Naqvi, S.M., Rana Prathap, J.G., 2007. Geochemistry of adakites from Neoarchaean active continental margin of Shimoga schist belt, western Dharwar craton, India: implica- tions for the genesis of TTG. Precambrian Research 156 (1), 32 – 54.

Newton, R.C., Perkins, D.I., 1982. Thermodynamic calibration of geobarometers based on the assemblages garnet-plagioclase-orthopyroxene (clinopyroxene)-quartz. American Mineralogist 67(3–4), 203–222.

Patiño Douce, A.E., Johnston, A.D., 1991. Phase equilibria and melt productivity in the pelitic system: implications for the origin of peraluminous granitoids and aluminous granulites. Contributions to Mineralogy and Petrology 107(2), 202–218.

Pattison, D.R.M., 2003. Petrogenetic significance of orthopyroxene-free garnet + clinopyroxene + plagioclase ± quartz-bearing metabasites with respect to the amphibolite and granulite facies. Journal of Metamorphic Geology 21(1), 21–34.

Pearce, J.A., Harris, N.B.W., Tindle, A.G., 1984. Trace element discrimination diagrams for the tectonic interpretation of granitic rocks. Journal of Petrology 25, 956-983.

Perchuk, L.L., Aranovich, L.Y., Podlesskii, K.K., Lavrant'eva, I.V., Gerasimov, V.Y., Fed'Kin, V.V., Kitsul, V.I., Karsakov, L.P., Berdnikov, N.V., 1985. Precambrian granulites of the Aldan shield, eastern Siberia, USSR. Journal of Metamorphic Geology 3(3), 265–310.

Perchuk, L. L., Lavrent'eva, L. Y., 1983. Experimental investigation of exchange equilibria in the system cordierite–garnet–biotite. In: Saxena, S.K., (Ed.), Kinetics and Equilibrium in Mineral Reactions. Advances in Physical Geochemistry 3, 199–239.

Pesonen, L.J., Elming, S.Å., Mertanen, S., Pisarevsky, S., D'Agrella-Filho, M.S., Meert, J.G., Schmidt, P.W., Abrahamsen, N., Bylund, G., 2003. Palaeomagnetic configuration of continents during the Proterozoic. Tectonophysics 375 (1), 289 – 324.

Petterson, M.G., Windley, B.F., 1985. Rb-Sr dating of the Kohistan arc-batholith in the Trans-Himalaya of north Pakistan, and tectonic implications. Earth and Planetary Science Letters 74, 45-57.

Piper, J.D., 2000. The Neoproterozoic Supercontinent: Rodinia or Palaeopangaea? Earth and Planetary Science Letters 176 (1), 131 – 146.

Pisarevsky, S.A., Wingate, M.T., Powell, C.M., Johnson, S., Evans, D.A., 2003. Models of Rodinia assembly and fragmentation.Geological Society,London,Special Publications 206 (1), 35 – 55.

Pouchou, J.L., Pichoir, F., 1985. Pap. phi-rho-Z) procedure for improved quantitative microanalysis. In: Armstrong, J.T. (Ed.), Microbeam, analysis, pp. 104 – 106.

Powell, R., Holland, T.J.B., 1988. An internally consistent dataset with uncertainties and correlations: 3. Applications to geobarometry, worked examples and a computer program. Journal of Metamorphic Geology 6(2), 173-204.

Powell, R., Holland, T.J.B., 1999. Relating formulations of the thermodynamics of mineral solid solutions: activity modeling of pyroxenes, amphiboles, and micas. American Mineralogist 84, 1–14.

Powell, R., Holland, T.J.B., 2008. On thermobarometry. Journal of Metamorphic Geology 26(2), 155-179.

Proyer, A., Mposkos, E., Baziotis, I., Hoinkes, G., 2008. Tracing high-pressure metamorphism in marbles: Phase relations in high-grade aluminous calcite–dolomite marbles from the Greek Rhodope massif in the system $CaO–MgO–Al_2O_3–SiO_2–CO_2$ and indications of prior aragonite. Lithos 104(1), 119–130.

Pyle, J.M., Spear, F.S., 1999. Yttrium zoning in garnet: coupling of major and accessory phases during metamorphic reactions. Geological Materials Research 1(6), 1-49.

Rahmati-Ilkhchi, M., Faryad, S.W., Holub, F.V., Košler , J., Frank, W., 2011. Magmatic and metamorphic evolution of the Shotur Kuh metamorphic complex (Central Iran). International Journal of Earth Sciences 100 (1), 45 – 62.

Ramezani, J., Tucker, R.D., 2003. The Saghand region, central Iran: U-Pb geochronology, petrogenesis and implications for Gondwana tectonics. American Journal of Science 303 (7), 622 – 665.

Rehman, H.U., Seno, T., Yamamoto, H., Khan, T., 2011. Timing of collision of the Kohistan–Ladakh Arc with India and Asia: Debate. Island Arc 20, 308-328.

Resch, M., 1971. Zur geologie des westlichen Hindukush zwischen Salang und Sekari-Schlucht. Bonn, Reinische Friedrich-Wilhelms-Univeristat, PhD thesis, 82 p., scale 1:304,960

Rex, A.J., Searle, M.P., Tirrul, R., Crawford, M., Prior, D., Rex, D., Barnicoat, A., Bertrand, J., 1988. The geochemical and tectonic evolution of the central Karakoram, North Pakistan. Philosophical Transactions of the Royal Society of London 326, 229-255.

Rogers, J.J., Santosh, M., 2002. Configuration of Columbia, a Mesoproterozoic supercontinent. Gondwana Research 5(1), 5 – 22.

Ross, G.M., Parrish, R.R., Winston, D., 1992. Provenance and U-Pb geochronology of the Mesoproterozoic Belt Supergroup (northwestern United States): Implications for age of deposition and pre-Panthalassa plate reconstructions. Earth and Planetary Science Letters 113 (1), 57 – 76.

Ruleman, C.A., Crone, A.J., Machette, M.N., Haller, K.M., Rukstales, K.S., 2007. Map and database of probable and possible Quaternary faults in Afghanistan (No. 2007-1103). Geological Survey (US).

Samuel, V.O., Santosh, M., Liu, S., Wang, W., Sajeev, K., 2014. Neoarchean continental growth through arc magmatism in the Nilgiri Block, southern India. Precambrian Research 245, 146 – 173.

Sarkar, T., Schenk, V., 2014. Two-stage granulite formation in a Proterozoic magmatic arc (Ongole domain of the Eastern Ghats Belt, India): Part 1. Petrology and pressure–temperature evolution, Precambrian Research 255, 485-509.

Satish-Kumar, M., Wada, H., Santosh, M., Yoshida, M. 2001. Fluid-rock history of granulite facies humite-marbles from Ambasamudram, southern India. Journal of Metamorphic Geology 19(4), 395–410.

Schreyer, W., Abraham, K., 1975. Peraluminous sapphirine as a metastable reaction product in kyanite-gedrite-talc schist from Sar e Sang, Afghanistan. Mineralogical Magazine 40, 171–180.

Schuth, S., Gornyy, V.I., Berndt, J., Shevchenko, S.S., Sergeev, S.A., Karpuzov, A.F., Mansfeldt, T., 2012. Early Proterozoic U-Pb Zircon Ages from Basement Gneiss at the Solovetsky Archipelago, White Sea, Russia. International Journal of Geosciences 3, 289-296.

Schwandt, C.S., Papike, J.J., Shearer, C.K., 1996. Trace element zoning in pelitic garnet of the Black Hills, South Dakota. American Mineralogist 81(9), 1195-1207.

Searle, M.P., 1991. Geology and tectonics of the Karakoram Mountains. John Wiley & Sons Inc.

Sears, J.W., Price, R.A., 2000. New look at the Siberian connection: no SWEAT. Geology 28(5), 423 – 426.

Şengör, A.M.C., 1984. The Cimmeride orogenic system and the tectonics of Eurasia. Geological Society of America Special Papers 195, 1-74.

Şengör, A.M.C., Altıner, D., Cin, A., Ustaömer, T., Hsü, K.J., 1988. Origin and assembly of the Tethyside orogenic collage at the expense of Gondwana Land. Geological Society, London, Special Publications 37(1), 119-181.

Şengör, A.M.C., Cin, A., Rowley, D.B., Nie, S.Y., 1993. Space-time patterns of magmatism along the Tethysides: a preliminary study. The Journal of Geology 101, 51 – 84.

Shaji, E., Santosh, M., He, X.F., Fan, H.R., Dev, S.G., Yang, K.F., Thangal, M.K., Pradeepkumar, A.P., 2014. Convergent margin processes during Archean – Proterozoic transition in southern India: Geochemistry and zircon U-Pb geochronology of gold-bearing am- phibolites, associated metagabbros, and TTG gneisses from Nilambur. Precambrian Research 250, 68 – 96.

Shi, Y., Wilde, S.A., Zhao, X., Ma, Y., Du, L., Liu, D., 2012. Late Neoarchean magmatic and subsequent metamorphic events in the northern North China Craton: SHRIMP zircon dating and Hf isotopes of Archean rocks from Yunmengshan Geopark, Miyun, Beijing. Gondwana Research 21 (4), 785 – 800.

Slavin, V.I., Federov, T.O., Feruz, N.M., 1972. The geology and age of the metamorphic complex in the Kabul district. Vestnik Moskovskogo Universiteta, Moscow

Smethurst, M.A., Khramov, A.N., Torsvik, T.H., 1998. The Neoproterozoic and Palaeozoic palaeomagnetic data for the Siberian Platform: from Rodinia to Pangea. Earth- Science Reviews 43 (1), 1 – 24.

Smithies, R.H., 2000. The Archaean tonalite – trondhjemite – granodiorite (TTG) series is not an analogue of Cenozoic adakite. Earth and Planetary Science Letters 182 (1), 115 – 125.

Smye, A.J., Greenwood, L.V., Holland, T.J.B., 2010. Garnet–chloritoid–kyanite assemblages: eclogite facies indicators of subduction constraints in orogenic belts. Journal of Metamorphic Geology 28(7), 753-768.

Sommer, H., Kröner, A., 2013. Ultra-high temperature granulite-facies metamorphic rocks from the Mozambique belt of SW Tanzania. Lithos 170, 117–143.

Song, S., Su, L., Li, X.H., Niu, Y., Zhang, L., 2012. Grenville-age orogenesis in the Qaidam- Qilian block: The link between South China and Tarim. Precambrian Research 220, 9 – 22.

Spear, F.S., Peacock, S.M., 1989. Petrologic Determination of Metamorphic Pressure-Temperature-Time Paths. American Geophysical Union. 102p.

Spear, F.S., Kohn, M.J., Cheney, J.T., 1999. P-T paths from anatectic pelites. Contributions to Mineralogy and Petrology 134(1), 17–32.

Stacey, S., Kramers, J.D., 1975. Approximation of terrestrial lead isotope evolution by a two-stage model. Earth and Planetary Science Letters 26, 207–221.

Stampfli, G.M., Borel, G.D., 2004. The TRANSMED transects in space and time: constraints on the paleotectonic evolution of the Mediterranean domain. The TRANSMED Atlas. The Mediterranean region from crust to mantle. Springer Berlin Heidelberg, pp. 53 – 80.

Stampfli, G.M., von Raumer, J.F., Borel, G.D., 2002. Paleozoic evolution of pre-Variscan terranes: from Gondwana to the Variscan collision. Special Papers-Geological Society Of America pp. 263 – 280.

Stampfli, G.M., Von Raumer, J., Wilhem, C., 2011. The distribution of Gondwana derived terranes in the early Paleozoic. The Ordovician of the World 14, 567 – 574.

Stazhilo-Alekseev, K.F., Dovgal', Y.M., Chal'yan, M.A., Kochetkov, A.Y., 1973. O svyazi magmatizma s tektonikoi v Afganistane. Sovetskaya Geologiya 1973, 102-112.

Steiger R.H., Jäger, E., Subcommission on geochronology: convention on the use of decay constants in geo- and cosmochronology. Earth and Planetary Science Letters 36, 359–362.

Stöcklin, J., 1974. Possible ancient continental margins in Iran. The geology of continental margins. Springer Berlin Heidelberg, pp. 873 – 887.

Stöcklin, J., 1977. Structural correlation of the alpine ranges between Iran and Central Asia. Societe Geologique de France, Memoire Hors Serie 8, 333-353.

Sun, S.S., McDonough, W., 1989. Chemical and isotopic systematics of oceanic basalts: implications for mantle composition and processes. Geological Society, London, Special Publications 42 (1), 313 – 345.

Tajčmanová, L., Connolly, J.A.D., Cesare, B., 2009. A thermodynamic model for titanium and ferric iron solution in biotite. Journal of Metamorphic Geology 27, 153-64.

Tapponnier, P., Mattauer, M., Proust, F., Cassaigneau, C., 1981. Mesozoic ophiolites, sutures, and large-scale tectonic movements in Afghanistan. Earth and Planetary Science Letters 52 (2), 355 – 371.

Timmermann, H., Jamieson, R.A., Parrish, R.R., Culshaw, N.G., 2002. Coeval migmatites and granulites, Muskoka domain, south-western Grenville Province, Ontario. Canadian Journal of Earth Sciences 39(2), 239–258.

Tinkham, D.K., Zuluaga, C. Stowell, H., 2001. Metapelite phase equilibria modeling in MnNCKFMASH: the effect of variable Al_2O_3 and MgO/(MgO+FeO) on mineral stability. Geological Materials Research 3, 1–42.

Torsvik, T.H., Smethurst, M.A., Meert, J.G., Van der Voo, R., McKerrow, W.S., Brasier, M.D., Sturt, B.A., Walderhaug, H., 1996. Continental breakup and collision in the Neoproterozoic and Phanerozoic-A tale of Baltica and Laurentia. Earth-Science Reviews 40, 229 – 258.

Treloar, P.J., Izatt, C.N., 1993. Tectonics of the Himalayan collision between the Indian plate and the Afghan block: A synthesis. Geological Society, London, Special Publications 74(1), 69 – 87.

Treloar, P.J., Rex, D.C., 1990. Post-metamorphic cooling history of the Indian Plate crystalline thrust stack, Pakistan Himalaya. Journal of the Geological Society 147, 735-738.

Wallbrecher, E., 1974. Zur Geologie der Südflanke des afganischen Hindukush zwischen den Flüssen Salang und Parandeh. (PhD thesis) Freien Universität, Berlin, 150p.

Wang, A., Liu, Y.-C., 2012. Neoarchean (2.5 – 2.8 Ga) crustal growth of the North China Craton revealed by zircon Hf isotope: A synthesis. Geoscience Frontiers 3, 147 – 173.

Wang, Q., Pan, Y., Chen, N., Li, X., Chen, H., 2009. Proterozoic polymetamorphism in the Quanji Block, northwestern China: evidence from microtextures, garnet compositions and monazite CHIME ages. Journal of Asian Earth Sciences 34(5), 686 – 698.

Wang, X.C., Li, X.H., Li, Z.X., Li, Q.L., Tang, G.Q., Gao, Y.Y., Zhang, Q.R., Liu, Y., 2012. Episodic Precambrian crust growth: evidence from U – Pb ages and Hf – O isotopes of zircon in the Nanhua Basin, central South China. Precambrian Research 222, 386 – 403.

Waters, D.J., Lovegrove, D.P., 2002. Assessing the extent of disequilibrium and overstepping of prograde metamorphic reactions in metapelites from the Bushveld Complex aureole, South Africa. Journal of Metamorphic Geology 20(1), 135-149.

Wetherill, G.W., 1956. Discordant uranium-lead ages. Transactions American Geophysical Union 37, 320 – 326.

White, R.W., Powell, R., Holland, T.J.B., Worley, B.A., 2000. The effect of TiO_2 and Fe_2O_3 on metapelitic assemblages at greenschist and amphibolite facies conditions: mineral equilibria calculations in the system K_2O-FeO-MgO-Al_2O_3-SiO_2-H_2O-TiO_2-Fe_2O_3. Journal of Metamorphic Geology 18, 497-512.

White, R.W., Powell, R., Holland, T.J.B., 2001. Calculation of partial melting equilibria in the system Na_2O–CaO–K_2O–FeO–MgO–Al_2O_3–SiO_2–H_2O (NCKFMASH). Journal of Metamorphic Geology 19(2), 139-153.

White, R.W., Pomroy, N.E., Powell, R., 2005. An in situ metatexite–diatexite transition in upper amphibolite facies rocks from Broken Hill, Australia. Journal of Metamorphic Geology 23(7), 579-602.

White, R.W., Powell, R., Holland, T.J.B., 2007. Progress relating to calculation of partial melting equilibria for metapelites. Journal of Metamorphic Geology 25(5), 511-527.

Whitney, D.L., Evans, B.W., 2010. Abbreviations for names of rock-forming minerals. American Mineralogist 95, 185.

Wiedenbeck, M., Allé, P., Corfu, F., Griffin, W.L., Meier, M., Oberli, F., Von Quadt, A., Roddick, J.C., Spiegel, W., 1995. Three natural zircon standards for U–Th–Pb, Lu–Hf, trace elements and REE analyses. Geostandards Newsletter 19, 1–23.

Williams, I.S., 1998. U – Th – Pb geochronology by ion microprobe. In: McKibben, M.A., Shanks III, W.C., Ridley, W.I. (Eds.), Applications of microanalytical techniques to understanding mineralizing processes. Reviews in Economic Geology 7, pp. 1 – 35.

Wing, B.A., Ferry, J.M., Harrison, T.M., 2003. Prograde destruction and formation of mon- azite and allanite during contact and regional metamorphism of pelites: petrology and geochronology. Contributions to Mineralogy and Petrology 145 (2), 228 – 250.

Wittekindt, H., Weippert, D., 1973. Geologische Karte Von Zentral-und Suedafghanistan: Geological Map of Central and Southern Afghanistan, 1: 500,000. Bundesanstalt für Bodenforschung.

Wolfart, R., Wittekindt, H., 1980. Geology von Afghanistan. Beiträge Regionale Geologie Erde.

Wu, C.M., Zhang, J., Ren, L.D., 2004. Empirical garnet–biotite–plagioclase–quartz (GBPQ) geobarometry in medium-to high-grade metapelites. Journal of Petrology 45(9), 1907–1921.

Wu, C.M., Zhao, G., 2006. Recalibration of the garnet–muscovite (GM) geothermometer and the garnet–muscovite– plagioclase–quartz (GMPQ) geobarometer for metapelitic assemblages. Journal of Petrology 47, 2357-2368.

Xia, B., Zhang, L., Xia, Y., Bader, T., 2014. The tectonic evolution of the Tianshan Orogenic Belt: Evidence from U – Pb dating of detrital zircons from the Chinese southwestern Tianshan accretionary mélange. Gondwana Research 25 (4), 1627 – 1643.

Xiao, W., Windley, B.F., Allen, M.B., Han, C., 2013. Paleozoic multiple accretionary and collisional tectonics of the Chinese Tianshan orogenic collage. Gondwana Research 23 (4), 1316 – 1341.

Xu, B., Jian, P., Zheng, H., Zou, H., Zhang, L., Liu, D., 2005. U – Pb zircon geochronology and geochemistry of Neoproterozoic volcanic rocks in the Tarim Block of northwest Chi na: implications for the breakup of Rodinia supercontinent and Neoproterozoic glaciations. Precambrian Research 136 (2), 107 – 123.

Yang, P., Pattison, D., 2006. Genesis of monazite and Y zoning in garnet from the Black Hills, South Dakota. Lithos 88(1), 233-253.

Yang, Q.Y., Santosh, M., Tsunogae, T., 2014. First report of Paleoproterozoic incipient charnockite from the North China Craton: Implications for ultrahigh-temperature metasomatism. Precambrian Research 243, 168 – 180.

Zegers, T.E., De Keijzer, M., Passchier, C.W., White, S.H., 1998. The Mulgandinnah shear zone; an Archean crustal scale strike-slip zone, eastern Pilbara, Western Australia. Precambrian Research 88 (1), 233 – 247.

Zhang, C.L., Li, Z.X., Li, X.H., Yu, H.F., Ye, H.M., 2007. An early Paleoproterozoic high-K intrusive complex in southwestern Tarim Block, NW China: age, geochemistry, and tectonic implications. Gondwana Research 12 (1), 101 – 112.

Zhang, C.L., Li, Z.X., Li, X.H., Ye, H.M., 2009a. Neoproterozoic mafic dyke swarms at the northern margin of the Tarim Block, NW China: age, geochemistry, petrogenesis and tectonic implications. Journal of Asian Earth Sciences 35 (2), 167 – 179.

Zhang, C.L., Yang, D., Wang, H., Dong, Y., Ye, H., 2010. Neoproterozoic mafic dykes and basalts in the southern margin of Tarim, Northwest China: age, geochemistry and geodynamic implications. Acta Geologica Sinica English Edition 84 (3), 549 – 562.

Zhang, C.L., Yang, D.S., Wang, H.Y., Takahashi, Y., Ye, H.M., 2011. Neoproterozoic mafic- ultramafic layered intrusion in Qur- uqtagh of northeastern Tarim Block, NW China: two phases of mafic igneous activity with different mantle sources. Gondwana Research 19 (1), 177 – 190.

Zhang, C.L., Li, H.K., Santosh, M., Li, Z.X., Zou, H.B., Wang, H., Ye, H., 2012. Precambrian evolution and cratonization of the Tarim Block, NW China: Petrology, geochemistry, Nd-isotopes and U – Pb zircon geochronology from Archaean gabbro-TTG – potassic granite suite and Paleoproterozoic metamorphic belt. Journal of Asian Earth Sciences 47, 5 – 20.

Zhang, C.L., Zou, H.B., Li, H.K., Wang, H.Y., 2013. Tectonic framework and evolution of the Tarim Block in NW China. Gondwana Research 23 (4), 1306 – 1315.

Zhang, Z., Zhu, W., Shu, L., Su, J., Zheng, B., 2009b. Neoproterozoic ages of the Kuluketage diabase dyke swarm in Tarim, NW China, and its relationship to the breakup of Rodinia. Geological Magazine 146 (01), 150 – 154.

Zhao, G., Cawood, P.A., Wilde, S.A., Sun, M., 2002. Review of global 2.1 – 1.8 Ga orogens: implications for a pre-Rodinia super- continent. Earth-Science Reviews 59 (1), 125 – 162.

Zhao, G., Sun, M., Wilde, S.A., Li, S., 2003. Assembly, accretion and breakup of the Paleo- Mesoproterozoic Columbia Supercon- tinent: records in the North China Craton. Gondwana Research 6 (3), 417 – 434.

Zhao, G., Sun, M., Wilde, S.A., Li, S., 2004. A Paleo-Mesoproterozoic supercontinent: assembly, growth and breakup. Earth- Science Reviews 67 (1), 91 – 123.

Zhu, W., Zhang, Z., Shu, L., Lu, H., Su, J., Yang, W., 2008. SHRIMP U – Pb zircon geochronology of Neoproterozoic Korla mafic dykes in the northern Tarim Block, NW China: implications for the long-lasting breakup process of Rodinia. Journal of the Geological Society 165 (5), 887 – 890.

Zhu,W., Zheng, B., Shu, L., Ma, D., Wan, J., Zheng, D., Zhang,Z., Zhu, X., 2011. Geochemistry and SHRIMP U – Pb zircon geochronology of the Korla mafic dykes: constrains on the Neoproterozoic continental breakup in the Tarim Block, northwest China. Journal of Asian Earth Sciences 42 (5), 791 – 804.

Part VIII

Appendix

A   Sampling

Sampling of Precambrian basement rocks has been carried out from several localities in and around the city of Kabul over several field seasons. Additional sampling was also undertaken along the three major mountain passes (the Ghor Band, Salang, and Panjshir) that traverse the Western Hindu Kush, north from Kabul. The location of each of these sample localities are shown in Figures 9 and 10 of Part I, approximate GPS co-ordinates of the localities and the field season during which each locality has been visited is listed in Table A and the principal investigators for each field season shown in Table B. Below is presented a brief outline of each sample locality and the lithologies which were collected from each.

Table A: Table of the sample localities approximate GPS co-ordinates and the field season during which each were visited

#	Locality	GPS co-ordinates	Field Season							
			2006a	2006b	2007	2009	2011	2012a	2012b	2013
1	Khair Khana	34°35′45 N 69°06′30 E	x		x	x		x	x	x
2	Kabul Airport	34°35′00 N 69°13′15 E						x		x
3	Badam Bagh	34°33′15 N 69°06′15 E						x		
4	Bagh-e Bala	34°31′45 N 69°07′45 E		x		x		x		
5	T.V. Hill	34°31′15 N 69°09′15 E	x	x						
6	Sherdarwaza Hill	34°30′30 N 69°10′00 E					x			
7	Chehel Sotoon North	34°28′15 N 69°10′45 E	x					x		
8	Chehel Sotoon South	34°27′30 N 69°10′30 E			x					
9	North East Kabul	34°33′35 N 69°17′15 E						x		
10	North Kabul	34°38′45 N 69°05′30 E						x		
11	Bagram Road Quarry	34°46′00 N 69°13′45 E								x
12	Ghor Band Valley	35°05′45 N 69°10′45 E*	x					x		
13	Salang Valley	35°08′15 N 69°13′45 E*	x					x		
14	Lower Salang Batholith	35°11′30 N 69°13′00 E	x					x		
15	Upper Salang Batholith	35°17′45 N 69°03′45 E						x		
16	Panjshir Valley	35°09′30 N 69°17′15 E*			x			x		x

* - GPS co-ordinates for the mountain passes indicate the beginning of the pass, samples were collected at several localities along each pass

Table B: Principal field investigators for each of the field seasons

Principal Investigators	Field Season							
	2006a	2006b	2007	2009	2011	2012a	2012b	2013
Stephen Collett MGeol.						x		x
Prof. Shah Wali Faryad	x		x	x	x	x		x
Prof. Mike Petterson		x						
Prof. Amid Mohammad Mosazai	x		x	x			x	x

Kabul Block localities

Locality 1 – Khair Khana Mountains

The Khair Khana Mountains are located in the north west of the city of Kabul. The area was identified by Karapetov et al., (1981) as containing granulite-facies assemblages belonging to the possibly Archean

age Khair Khana Formation as xenolithic veins within migmatite and gneiss of the Sherdarwaza Formation. During our fieldwork we identified elongate bodies of orthopyroxene- and garnet-bearing felsic granulite and orthogneiss which were enclosed by strongly foliated garnet-absent migmatite. Small mafic lenses (< 25 cm across) containing orthopyroxene and/or clinopyroxene were identified within the felsic granulite. The migmatite also contains layers of amphibolite and quartzite. A large body of marble and calc-silicate cuts across the eastern flank of the mountain, granulite-facies assemblages are also identified within the marble by the presence of olivine. Additional samples were also collected from a highly deformed dyke of tonalitic composition and from largely undeformed mafic dykes.

FELSIC GRANULITE

Samples: *F74/6, af159c, af159d, af159h, af101, af102, af103, C20/13, C22/13, C30/13*

The felsic granulites are defined by the presence of orthopyroxene, which occurs as sub-idioblastic to xenomorphic grains with variable abundances depending on the amount of retrogression. The orthopyroxene is partially replaced by a fine grained intergrowth of biotite with quartz and rare amphibole. The rocks contain a granoblastic matrix of plagioclase, quartz, K-feldspar and opaque minerals (usually ilmenite but also some rare magnetite). Tabular biotite defines a weak foliation and accessory amounts of apatite, zircon, monazite, and in some instances graphite are also present. Three types of garnet are present in the felsic granulite (Fig. A) a very rare Mg-rich garnet occurs as small inclusions inside plagioclase feldspar, porphyroblastic grains include rounded inclusions of all the other phases include occasionally orthopyroxene, a third variety occurs as fine grained overgrowths which typically occur at contact between biotite or orthopyroxene with plagioclase but is also observed between the porphyroblastic garnet and plagioclase. The textural relations indicate that the rocks underwent a polymetamorphic history and they formed the backbone of the paper presented in Part II as well as significant contributions to the paper presented in Part IV. These samples have been extensively studied on both electron microprobe (E.M.P.A.) and scanning electron microprobe (S.E.M.), whole rock geochemistry was collected for selected samples and both U/Pb dating of zircon and U-Th-Pb dating of monazite has been undertaken.

Figure A: Composition of the different varieties of garnet found in felsic granulite at Khair Khana (Grt$_I$ - small inclusions in plagioclase; Grt$_{II}$ - porphyroblastic garnet; Grt$_{III}$ - fine grained overgrowths), mafic granulite at Khair Khana, and orthogneiss at Kabul Airport (Grt$_I$ - porphyroblastic garnet; Grt$_{II}$ - fine-grained overgrowths).
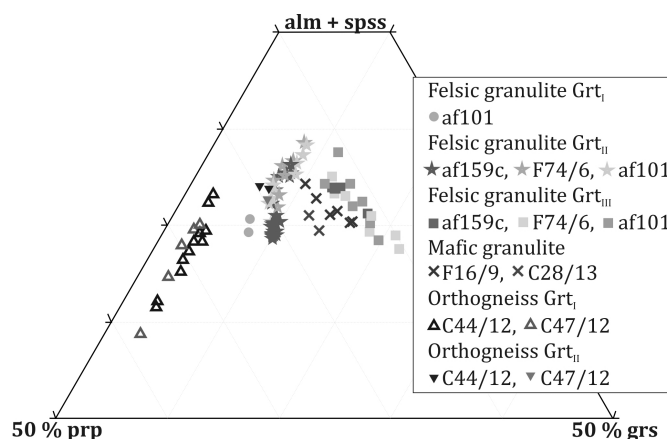
ORTHOGNEISS

Samples: *F71/6, F73/6, af159a, af159b, af159e, af159f, af159i, af159l, af159o, C18/13, C19/13, C21/13, C26/13*

The orthogneiss primarily differs from the felsic granulite by the absence of orthopyroxene. In general the samples tend to be slightly coarser grained and none of the small Mg-rich garnet in plagioclase was

identified. Another apparent difference is a relatively lower abundance of the fine grained garnet over-growths; however, in one sample (af159a) the fine grained overgrowth can clearly be seen overgrowing an older garnet grain. A clear jump to more Ca rich compositions can be seen for the garnet overgrowth. Samples of orthogneiss were studied as part of the articles presented in Parts II and IV. Two samples (af159a, af159b, labelled as AF-59a and AF-59b) have undergone U/Pb zircon dating and several of the samples were analysed using S.E.M. and E.M.P.A.

MAFIC GRANULITE

Samples: *af159m, F16/9, C28/13*

The samples of mafic granulite occur as thin lenses within the felsic granulite, granulite-facies condi-tions are recognised by the presence of ortho- or clinopyroxene; however, both are not present together. Coarse grained amphibole of pargasitic composition is common to both the orthopyroxene and the clinopyroxene bearing varieties. A fine grained more Al-rich, Ti-poor amphibole overgrows the coarse grained amphibole at contact with plagioclase (Fig. B). Quartz and biotite are both present but have re-latively low abundances, while accessory amounts of apatite, ilmenite, and magnetite are also present. Sample F16/9 (orthopyroxene-bearing) was studied extensively as part of the article presented in Part II, it differs from the other two samples owing to the presence of fine grained garnet which overgrows the othopyroxene and coarse-grained amphibole at contact with plagioclase. In some instances this fine grained is intergrown with ilmenite.

Figure B: Total Al against Ti in the two amphibole varieties in the mafic granulite. Amp_I is coarse grained granulite-facies amphibole, Amp_{II} is the fine grained overgrowths.
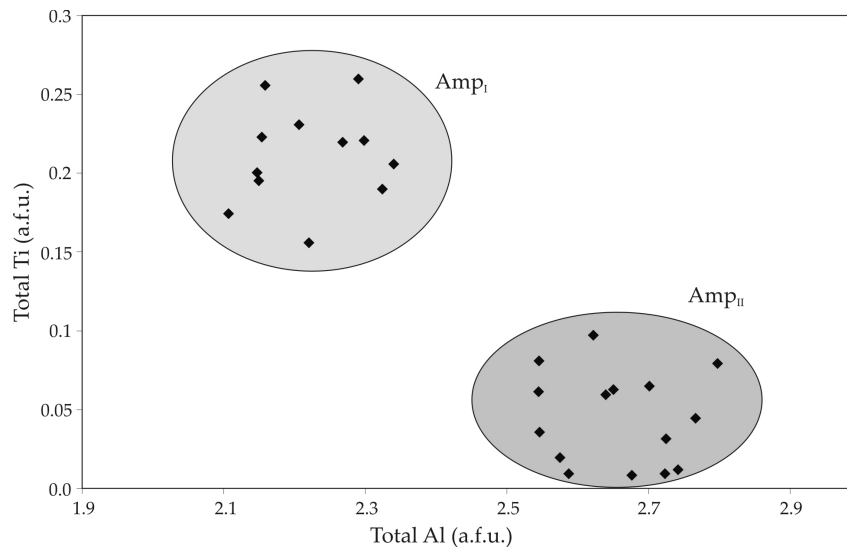
MARBLE / CALC-SILICATE

Samples: *F72/6, af159q, af159s, C8/12*

The marbles are calcite rich with subordinate dolomite, granulite-facies conditions are recognised within the marbles by the presence of olivine. All the samples additionally contain amphibole typically of edenitic to pargasitic composition. Sample af159q differs from the others by the occurrence of large diopside grains; in the other samples diopside is present only as an inclusion in other phases or as a fine-grained replacement around amphibole. Phlogopite is present in sample F72/6, af159s, and C8/12 as porphyroblastic flakes which contain exsolution lammelae of rutile. Additionally, sample C8/12 contains clusters of yellow coloured clino-humite. Apatite is present in all samples and minor amounts of titanite is also observed. Samples F72/6 (labelled as F15-9) and af159s (as F-6) were dated using

Ar/Ar technique on phlogopite as reported in Part IV. Samples F72/6 and C8/12 were also studied in detail as part of the article presented in Part II.

MIGMATITE

Samples: *F70/6, af159g, af159k, af159n, C2/12, C4/12, C5/12, C6/12*

Two varieties of migmatite are observed at Khair Khana a strongly foliated garnet absent variety *(F70/6, C2/12, C4/12, C5/12, C6/12)* consists of a quartz-feldspathic leucosome with minor apatite, the feldspars are both perthite and anti-perthite and some quartz grains exhibit myrmekitic textures. The foliation is typically dominated by biotite with variable amounts of amphibole depending on composition, increasing amounts of epidote and muscovite are observed in more retrogressed samples.

The second variety contains minor amounts of garnet, or clusters of biotite grains that appear to pseudomorph after garnet. They are typically finer grained than the other migmatite samples and display a weaker foliation. In addition plagioclase is partially replaced by scapolite and minor amounts of calcite is present as a replacement phase.

AMPHIBOLITE / AMPHIBOLE GNEISS

Samples: *C1/12, C3/12, C13/12, C24/13*

The amphibolite consists of medium grained crystalline assemblage of amphibole and plagioclase with minor quartz and opaque phases. The amphibole gneiss differs from the amphibolite by a significantly higher quartz abundance (and lower amphibole abundance) as well as minor amounts of biotite which define a weak foliation.

META-TONALITE

Samples: *C10/12, C29/13*

The meta-tonalite consists of a medium to coarse grained crystalline matrix of plagioclase and quartz with minor K-feldspar and apatite. Clinopyroxene occurs as highly fractured rounded grains which are replaced by fine grained greenish brown amphibole. Plagioclase is partially replaced by epidote and both epidote and amphibole are observed enclosing a magnetite grain.

Locality 2 – Kabul Airport

The Kabul Airport locality is located in the north of the city approximately 9 km east of the Khair Khana Mountains. On the geological map of Kabul by Bohannon (2010) this area is mapped as being comprised of a meta-igneous body of anorthositic to granodioritic composition. Our field investigations identified a garnet-bearing orthogneiss body in the lower slopes of the mountains overlain by garnet-absent paragneiss and migmatite. The paragneiss includes several thin (< 1m thick) lenses of quartzite and amphibolite. Both the orthogneiss and paragneiss are cut by numerous unmetamorphosed mafic dykes.

ORTHOGNEISS

Samples: *C44/12, C45/12, C46/12, C47/12, C1/13, C2/13, C3/13, C5/13, C7/13*

The orthogneiss is a medium to coarse grained garnet-biotite gneiss, foliation is discrete and defined primarily by biotite. The rocks consist of feldspars, quartz, biotite and garnet. The feldspars are both antiperthite, exhibiting exsolved alkali feldspar blobs within plagioclase and perthite with fine grained lamellae of plagioclase within K-feldspar. In addition to relic tabular grains of biotite with exsolution lamellae of rutile/ilmenite, fine grained biotite intergrown with sillimanite, quartz and plagioclase is

present. It usually forms after tabular biotite or garnet. Needles of sillimanite occur within garnet and partly rim grain boundary of plagioclase with quartz. Garnet forms as large often highly fractured porphyroblasts containing rounded inclusions of quartz and feldspar as well as small needles of sillimanite, a rare secondary garnet developed as fine grained mass develops adjacent to garnet porphyroblast rims. Alumino-silicate in the matrix is mostly sillimanite, but small kyanite grains were also observed. Monazite occurs as an inclusion in garnet, usually towards the garnet rim although rare grains also observed in the core, and within the matrix. Samples of orthogneiss have been studied extensively for mineral chemistry using both S.E.M. and E.M.P.A. analysis. Whole rock geochemistry has been carried out on selected samples (C44/12, C47/12, C3/13); U/Pb zircon dating was obtained for samples C1/13 and C5/13, and U-Th-Pb dating was undertaken on sample C44/12. The samples of orthogneiss figure prominently in two of the published articles (parts II and IV of the thesis).

Paragneiss / Migmatite

Samples: *C11/13, C12/13, C13/13, C15/13*

The samples of paragneiss / migmatite are quite varied and have often undergone strong retrogression to low-grade assemblages. The best preserved examples display a finer grained assemblage than in the orthogneiss consisting of plagioclase, K-Feldspar, quartz, biotite, muscovite, and rare epidote. The mica and epidote define a strong foliation that is continuous throughout the samples. Garnet is usually absent or very rare, fine grained clusters were observed in one sample. These samples have not been studied in detail but are reminiscent of other Sherdarwaza Formation lithologies and form part of the background knowledge of the region.

Locality 3 – Badam Bagh

Badam Bagh is an approximately 1.5 km^2 area of farmland located approximately 4.5 km south from the Khair Khana Mountains. A small number of samples were collected from the mountains located behind the farmland during the 2012 field excursions. These samples consist of garnet-muscovite and muscovite schists, impure marble, and amphibolite. On the geological maps of Karapetov et al. (1981) and Bohannon (2010) this area belongs to the Sherdarwaza Formation.

Garnet-muscovite schist

Samples: *C49/12, C50/12*

The Garnet-muscovite schist consists of garnet, muscovite, quartz, and opaque minerals. The muscovite defines a well developed underlose foliation that partially wraps around the garnet grains. The garnet is highly xenomorphic and poikiolitic, it is often strongly replaced primarily by chlorite; the inclusions are almost exclusively quartz and the largest grains are little more than 500 μm across. These samples haven't been studied in detail as part of this project and lack the high-grade assemblages seen elsewhere in the Sherdarwaza Formation.

Locality 4 – Bagh-e Bala

Bagh-e Bala is situated south east from the Badam Bagh locality and adjacent to the Kabul Intercontinental Hotel. The rocks at this locality are almost exclusively migmatite, typical of the Sherdarwaza Formation; these are garnet-absent and often retrogressed with muscovite and epidote along foliation. Only a small number of samples were collected from this locality during the 2009 and 2012 field excursions. Additionally, two samples from this locality were also collected by Prof. Mike Petterson during field excursions in 2006 that were studied as part of the authors Masters Dissertation.

MIGMATITE

Samples: *F12/9, F13/9, F14/9, C11/12, C12/12, (KB INT 1, KB INT 2)*

The samples of migmatite from Bagh-e Bala are typical for the Sherdarwaza Formation in that they contain a quartz-feldspathic leucosome, a strong foliation defined primarily by biotite with minor muscovite and epidote and are typically garnet absent (small accessory grains were observed in F14/9). Ar/Ar age dating has been carried out on biotite from samples F12/9 and F14/9 and of muscovite on sample F13/9. The results of which are presented in the article in Part IV. In addition U/Pb zircon dating was carried out on sample KB INT 1 as part of the authors masters project (Fig. C). While samples from Bagh-e Bala haven't been studied in detail they do provide useful insight into the overall regional geology.
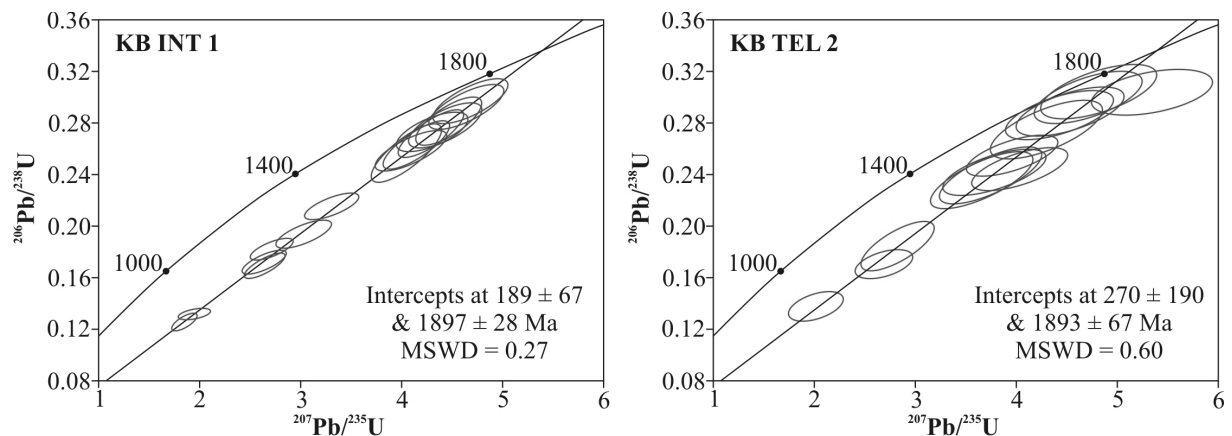

Figure C: U/Pb SHRIMP zircon dating for samples of migmatite from Bagh-e Bala (KB INT 1) and Television Hill (KB TEL 2).

Locality 5 – Television Hill

The Television Hill locality is located approximately 3 km south east from Bagh-e Bala and is so named because of the antennas located at the summit of the mountain. This area is mapped by Karapetov et al. (1981) as part of the Sherdarwaza Formation and consists of the characteristic, garnet-absent, migmatite and minor amphibolite. A small number of samples from this locality were collected by Prof. Faryad in 2006 and additional samples from this locality, collected in 2006 by Prof. Petterson, were studied as part of the author's Masters Dissertation.

MIGMATITE

Samples: *F107/6, F108/6, (KB TEL 1, KB TEL 2, KB TEL 3, KB TEL 4, KB TEL 5, KB TEL 6, KB TEL 7)*

The samples from the television hill locality are almost identical to those studied from Bagh-e Bala consisting of K-Feldspar, plagioclase, quartz, biotite, muscovite, epidote, and ilmenite. Accessory amounts of apatite and zircon are present and in rare instances also rutile. Whole rock geochemistry, both major oxides and trace elements were collected for samples KB TEL 1 - 7, and this was studied as part of the authors masters project (Fig. D). However, these samples were not studied in detail for this thesis.

Locality 6 – Sherdarwaza Hill

This locality is about 1.5 km south of Television Hill and is separated from it by the Kabul River. Samples from here belong to the Sherdarwaza Formation. Both garnet-bearing and garnet-absent migmatites
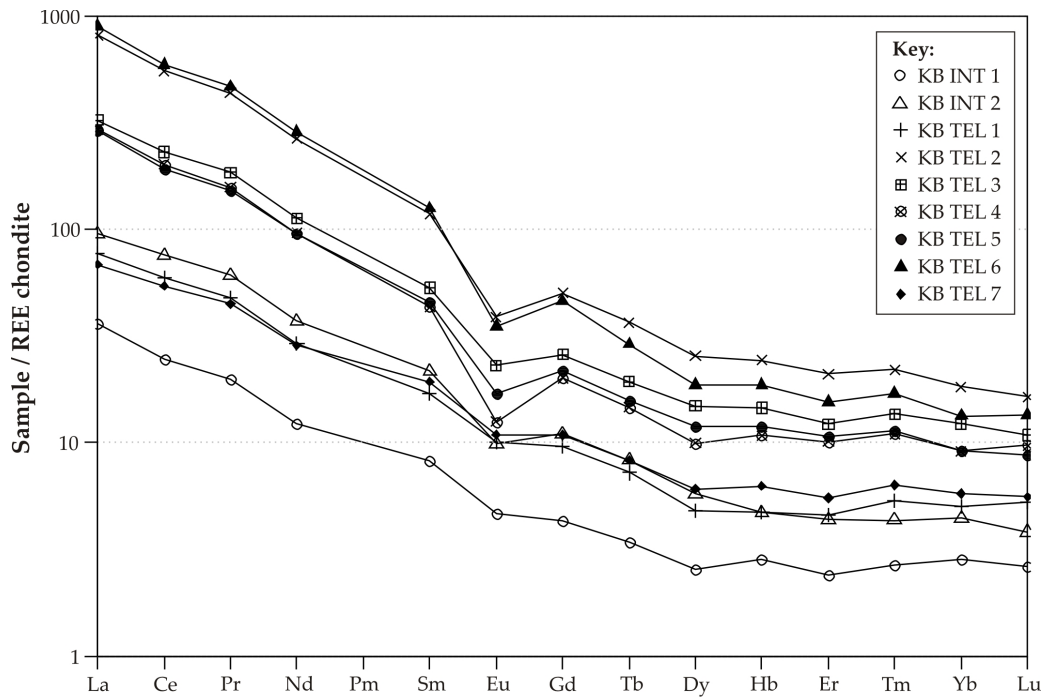
Figure D: REE geochemistry of migmatites from Television Hill and Bagh-e Bala normalised to chondritic values of Nakamura (1974).

were sampled here along with amphibolite.

MIGMATITE

Samples: *Afg 1/11, Afg 2/11, Afg 3/1, Afg 4/11*

Sample Afg 1/11 contains large garnet porphyroblasts that are partially wrapped by a continuous foliation of biotite and epidote. The sample still contains the quartz-feldspathic leucosome typical of Sherdarwaza migmatites. The garnet porphyroblasts are Ca-rich and display complex almost soap bubble like zoning (Fig. E). The sample has been studied extensively using S.E.M. and E.M.P.A. analysis and whole rock geochemical data was collected. However, the data did not form part of any of the presented articles. The other samples from this area are garnet-absent and are texturally similar to migmatite seen elsewhere.

Locality 7 – Chehel Sotoon North

The Chehel Sotoon North locality is around 3 km south from the Sherdarwaza Hill locality and marks the boundary between the Sherdarwaza Formation and the overlying Welayati Formation. On the geological map of Karapetov et al. (1981) a thin segment of the Kharog Formation crops out between the Sherdarwaza and Welayati Formations; however, this is not shown on the map of Bohannon (2010) or the cross-section of Andritzky (1967) and was interpreted as Welayati Formation in Collett and Faryad (2015, Part III of this report). A variety of lithologies were sampled here including both garnet-bearing and garnet-absent migmatite of the Sherdarwaza Formation, garnet-kyanite micaschist and amphibolite from the Welayati Formation and garnet-bearing amphibolite of uncertain affinity (see Parts III (Collett and Faryad, 2015) and IV (Faryad et al. 2015) for discussion). The samples from this locality were collected during the 2006 and 2012 field excursions.

Figure E: Compositional maps for Fe, Mg, Mn, Ca, Y, and P in garnet from migmatite at Sherdarwaza Hill
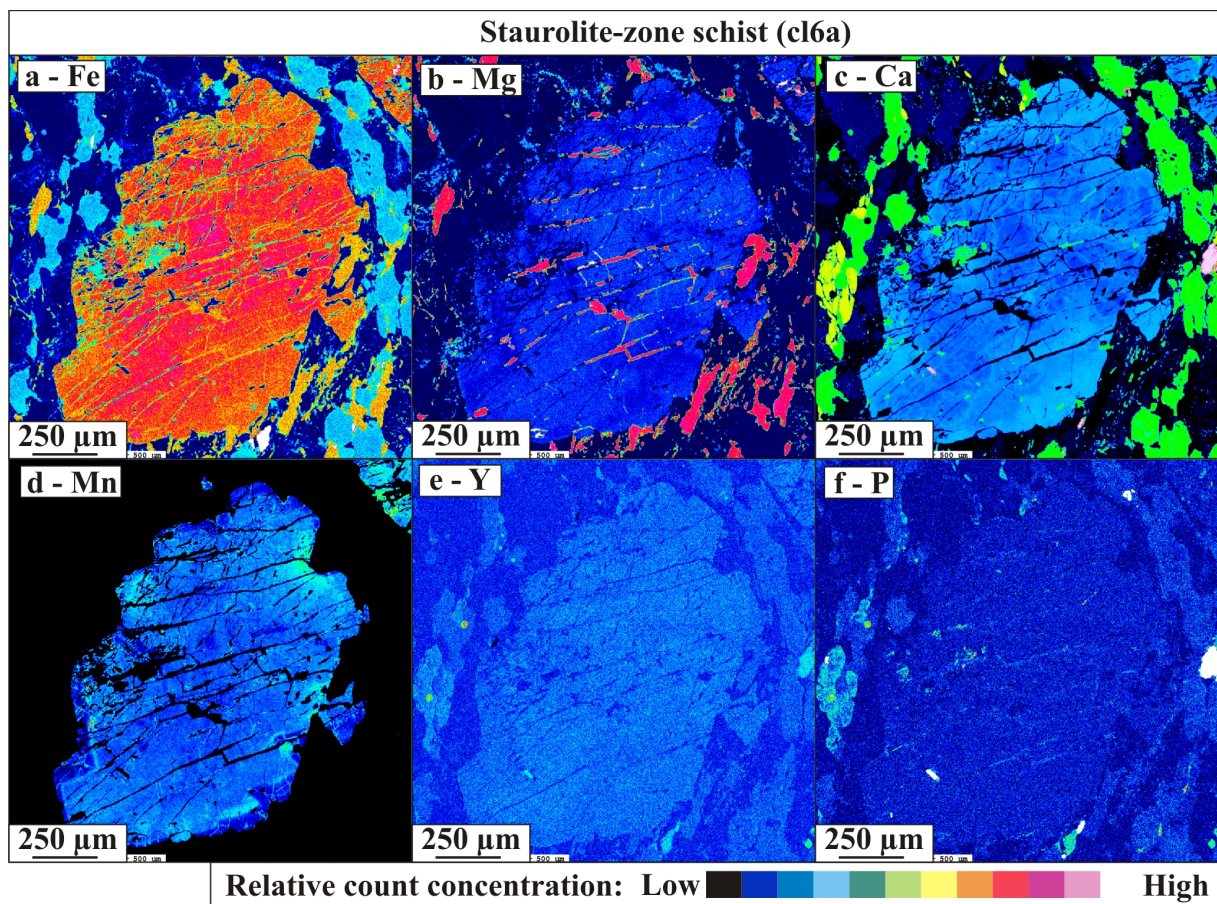
Migmatite

Samples: *C25/12, C26/12, C29/12, C32/12, C40/12*

Both garnet-bearing (C25/12, C32/12, C40/12) and garnet-absent (C26/12, C29/12) migmatite was sampled from the Chehel Sotoon locality. There is little textural difference between the two other than the presence of garnet porphyroblasts which are partially wrapped by the foliation. As with elsewhere the foliation is biotite dominated with increasing muscovite and epidote in more retrogressed samples. Plagioclase, K-feldspar, quartz, and accessory apatite and opaque minerals form the leucosome. Both perthitic and myrmekitic textures are observed. These samples come mostly from the northern section of the study area and their assemblages suggest that they belong to the Sherdarwaza Formation; although, this hasn't been tested and the samples were not studied in detail during this project.

Garnet-kyanite schist

Samples: *C31/12, C33/12, C36/12*

The matrix of the garnet-kyanite schist consists of quartz and plagioclase with accessory amounts of rutile, ilmenite, apatite and tourmaline. Garnet porphyroblasts are up to 6 mm in diameter, are sub-idiomorphic, and poikiolitic, inclusions are mostly micro grains of quartz but also include epidote and larger (up to 0.5 mm across) ilmenite and rutile. The inclusions have an alignment approximately perpendicular to the main foliation and show some evidence for rotation. Kyanite forms as elongate grains often mantled by muscovite, and can be seen to follow the foliation around garnet grains. Muscovite along with biotite defines the main foliation. Two varieties of biotite are observed, as elongate grains with the long axis parallel to the main foliation , and as tabular porphyroblasts seen to cut or overgrow the white mica. Plagioclase forms as highly irregular grains, which overgrows the main foliation and contains abundant inclusions of muscovite and minor quartz and epidote. Rutile is observed as both inclusions in garnet and within the matrix and is often intergrown with or enclosed by ilmenite. The samples have been extensively studied as part of the article presented in Part III. E.M.P.A. and S.E.M. mineral chemistry data was collected for each of the samples and whole rock geochemistry was collected for sample C33/12.

Garnet-absent amphibolite

Samples: *C28/12, C34/12, C35/12*

The garnet-absent amphibolite occurs as thin layers and lenses within the garnet-kyanite schist it is typically fine grained and strongly foliated. The assemblage is amphibole dominated with subordinate plagioclase, quartz and opaque phases. In places amphibole is partially replaced by chlorite and/or epidote. These samples were not studied in detail during this project.

Garnet-bearing amphibolite / amphibole gneiss

Samples: *F81/6, F82/6, F83/6, C38/12, C39/12*

The garnet-bearing samples are significantly coarser grained than the garnet-absent samples. The distinction between amphibolite and amphibole gneiss is made by the relative abundance of quartz and amphibole with the more quart-rich samples termed as gneiss. Garnet in the amphibolite is highly corroded and replaced in part by chlorite and occasionally calcite. It contains abundant inclusions of quartz and minor feldspar which show weak alignment. The amphibolite is highly crystalline and sub-granoblastic. In contrast to the amphibolite, the gneiss is rich in quartz and it is not clear if it represents a leucocratic variety in the amphibolite or represents a mixture of basaltic and sedimentary rocks. It consists of amphibole, garnet, plagioclase, biotite, and small, accessory amounts of epidote and ilmenite, respectively. One sample of amphibole gneiss (F82/6) was analysed for U/Pb dating in zircon and is described in Part IV.

Locality 8 – Chehel Sotoon South

The Chehel Sotoon South locality is just over 2 km south from the northern locality. The rocks here are universally classified as belonging to the Welayati Formation and consist of garnet-staurolite micaschist and garnet-bearing amphibolite. One sample each of quartz-rich amphibole gneiss and garnet-biotite gneiss were also collected at this locality. The samples were collected by Prof. Faryad during 2007 field excursions.

GARNET-STAUROLITE SCHIST

Samples: *cl4, cl5, cl6a, cl7*

The samples of garnet-staurolite schist are characterized by the presence of garnet and staurolite porphyroblasts wrapped by a continuous foliation defined by white mica and minor biotite. The matrix is dominated by quartz with accessory amounts of apatite, ilmenite, monazite, and zircon. Porphyroblasts of plagioclase and biotite are observed overgrowing the foliation. Epidote is present exclusively as an inclusion phase in garnet and replacing plagioclase. The staurolite grains are often poikiloblastic, with inclusions consisting almost exclusively of quartz and ilmenite and show little or no orientation. Garnet porphyroblasts are up to 5 mm in diameter and exhibit well defined textural core and rim relationships. The cores of the garnet grains are typically rich in inclusions of quartz, ilmenite, apatite, and epidote. The inclusions show orientation roughly perpendicular to the main foliation and a small rotational component. The main foliation is defined by elongate, tabular grains of muscovite and paragonite. As well as occurring within the foliation biotite is present as tabular porphyroblasts cross-cutting the main foliation and overgrowing muscovite. The plagioclase porphyroblasts occur as xenomorphous growths that contain inclusions of paragonite, muscovite, and quartz. Unlike the garnet porphyroblasts where the main foliation wraps around the porphyroblastic grains, the foliation is continuous either side of the plagioclase and biotite porphyroblasts. Kyanite is usually absent from these samples, but one sub-idiomorphic grain is observed in sample cl6a. The samples were extensively studied as part of the article in Part III and also age dating from this samples played an important role in Part IV. Samples cl5, cl6, and cl7 all underwent Ar/Ar dating of micas and sample cl7 additionally was analysed for U-Th-Pb in monazite.

GARNET AMPHIBOLITE / AMPHIBOLE GNEISS

Samples: *cl1, cl2, cl8, cl9*

The garnet amphibolite and amphibole gneiss from the southern locality is very similar both compositionally and texturally to those studied from the northern locality. The large amphibolite body that causes some confusion as to its relations in the geological map of Karapetov et al. (1981) is not marked at this locality. This could indicate that all of the amphibolite may belong to the Welayati Formation.

Locality 9 – North East Kabul

The north east Kabul locality is approximately 6.5 km east from the Kabul Airport locality on the outskirts of the city. Similar to the Kabul Airport locality, this area was also identified as meta-igneous rocks belonging to the Sherdarwaza Formation on the geological map of Bohannon (2010). Samples of garnet-absent biotite gneiss and amphibolite were collected from this locality during the 2012 field excursions.

Locality 10 – North Kabul

The North Kabul locality is also on the outskirts of the city around 4 km to the north of the Khair Khana locality; this is identified as Sherdarwaza Formation on the map of Bohannon (2010). Only two samples were collected here during the 2012 field excursions. One is a sample of garnet-absent amphibolite similar to other Sherdarwaza localities; the other is a calc-silicate which contains porphyroblastic zircon crystals of uncertain age.

CALC-SILICATE

Sample: *C23/12*

The calc-silicate sample is interesting owing to the presence of large zircon crystals. These were studied using CL imaging which reveals complex zoning patterns (Fig. F). In addition to zircon the samples also contain coarse-grained mesoperthite, calcite and fine grained clusters of amphibole.

Figure F: CL imaging of zircon from the calc-silicate sampled North of Kabul
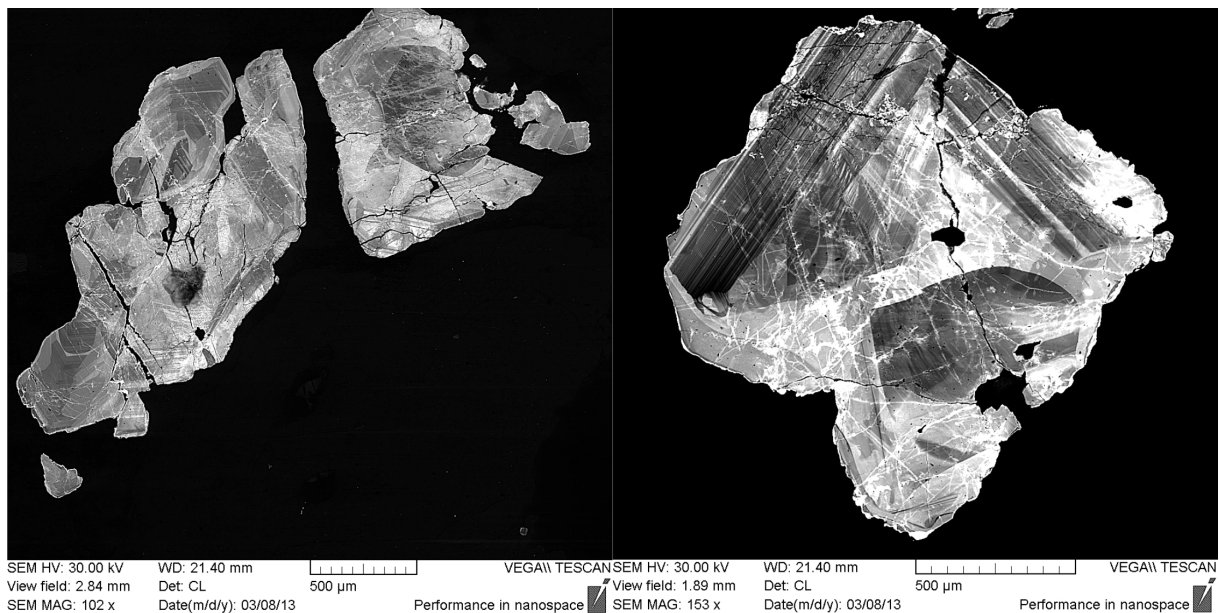
Locality 11 – Bagram Road Quarry

A small number of samples were collected during the 2013 fieldwork from a quarry site on the Bagram road around 25 km north from Kabul. The area is identified as Proterozoic basement on the maps of Kafarsky et al. (1975) and Bohannon and Turner (2007). The collected samples consisted of garnet-absent migmatite, and garnet-biotite gneiss; both of which are petrographically similar to other Sherdarwaza Formation rocks.

Hindu Kush Mountain Localities

Locality 12 – Ghor Band Valley

The Ghor Band valley follows the boundary between the Western Hindu Kush and the Paghman Terrane to the north west of the Kabul Block. Samples were collected at roadside cuttings along the mountain pass during 2006 and 2012 field excursions. These samples consist of micaschist, phyllite, migmatite.

On the geological map of Kafarsky et al., (1975) the migmatite is assigned a Proterozoic age, while the micaschist and phyllite have Early Paelozoic ages.

The migmatite comes from nearby to the contact between the Proterozoic and Paleozoic basement in the Ghorband Valley. Relatively massif white colour migmatite forms a thin (2–5 m) and about 200 m long crest striking parallel to the Panjshir fault zone (SW–NE). It consists of K-feldspar, quartz, plagioclase, sillimanite and small amounts of garnet and accessory biotite. Sillimanite defines the foliation in the rocks. Backscatter images show that sillimanite together with K-feldspar forms thin bands in quartz aggregate, suggesting dehydration melting of former muscovite. K-feldspar encloses plagioclase. Garnet has inclusions of quartz and sillimanite. It contains accessory muscovite, replacing K-feldspar.

The Paleozoic phyllitic rocks are usually fine-grained and some may contain small garnet, biotite and in some case also staurolite. Garnet contains inclusions of quartz, ilmenite and, rarely, staurolite. The selected two mica-schist samples from the Ghorband Valley contain garnet, muscovite, biotite, staurolite and plagioclase. Some large garnet porphyroblasts may have two different inclusion patterns and their backscatter images indicate that they represent two generations of garnet growth. Garnet (I) has irregular shapes and its boundary with garnet (II) is followed by opaque minerals. Staurolite crystals enclose small grains of garnet. No garnet was found in amphibolite and amphibole gneisses in the study area.

Locality 13 – Salang Valley

The Salang valley traverses north through the Western Hindu Kush from the tip of the Kabul Block. On the geological maps of Kafarsky et al. (1975) and Bohannon and Turner (2007) the area consists of Proterozoic gneiss and migmatite and Early Paleozoic meta-sediments. The lower reaches of the pass is intruded by granitoid bodies of Cretaceous age (Lower Salang Batholith) while Triassic granite (Upper Salang Batholith) intrudes the Paleozoic rocks higher up the pass. Samples of migmatite and phyllite were collected from the Salang valley during 2006a, 2007, and 2012a field excursions.

Locality 14 – Lower Salang Batholith

The Lower Salang Batholith is a small granitoid body of Cretaceous age with an Eocene metamorphic overprint. Samples of garnet-bearing meta-granite were collected here during the 2006a and 2012a field excursions. The rocks from the Lower Salang Batholith show weak foliation in the central part of bodies, but strong foliation at contact with surrounding phyllites. The foliation strikes SW–NE almost vertical and parallel to the thrust faults of the Panjshir and Ghor Band valleys. These rocks preserve igneous textures with zoned plagioclase and K-feldspar porphyroclasts, but they also show various degrees of recrystallization and deformation. In addition to garnet porphyroblasts, metamorphic minerals are biotite, titanite and epidote. Biotite along with quartz aggregates defines the foliation in this sample. Garnet crystals contain inclusions of biotite, quartz, plagioclase and apatite. Some large plagioclase grains exhibit oscillatory zoning that is visible in back scattered electron (BSE) images with anorthite-rich cores. Accessory allanite, rimmed by epidote, is also present. The metagranite contains white mica in addition to garnet and biotite and shows no foliation. The sample exhibits a low-degree of recrystallization with the exception of garnet grains that form at contact with biotite. Some mafic varieties may contain brown hornblende which is replaced or rimmed by actinolite. If the rock is foliated, the foliation is defined by biotite, white mica and aggregates of quartz.

Locality 15 – Upper Salang Batholith

The Upper Salang Batholith occurs 20 km north of the Lower Salang Batholith its surface expression is considerably larger and it is of Triassic age with minimal metamorphic overprint. Two samples of granite were collected here during the 2012a field excursion along with a mafic xenolith. In contrast to the South Salang batholith, the granite sampled here shows only brittle deformation with new chlorite, prehnite and white mica.

Locality 16 – Panjshir Valley

The Panjshir Valley is the easternmost of the three Hindu Kush mountain passes at the northern juncture of the Kabul Block. The Panjshir valley initially passes through Proterozoic gneiss and migmatite belonging to the Nuristan Block before following the Herat-Panjshir Suture Zone to the north east of the Kabul Block. Meta-granitoid of apparent Proterozoic basement affinity was sampled here along with a mafic granulite-facies xenolith of uncertain age during 2007 field excursions. the Metagranitoids are strongly foliated with characteristic augen texture that is represented by porphyroclasts of feldspar in a fine-grained matrix. These rocks are mostly free of garnet, but contain biotite and hornblende (Table 1), depending on their composition. Sample af170 contains plagioclase porphyroclasts which are surrounded by a medium-grained foliated matrix, consisting of quartz, plagioclase, biotite, hornblende and titanite. Sample af168a consists of plagioclase and biotite with porphyroblasts of garnet and allanite. Both garnet and allanite contain inclusions of biotite, apatite and garnet in addition to quartz.

The mafic xenolith sample (af168b) contains amphibole, orthopyroxene, plagioclase, quartz, biotite, and ilmenite. Both prograde and retrograde reactions can be observed in this sample, prograde is preserved by the appearance of hornblende as inclusions within orthopyroxene, and the retrograde by the development of cummingtonite coronae between grains of hornblende and orthopyroxene. The sample has a decussate granoblastic texture defined by the tabular nature of the biotite as well as a slight elongation of the fairly irregular hornblende and orthopyroxene. Ilmenite occurs both within the main assemblage and as inclusions occurring within both hornblende and orthopyroxene.

B   Analytical Techniques

Various different analytical techniques have been employed in order to fulfil the project objectives. The principal analytical methods are summarised in Table C.

Table C: Table of the different analytical methods applied to each of the samples

Sample #	Lithology	Locality	Geochemistry		Mineral Chemistry		Geochronology		
			Major Oxides	Trace + REE	S.E.M.	E.M.P.A.	U/Pb Zircon	Ar/Ar Mica	U-Th-Pb Monazite
F70/6	Migmatite	1	x	x		x*	x		
F72/6	Marble	1			x			x	
F74/6	Felsic Granulite	1			x				
F82/6	Amphibole Gneiss	7	x	x		x*	x		
af159a	Orthogneiss	1			x	x*	x		
af159b	Orthogneiss	1			x		x		
af159c	Felsic Granulite	1	x	x	x				
af159d	Felsic Granulite	1			x				
af159f	Orthogneiss	1			x				
af159g	Migmatite	1			x				
af159k	Migmatite	1			x				
af159m	Mafic Granulite	1	x	x	x	x*			
af159n	Migmatite	1	x		x				
af159q	Marble	1			x	x*			
af159s	Marble	1			x	x*		x	
cl1	Amphibolite	8				x*			
cl4	Grt-St Schist	8				x*			
cl5	Grt-St Schist	8				x*		x	
cl6a	Grt-St Schist	8	x		x	x		x	
cl7	Grt-St Schist	8	x		x	x*		x	x
cl8	Amphibolite	8			x	x*			
cl9	Amphibolite	8				x*			
F12/9	Migmatite	4						x	
F13/9	Migmatite	4						x	
F14/9	Migmatite	4				x*		x	
F16/9	Mafic Granulite	1			x				
afg 1/11	Migmatite	6	x		x	x			
C8/12	Marble	1			x				
C10/12	Meta-tonalite	1	x		x				
C23/12	Calc-silicate	10			x				
C24/12	Amphibolite	10	x	x					
C31/12	Grt-Ky Schist	7			x				
C32/12	Migmatite	7	x						
C33/12	Grt-Ky Schist	7	x		x	x			
C36/12	Grt-Ky Schist	7			x				
C38/12	Amphibolite	7	x						
C40/12	Migmatite	7	x						
C44/12	Orthogneiss	2	x	x	x	x*			x
C47/12	Orthogneiss	2	x	x	x				
af101	Felsic Granulite	1			x		x		x
af102	Felsic Granulite	1	x	x	x				x
af103	Felsic Granulite	1			x				
C1/13	Orthogneiss	2				x*	x		
C3/13	Orthogneiss	2	x	x	x	x*			
C5/13	Orthogneiss	2				x*	x		
C28/13	Mafic Granulite	1			x				
C30/13	Felsic Granulite	1			x	x*			

* EPMA analysis performed by the project supervisor

Whole-rock geochemistry

The whole rock geochemistry was undertaken at the Geological Laboratory at Charles University in Prague. Major elements were analysed by wet chemical analyses and trace elements were determined using a modified total digestion in mineral acids (HF + HClO$_4$) and borate fusion (Na2CO3 + Na2B4O7) followed by conventional solution nebulisation of ICP-MS Thermo X-Series II. The analytical precision, calculated as one relative standard deviation RSD, ranged from 0.5 to 5 % for most elements. The QA/QC was controlled using the AGV-2 and BCR-2 (USGS) reference materials.

Table D: Whole rock geochemical data

Oxide Weight %	F70-6	F75/6	F82-6	af159c	af159m	af159n	cl6a	cl7	afg 1-11	C10-12	C26-12	C32-12	C33-12	C38-12	C40-12	C44-12	C47-12	af103	C3-13
SiO2	70.99	48.52	71.03	59.67	47.76	73.54	58.42	61.48	57.38	67.42	47.92	72.28	59.24	51.86	66.58	67.96	66.18	66.62	72.86
TiO2	0.34	2.64	0.53	0.66	0.53	0.58	0.52	0.69	0.65	0.08	2.96	0.40	0.87	1.06	0.74	0.52	0.87	0.49	0.28
Al2O3	13.72	13.07	11.38	18.49	16.69	11.63	19.54	18.39	19.58	15.65	11.71	12.14	21.74	14.74	13.56	14.95	16.16	15.33	13.07
Fe2O3		4.08		1.04	2.74	1.37	2.35	2.13	3.36	1.28	4.52	1.38	2.62	3.71	2.14	1.67	1.23	2.42	1.41
FeO	2.48	12.29	6.58	5.48	5.54	2.99	7.17	5.84	3.51	0.99	13.41	4.07	5.79	9.58	5.22	4.06	3.77	2.98	2.33
MnO	0.03	0.20	0.11	0.10	0.14	0.07	0.07	0.07	0.25	0.05	0.24	0.13	0.08	0.15	0.06	0.09	0.06	0.09	0.06
MgO	0.91	5.34	2.42	2.07	8.68	1.41	3.19	3.06	0.92	1.84	4.89	0.22	1.78	6.58	2.35	1.86	2.16	1.45	1.14
CaO	1.77	9.77	4.85	4.26	12.65	2.37	0.92	0.73	6.32	6.21	8.98	1.67	1.96	7.71	1.69	1.58	2.23	2.88	1.04
Na2O	3.64	2.07	1.60	3.08	2.93	2.62	0.98	0.93	4.48	4.33	2.56	1.69	0.83	1.72	2.92	2.23	2.74	2.52	1.76
K2O	5.28	0.55	0.64	3.32	0.54	2.24	3.53	3.65	1.56	1.17	0.47	4.96	3.09	0.13	2.28	3.34	2.67	3.76	4.81
P2O5	0.09	0.29	0.14	0.27	0.05	0.04	0.09	0.17	0.16	0.06	0.31	0.08	0.16	0.13	0.21	0.08	0.06	0.14	0.06
Total	99.25	98.82	99.28	98.44	98.25	98.86	96.78	97.14	98.17	99.08	97.97	99.02	98.16	97.37	97.75	98.34	98.13	98.68	98.82
ppm																			
Rb	165		21.3	107.63	7.9						12.2					105.37	96.3	118.87	112.07
Sr	215		31.4	365.43	141.8						145.0					234.5	331.8	344.5	242.7
Zr	189.4		233.7	187.45	37.1						234.0					202.3	212.1	191.0	193.0
Ba	1190.3		231.4	1324.30	435						153					1089.5	868	1611.4	1894.7
Y	13.3		23.2	12.79	10.8						42.1					28.85	17.2	14.6	19.07
Nb	11		9.6	8.64	1.7						15.7					12.3	8.0	9.3	6.5
La	51.3		29.7	33.46	3.11						18.87					52.50	37.48	35.08	39.63
Ce	103.8		62.9	52.17	7.45						44.73					94.29	67.97	58.88	73.61
Pr	11.95		7.15	5.23	1.00						5.85					10.19	6.84	5.90	7.92
Nd	42.3		29.1	19.90	4.77						28.38					36.66	25.06	20.94	29.06
Sm	8		6	3.13	1.43						7.46					6.27	4.41	3.34	5.16
Eu	1.02		0.94	1.23	0.66						2.14					1.61	1.77	1.32	1.34
Gd	5.08		4.32	3.41	1.70						8.31					6.41	4.85	3.26	5.09
Tb	0.73		0.75	0.40	0.30						1.31					0.90	0.62	0.41	0.64
Dy	3.18		3.71	2.11	2.19						8.49					5.46	3.64	2.39	3.57
Ho	0.48		0.71	0.50	0.44						1.68					1.03	0.65	0.52	0.69
Er	1.04		2.34	1.75	1.32						5.08					3.12	1.99	1.81	2.17
Tm	0.13		0.41	0.23	0.17						0.69					0.41	0.27	0.29	0.30
Yb	0.83		3.2	2.04	1.26						4.68					2.78	1.74	2.18	2.08
Lu	0.13		0.54	0.36	0.17						0.64					0.39	0.24	0.35	0.32
Pb	10.9		0.8	67.23	4.44						1.83					53.50	25.16	78.42	74.06
Th	31.3		15.2	4.10	0.72						3.55					18.32	6.70	4.97	13.95
U	3.2		2.6	0.80	0.25						0.68					1.86	0.69	0.88	1.43

Mineral chemistry

Mineral chemistry data was acquired using a scanning electron microscope (S.E.M.) fitted with an energy-dispersive X-ray spectroscopy (EDX) analyser at the Institute of Petrology and Structural Geology at Charles University in Prague. High precision data was acquired using electron micro probe analyser (EMPA) at the Institute of Mineralogy and Crystal Chemistry, University of Stuttgart and the Institute of Earth Sciences of the University of Graz. The microprobe at Stuttgart is equipped with four wavelength-dispersive spectrometers during analysis the following standards were used: pyrope (Si, Al, Mg), andradite (Ca, Fe), jadeite (Na), spessartine (Mn), K-silicate glass (K), Ba-silicate glass (Ba), NaCl (Cl), as well as natural rutile (Ti) and topaz (F). The operating voltage was 15 kV using a beam current between 10 and 15 nA, and the beam was focused to a 1- to 2-μm diameter except for mica, for which an 8- to 10-μm beam was used. Analyses at Stuttgart was undertaken purely by the project supervisor. Data collection in Graz was carried out by both the research student and the project supervisor. The microprobe in Graz is equipped with wavelength- and energy-dispersive spectrometers. Standards were pyrope (Mg, Al), adularia (K), rutile (Ti), tephroite (Mn), jadeite (Na, Si), and andradite (Fe, Ca). Na and F were measured with a Microspec wavelength-dispersive spectrometer, and operating conditions were 15 kV and 10 or 15 nA, with 20 s counting time on peak and 10 s on each background.

Geochronological dating

U/Pb Zircon

U-Pb zircon geochronological analyses were performed at the SIMS SHRIMP-II facility at the Centre of Isotopic Research (CIR) in St. Petersburg, Russia. The results were obtained with a secondary electron multiplier in peak-jumping mode following the procedure described by Williams (1998) and adapted for CIR (e.g. Schuth et al., 2012). Individual corrected ratios and ages are reported with $1y$ analytical errors (68% confidence), as are the error ellipses presented in the concordia diagrams.

Ar/Ar Mica

Ar-Ar analyses were performed by measuring the $^{40}Ar^*/^{39}Ar$ isotopic ratio of mica aggregates at the Central European Ar-Laboratory (CEAL) in Bratislava, equipped with VG 5400 Noble Gas Mass Spectrometer and special own built Ar gas extraction line. Parts of samples were analysed at Lund University $^{40}Ar/^{39}Ar$ Geochronology Laboratory. It is equipped with a Micromass 5400 Gas Source MS with custom designed UHV gas metal extraction line and a New-Wave Dual-Lase system – CO_2 and UV Laser. Step-wise progressive outgassing of the sample was done mostly in 8–10 temperature steps from 610 to 1250 °C.

U-Th-Pb Monazite

Chemical composition of monazite was investigated using a CAMECA SX100 electron microprobe in the wavelength-dispersion mode in Laboratory of the Masaryk University and at University of Salzburg. Operating conditions included an accelerating voltage of 15 kV, a beam current of 120 nA, and a beam diameter of 3 μm. Peak counting times vary from 20 to 220 s in order to optimise detection limits. Uranium was determined on the U Mβ line (counting time 80 s, detection limit 270 ppm), Th on the Th Mα line (counting time 60 s, detection limit 280 ppm) and Pb on the Pb Mα line (counting time

220 s, detection limit 150 ppm). Synthetic and natural phases (U – metallic U, Pb – vanadinite, Th – $CaTh(PO_4)2$, P – $LaPO_4$, Y – YAG, La – $LaPO_4$, Ce – $CePO_4$, Pr – $PrPO_4$, Nd – $NdPO_4$, Sm – $SmPO_4$, Eu - $EuPO_4$, Gd – $GdPO_4$, Dy – $DyPO_4$, Er – YErAG, Al – sanidine, Si – sanidine, Ca – $CaTh(PO_4)_2$, Fe – andradite, S – $BaSO_4$, Sr – $SrSO_4$) were used as standards. Data was reduced using the PAP matrix correction routine (Pouchou and Pichoir, 1985). Overlapping of peaks and background positions were carefully tested and chosen using detailed WDS angle scans on natural and synthetic REE-phases. The background model on $PbM\alpha$ according to Jercinovic and Williams (2005) using exponential interpolation was chosen. Concentrations of Pb were additionally manually corrected for $YL\gamma_2$, $ThM\zeta_1$ and $ThM\zeta_2$ overlap on $PbM\alpha$ and concentrations of U were corrected for overlapping with $ThM\gamma$. The concentration of Si (and Eu) was calculated by empirical correction for the interference of Nd (Dy respectively) on $SiK\alpha$ ($EuL\beta$ respectively). The monazite age was calculated using the method of Montel et al. (1996). Three monazite age-standards of known age (498 Ma, 868 Ma and 1023 Ma) were measured together with studied samples.

C   Pseudosection modelling

A big part of resolving the metamorphic history of the rocks has invoked pseudosection modelling. A pseudosection, alternatively known as an equilibrium phase diagram, is a type of phase diagram that shows the relative of stability of different equilibrium mineral assemblages over a range of P-T conditions for a single bulk-rock composition. Pseudosections are very useful tool in understanding the behaviour of rocks within a metamorphic system. Many assemblages have restricted stability fields for a set composition and it is therefore possible to constrain P-T limits. Univariant reaction lines are also calculated that can be related back to textural relations to define a prograde or retrograde evolution. However, there are some limitations when it comes to pseudosection modelling that are important to understand. A key assumption made when calculating for a fixed-bulk composition is that the system is in total equilibrium. This is rarely a valid assumption for crustal rocks, minerals often preserve compositional zoning reflecting different stages of crystallisation additionally relicts of several different equilibria may be preserved within the same rock. Furthermore, rocks are often heterogeneous and a bulk rock composition may not be representative of thin-section scale observations. Therefore any calculated pseudosection must be treated with a certain amount of caution and checked against other geothermobarometric methods (conventional thermobarometry) and an understanding of petrological essentials.

The vast majority of pseudosections produced during this study were calculated using the Perple_X software package (available at: http://www.perplex.ethz.ch/). Perple_X is a Gibbs free energy minimiser, which calculates the assemblage with the lowest Gibbs free energy at different P-T conditions. This data is plotted on a Cartesian grid which and is typically refined over several iterations. The position of univariant reactions are drawn around the changes in the assemblage with the lowest Gibbs free energy. The accuracy of the diagram is therefore constrained in part by the resolution of the Cartesian grid.

Calculations in Perple_X rely on two principle datasets, a thermodynamic database that gives properties of a wide range of end-members (both mineral, liquid, and melt) and activity models that describe how the energies of the end-members contribute to the energies of intermediate compositions. Several different thermodynamic databases exist but the most comprehensive and widely used is the database of Holland and Powell. The 2003 version of the dataset (Perple_X file: hp04ver.dat) has been used for most of the pseudosection calculations. A newer version of the dataset, published in 2011 (filename hp11ver.dat), is available; however, at the time the calculations were being carried this dataset had not been rigorously tested and most of the activity models were still calibrated with the older dataset. The big advantage of the Perple_X software package is the sheer number of activity models available for use in the calculations (see Perple_x file: solution_models.dat). It is important however when choosing activity models to consider the compositions and P-T conditions that it has been calibrated for and which other models it is designed to work with. As a result there is no one clear set of activity models that are applicable to every sample. However, rough guidelines from the calculations are provided below:

- Biotite: High Ti contents - Bio(TCC); normal Ti content - TiBio(WPH).

- Plagioclase: Low-grade conditions (up to 650 °C) - Pl(h); High-grade conditions - feldspar_B

- K-Feldspar: Low-grade conditions (< 500 °C) - Kf; High-grade conditions - San

- Garnet: Basic model - Gt(HP); O2 considered in the model system - Gt(WPH); Modelling with SGH mica model - Gt(WPPH)

- White mica: Basic model - Mica(CHA); Considering Ca and Fe^{3+} end-members - Mica(SGH)

- Amphibole: Basic calcium amphibole model - Ca-Amph(D); Complex clino-amphibole model: cAmph(DP2); Complex ortho-amphibole model - oAmph(DP2)

- Pyroxene: Orthopyroxene - Opx(HP); Clinopyroxene - Cpx(HP)

- Olivine: O(HP)

- Chlorite: Chl(HP)

- Cordierite: hCrd

- Ilmenite: Ilm(WPH)

- Chloritoid: Ctd(HP); if considering SGH mica model - Ctd(SGH)

- Epidote: Ep(HP)

- Melt: melt(HP)

Pure end-member phases such as quartz, rutile, and alumino-silicate do not require an activity model for their calculation.

D   Curriculum Vitae

Name:

Stephen Paul Collett

Date of Birth:

21st August 1989

Nationality:

British

Home Address:

Sudoměřská1096/28

130 00 Praha 3 - Žižkov

Czech Republic

Work Address:

Institute of Petrology and Structural Geology

Faculty of Science, Charles University

Albertov 6

128 43 Praha 2

Czech Republic

Telephone:

+420 775485263 (CZE) / +44 7960611886 (GBR)

Email:

colletts@natur.cuni.cz / scollett311@gmail.com

Education:

- 2000 - 2007 Aylesbury Grammar School, Buckinghamshire, United Kingdom

    - 2005: 12 GCSE's (A*-C) including: Mathematics, English, Physics, Chemistry, Biology, French
    - 2006: 4 AS-Levels (A-C) in Mathematics, Physics, Chemistry, Ancient History
    - 2007: 3 A-Levels (A-C) in Mathematics, Physics, Ancient History

- 2007 - 2011 Department of Geology, University of Leicester, United Kingdom

    - Master of Geology (Upper second class honours degree)
    - Dissertation title: The Himalayan Syntaxes: A review and analysis of the literature on models for the formation of the Nanga Parbat and Namche Barwa syntaxes
    - Thesis: Crustal Evolution in the Palaeo Proterozoic of Afghanistan: Insights from the Sherdawaza Gneisses of the Kabul Block

- 2011 - Present Institute of Petrology and Structural Geology, Faculty of Science, Charles University in Prague, Czech Republic

    - PhD. study under the supervision of Prof. Ing. Shah Wali Faryad, CSc.
    - Thesis: Metamorphism and geodynamics of the Proterozoic Kabul Block: Preservation and modification of crustal fragments within an orogenic zone

Publications:

- Faryad, S. W., **Collett, S.**, Petterson, M., & Sergeev, S. A. (2013). Magmatism and metamorphism linked to the accretion of continental blocks south of the Hindu Kush, Afghanistan. Lithos, 175, 302-314.

- Faryad, S. W., Jedlicka, R., & **Collett, S.** (2013). Eclogite facies rocks of the Monotonous unit, clue to Variscan suture in the Moldanubian Zone (Bohemian Massif). Lithos, 179, 353-363.

- **Collett, S.**, Faryad, S. W., & Mosazai, A. M. (2015). Polymetamorphic evolution of the granulite-facies Paleoproterozoic basement of the Kabul Block, Afghanistan. Mineralogy and Petrology. doi:10.1007/s00710-015-0371-9

- Faryad, S. W., **Collett, S.**, Finger, F., Sergeev, S. A., Čopjaková, R., & Siman, P. (2015). The Kabul Block (Afghanistan), a segment of the Columbia Supercontinent, with a Neoproterozoic metamorphic overprint. Gondwana Research. doi:10.1016/j.gr.2015.02.019

- **Collett, S.**, & Faryad, S. W. (2015). Pressure-temperature evolution of Neoproterozoic metamorphism in the Welayati Formation (Kabul Block), Afghanistan. Journal of Asian Earth Sciences. doi:10.1016/j.jseaes.2015.06.002

Abstracts:

- **Collett, S.**, Faryad, S. W., & Petterson, M. (2011). Geochemistry and age dating of the Proterozoic Shedarwaza Formation, Kabul Block, Afghanistan. 3rd International Hindu Kush Geoscience Conference, September, 20-23. 2011, Kabul, Afghanistan. *(presented in absentia)*

- **Collett, S.**, Faryad, S. W., & Petterson, M. (2011). Metamorphism & Geodynamics of the Palaeo-Proterozoic Kabul Block. Strengthening Kabul University – Shared Experiences from Afghanistan, Pakistan, Kurdistan Iraq, UK, Germany and the Czech Republic, December, 7-10. 2011, Leicester, U.K..

- **Collett, S.**, & Faryad, S. W. (2012). Granulite Facies Metamorphism in the Kabul Block, Afghanistan. European Geosciences Union General Assembly, April, 22-27. 2012, Vienna, Austria.

- **Collett, S.**, Faryad, S. W., Petterson, M., Mosazai, A. M. (2012). HT-LP Metamorphism within the Palaeo-Proterozoic Basement of the Kabul Block, Afghanistan. 1st European Mineralogical Conference, September, 2-6. 2012, Frankfurt, Germany.

- **Collett, S.**, & Faryad, S. W. (2013). P-T-X evolution of transitional amphibolite- to granulite- facies para- and ortho- gneisses from the Proterozoic basement of the Kabul Block, Afghanistan. Metamorphic Studies Group Research in Progress Meeting, March, 20. 2013, Cambridge, U.K.

- Faryad, S. W., **Collett, S.**, Petterson, M., & Sergeev, S. A. (2013). Magmatic and metamorphic events in the Western Hindu Kush, Afghanistan. 4th International Hindu Kush Geoscience Conference, September, 29-30. 2013, Kabul, Afghanistan.

- **Collett, S.**, Faryad, S. W., Mosazai, A. M., & Yousufi, A. (2013). P-T evolution of low pressure granulite facies assemblages in Paleo-Proterozoic basement of the Kabul Block, Afghanistan. 4th International Hindu Kush Geoscience Conference, September, 29-30. 2013, Kabul, Afghanistan.

- **Collett, S.**, Faryad, S. W., & Mosazai, A. M. (2014). Metamorphic history of the Palaeo-Proterozoic basement of the Kabul Block, Afghanistan. Metamorphic Studies Group Research in Progress Meeting, March, 12. 2014, Milton Keynes, U.K.

- **Collett, S.**, Faryad, S. W., & Mosazai, A. M. (2015). Proterozoic metamorphism in the Neoarchean Kabul Block, Afghanistan. European Geosciences Union General Assembly, April, 12-17. 2015, Vienna, Austria.

- Faryad, S. W., **Collett, S.**, Sergeev, S. A., & Finger, F. (2015). Mineralogical and Geochronological Records of Paleo- and Neoproterozoic Orogenies in the Kabul Block (Afghanistan). 25th Goldschmidt Conference, August, 16-21. 2015, Prague, Czech Republic.